

Pacific Northwest National Laboratory

Operated by Battelle for the
U.S. Department of Energy

STOMP Subsurface Transport Over Multiple Phases

Application Guide

**W. E. Nichols
N. J. Aimo
M. Oostrom
M. D. White**

**RECEIVED
OCT 22 1997
OSTI**

October 1997

Prepared for the U.S. Department of Energy
under Contract DE-AC06-76RLO 1830

DISCLAIMER

This report was prepared as an account of work sponsored by an agency of the United States Government. Neither the United States Government nor any agency thereof, nor Battelle Memorial Institute, nor any of their employees, makes any warranty, express or implied, or assumes any legal liability or responsibility for the accuracy, completeness, or usefulness of any information, apparatus, product, or process disclosed, or represents that its use would not infringe privately owned rights. Reference herein to any specific commercial product, process, or service by trade name, trademark, manufacturer, or otherwise does not necessarily constitute or imply its endorsement, recommendation, or favoring by the United States Government or any agency thereof, or Battelle Memorial Institute. The views and opinions of authors expressed herein do not necessarily state or reflect those of the United States Government or any agency thereof.

PACIFIC NORTHWEST NATIONAL LABORATORY

operated by

BATTELLE

for the

UNITED STATES DEPARTMENT OF ENERGY

under Contract DE-AC06-76RLO 1830

Printed in the United States of America

Available to DOE and DOE contractors from the
Office of Scientific and Technical Information, P.O. Box 62, Oak Ridge, TN 37831;
prices available from (615) 576-8401.

Available to the public from the National Technical Information Service,
U.S. Department of Commerce, 5285 Port Royal Rd., Springfield, VA 22161



This document was printed on recycled paper.

(9/97)

DISCLAIMER

**Portions of this document may be illegible
in electronic image products. Images are
produced from the best available original
document.**

STOMP

Subsurface Transport Over Multiple Phases Application Guide

W. E. Nichols
N. J. Aimo
M. Oostrom
M. D. White

September 1997

Prepared for the U.S. Department of Energy
under Contract DE-AC06-76RLO1830

MASTER

This work is funded by the Office of Science and Technology,
within the U.S. Department of Energy's Office of Environmental
Management, under the Plumes Focus Area.

DISTRIBUTION OF THIS DOCUMENT IS UNLIMITED

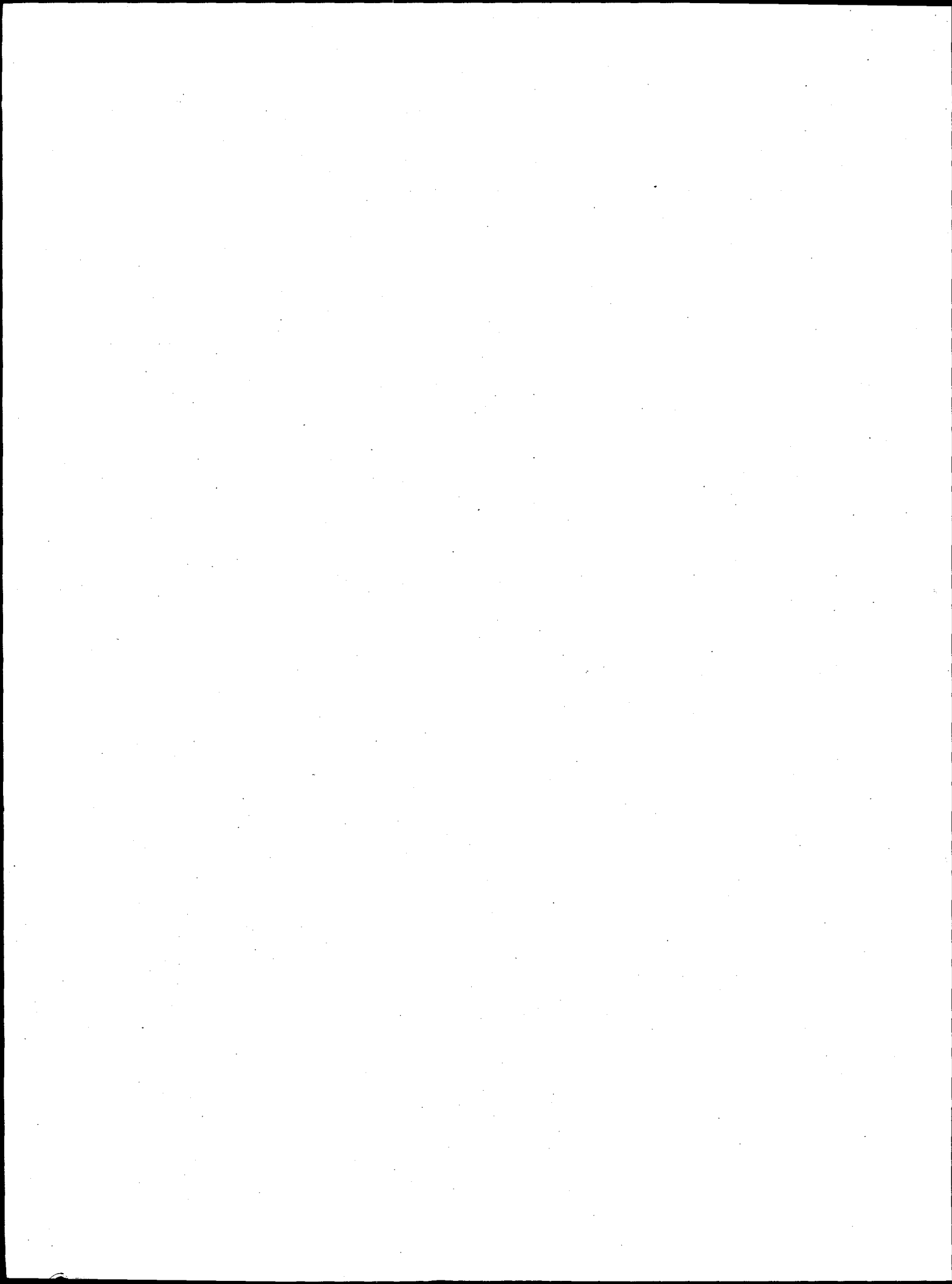
Pacific Northwest National Laboratory
Richland, Washington 99352

ph

Preface

This Application Guide is a software document written to provide a suite of example applications of the STOMP (Subsurface Transport Over Multiple Phases) simulator, a scientific tool for analyzing multiple phase subsurface flow and transport. A description of STOMP's governing equations and constitutive functions and numerical solution algorithms are provided in a companion document, the STOMP Theory Guide. The use, compilation, and execution of the STOMP simulator are described in a second companion document, the STOMP User's Guide. Creation of input files for the STOMP simulator with the sTeP utility is described in a third companion document, the sTeP User's Guide. In writing these guides to the STOMP simulator, the authors have assumed that the reader or code user has received training or is knowledgeable on the topics of multiple phase hydrology, thermodynamics, radioactive chain decay, and nonhysteretic relative permeability-saturation-capillary pressure (k - S - P) functions. The authors further assume that the reader is familiar with the computing environment on which they plan to compile and execute the STOMP simulator.

Computer requirements for the STOMP simulator are strongly dependent on the complexity of the simulated system and the translation of the physical domain into a computational domain. The simulator requires an ANSI FORTRAN 77 compiler to generate an executable code. The speed at which the STOMP simulator solves subsurface flow and transport problems depends on the computing platform, problem complexity, and computational domain size and dimensionality. One-dimensional problems of moderate complexity can be solved on conventional desktop computers, but multidimensional problems involving complex flow and transport phenomena typically require the power and memory capabilities of workstation or mainframe computer systems.



Summary

The U.S. Department of Energy (DOE), through the Office of Technology Development, has requested the demonstration of remediation technologies for the cleanup of volatile organic compounds and associated radionuclides within the soil and ground water at arid sites. This demonstration program, called the VOC-Arid Soils Integrated Demonstrated Program (Arid-ID), has been initially directed at a volume of unsaturated and saturated soil contaminated with carbon tetrachloride on the Hanford Site near Richland, Washington. A principal subtask of the Arid-ID program involves the development of an integrated engineering simulator for evaluating the effectiveness and efficiency of various remediation technologies. The engineering simulator's intended users include scientists and engineers who are investigating soil physics phenomena associated with remediation technologies. Principal design goals for the engineering simulator include broad applicability, verified algorithms, quality assurance controls, and validated simulations against laboratory and field-scale experiments. An important goal for the simulator development subtask involves the ability to scale laboratory and field-scale experiments to full-scale remediation technologies, and to transfer acquired technology to other arid sites. The STOMP (Subsurface Transport Over Multiple Phases) simulator has been developed by the Pacific Northwest Laboratory¹ for modeling remediation technologies. Information on the use, application, and theoretical basis of the STOMP simulator are documented in three companion guide guides. This document, the Application Guide, provides a suite of example applications of the STOMP simulator.

The STOMP simulator's fundamental purpose is to produce numerical predictions of thermal and hydrogeologic flow and transport phenomena in variably saturated subsurface environments, which are contaminated with volatile or nonvolatile organic compounds. Auxiliary applications include numerical predictions of solute transport processes including radioactive chain decay processes. Quantitative predictions from the STOMP simulator are generated from the numerical solution of partial differential equations that describe subsurface environment transport phenomena. Description of the contaminated subsurface environment is founded on governing conservation equations and constitutive functions. Governing coupled flow equations are partial differential equations for the conservation of water mass, air mass, volatile organic compound (VOC) mass, and thermal energy. Constitutive functions relate primary variables to secondary variables. Solution of the governing partial differential equations occurs by the integral volume

¹ Pacific Northwest National Laboratory is operated for the U.S. Department of Energy by Battelle Memorial Institute, under Contract DE-AC06-76RLO1830.

finite difference method. The governing equations that describe thermal and hydrogeological flow processes are solved simultaneously using Newton-Raphson iteration to resolve the nonlinearities in the governing equations. Governing transport equations are partial differential equations for the conservation of solute mass. Solute mass conservation governing equations are solved sequentially, following the solution of the coupled flow equations, by a direct application of the integral volume finite difference method. The STOMP simulator is written in the FORTRAN 77 language, following the American National Standards Institute (ANSI) standard. The simulator utilizes a variable source code configuration, which allows the execution memory and speed to be tailored to the problem specifics and essentially requires that the source code be assembled and compiled through a software maintenance utility.

KEYWORDS: subsurface, porous media, multiple phase, groundwater, nonaqueous phase liquid (NAPL), volatile organic compound (VOC), variably saturated, solute transport, radioactive chain decay, hysteretic, fluid entrapment, finite difference, Newton-Raphson, nonlinear, modeling.

Acknowledgments

This work was funded by the Office of Science and Technology, within the Department of Energy's Office of Environmental Management, under the Plumes Focus Area, with the support of the following contributors:

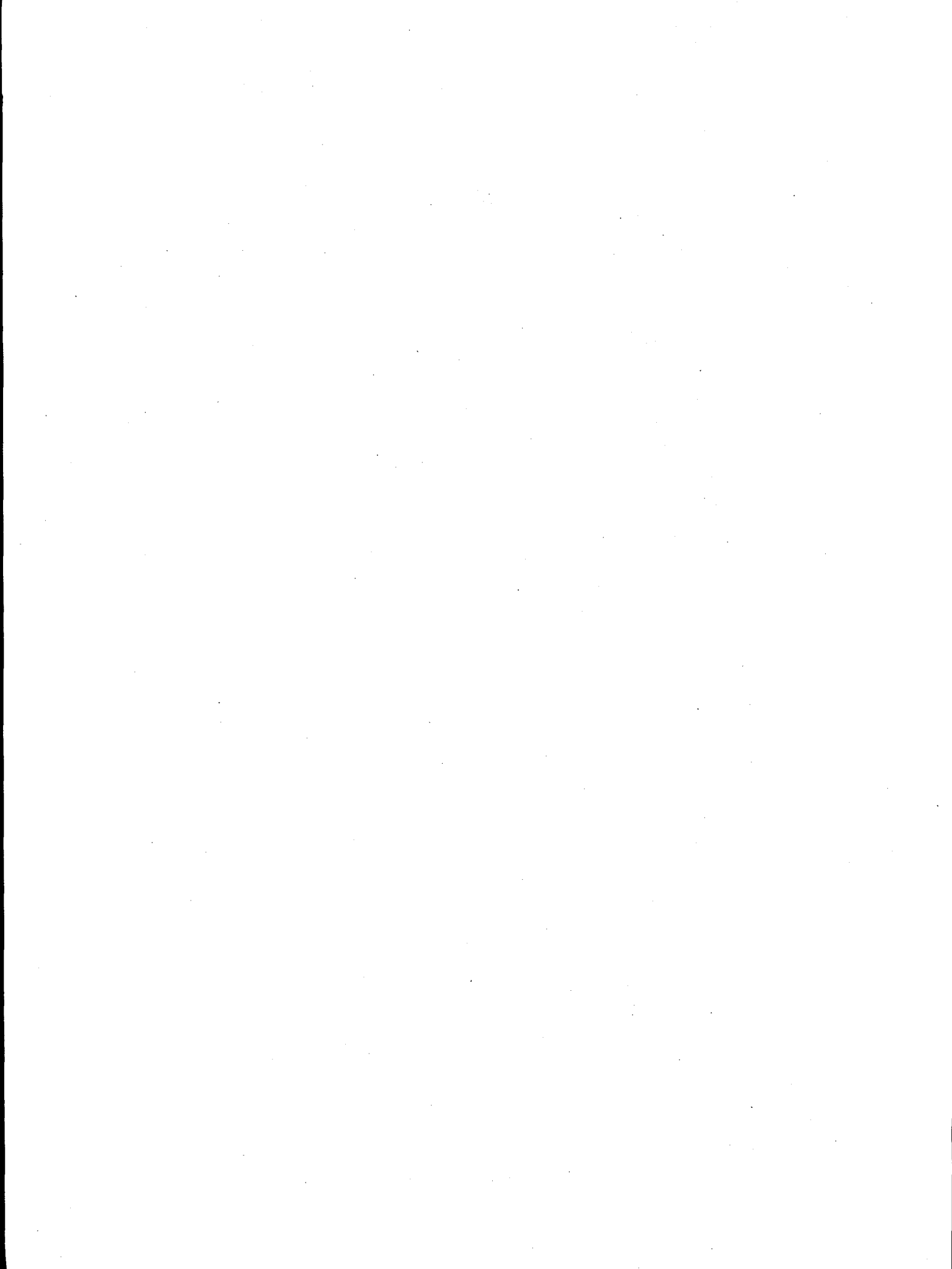
Headquarters: Office of Science and Technology
David Biancosino

Focus Area/Program: Plumes Focus Area
James A. Wright

Operations Office: Richland Operations Office
Science and Technology Programs Division
Jeffrey A. Frey, Technical Program Officer

Contractor: Pacific Northwest National Laboratory
Environmental Management
Technology Development Program
Steven C. Slate, Manager

Financial assistance for the technical review of this document was provided by the Office of Nuclear Regulatory Research of the U.S. Nuclear Regulatory Commission (NRC) under project JCN W6503. STOMP has been used by PNNL staff to support NRC projects JCN W6503 and JCN L2466.



Contents

Preface	i
Executive Summary	ii
Acknowledgments	iv
1.0 Introduction	1.1
1.1 STOMP Simulator Development.....	1.1
1.2 STOMP Application Guide Organization	1.2
1.3 References.....	1.2
2.0 Flow in Saturated Media.....	2.1
2.1 Theis's Problem.....	2.1
2.1.1 Problem Description and Parameters	2.1
2.1.2 Simulation	2.2
2.1.3 Analysis.....	2.3
2.1.4 Summary.....	2.3
2.2 The Two-Aquifer Problem.....	2.10
2.2.1 Problem Description and Parameters	2.10
2.2.2 Simulation	2.11
2.2.3 Analysis.....	2.12
2.2.4 Summary.....	2.13
2.3 Flow to Two Wells in a Nonhomogeneous Domain.....	2.19
2.3.1 Problem Description and Parameters	2.19
2.3.2 Simulation	2.19
2.3.3 Analysis.....	2.21
2.3.4 Summary.....	2.23
2.4 References.....	2.30
3.0 Mass Transport in Saturated Media.....	3.1
3.1 One-Dimensional Transport in a Uniform Steady Flow Field.....	3.2
3.1.1 Problem Description and Parameters.....	3.2
3.1.2 Simulation	3.3
3.1.3 Analysis.....	3.3

3.1.4 Summary	3.4
3.2 The Patch Source	3.13
3.2.1 Problem Description and Parameters	3.13
3.2.2 Simulation	3.14
3.2.3 Analysis	3.15
3.2.4 Summary	3.16
3.3 References	3.22
4. 0 Salt-Water Intrusion and Density-Driven Flow	4.1
4.1 Henry's Problem (Salt Water Intrusion)	4.1
4.1.1 Problem Description and Parameters	4.1
4.1.2 Simulation	4.2
4.1.3 Analysis	4.4
4.1.4 Summary	4.4
4.2 Elder's Problem (Density Driven Flow)	4.10
4.2.1 Problem Description and Parameters	4.10
4.2.2 Simulation	4.11
4.2.3 Analysis	4.13
4.2.4 Summary	4.17
4.3 References	4.24
5. 0 Flow and Transport in Unsaturated Porous Media	5.1
5.1 Haverkamp et al.'s Infiltration Experiments	5.1
5.1.1 Problem Description and Parameters	5.1
5.1.2 Simulations	5.4
5.1.3 Analysis	5.4
5.2 Tank Leak Simulation	5.14
5.2.1 Problem Description and Parameters	5.14
5.2.2 Simulation	5.14
5.2.3 Analysis	5.15
5.2.4 Summary	5.19
5.3 Two-Phase, One-Dimensional Infiltration	5.28
5.3.1 Problem Domain and Input Parameters	5.28
5.3.2 Simulations	5.31
5.3.3 Analysis	5.34
5.3.4 Summary	5.34

5.4 Radon Vapor Transport into Dwellings	5.44
5.4.1 Problem Description and Parameters	5.44
5.4.2 Simulations	5.46
5.4.3 Analysis.....	5.46
5.4.4 Summary.....	5.46
5.5 References	5.53
6.0 Mass and Energy Conservation Tests.....	6.1
6.1 Single Node Evaporation	6.1
6.1.1 Problem Description and Parameters	6.1
6.1.2 Simulation	6.2
6.1.3 Analysis (Mass Balance Check).....	6.2
6.1.4 Summary.....	6.5
6.2 Single Node Condensation	6.8
6.2.1 Problem Domain and Input Parameters	6.8
6.2.2 Simulation	6.8
6.2.3 Analysis (Mass Balance Check).....	6.9
6.2.4 Summary.....	6.11
6.3 Single Node Freezing	6.14
6.3.1 Problem Domain and Input Parameters	6.14
6.3.2 Simulation	6.14
6.3.3 Analysis (Mass Balance Check).....	6.16
6.3.4 Summary.....	6.18
6.4 Single Node Thawing.....	6.21
6.4.1 Problem Domain and Input Parameters	6.21
6.4.2 Simulation	6.21
6.4.3 Analysis (Mass Balance Check).....	6.23
6.4.4 Summary.....	6.24
6.5 Flow from Hot Two-Phase Conditions	6.27
6.5.1 Problem Domain and Input Parameters	6.27
6.5.2 Simulation	6.27
6.5.3 Analysis (Energy Conservation Check).....	6.28
6.5.4 Summary.....	6.30
6.6 References	6.33
7.0 Heat Pipe Effect.....	7.1

7.1 Evaporation / Condensation Heat Pipe	7.1
7.1.1 Problem Description and Parameters	7.2
7.1.2 Simulation	7.4
7.1.3 Analysis.....	7.6
7.1.4 Summary.....	7.8
7.2 Freezing / Thawing Heat Pipe.....	7.13
7.2.1 Problem Description and Parameters	7.13
7.2.2 Simulation	7.17
7.2.3 Analysis.....	7.17
7.2.4 Summary.....	7.20
7.3 References.....	7.25
8.0 Nonaqueous Phase Liquid Flow and Transport.....	8.1
8.1 Infiltration and Redistribution of Oil in a Hypothetical, Two-Dimensional Aquifer	8.1
8.1.1 Problem Description and Parameters	8.1
8.1.2 Simulations	8.2
8.1.3 Analysis.....	8.3
8.1.4 Summary.....	8.8
8.2 Infiltration and Redistribution of Dense and Light Nonaqueous Phase Liquids in Partially Saturated Sand Columns.....	8.14
8.2.1 Problem Description and Parameters	8.14
8.2.2 Simulations	8.15
8.2.3 Analysis.....	8.15
8.2.4 Summary.....	8.18
8.3 Density-Dependent Gas Advection of Trichlorethylene (TCE).....	8.23
8.3.1 Problem Description and Parameters	8.23
8.3.2 Simulations	8.26
8.3.3 Analysis.....	8.26
8.3.4 Summary.....	8.30
8.4 References.....	8.38

Figures

2.1-1. Drawdown After 5 Days of Pumping Predicted by STOMP for Various Initial Time Steps Compared to Theis's Analytical Solution.....	2.4
2.1-2. Drawdown After 10 Days of Pumping Predicted by STOMP for Various Initial Time Steps Compared to Theis's Analytical Solution	2.5
2.2-1. Illustrative Sketch of the Two-Aquifer Problem	2.11
2.2-2. STOMP-Predicted Drawdown Versus Time in the Pumped (Lower) Aquifer at $r = 3.16$ m and $r = 31.6$ m and in the Non-pumped (Upper) Aquifer at $r = 3.16$ m	2.12
2.2-3. Drawdown versus Time in the Pumped Aquifer A) at $r = 3.16$ m and $r = 31.6$ m and B) in the Non-pumped (Upper) Aquifer at $r = 3.16$ m	2.13
2.2-4. Contour Plot of Final Head (m) Distribution Predicted by STOMP for Two-Aquifer Problem	2.14
2.2-5. Contour Plot of Final Drawdown (m) Distribution Predicted by STOMP for Two-Aquifer Problem	2.14
2.3-1. Two Wells in a Nonhomogeneous Domain: Problem Definition.....	2.20
2.3-2. Drawdown in Aquifer for an East-West Cross Section that Intersects One Pumping Well ($500 \text{ m}^3/\text{day}$)	2.22
2.3-3. Response of the Two Wells During Pumping Interval of 2 Days.....	2.22
2.3-4. Volume Rate of Water Supplied by Fixed-Head Boundaries in Response to Pumping Stress	2.23
3.1-1. Concentration Profiles for the Analytical and Patankar Solution Scheme One-Dimensional Transport in a Uniform Steady Flow Field Problem ($Pe = 2.0$).....	3.5
3.1-2. Concentration Profiles for the Analytical and TVD Solution Scheme One-Dimensional Transport in a Uniform Steady Flow Field Problem ($Pe = 2.0$).....	3.5
3.1-3. Concentration Profiles for the Analytical and Patankar Solution Scheme One-Dimensional Transport in a Uniform Steady Flow Field Problem ($Pe = 0.2$).....	3.6
3.1-4. Concentration Profiles for the Analytical and TVD Solution Scheme One-Dimensional Transport in a Uniform Steady Flow Field Problem ($Pe = 0.2$).....	3.6
3.1-5. Concentration Profiles for the Analytical and Patankar Solution Scheme One-Dimensional Transport in a Uniform Steady Flow Field Problem ($Pe = 20.0$)	3.7
3.1-6. Concentration Profiles for the Analytical and TVD Solution Scheme One-Dimensional Transport in a Uniform Steady Flow Field Problem ($Pe = 20.0$)	3.7

3.2-1. Daus and Frind's Representation of the Patch-Source Problem with Dirichlet Boundary Conditions.....	3.14
3.2-2. Longitudinal Concentration Profiles at $y = 1$ Along the x -Direction for the Patch Source Problem	3.15
3.2-3. Transverse Concentration Profiles at $x = 41$ Along the y -Direction for the Patch Source Problem	3.16
4.1-1 Henry's Problem and Computational Grid	4.2
4.1-2 Steady-State Concentration Distribution from the STOMP Solution (Solid Lines) with Henry's Salt-Water Density and Viscosity Functions and from the Ségol Analytical Solution (Dashed Lines).....	4.5
4.1-3 Steady-State Concentration Distribution from the STOMP Solution (Solid Lines) with Leijnse's Salt-Water Density and Viscosity Functions and from the Ségol Analytical Solution (Dashed Lines).....	4.5
4.2-1 Schematic Definition for Elder's Problem	4.11
4.2-2 Contours of Solute Concentration at 2 yr (STOMP Results with Voss and Souza Aqueous Property Functions).....	4.14
4.2-3 Contours of Solute Concentration at 4 yr (STOMP Results with Voss and Souza Aqueous Property Functions).....	4.14
4.2-4 Contours of Solute Concentration at 10 yr (STOMP Results with Voss and Souza Aqueous Property Functions).....	4.15
4.2-5 Contours of 0.2 and 0.6 Solute Concentration at 2 yr Results from Elder's Analogous Thermal Problem	4.15
4.2-6 Contours of 0.2 and 0.6 Solute Concentration at 4 yr Results from Elder's Analogous Thermal Problem	4.16
4.2-7 Contours of 0.2 and 0.6 Solute Concentration at 10 yr Results from Elder's Analogous Thermal Problem	4.16
4.2-.8 Contours of 0.2 and 0.6 Solute Concentration at 2 yr (Solid Lines- STOMP with Voss and Souza Aqueous Property Functions, Dashed Lines- STOMP with Leijnse Aqueous Property Functions).....	4.18
4.2-9 Contours of 0.2 and 0.6 Solute Concentration at 4 yr (Solid Lines- STOMP Results with Voss and Souza Aqueous Property Functions, Dashed Lines- STOMP Results with Leijnse Aqueous Property Functions).....	4.18
4.2-10 Contours of 0.2 and 0.6 Solute Concentration at 10 yr (Solid Lines- STOMP Results with Voss and Souza Aqueous Property Functions, Dashed Lines- STOMP Results with Leijnse Aqueous Property Functions).....	4.19

5.1-1	Comparison of STOMP and Hills et al. Solutions to the Haverkamp et al. Infiltration Problem.....	5.5
5.2-1	Tank Leak Simulation Domain Schematic	5.15
5.2-2	Flow Field Predicted by STOMP for Tank Leak Simulation.....	5.17
5.2-3	Water Content Distribution, Showing Leakage From the Tank Being Diverted Around Both the Clay and Gravel Lenses	5.17
5.2-4	Contaminant Distribution at $t = 2$ yr for Tank Leak Simulation.....	5.18
5.2-5	Contaminant Distribution at $t = 5$ yr for Tank Leak Simulation.....	5.18
5.3-1	Moisture Retention and Relative Permeability Functions for the Two Phase, One Dimensional Infiltration Problem: A) Relationship Between Volumetric Moisture Content and Tension Head, B) Relationship Between Volumetric Water Content and Aqueous and Gas Relative Permeabilities.....	5.30
5.3-2	Aqueous Moisture Content Profiles Predicted by STOMP for Poned Infiltration in the One-Dimensional, Two-Phase Infiltration Problem: Open Column.....	5.32
5.3-3	Aqueous Moisture Content Profiles Predicted by STOMP for Poned Infiltration in the One-Dimensional, Two-Phase Infiltration Problem: Bounded Column.....	5.33
5.3-4	Poned infiltration: water content profiles in the open (a) and bounded (b) columns. Horizontal bars represent experimental uncertainties.....	5.35
5.4-1	Radon Concentration Profiles for Porous Medium Permeability of (a) 10^{-10} m^2 and (b) 10^{-11} m^2	5.45
5.4-2	Radon Concentration Profiles for Porous Medium Permeability of (a) 10^{-10} m^2 and (b) 10^{-11} m^2	5.47
6.1-1	STOMP-Predicted Temperature and Aqueous-Phase Saturation Variation with Time for the Single Node Evaporation Problem	6.2
6.2-1	STOMP-Predicted Temperature and Aqueous Saturation Variation with Time for the Single Node Condensation Problem	6.9
6.3-1	STOMP Predicted Temperature and Saturation Change with Time for the Single Node Freezing Problem.....	6.15
6.4-1	STOMP Predicted Temperature and Phase Change with Time for the Single Node Thawing Problem.....	6.22
7.1-1	Temperature, Total-Liquid Saturation, and Water Vapor Mass Fraction Profiles Versus Distance from Saturated Boundary after 2 Days	7.4

7.1-2	Temperature, Total-Liquid Saturation, and Water Vapor Mass Fraction Profiles Versus Distance from Saturated Boundary after 5 Days	7.5
7.1-3	Temperature, Total-Liquid Saturation, and Water Vapor Mass Fraction Profiles Versus Distance from Saturated Boundary after 10 Days	7.5
7.1-4	Temperature, Total-Liquid Saturation, and Water Vapor Mass Fraction Profiles Versus Distance from Saturated Boundary after 50 Days	7.7
7.1-5	Temperature, Total-Liquid Saturation, and Water Vapor Mass Fraction Profiles Versus Distance from Saturated Boundary after 876.6 Days	7.7
7.2-1	Unfrozen Water Content versus Temperature for the Freezing / Thawing Heat Pipe Problem	7.15
7.2-2	Total Moisture Content Versus Distance from the Cold Boundary for the High Conductivity Soil (256. cm/day)	7.18
7.2-3	Temperature Versus Distance from the Cold Boundary for the High Conductivity Soil (256. cm/day)	7.18
7.2-4	Total Moisture Content Versus Distance from the Cold Boundary for the Low Conductivity Soil (25.6 cm/day)	7.19
7.2-5	Temperature Versus Distance from the Cold Boundary for the Low Conductivity Soil (25.6 cm/day)	7.19
8.1-1	Conceptual Model of the Flow Domain	8.2
8.1-2	NAPL saturations for $\rho_n = 1200 \text{ kg/m}^3$, and $\mu_n = 0.002 \text{ Pa s}$ after (a) 25 days, (b) 50 days, and (c) 100 days	8.4
8.1-3	NAPL saturations for $\rho_n = 1200 \text{ kg/m}^3$, and $\mu_n = 0.0005 \text{ Pa s}$ after (a) 25 days, (b) 50 days, and (c) 100 days	8.5
8.1-4	NAPL saturations for $\rho_n = 800 \text{ kg/m}^3$, and $\mu_n = 0.002 \text{ Pa s}$ after (a) 25 days, (b) 50 days, and (c) 100 days	8.6
8.1-5	NAPL saturations for $\rho_n = 800 \text{ kg/m}^3$, and $\mu_n = 0.002 \text{ Pa s}$ after (a) 25 days, (b) 50 days, and (c) 100 days	8.7
8.2-1	Soltrol® saturation versus elevation at $t = 4 \text{ hr}$. A total of 100 ml Soltrol® infiltrated into the column at a rate of $2 \mu\text{l/min}$	8.16
8.2-2	Soltrol® saturation versus elevation at $t = 72 \text{ hr}$	8.16
8.2-3	Carbon tetrachloride breakthrough curve at $z = 74 \text{ cm}$. A total of 60 ml was allowed to infiltrate into the column at a rate of $2 \mu\text{l/min}$	8.17

8.2-4	Carbon tetrachloride saturation versus elevation at $t = 4$ hr.....	8.17
8.3-1	Illustration of the Configuration of the Flow Cell Including the Measurement Ports with Associated Numbers, the Vapor Chamber, and the Water Table.....	8.25
8.3-2	Comparison Between Experimental TCE Concentrations and Predictions Made by STOMP when Vapor Density is Considered (solid lines) and Ignored (broken lines) for Port 6.	8.27
8.3-3	Comparison Between Experimental TCE Concentrations and Predictions Made by STOMP when Vapor Density is Considered (solid lines) and Ignored (broken lines) for Port 9	8.28
8.3-4	Comparison Between Experimental TCE Concentrations and Predictions Made by STOMP when Vapor Density is Considered (solid lines) and Ignored (broken lines) for Port 45.....	8.29
8.3-5	Darcian Velocities (m/s) of the Gas Phase in the Experimental Cell Predicted Using STOMP when Vapor Density Effects are Considered for (a) $t = 1$ h, and (b) $t = 180$ h.....	8.31

Tables

2.3-1	Physical Parameters of Aquifer Materials for Flow to Two Wells in Nonhomogeneous Domain Problem.....	2.20
4.1-1	Parameters for Henry's Problem.....	4.3
4.2-1	Parameters for Elder's Problem.....	4.12
5.1-1	Input Parameters for Haverkamp et al.'s Infiltration Experiment Problem	5.3
5.2-1	Input Parameters for the Field-Scale Layered Lysimeter Infiltration Problem.....	5.16
5.5-1	Input Parameters for the Touma and Vauclin Infiltration Problems.....	5.29
6.1-1	Single Node Evaporation Problem Initial and Final Conditions.....	6.4
6.2-1	Single Node Condensation Problem Initial and Final Conditions.....	6.10
6.3-1	Single Node Freezing Problem Initial and Final Conditions.....	6.15
6.4-1	Single Node Freezing Problem Initial and Final Conditions.....	6.22
6.5-1	Hot Two-Phase Flow Problem Initial and Final Conditions.....	6.28
7.1-1	Initial and Boundary Conditions for the Evaporation / Condensation Heat Pipe Problem	7.3
7.1-2	Constitutive Function and Physical Parameters for the Evaporation / Condensation Heat Pipe Problem.....	7.3
7.2-1	Initial and Boundary Conditions for Freezing/Thawing Heat Pipe Problem.....	7.14
7.2-2	Constitutive Function and Physical Parameters for Freezing / Thawing Heat Pipe Problem	7.15
8.1-1	NAPL Densities and Viscosities	8.3

Exhibits

2.1-1. STOMP Input File for Theis' Problem.....	2.6
2.1-2. STOMP Parameters File for Theis' Problem.....	2.8
2.2-1. STOMP Input File for the Two-Aquifer Problem.....	2.15
2.2-2. STOMP Parameters File for the Two Aquifer Problem.....	2.17
2.3-1. STOMP Input File for the Two Wells in Nonhomogeneous Domain Problem.....	2.24
2.3-2. STOMP Parameters File for Two Wells in Nonhomogeneous Domain Problem.....	2.28
3.1-1 STOMP Input File for 1D Transport in Uniform Steady Flow Problem.....	3.8
3.1-2 STOMP Parameters File for 1D Transport in Uniform Steady Flow Problem.....	3.11
3.2-1 STOMP Input File for Patch Source Problem.....	3.17
3.2-2 STOMP Parameters File for Patch Source Problem.....	3.20
4.1-1 STOMP Input File for Henry's Problem.....	4.6
4.1-2 STOMP Parameters File for Henry's Problem.....	4.8
4.2-1 STOMP Input File for Elder's Problem.....	4.20
4.2-2 STOMP Parameters File for Elder's Problem.....	4.22
5.1-1 STOMP Input File for Haverkamp et al.'s Infiltration Experiment - Case 3.....	5.6
5.1-2 STOMP Input File for Haverkamp et al.'s Infiltration Experiments - Case 6.....	5.9
5.1-3 STOMP Parameters File for Haverkamp et al.'s Infiltration Experiments.....	5.12
5.2-1 STOMP Input File for Tank Leak Simulation, Step I.....	5.20
5.2-2 STOMP Input File for Tank Leak Simulation, Step II.....	5.23
5.2-3 STOMP Parameters File for Tank Leak Simulation.....	5.26
5.3-1 STOMP Input File for Two-Phase Infiltration Problem: Open Column.....	5.36
5.3-2 STOMP Parameters File for Two-Phase Infiltration Problem: Open Column.....	5.39

5.3-3	STOMP Input File for Two-Phase Infiltration Problem: Bounded Column	5.41
5.4-1	STOMP Input File for Vapor Transport of Radon Into Dwellings Problem.....	5.48
5.4-2	STOMP Parameters File for Vapor Transport of Radon Problem.....	5.51
6.1-1	STOMP Input File for Single Node Evaporation Problem.....	6.6
6.2-1	STOMP Input File for Single Node Condensation Problem.....	6.12
6.3-1	STOMP Input File for Single Node Freezing Problem.....	6.19
6.4-1	STOMP Input File for Single Node Thawing Problem	6.25
6.5-1	STOMP Input File for Hot Two-Phase Problem.....	6.31
7.1-1	STOMP Input File for Evaporation/Condensation Heat Pipe Problem.....	7.9
7.1-2	STOMP Parameters File for Evaporation/Condensation Heat Pipe Problem	7.11
7.2-1	STOMP Input File for the Freezing/Thawing Heat Pipe Problem	7.21
7.2-2	STOMP Parameters File for the Freezing/Thawing Heat Pipe Problem.....	7.23
8.1-1	STOMP Input File for Oil Redistribution in 2D Aquifer	8.10
8.1-2	Parameters File for Oil Redistribution in 2D Aquifer.....	8.12
8.2-1	STOMP Input File for LNAPL and DNAPL Problem (Soltrol).....	8.19
8.2-2	STOMP Input File for LNAPL and DNAPL Problem (Carbon Tetrachloride).....	8.21
8.3-1	STOMP Input File for Two-Dimensional Vapor Flow Problem	8.32
8.3-2	STOMP Parameters File for Two-Dimensional Vapor Flow Problem	8.36

1.0 Introduction

The VOC-Arid Soils Integrated Demonstration Program, abbreviated as Arid-ID and funded by the U.S. Department of Energy (DOE), Office of Technology Development (OTD), is directed at the cleanup of volatile organic compounds and associated radionuclides and heavy metals in soils and ground-water at arid sites. The initial demonstration site is located within the 200 West Area on the Hanford Site near Richland, Washington. The site contains a volume of soil contaminated with carbon tetrachloride, which includes approximately 200 vertical feet of contaminated unsaturated sediments underlying inactive disposal sites and overlying a 7-square-mile plume of contaminated ground water. A critical component of the Arid-ID program involves assessing the impact of spatial heterogeneity of subsurface materials on remediation process and evaluating the effectiveness and efficiency of demonstrated remedial technologies. Because of the complexity of subsurface flow and heat transport phenomena, these assessments and evaluations will require complex numerical tools for their completion. Numerical tools allow scientists and engineers to integrate the current knowledge of contaminant behavior in the subsurface environment to predict and evaluate the performance of proposed remediation methods against established technologies.

1.1 STOMP Simulator Development

A principal subtask of the Arid-ID program involves the development of an engineering simulator (numerical tool), which is capable of numerically simulating proposed remediation processes. The design goals are that the engineering simulator: 1) be accessible and exploitable to scientists and engineers familiar with subsurface environment phenomena, but not necessarily numerical modeling technicalities, 2) have enough general applicability to recruit a user group that is capable of supporting training, maintenance, and enhancement activities, 3) be verified by comparison to analytical solutions and benchmarked against existing simulators, 4) be validated against germane laboratory and field experiments, and 5) have controlled configuration and documentation under an appropriate quality assurance program. An engineering simulator named STOMP, an acronym for Subsurface Transport Over Multiple Phases, has been developed by the Pacific Northwest Laboratory which achieves the five design goals described above. This document, one of three companion documents, has been written to provide users of the STOMP simulator with examples of applications of the simulator to solve classical groundwater problems.

Another companion document is the STOMP User's Guide (White and Oostrom 1997), which provides users of the STOMP simulator with the necessary information for selecting an appropriate operation model, understanding the code flow path and design, creating input files, dimensioning the executable, compiling and executing, and interpreting the simulation outputs. The final companion document, the STOMP Theory Guide (White and Oostrom 1996), provides users of the STOMP simulator with information about the solved governing and constitutive equations, numerical algorithms, and solution techniques used in the STOMP code.

1.2 STOMP Application Guide Organization

This guide has been organized into several sections that group similar classical groundwater problems and presents their solution using the STOMP simulator. The examples in this guide were selected to demonstrate the application of the STOMP simulator to a variety of thermal and hydrogeologic flow and transport problems while illustrating a range of features available in the simulator. Simultaneously, the application examples serve as verification and benchmark cases wherever possible through comparison to analytic solutions or results reported elsewhere in the literature for similar problems solved using other computer codes.

In all applications documented in this guide, the STOMP simulator input file used to direct the executions are shown as "Exhibits," provided at the end of each application example. Any Exhibit in this guide is a verbatim copy of an input or other STOMP-related file provided to assist in understanding how the input file is prepared for a specific problem and to show complete examples. Line numbers are provided on the left side of each exhibit; these are not a part of the actual file, but serve to assist in reading the input file and referencing portions of it in the discussion.

1.3 References

White MD, and M Oostrom. 1996. *STOMP Subsurface Transport Over Multiple Phases Theory Guide*, PNNL-11217, Pacific Northwest National Laboratory, Richland, Washington.

White MD, and M Oostrom. 1997. *STOMP Subsurface Transport Over Multiple Phases User's Guide*, PNNL-11218, Pacific Northwest National Laboratory, Richland, Washington.

2.0 Flow in Saturated Media

STOMP can solve for flow in saturated media using operational mode 1 ("Water"). Solutions generated with the STOMP simulator for three classic ground-water problems are presented in this section. Theis's problem examines the classic transient radial flow problem in which water is extracted by a well that fully penetrates a single aquifer, and allows for comparison to an analytical solution. The two-aquifer, or *leaky aquifer*, problem is a case of flow to a well in a confined multiple-layer system in which water is extracted from the lower aquifer by a fully penetrating well. Both published numerical and analytical solutions to the two-aquifer problem are available for comparison with the STOMP solution. Finally, STOMP is used to solve for water flow to two wells in a nonhomogeneous domain. This is a three-dimensional (rectangular) problem that illustrates the effects of pumping in a complex confined aquifer made up of several anisotropic soil/rock types. There is no analytical solution to this problem (due to the heterogeneous material distribution and mixed boundary conditions).

2.1 Theis's Problem

This test case concerns the classic transient radial flow problem, resulting from pumping a fully penetrating well. An analytical solution to this problem was obtained by Theis (1935) by analogy to heat transfer (see Carslaw and Jaeger (1959), pp.261-262). Here Theis's analytical solution is compared to STOMP simulations. Several time-stepping schemes are used to illustrate the effect of time-step size on accuracy of the predicted drawdowns.

Problem Features: 2.1

- "Water" operational mode
- one dimensional
- saturated flow
- confined aquifer
- radial grid
- homogeneous, isotropic media

2.1.1 Problem Description and Parameters

The mathematical aquifer is confined, horizontal, with constant thickness, homogeneous, isotropic, and extends to infinity. For this simulation of Theis's problem, the aquifer extends to a maximum radial distance of 22,254 m. The pump test is conducted so that drawdown at the simulated aquifer boundaries is negligible. The values for permeability, storage coefficient,

porosity and aquifer thickness are: $2.35965 \times 10^{-11} \text{ m}^2$, $2.0 \times 10^{-6} \text{ m}^{-1}$, 0.35, and 50. m, respectively.

A fully screened, fully penetrating well is pumped at a constant rate Q of 1,000 m^3/day , starting at $t > 0$. In addition, the well is of small diameter, radius 0.001 m, and there are no head losses due to well construction.

The governing equation for transient flow in radial coordinates is

$$\frac{S_s}{K} \frac{\partial h}{\partial t} - \frac{\partial^2 h}{\partial r^2} - \frac{1}{r} \frac{\partial h}{\partial r} = 0$$

Equation 2.1-1

where S_s , K , h , t , and r , are the specific storage coefficient, hydraulic conductivity, hydraulic head, time, and radial distance from the well respectively.

The following initial and boundary conditions apply;

$$\begin{aligned} h(\infty, t) &= h_0 \\ \lim_{r \rightarrow 0} \left(r \frac{\partial h}{\partial r} \right) &= \frac{Q}{2\pi T} \\ h(r, 0) &= h_0 \end{aligned}$$

Equation 2.1-2

2.1.2 Simulation

Simulation of this problem requires a closely spaced grid near the well, in order to accurately represent the steep head gradient caused by pumping. Thus a grid with progressively finer spacing close to the well is used. The radial symmetry of the problem allows the use of the "Cylindrical Grid" feature of STOMP to simulate a quasi- three-dimensional domain. The aquifer is constructed as a 90-degree wedge with 60 nodes in the radial direction and one node in the z -direction.

Simulations were performed for maximum pumping times of 5 and 10 days. For each of these times, six simulations with different time-stepping schemes were made. The time-stepping schemes differ in the value of the initial time-step; with all simulations having a time-step growth factor of 1.5. The initial time-steps used for the 5 day simulations are: 10 min, .25 days, 0.5 days, 1 day, 2.5 days, and 5 days. For the 10-day simulations initial time-steps of 10 min, 0.5 days, 1.125 days, 2.5 days, 5 days and 10 days were used. These particular choices parallel those used by Moridis and Reddell (1991). A copy of the STOMP input and parameters files for this problem are presented in Exhibit 2.1-1 and Exhibit 2.1-2, respectively.

2.1.3 Analysis

The results for 5 days of pumping are compared to Theis's analytical solution in Figure 2.1-1. The comparison for 10 days of pumping is shown in Figure 2.1-2. As would be expected, both figures show that better accuracy is achieved with smaller initial time-step size. In general, the results from the STOMP simulations are comparable to the finite difference results reported in Moridis and Reddell (1991) and Ségol (1994).

2.1.4 Summary

The classical transient radial flow problem is simulated using STOMP, and the results are compared to Theis's analytical solution. The effect time step size has on accuracy of the predicted drawdown is presented. It was found that the smaller the time-step the more accurate the numerical predictions. In general, the results obtained by STOMP are similar to those obtained with other finite difference codes.

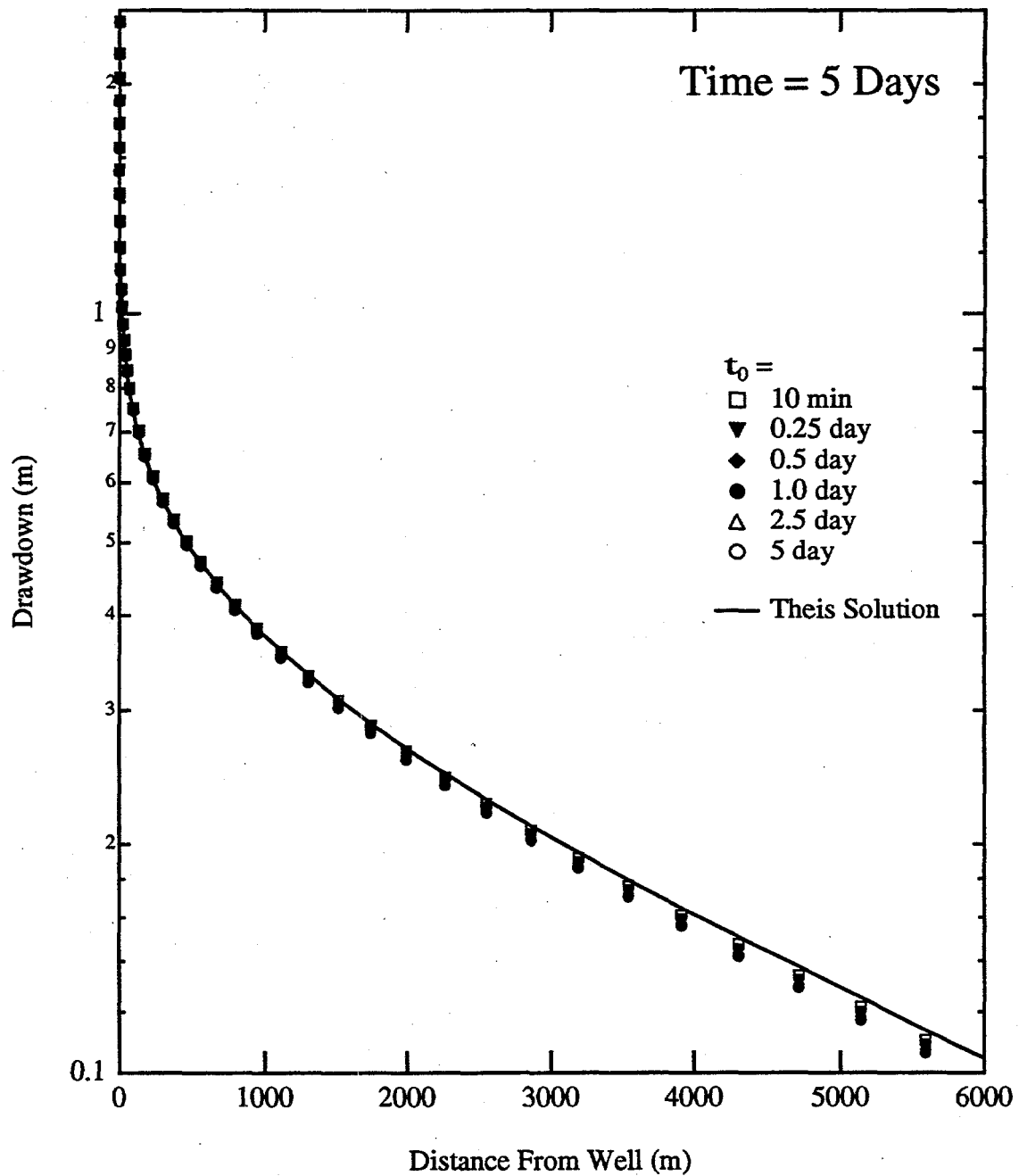


Figure 2.1-1. Drawdown After 5 Days of Pumping Predicted by STOMP for Various Initial Time Steps Compared to Theis's Analytical Solution

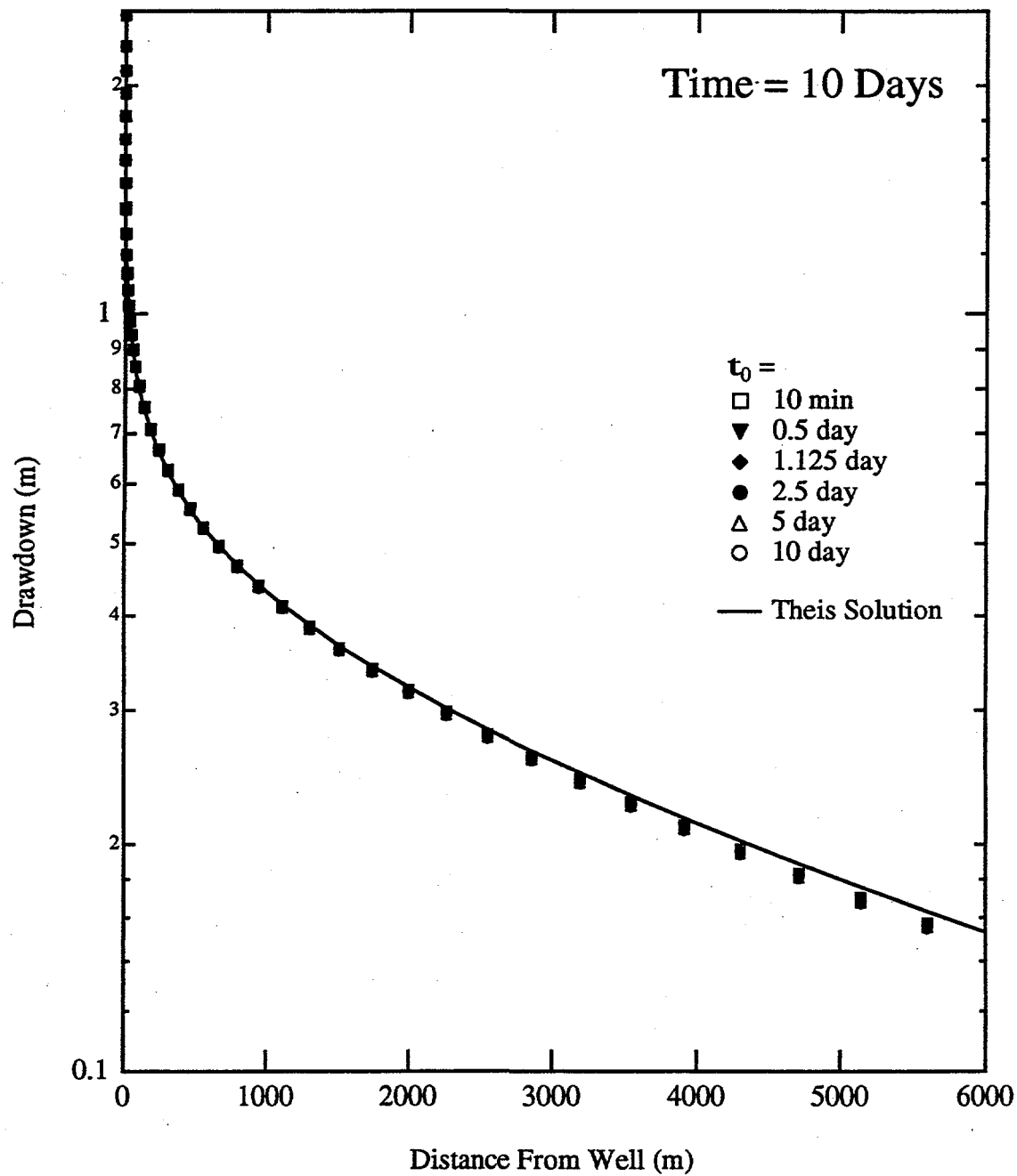


Figure 2.1-2. Drawdown After 10 Days of Pumping Predicted by STOMP for Various Initial Time Steps Compared to Theis's Analytical Solution

Exhibit 2.1-1. STOMP Input File for Theis' Problem

<u>Line</u>	<u>Input File</u>
1	#####
2	# STOMP APPLICATION GUIDE --- Case 2.1 #
3	# #
4	# THEIS'S PROBLEM (Segol 1994, p.15,32-45) #
5	# #
6	# Showcased features: radial solution #
7	# Neumann boundary #
8	# confined aquifer #
9	# #
10	# Domain: One-dimensional "radial" aquifer with maximum radius of 22,254 m. #
11	# and a depth of 50 m. No drawdown allowed at r= 22,254 m. #
12	#####
13	
14	
15	-Simulation Title Card
16	1,
17	THEIS'S PROBLEM (Segol 1994, p.15,32-45)
18	NJ Aimo,
19	Pacific Northwest Laboratory,
20	June 1995,
21	4:00:00 PM PST,
22	3,
23	Case 2.1 --- STOMP Application Guide
24	Domain: One-dimensional "radial" aquifer with a maximum radius of 22,254 m.
25	and a depth of 50 m. No drawdown allowed at r= 22,254 m.
26	
27	
28	-Solution Control Card
29	Normal,
30	Water,
31	1, Number of Simulation periods
32	0.,s,5.,day,10.,min,5.,day,1.5,18,1.e-6, Run #1
33	#
34	1,day,1,day,100000, Max. machine times
35	0, Variables to average
36	
37	-Grid Card
38	Cylindrical,
39	60,1,1,
40	.001,m,.011,m,.031,m,.071,m,.151,m,.311,m,.631,m,1.131,m,2.131,m,4.131,m,
41	7.131,m,11.131,m,16.131,m,22.131,m,30.131,m,39.131,m,49.131,m,64.131,m,84.131,m,
42	114.131,m,154.131,m,204.131,m,264.131,m,334.131,m,414.131,m,504.131,m,604.131,m,
43	724.131,m,864.131,m,1024.131,m,1204.131,m,1404.131,m,1624.131,m,1864.131,m,
44	2124.131,m,2404.131,m,2704.131,m,3024.131,m,3364.131,m,3724.131,m,4104.131,m,
45	4504.131,m,4924.131,m,5364.131,m,5824.131,m,6304.131,m,6804.131,m,7354.131,m,
46	7954.131,m,8604.131,m,9304.131,m,10054.131,m,10854.131,m,11704.131,m,
47	12604.131,m,13554.131,m,14554.131,m,15754.131,m,17254.131,m,19254.131,m,
48	22254.131,m,
49	0.,deg,90.,deg,
50	0.,m,50.,m,
51	
52	-Rock/Soil Zonation Card
53	1,
54	AQFR1,1,60,1,1,1,1,
55	

Exhibit 2.1-1. (Contd)

<u>Line</u>	<u>Input File</u>
56	
57	-Mechanical Properties Card
58	AQFR1,2.65E+06,g/m ³ ,0.35,0.35,2.E-06,1/m, Millington and Quirk,
59	
60	-Hydraulic Properties Card
61	AQFR1,2.35965E-11,m ² ,,,,,,
62	
63	-Saturation Function Card
64	AQFR1,Nonhysteretic van Genuchten,.133,1/cm,1.88,0.268,,
65	
66	-Aqueous Relative Permeability Card
67	AQFR1,Mualem,,
68	
69	-Initial Conditions Card
70	Gas Pressure, Aqueous Pressure,
71	1,
72	Aqueous Pressure,600000.,Pa,,,,,,1,60,1,1,1,1,
73	
74	-Boundary Conditions Card
75	2,
76	West,Neumann,
77	1,1,1,1,1,1,1,
78	0.0,day,-0.03684142201,m/s,,,
79	East, Dirichlet,
80	60,60,1,1,1,1,1,
81	0.0,day,600000.,Pa,
82	
83	-Output Control Card
84	2,
85	1,1,1,
86	60,1,1,
87	1,1,hr,m,6,6,6,
88	3,
89	Aqueous Hydraulic Head,m,
90	Aqueous Pressure, Pa,
91	Aqueous Saturation,,
92	2,
93	0.,day,
94	5.,day,
95	3,
96	Aqueous Hydraulic Head,m,
97	Aqueous Pressure, Pa,
98	Aqueous Saturation,,
99	

Exhibit 2.1-2. STOMP Parameters File for Theis' Problem

<u>Line</u>	<u>Parameters File</u>
1	C-----C
2	C STOMP Parameter File
3	C-----C
4	C
5	C--- Number of lines of simulation notes
6	C Number of execution periods ---
7	C
8	PARAMETER(LNOTES=10, LEPD=2)
9	C
10	C--- Number of nodes in the x or r coordinate direction
11	C Number of nodes in the y or theta coordinate direction
12	C Number of nodes in the z coordinate direction
13	C Number of active nodes
14	C Number of active dimensions
15	C Minimum of (LFX*LFY, LFX*LFZ, LFY*LFZ) ---
16	C
17	PARAMETER(LFX=60, LFY=1, LFZ=1)
18	PARAMETER(LAN=60, LAD=2, LMNP=60)
19	C
20	C--- Energy equation switch (0 = off, 1 = on)
21	C Water mass equation switch (0 = off, 1 = on)
22	C Air mass equation switch (0 = off, 1 = on)
23	C VOC mass equation switch (0 = off, 1 = on)
24	C Solute transport equation switch (0 = off, 1 = on)
25	C Freezing conditions switch (0 = off, 1 = on) ---
26	C Dissolved salt transport equation switch (0 = off, 1 = on) ---
27	C Dissolved oil transport equation switch (0 = off, 1 = on) ---
28	C
29	PARAMETER(LT=0, LL=1, LG=0, LN=0, LC=0, LFC=0, LS=0, LD=0)
30	C
31	C--- Banded matrix linear equation solver switch (0 = off, 1 = on)
32	C Conjugate gradient linear equation solver switch (0 = off, 1 = on) ---
33	C Unsymmetric-pattern multifrontal package switch (0 = off, 1 = on) ---
34	C
35	PARAMETER(LBD=1, LCG=0, LUM=0)
36	C
37	C--- Number of boundary condition surfaces
38	C Number of boundary condition times ---
39	C
40	PARAMETER(LBC=2, LBTM=1)
41	C
42	C--- Number of sources
43	C Number of source times ---
44	C
45	PARAMETER(LSR=1, LSTM=1)
46	C
47	C--- Number of rock/soil types
48	C Number of solutes
49	C
50	PARAMETER(LRC=1, LSOLU=1)
51	C
52	C--- Number of reference nodes
53	C Number of print times
54	C Number of integration surfaces ---
55	C

Exhibit 2.1-2. (Contd)

<u>Line</u>	<u>Parameters File</u>
56	PARAMETER(LREF=10, LPTM=10, LSF=10)
57	C
58	C--- Number saturation and relative permeability table entries
59	C Number of hysteretic scanning paths
60	C Number of chemical reactions
61	C
62	PARAMETER(LTBL=10, LPATH=3, LCHEM=1)
63	C
64	C--- Computed Parameters ---
65	C
66	PARAMETER(LUK=LT+LL+LG+LN+LS+LD, LPH=LL+LG+LN, LCMP=LL+LS+LD)
67	PARAMETER(LFX=LFY*LFZ, LFYZ=LFY*LFZ, LFZX=LFZ*LFX)
68	PARAMETER(LFD=LFX*LFY*LFZ)
69	PARAMETER(LNE=(LUK*LUK*(7*LFD-2*LFY-2*LFZ-2*LFZX))**LUM)
70	PARAMETER(LHBW=LUK*LMNP+LUK-1)
71	PARAMETER(LJA=LBD + LCG*LAN*LUK + LUM*LAN*LUK)
72	PARAMETER(LJB=(2*LAN*LUK)**LUM, LJC=LAN**LUM)
73	PARAMETER(LJD=LBD*(3*LHBW+1) + LCG*LAN*LUK + LUM*6*LNE)
74	PARAMETER(LJE=LBD*LAN*LUK + LCG*((2*LAD+1)*LUK+2*LAD) + LUM)
75	PARAMETER(LJF=LAN*LUK)
76	PARAMETER(LJG=LBD*(3*LHBW+1) + LCG*LAN*LUK + LUM)
77	PARAMETER(LJH=LBD*LAN*LUK + LCG*(2*LAD+1) + LUM)
78	PARAMETER(LJJ=LBD*LAN*LUK + LCG + LUM)
79	PARAMETER(LSV=LUK+2, LSFV=2*LUK+1)
80	PARAMETER(LSX=(LFX+1)*LFY*LFZ)
81	PARAMETER(LSY=LFY*(LFY+1)*LFZ)
82	PARAMETER(LSZ=LFY*LFY*(LFZ+1))
83	PARAMETER(LFDT=LFD**LT, LFDL=LFD**LL, LFDG=LFD**LG, LFDN=LFD**LN)
84	PARAMETER(LFDC=LFD**LC, LFDI=LFD**LFC, LFDS=LFD**LS, LFDD=LFD**LD)
85	PARAMETER(LSXT=LSX**LT, LSXL=LSX**LL, LSXG=LSX**LG, LSXN=LSX**LN)
86	PARAMETER(LSXC=LSX**LC, LSXS=LSX**LS, LSXD=LSX**LD)
87	PARAMETER(LSYT=LSY**LT, LSYL=LSY**LL, LSYG=LSY**LG, LSYN=LSY**LN)
88	PARAMETER(LSYC=LSY**LC, LSYS=LSY**LS, LSYD=LSY**LD)
89	PARAMETER(LSZT=LSZ**LT, LSZL=LSZ**LL, LSZG=LSZ**LG, LSZN=LSZ**LN)
90	PARAMETER(LSZC=LSZ**LC, LSZS=LSZ**LS, LSZD=LSZ**LD)
91	PARAMETER(LRCT=LRC**LT, LRCL=LRC**LL, LRCG=LRC**LG, LRCN=LRC**LN)
92	PARAMETER(LRCC=LRC**LC, LRCL=LRC**LFC, LRCS=LRC**LS, LRCD=LRC**LD)
93	PARAMETER(LBCT=LBC**LT, LBCL=LBC**LL, LBCG=LBC**LG, LBCN=LBC**LN)
94	PARAMETER(LBCC=LBC**LC, LBCI=LBC**LFC, LBCS=LBC**LS, LBCD=LBC**LD)
95	PARAMETER(LBCU=LUK+LPH+LT+2, LBCV=LBCU+LSOLU)
96	PARAMETER(LOUPV=200+11*(LSOLU))
97	PARAMETER(LJI=LBD*LAN*LUK + LCG + (3*LNE+23*LFD*LUK+9)*LUM)
98	PARAMETER(LSCHR=18)
99	

2.2 The Two-Aquifer Problem

Problem Features: 2.2

- "Water" operational mode
- two dimensional (xz section)
- saturated flow
- confined aquifer
- radial grid
- layered media

This test case illustrates flow to a well in a confined multi-layer system, where two identical aquifers (upper and lower) are separated by an aquitard. The well produces only from the lower aquifer, where it is fully penetrating. This problem is known in the literature as the *leaky aquifer* problem. Numerical simulations of this problem have been published by Chorley and Frind (1978) and Huyakorn et al. (1986), while analytical solutions have been developed by Hantush and Jacob (1955) and Neuman and Witherspoon ((1969a; 1969b; 1972)).

2.2.1 Problem Description and Parameters

Two identical aquifers, confined, horizontal, homogeneous, isotropic, 5 m thick, with hydraulic conductivity of 2×10^{-5} m/s and a storage coefficient of 10^{-4} m⁻¹, are separated by an aquitard. The aquitard has a thickness of 10 m, hydraulic conductivity of 10^{-8} m/s, and storage coefficient of 8×10^{-4} m⁻¹ (see Ségol (1994), pp.423-432). Figure 2.2-1 shows a sketch of the conceptual model.

A pumping well penetrates through to the lower aquifer. The well is only open to the full thickness of the lower aquifer, and it is sealed to the aquitard and upper aquifer. In addition, it is assumed the well is of small diameter, and there are no head losses due to well construction. The well is pumped at a constant rate Q , for $t > 0$. Uniform head prevails over the entire domain at $t = 0$, i.e. zero drawdown, and no drawdown is allowed at a radial distance of 10,000 m for $t > 0$.

The governing equation for transient flow in radial coordinates is

$$\frac{S_s}{K} \frac{\partial h}{\partial t} - \frac{\partial^2 h}{\partial r^2} - \frac{1}{r} \frac{\partial h}{\partial r} = 0$$

Equation 2.2-1

where S_s , K , h , t , and r , are the specific storage coefficient, hydraulic conductivity, hydraulic head, time, and radial distance from the well, respectively. The solution obtained by STOMP is

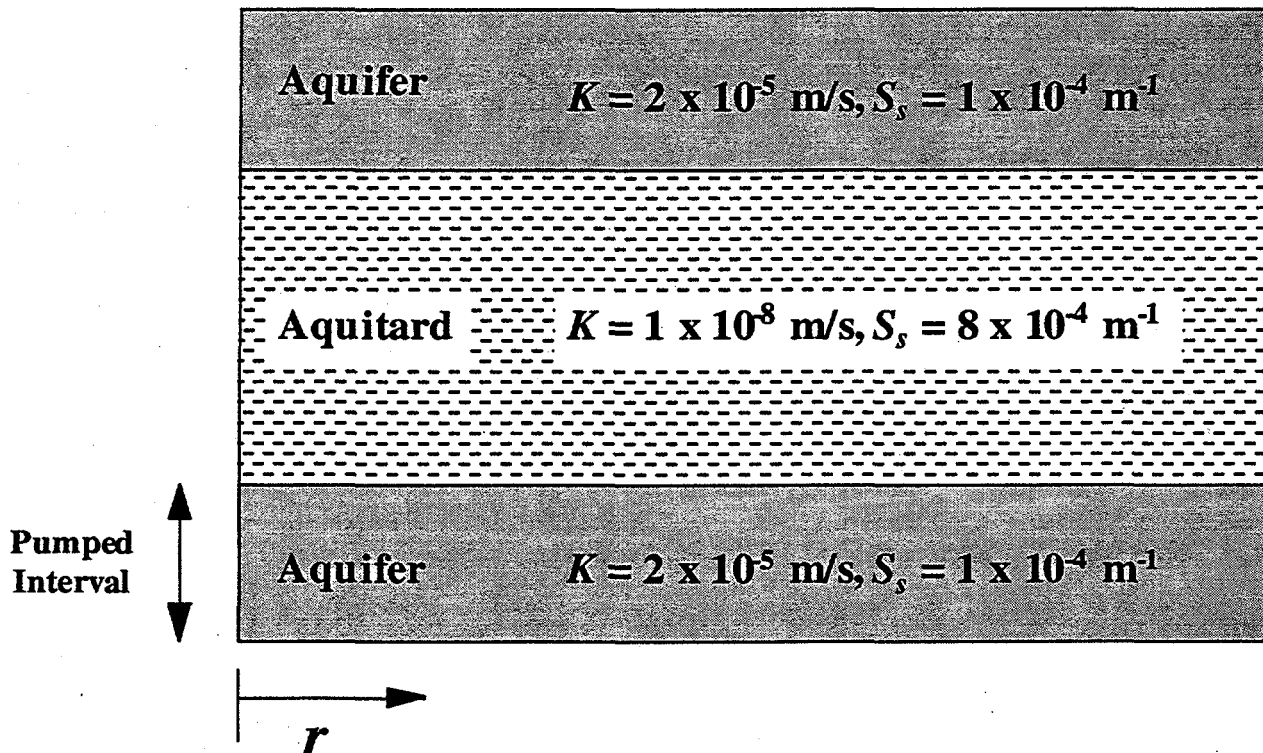


Figure 2.2-1. Illustrative Sketch of the Two-Aquifer Problem

compared to that report by Huyakorn et al (1986), and the analytical solution of Neuman and Witherspoon.

2.2.2 Simulation

Simulation of this problem requires a closely spaced grid near the well, in order to accurately represent the steep head gradient caused by pumping. Thus a grid with progressively finer spacing close to the well is used in the radial direction. A uniform grid spacing is used to discretize the vertical direction. The resulting grid has 12 nodes in the radial direction and 20 nodes in the vertical direction. The radial symmetry of the problem allows the use of the "Cylindrical Grid" feature of STOMP. An 18° arc is used for the third dimension.

A STOMP simulation was performed with duration of 100,000 hours, initial time-step of 36 s, and a time-step growth factor of 1.414. The simulation was started with uniform head initial conditions (hydrostatic pressure). Pumping at the well was implemented via a Neumann boundary

condition, while a Dirichlet boundary condition was prescribed at $r = 10,000$ m. A copy of the STOMP input and parameters files for this problem are presented in Exhibit 2.2-1 and Exhibit 2.2-2, respectively.

2.2.3 Analysis

Figure 2.2-2 shows the results of the STOMP simulation for two locations on the lower (pumped) aquifer, and one location on the upper (unpumped) aquifer. The results obtained by Huyakorn et al. (1986), and the analytical solution predictions are shown in Figure 2.2-3 for the same locations. Comparison of the results shows some differences. The STOMP simulation predicted more drawdown at any given time. The analytical solution of Neuman and Witherspoon and the numerical approach of Huyakorn et al. both assume the flow within the aquitard is purely vertical because of the contrast in conductivities and streamline refraction, and do not explicitly

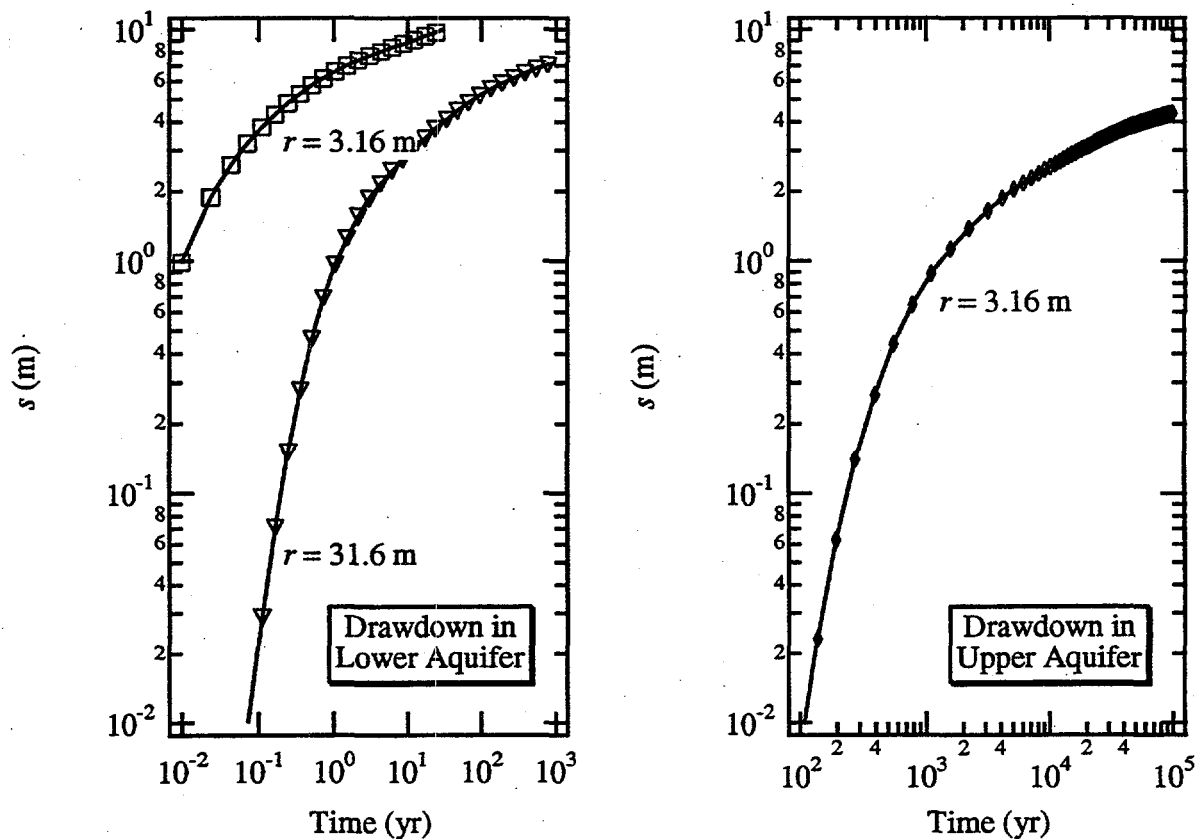


Figure 2.2-2. STOMP-Predicted Drawdown Versus Time in the Pumped (Lower) Aquifer at $r = 3.16$ m and $r = 31.6$ m and in the Non-pumped (Upper) Aquifer at $r = 3.16$ m

account for flow within the aquitard. STOMP, however, takes into consideration the entire domain, without any assumptions. Figure 2.2-4 shows a contour plot of the final head distribution. It is evident that flow within the aquitard is not vertical for $1,000 < r < 10,000$ m; which may account for the discrepancy between the different predictions. Figure 2.2-5 shows the final drawdown distribution.

2.2.4 Summary

The leaky aquifer problem is simulated using STOMP, and the results are compared to previous work by Huyakorn et al. (1986) and Neuman and Witherspoon's analytical solution. The difference between STOMP's predictions and both the analytical solution and the numerical work of Huyakorn et al. may be attributable to the assumption of vertical flow in the aquitard made by Huyakorn et al. and Neuman and Witherspoon.

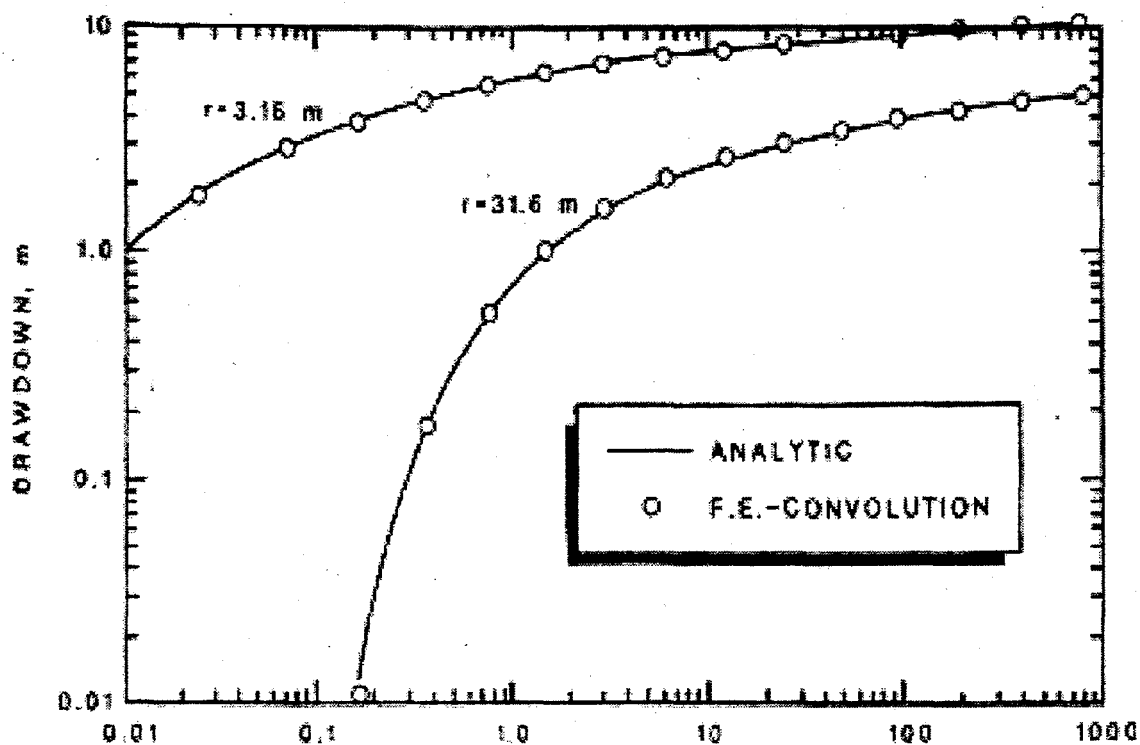


Figure 2.2-3. Drawdown versus Time in the Pumped Aquifer A) at $r = 3.16$ m and $r = 31.6$ m and B) in the Non-pumped (Upper) Aquifer at $r = 3.16$ m (SOURCE: Ségol (1994))

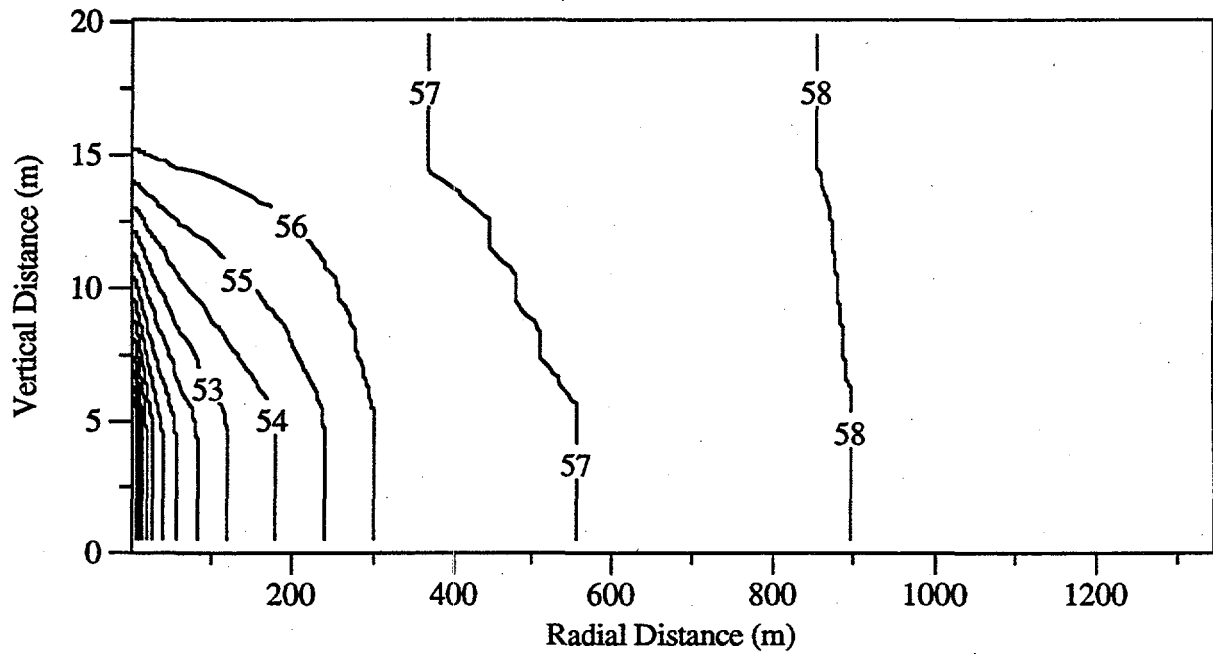


Figure 2.2-4. Contour Plot of Final Head (m) Distribution Predicted by STOMP for Two-Aquifer Problem

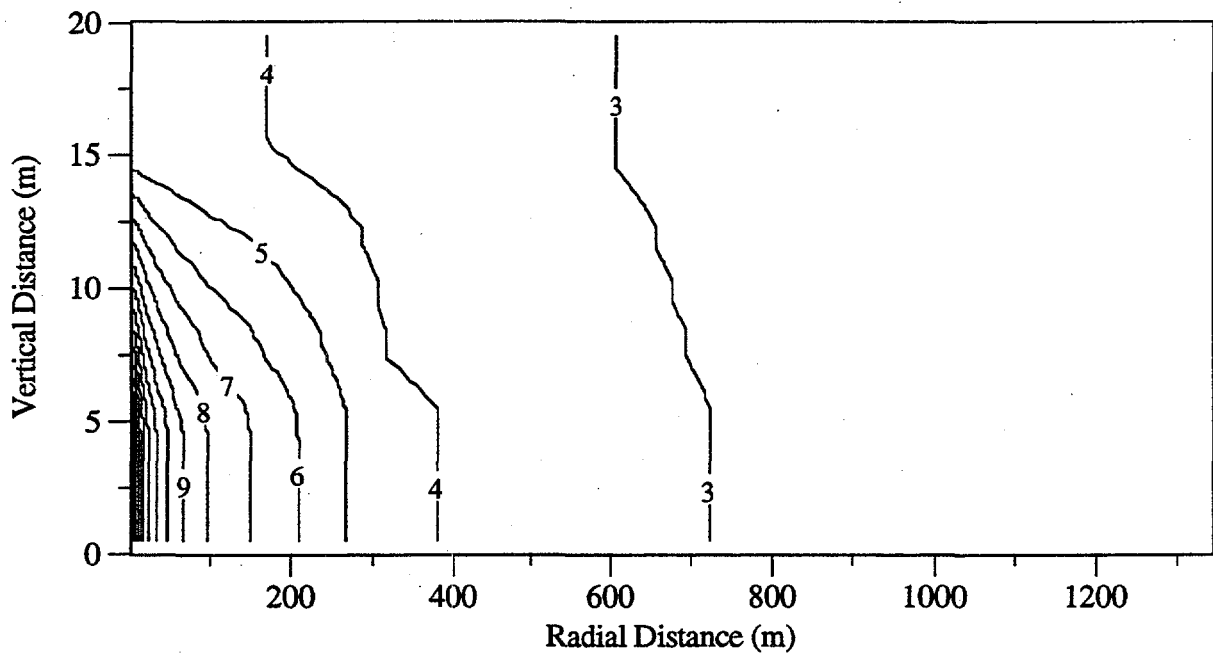


Figure 2.2-5. Contour Plot of Final Drawdown (m) Distribution Predicted by STOMP for Two-Aquifer Problem

Exhibit 2.2-1. STOMP Input File for the Two-Aquifer Problem

<u>Line</u>	<u>Input File</u>
1	#####
2	# STOMP APPLICATION GUIDE --- Case 2.2 #
3	# #
4	# THE TWO AQUIFER PROBLEM (Segol 1994, p.423-432) #
5	# #
6	# Showcased features: radial solution #
7	# Neumann boundary #
8	# confined aquifer #
9	# #
10	# Domain: Two-dimensional "radial" aquifers with maximum radius of 10,000 m. #
11	# Two aquifers (5 m. thick) separated by an aquitard (10 m. thick). #
12	# Pumping well is screened in the lower aquifer only. No drawdown #
13	# allowed at r=10,000 m. #
14	#####
15	
16	
17	-Simulation Title Card
18	1,
19	TWO AQUIFER PROBLEM (Segol 1994, p.423-432)
20	NJ Aimo,
21	Pacific Northwest Laboratory,
22	June 1995,
23	4:00:00 PM PST,
24	5,
25	Case 2.2 --- STOMP Application Guide
26	Domain: Two-dimensional "radial" aquifers with maximum radius of 10,000 m.
27	Two aquifers (5 m. thick) separated by an aquitard (10 m. thick).
28	Pumping well is screened in the lower aquifer only. No drawdown
29	allowed at r=10,000 m.
30	
31	-Solution Control Card
32	Normal,
33	Water,
34	1, Number of Simulation periods
35	0.,s,1.E+05,hr,36.,s,3.6E+06,s,1.414,24,1.E-6,
36	1,day,1;day,100000, Max. machine times
37	0,
38	
39	-Grid Card
40	Cylindrical,
41	13,1,20,
42	1.0,m,1.195,m,2.365,m,3.955,m,7.285,m,12.715,m,22.885,m,40.315,m,72.085,m,
43	127.915,m,504.485,m,1495.515,m,4828.485,m,10000.,m,
44	0.,deg,18.,deg,
45	0.,m,1.,m,2.,m,3.,m,4.,m,5.,m,6.,m,7.,m,8.,m,9.,m,
46	10.,m,11.,m,12.,m,13.,m,14.,m,15.,m,16.,m,17.,m,18.,m,19.,m,
47	20.,m,
48	
49	-Rock/Soil Zonation Card
50	3,
51	AQFR1,1,13,1,1,16,20,
52	AQFR2,1,13,1,1,6,15,
53	AQFR3,1,13,1,1,1,5,
54	
55	-Mechanical Properties Card

Exhibit 2.2-1. (Contd)

<u>Line</u>	<u>Input File</u>
56	AQFR1,2.65E+06,g/m ³ ,0.30,0.30,1.E-04,1/m, Millington and Quirk,
57	AQFR2,2.65E+06,g/m ³ ,0.43,0.43,8.E-04,1/m, Millington and Quirk,
58	AQFR3,2.65E+06,g/m ³ ,0.30,0.30,1.E-04,1/m, Millington and Quirk,
59	
60	-Hydraulic Properties Card
61	AQFR1,2.E-05,hc m/s,2.E-05,hc m/s,2.E-05,hc m/s,
62	AQFR2,1.E-08,hc m/s,1.E-08,hc m/s,1.E-08,hc m/s,
63	AQFR3,2.E-05,hc m/s,2.E-05,hc m/s,2.E-05,hc m/s,
64	
65	-Saturation Function Card
66	AQFR1,Nonhysteretic van Genuchten,.133,1/cm,1.88,0.268,,
67	AQFR2,Nonhysteretic van Genuchten,.133,1/cm,1.88,0.268,,
68	AQFR3,Nonhysteretic van Genuchten,.133,1/cm,1.88,0.268,,
69	
70	-Aqueous Relative Permeability Card
71	AQFR1,Mualem,,
72	AQFR2,Mualem,,
73	AQFR3,Mualem,,
74	
75	-Initial Conditions Card
76	Gas Pressure, Aqueous Pressure,
77	1,
78	Aqueous Pressure,688935.,Pa,,,,,-9793.5,1/m,1,13,1,1,1,20,
79	
80	-Boundary Conditions Card
81	2,
82	West,Neumann,
83	1,1,1,1,1,5,1,
84	0.0,day,-5.02929620E-05,m/s,,,
85	East,Hydraulic Gradient Aqueous,
86	13,13,1,1,1,20,1,
87	0.0,day,688935.,Pa,,,,,
88	
89	-Output Control Card
90	5,
91	3,1,3,
92	3,1,4,
93	7,1,3,
94	3,1,18,
95	7,1,10,
96	1,1,hr,m,6,6,6,
97	3,
98	Aqueous Saturation,,
99	Aqueous Pressure,Pa,
100	Aqueous Hydraulic Head,m,
101	1,
102	0.,s,
103	7,
104	Aqueous Hydraulic Head,m,
105	Aqueous Pressure,Pa,
106	XNC Aqueous Volumetric Flux,m/hr,
107	ZNC Aqueous Volumetric Flux,m/hr,
108	X Aqueous Volumetric Flux,m/hr,
109	Z Aqueous Volumetric Flux,m/hr,
110	Aqueous Saturation,,

Exhibit 2.2-2. STOMP Parameters File for the Two Aquifer Problem

<u>Line</u>	<u>Parameters File</u>
1	C-----C
2	C STOMP Parameter File
3	C-----C
4	C
5	C--- Number of lines of simulation notes
6	C Number of execution periods ---
7	C
8	PARAMETER(LNOTES=10, LEPD=1)
9	C
10	C--- Number of nodes in the x or r coordinate direction
11	C Number of nodes in the y or theta coordinate direction
12	C Number of nodes in the z coordinate direction
13	C Number of active nodes
14	C Number of active dimensions
15	C Minimum of (LFX*LFY, LFX*LFZ, LFY*LFZ) ---
16	C
17	PARAMETER(LFX=13, LFY=1, LFZ=20)
18	PARAMETER(LAN=260, LAD=3, LMNP=13)
19	C
20	C--- Energy equation switch (0 = off, 1 = on)
21	C Water mass equation switch (0 = off, 1 = on)
22	C Air mass equation switch (0 = off, 1 = on)
23	C VOC mass equation switch (0 = off, 1 = on)
24	C Solute transport equation switch (0 = off, 1 = on)
25	C Freezing conditions switch (0 = off, 1 = on) ---
26	C Dissolved salt transport equation switch (0 = off, 1 = on) ---
27	C Dissolved oil transport equation switch (0 = off, 1 = on) ---
28	C
29	PARAMETER(LT=0, LL=1, LG=0, LN=0, LC=0, LFC=0, LS=0, LD=0)
30	C
31	C--- Banded matrix linear equation solver switch (0 = off, 1 = on)
32	C Conjugate gradient linear equation solver switch (0 = off, 1 = on) ---
33	C Unsymmetric-pattern multifrontal package switch (0 = off, 1 = on) ---
34	C
35	PARAMETER(LBD=1, LCG=0, LUM=0)
36	C
37	C--- Number of boundary condition surfaces
38	C Number of boundary condition times ---
39	C
40	PARAMETER(LBC=30, LBTM=1)
41	C
42	C--- Number of sources
43	C Number of source times ---
44	C
45	PARAMETER(LSR=1, LSTM=1)
46	C
47	C--- Number of rock/soil types
48	C Number of solutes
49	C
50	PARAMETER(LRC=3, LSOLU=1)
51	C
52	C--- Number of reference nodes
53	C Number of print times
54	C Number of integration surfaces ---
55	C

Exhibit 2.2-2. (Contd)

<u>Line</u>	<u>Parameters File</u>
56	PARAMETER(LREF=10, LPTM=10, LSF=10)
57	C
58	C--- Number saturation and relative permeability table entries
59	C Number of hysteretic scanning paths
60	C Number of chemical reactions
61	C
62	PARAMETER(LTBL=10, LPATH=3, LCHEM=1)
63	C
64	C--- Computed Parameters ---
65	C
66	PARAMETER(LUK=LT+LL+LG+LN+LS+LD, LPH=LL+LG+LN, LCPM=LL+LS+LD)
67	PARAMETER(LFX=LFY*LFZ, LFXZ=LFY*LFZ, LFZX=LFZ*LFX)
68	PARAMETER(LFD=LFX*LFY*LFZ)
69	PARAMETER(LNE=(LUK*LUK*(7*LFD-2*LFX-2*LFY-2*LFZ))*LUM)
70	PARAMETER(LHBW=LUK*LMNP+LUK-1)
71	PARAMETER(LJA=LBD + LCG*LAN*LUK + LUM*LAN*LUK)
72	PARAMETER(LJB=(2*LAN*LUK)**LUM, LJC=LAN**LUM)
73	PARAMETER(LJD=LBD*(3*LHBW+1) + LCG*LAN*LUK + LUM*6*LNE)
74	PARAMETER(LJE=LBD*LAN*LUK + LCG*((2*LAD+1)*LUK+2*LAD) + LUM)
75	PARAMETER(LJF=LAN*LUK)
76	PARAMETER(LJG=LBD*(3*LHBW+1) + LCG*LAN*LUK + LUM)
77	PARAMETER(LJH=LBD*LAN*LUK + LCG*(2*LAD+1) + LUM)
78	PARAMETER(LJJ=LBD*LAN*LUK + LCG + LUM)
79	PARAMETER(LSV=LUK+2, LSFV=2*LUK+1)
80	PARAMETER(LSX=(LFX+1)*LFY*LFZ)
81	PARAMETER(LSY=LFX*(LFY+1)*LFZ)
82	PARAMETER(LSZ=LFX*LFY*(LFZ+1))
83	PARAMETER(LFDT=LFD**LT, LFDL=LFD**LL, LFDG=LFD**LG, LFDN=LFD**LN)
84	PARAMETER(LFDC=LFD**LC, LFDI=LFD**LFC, LFDS=LFD**LS, LFDD=LFD**LD)
85	PARAMETER(LSXT=LSX**LT, LSXL=LSX**LL, LSXG=LSX**LG, LSXN=LSX**LN)
86	PARAMETER(LSXC=LSX**LC, LSXS=LSX**LS, LSXD=LSX**LD)
87	PARAMETER(LSYT=LSY**LT, LSYL=LSY**LL, LSYG=LSY**LG, LSYN=LSY**LN)
88	PARAMETER(LSYC=LSY**LC, LSYS=LSY**LS, LSYD=LSY**LD)
89	PARAMETER(LSZT=LSZ**LT, LSZL=LSZ**LL, LSZG=LSZ**LG, LSZN=LSZ**LN)
90	PARAMETER(LSZC=LSZ**LC, LSZS=LSZ**LS, LSZD=LSZ**LD)
91	PARAMETER(LRCT=LRC**LT, LRCL=LRC**LL, LRCG=LRC**LG, LRCN=LRC**LN)
92	PARAMETER(LRCC=LRC**LC, LRCL=LRC**LFC, LRCS=LRC**LS, LRCD=LRC**LD)
93	PARAMETER(LBCT=LBC**LT, LBCL=LBC**LL, LBCC=LBC**LG, LBCN=LBC**LN)
94	PARAMETER(LBCC=LBC**LC, LBCI=LBC**LFC, LBCS=LBC**LS, LBCC=LBC**LD)
95	PARAMETER(LBCU=LUK+LPH+LT+2, LBCV=LBCU+LSOLU)
96	PARAMETER(LOUPV=200+11*(LSOLU))
97	PARAMETER(LJI=LBD*LAN*LUK + LCG + (3*LNE+23*LFD*LUK+9)*LUM)
98	PARAMETER(LSCHR=18)
99	

2.3 Flow to Two Wells in a Nonhomogeneous Domain

This test case illustrates the effects of pumping in a complex confined aquifer made up of seven anisotropic soil/rock types. This problem was designed by Moridis and Reddell (1991) (see also Ségol (1994)). Two pumping wells produce only from the bottom fourth of the aquifer. The aquifer is bounded by a mix of fixed-head (Dirichlet) and no-flow (Neumann) boundary conditions. Due to the heterogeneous material distribution and mixed boundary conditions no analytical solution is available for comparison (Celia et al. 1990). The results originally published by Moridis and Reddell (1991) are in error (Moridis 1995). However, the problem serves as a good test for STOMP.

Problem Features: 2.3

- "Water" operational mode
- three dimensional
- saturated flow
- confined aquifer
- heterogeneous and anisotropic
- uniform cartesian grid
- pumping wells
- surface flux history

2.3.1 Problem Description and Parameters

A three-dimensional aquifer 50 m thick, and 7,200 m by 4,800 m in plan view consists of seven different anisotropic material types. The aquifer is surrounded by no-flow boundaries, except for two strips along the upper fourth of the aquifer where fixed-head is enforced. The physical parameters of each of the material types making up the aquifer are presented in Table 2.3-1, while a plan view of the aquifer showing the areal distribution of the material types is presented in Figure 2.3-1. Two pumping wells are turned on at $t = 0$, and pump at a rate of 500 m³/day and 400 m³/day. The wells are located areally at (2325, 2175) m and at (4875, 3375) m, respectively. Initial conditions of no drawdown due to the wells exist at $t = 0$.

2.3.2 Simulation

The simulated domain is divided vertically into 4 blocks of 12.5 m each. In plan view, the aquifer is divided into square blocks with 150 m sides. This discretization yields a grid with 48 blocks in the x -direction, 32 blocks in the y -direction, and 4 blocks in the z -direction, for a total of 6,144 blocks.

Table 2.3-1. Physical Parameters of Aquifer Materials for Flow to Two Wells in Nonhomogeneous Domain Problem

Material	K_x	K_y	Porosity
1	9.0×10^{-13}	7.0×10^{-13}	0.43
2	1.0×10^{-11}	6.0×10^{-12}	0.38
3	3.5×10^{-11}	1.0×10^{-11}	0.33
4	5.0×10^{-12}	2.0×10^{-12}	0.43
5	5.0×10^{-13}	3.0×10^{-13}	0.45
6	8.0×10^{-12}	3.0×10^{-12}	0.40
7	1.0×10^{-16}	1.0×10^{-16}	0.01

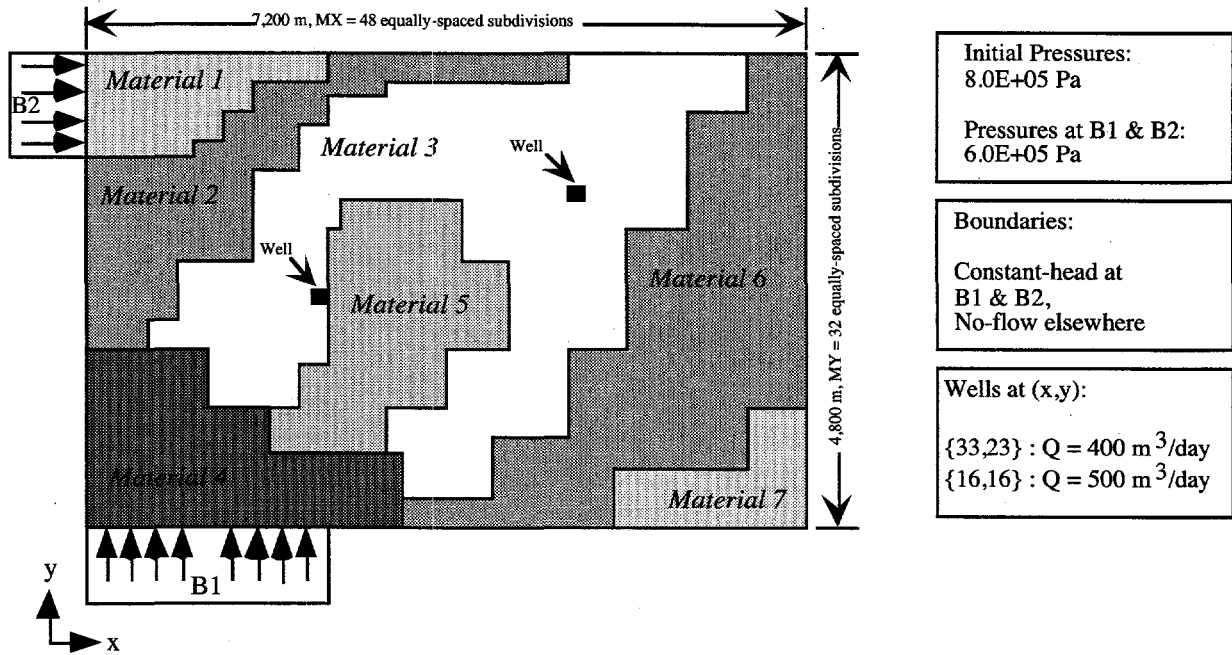


Figure 2.3-1. Two Wells in a Nonhomogeneous Domain: Problem Definition

Dirichlet boundary conditions are specified at the northern edge of the western boundary and at the western edge of the southern boundary, only for the upper fourth of the aquifer (z layer number 4). No-flow Neumann conditions exist everywhere else. Initial conditions of zero drawdown were specified. The initial pressures were assigned so that the aquifer would remain fully saturated (confined) during the pumping period. Two pumping wells, with (x,y,z) nodal locations (16,15,1) and (33,23,1) are simulated using nodal sinks. For illustrative purposes, the amount of water contributed to the aquifer via the fixed head boundaries was monitored using STOMP's Surface Flux Card option.

A STOMP simulation was performed for a maximum simulation time $t_{max} = 2$ days, with a time-step growth factor of 1.5. Initial time-step (Δt) of 6 s was used. A copy of the STOMP input file for this problem is presented in Exhibit 2.3-1, and the parameters file for this problem is presented in Exhibit 2.3-2.

2.3.3 Analysis

The flow problem presented here is arbitrary. The domain configuration and hydraulic parameters are such that a comparison to an analytical solution is not feasible. However, this problem illustrates the use of STOMP to solve flow problems within a complex domain.

Figure 2.3-2 shows the drawdown in the aquifer for a east-west cross-section which intersects one pumping well ($500 \text{ m}^3/\text{day}$), while Figure 2.3-3 shows the response of each of the two wells during the pumping interval of 2 days. The three-dimensional character of the flow-field due to the heterogeneous domain is evident in the non-symmetric shape of the drawdown cone.

Figure 2.3-3 shows the amount of water supplied by the fixed-head boundaries in response to the pumping stress. A time-lag between the pumping stress and the boundary response can be observed by comparison of Figure 2.3-2 and Figure 2.3-3.

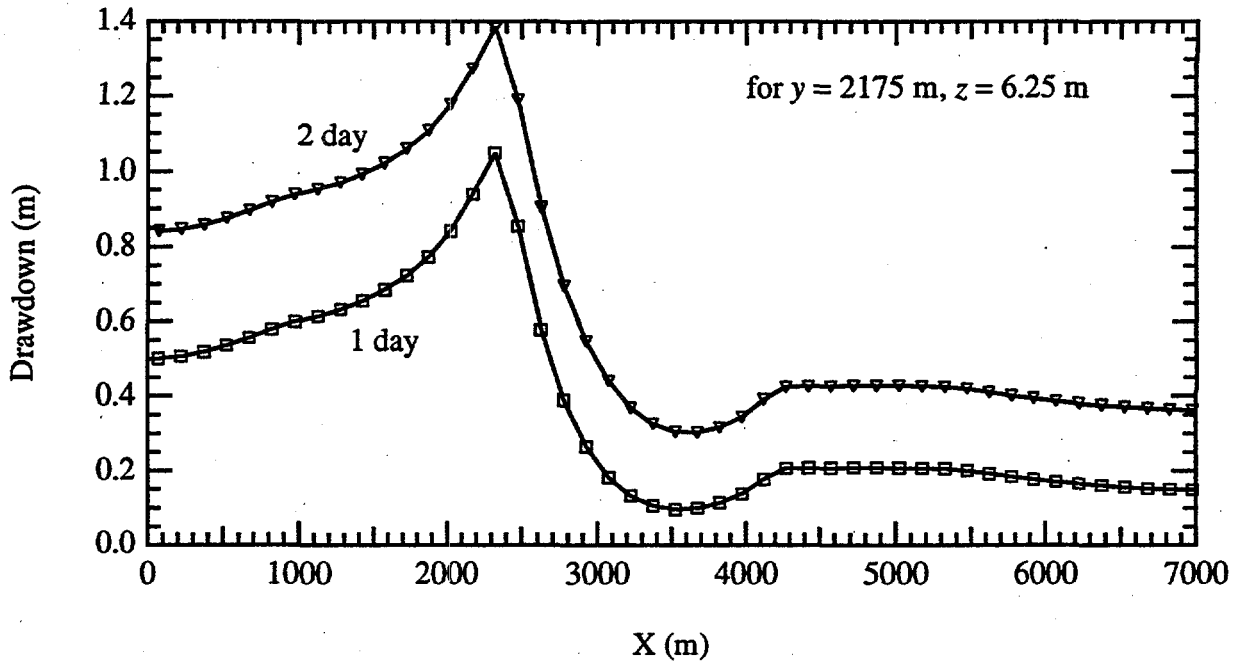


Figure 2.3-2. Drawdown in Aquifer for an East-West Cross Section that Intersects One Pumping Well ($500 \text{ m}^3/\text{day}$)

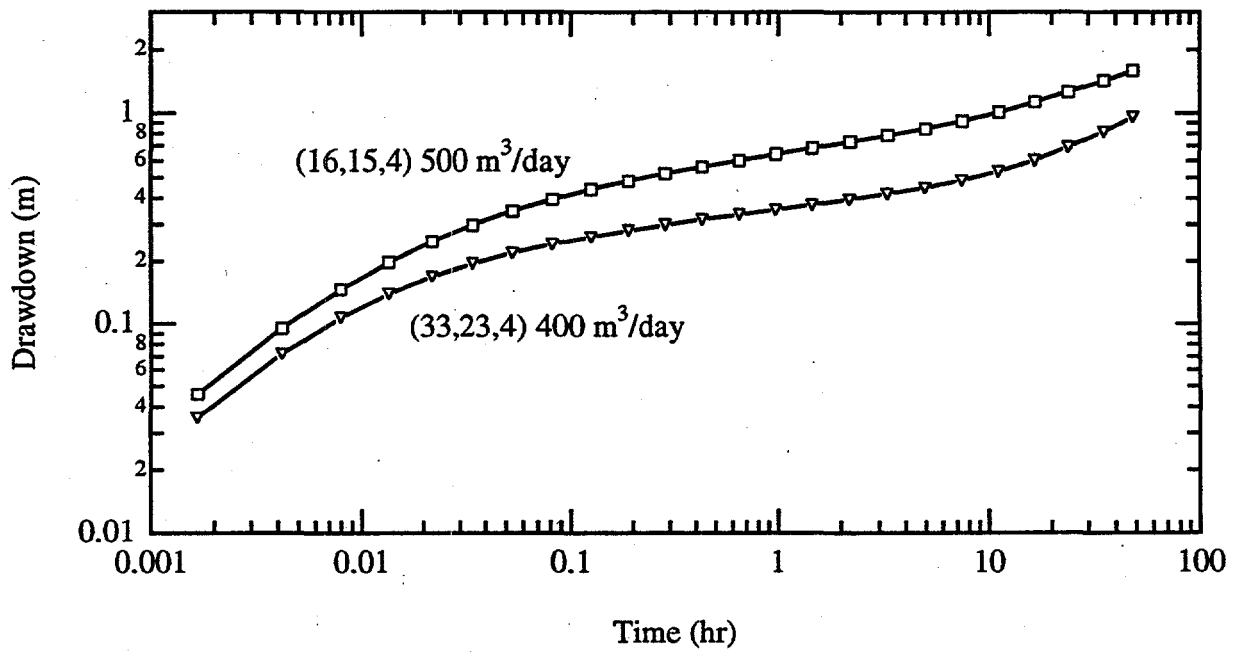


Figure 2.3-3. Response of the Two Wells During Pumping Interval of 2 Days

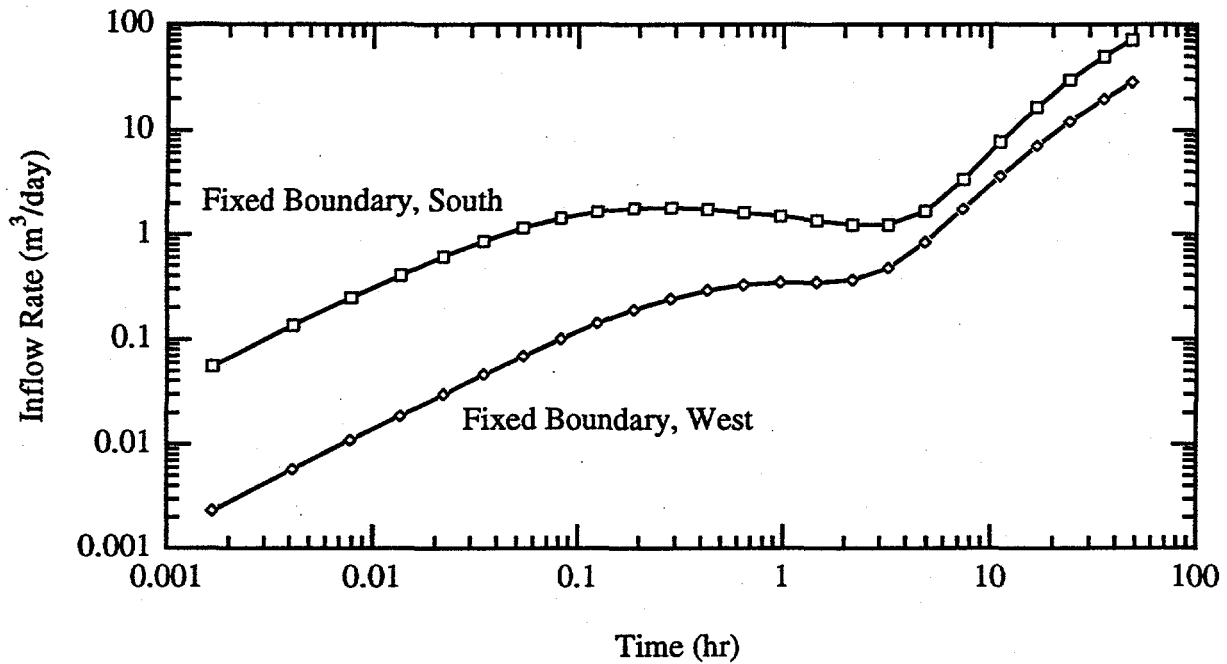


Figure 2.3-4. Volume Rate of Water Supplied by Fixed-Head Boundaries in Response to Pumping Stress

2.3.4 Summary

Confined flow within a highly heterogeneous aquifer, resulting from pumping at two wells was solved using STOMP. The results show a time-lag between the fixed-head boundary response and the pumping stress, as would be expected. The heterogeneous nature of the aquifer is also visible in the results.

Exhibit 2.3-1. STOMP Input File for the Two Wells in Nonhomogeneous Domain Problem

<u>Line</u>	<u>Input File</u>
1	#####
2	# STOMP APPLICATION GUIDE --- Case 2.3 #
3	# #
4	# FLOW TO TWO WELLS IN A NONHOMOGENEOUS DOMAIN (rectangular, 3D) #
5	# (Segol 1994, p.439-442) #
6	# #
7	# Showcased features: Multiple materials #
8	# Dirichlet Boundaries #
9	# anisotropic aquifer #
10	# #
11	# Domain: Three-dimensional rectangular aquifer, with 7 material types, two #
12	# pumping wells, and mixed Dirichlet and Neumann boundary conditions #
13	# #
14	#####
15	
16	
17	-Simulation Title Card
18	1,
19	Flow to Two Wells in a Non-Homogeneous Domain (Segol 1994, p.439-442).
20	NJ Aimo,
21	Pacific Northwest Laboratory,
22	August 1995,
23	4:00:00 PM PST,
24	2,
25	Case 2.3 --- STOMP Application Guide, STOMP Mode 1, 3D
26	Domain: Three-dimensional rectangular heterogeneous aquifer.
27	
28	
29	-Solution Control Card
30	Normal,
31	Water,
32	1, Number of Simulation periods
33	0.,s,2.,day,6. ,s, 2.,day,1.5,18,1.e-6,
34	1,day,1,day,100000, Max. machine times
35	0, Variables to average
36	
37	
38	-Grid Card
39	Uniform Cartesian,
40	48,32,4,
41	150.,m,
42	150.,m,
43	12.5,m,
44	
45	
46	-Rock/Soil Zonation Card
47	# the order of specification of materials is critical here, since new
48	# specifications override older ones.
49	33, Number of specification lines
50	# begin w/blanket assignment
51	MAT3,1,48,1,32,1,4,
52	#
53	# overwrite previous specification
54	MAT1, 1, 1,25,32,1,4,
55	MAT1, 2, 7,26,32,1,4,

Exhibit 2.3-1. (Contd)

<u>Line</u>	<u>Input File</u>
56	MAT1, 8, 9,27,32,1,4,
57	MAT1,10,11,29,32,1,4,
58	MAT1,12,16,31,32,1,4,
59	#
60	MAT2, 1, 1,13,24,1,4,
61	MAT2, 2, 4,13,25,1,4,
62	MAT2, 5, 6,15,25,1,4,
63	MAT2, 7, 7,19,25,1,4,
64	MAT2, 8, 9,19,26,1,4,
65	MAT2,10,11,19,28,1,4,
66	MAT2,12,14,25,30,1,4,
67	MAT2,15,16,28,30,1,4,
68	MAT2,17,20,30,32,1,4,
69	MAT2,21,32,31,32,1,4,
70	#
71	MAT4, 1, 8,1,12,1,4,
72	MAT4, 9,12,1, 8,1,4,
73	MAT4,13,21,1, 5,1,4,
74	#
75	MAT5,13,20, 6, 8,1,4,
76	MAT5,15,24, 9,11,1,4,
77	MAT5,17,24,12,12,1,4,
78	MAT5,17,28,13,18,1,4,
79	MAT5,17,25,19,20,1,4,
80	MAT5,18,25,21,22,1,4,
81	#
82	MAT6,22,27,1, 2,1,4,
83	MAT6,28,32,1, 6,1,4,
84	MAT6,33,36,1,12,1,4,
85	MAT6,37,40,5,20,1,4,
86	MAT6,41,44,5,28,1,4,
87	MAT6,45,48,9,32,1,4,
88	#
89	MAT7,36,48,1,4,1,4,
90	MAT7,45,48,5,8,1,4,
91	#
92	
93	
94	-Mechanical Properties Card
95	MAT1,2.65E+06,g/m^3,0.43,0.43,2.E-06,1/m, Millington and Quirk,
96	MAT2,2.65E+06,g/m^3,0.38,0.38,2.E-06,1/m, Millington and Quirk,
97	MAT3,2.65E+06,g/m^3,0.33,0.33,2.E-06,1/m, Millington and Quirk,
98	MAT4,2.65E+06,g/m^3,0.43,0.43,2.E-06,1/m, Millington and Quirk,
99	MAT5,2.65E+06,g/m^3,0.45,0.45,2.E-06,1/m, Millington and Quirk,
100	MAT6,2.65E+06,g/m^3,0.40,0.40,2.E-06,1/m, Millington and Quirk,
101	MAT7,2.65E+06,g/m^3,0.01,0.01,2.E-06,1/m, Millington and Quirk,
102	
103	
104	-Hydraulic Properties Card
105	MAT1,9.00E-13,m^2,7.00E-13,m^2,4.50E-14,m^2,,,,,
106	MAT2,1.00E-11,m^2,6.00E-12,m^2,5.00E-13,m^2,,,,,
107	MAT3,3.50E-11,m^2,1.00E-11,m^2,1.75E-12,m^2,,,,,
108	MAT4,5.00E-12,m^2,2.00E-12,m^2,2.50E-13,m^2,,,,,
109	MAT5,5.00E-13,m^2,3.00E-13,m^2,2.50E-14,m^2,,,,,
110	MAT6,8.00E-12,m^2,3.00E-12,m^2,4.00E-13,m^2,,,,,

Exhibit 2.3-1. (Contd)

<u>Line</u>	<u>Input File</u>
111	MAT7,1.00E-16,m^2,1.00E-16,m^2,5.00E-18,m^2,,,,,
112	
113	
114	-Saturation Function Card
115	MAT1,Nonhysteretic van Genuchten,.133,1/cm,1.88,0.268,,
116	MAT2,Nonhysteretic van Genuchten,.133,1/cm,1.88,0.268,,
117	MAT3,Nonhysteretic van Genuchten,.133,1/cm,1.88,0.268,,
118	MAT4,Nonhysteretic van Genuchten,.133,1/cm,1.88,0.268,,
119	MAT5,Nonhysteretic van Genuchten,.133,1/cm,1.88,0.268,,
120	MAT6,Nonhysteretic van Genuchten,.133,1/cm,1.88,0.268,,
121	MAT7,Nonhysteretic van Genuchten,.133,1/cm,1.88,0.268,,
122	
123	
124	-Aqueous Relative Permeability Card
125	MAT1,Mualem,,
126	MAT2,Mualem,,
127	MAT3,Mualem,,
128	MAT4,Mualem,,
129	MAT5,Mualem,,
130	MAT6,Mualem,,
131	MAT7,Mualem,,
132	
133	
134	-Initial Conditions Card
135	Gas Pressure, Aqueous Pressure,
136	1,
137	Aqueous Pressure,7.256619E+05,Pa,,,,,-9793.52,1/m,1,48,1,32,1,4,
138	
139	
140	-Boundary Conditions Card
141	2,
142	West,Dirichlet,
143	1,1,25,32,4,4,1,
144	0.,day,3.584049E+05,Pa,,,
145	South, Dirichlet,
146	1,16,1,1,4,4,1,
147	0.,day,3.584049E+05,Pa,
148	
149	
150	-Source Card
151	2,
152	Aqueous Volumetric,16,16,15,15,1,1,1,
153	0.,s,-500.,m^3/day,
154	Aqueous Volumetric,33,33,23,23,1,1,1,
155	0.,s,-400.,m^3/day,
156	
157	
158	-Output Control Card
159	2,
160	16,15,1,
161	33,23,1,
162	1,1,hr,m,6,6,6,
163	2,
164	Aqueous Hydraulic Head,m,
165	Aqueous Saturation,,

Exhibit 2.3-1. (Contd)

<u>Line</u>	<u>Input File</u>
166	3,
167	0.,s,
168	1.,day,
169	2.,day,
170	3,
171	Aqueous Hydraulic Head,m,
172	Aqueous Pressure,Pa,
173	Aqueous Saturation,,
174	
175	
176	-Surface Flux Card,
177	2,
178	Aqueous Volumetric Flux,m ³ /day,m ³ ,South,1,16,1,1,4,4,
179	Aqueous Volumetric Flux,m ³ /day,m ³ ,West,1,1,24,32,4,4,
180	

Exhibit 2.3-2. STOMP Parameters File for Two Wells in Nonhomogeneous Domain Problem

<u>Line</u>	<u>Parameters File</u>
1	C-----C
2	C STOMP Parameter File
3	C-----C
4	C
5	C--- Number of lines of simulation notes
6	C Number of execution periods ---
7	C
8	PARAMETER(LNOTES=10, LEPD=1)
9	C
10	C--- Number of nodes in the x or r coordinate direction
11	C Number of nodes in the y or theta coordinate direction
12	C Number of nodes in the z coordinate direction
13	C Number of active nodes
14	C Number of active dimensions
15	C Minimum of (LFX*LFY, LFX*LFZ, LFY*LFZ) ---
16	C
17	PARAMETER(LFX=48, LFY=32, LFZ=4)
18	PARAMETER(LAN=6144, LAD=3, LMNP=128)
19	C
20	C--- Energy equation switch (0 = off, 1 = on)
21	C Water mass equation switch (0 = off, 1 = on)
22	C Air mass equation switch (0 = off, 1 = on)
23	C VOC mass equation switch (0 = off, 1 = on)
24	C Solute transport equation switch (0 = off, 1 = on)
25	C Freezing conditions switch (0 = off, 1 = on) ---
26	C Dissolved salt transport equation switch (0 = off, 1 = on) ---
27	C Dissolved oil transport equation switch (0 = off, 1 = on) ---
28	C
29	PARAMETER(LT=0, LL=1, LG=0, LN=0, LC=0, LFC=0, LS=0, LD=0)
30	C
31	C--- Banded matrix linear equation solver switch (0 = off, 1 = on)
32	C Conjugate gradient linear equation solver switch (0 = off, 1 = on) ---
33	C Unsymmetric-pattern multifrontal package switch (0 = off, 1 = on) ---
34	C
35	PARAMETER(LBD=1, LCG=0, LUM=0)
36	C
37	C--- Number of boundary condition surfaces
38	C Number of boundary condition times ---
39	C
40	PARAMETER(LBC=24, LBTM=1)
41	C
42	C--- Number of sources
43	C Number of source times ---
44	C
45	PARAMETER(LSR=2, LSTM=1)
46	C
47	C--- Number of rock/soil types
48	C Number of solutes
49	C
50	PARAMETER(LRC=7, LSOLU=1)
51	C
52	C--- Number of reference nodes
53	C Number of print times
54	C Number of integration surfaces ---
55	C

Exhibit 2.3-2. (Contd)

Line Parameters File

```

56           PARAMETER(LREF=10, LPTM=10, LSF=10)
57    C
58    C--- Number saturation and relative permeability table entries
59    C    Number of hysteretic scanning paths
60    C    Number of chemical reactions
61    C
62           PARAMETER(LTBL=10, LPATH=3, LCHEM=1)
63    C
64    C--- Computed Parameters    ---
65    C
66           PARAMETER(LUK=LT+LL+LG+LN+LS+LD, LPH=LL+LG+LN, LCMP=LL+LS+LD)
67           PARAMETER(LFX=LFX*LFY, LFYZ=LFY*LFZ, LFZX=LFZ*LFX)
68           PARAMETER(LFD=LFX*LFY*LFZ)
69           PARAMETER(LNE=(LUK*LUK*(7*LFD-2*LFX-2*LFYZ-2*LFZX))**LUM)
70           PARAMETER(LHBW=LUK*LMNP+LUK-1)
71           PARAMETER(LJA=LBD + LCG*LAN*LUK + LUM*LAN*LUK)
72           PARAMETER(LJB=(2*LAN*LUK)**LUM, LJC=LAN**LUM)
73           PARAMETER(LJD=LBD*(3*LHBW+1) + LCG*LAN*LUK + LUM*6*LNE)
74           PARAMETER(LJE=LBD*LAN*LUK + LCG*((2*LAD+1)*LUK+2*LAD) + LUM)
75           PARAMETER(LJF=LAN*LUK)
76           PARAMETER(LJG=LBD*(3*LHBW+1) + LCG*LAN*LUK + LUM)
77           PARAMETER(LJH=LBD*LAN*LUK + LCG*(2*LAD+1) + LUM)
78           PARAMETER(LJJ=LBD*LAN*LUK + LCG + LUM)
79           PARAMETER(LSV=LUK+2, LSFV=2*LUK+1)
80           PARAMETER(LSX=(LFX+1)*LFY*LFZ)
81           PARAMETER(LSY=LFX*(LFY+1)*LFZ)
82           PARAMETER(LSZ=LFX*LFY*(LFZ+1))
83           PARAMETER(LFDT=LFD**LT, LFDL=LFD**LL, LFDG=LFD**LG, LFDN=LFD**LN)
84           PARAMETER(LFDC=LFD**LC, LFDI=LFD**LFC, LFDS=LFD**LS, LFDD=LFD**LD)
85           PARAMETER(LSXT=LSX**LT, LSXL=LSX**LL, LSXG=LSX**LG, LSXN=LSX**LN)
86           PARAMETER(LSXC=LSX**LC, LSXS=LSX**LS, LSXD=LSX**LD)
87           PARAMETER(LSYT=LSY**LT, LSYL=LSY**LL, LSYG=LSY**LG, LSYN=LSY**LN)
88           PARAMETER(LSYC=LSY**LC, LSYS=LSY**LS, LSYD=LSY**LD)
89           PARAMETER(LSZT=LSZ**LT, LSZL=LSZ**LL, LSZG=LSZ**LG, LSZN=LSZ**LN)
90           PARAMETER(LSZC=LSZ**LC, LSZS=LSZ**LS, LSZD=LSZ**LD)
91           PARAMETER(LRCT=LRC**LT, LRCL=LRC**LL, LRCG=LRC**LG, LRCN=LRC**LN)
92           PARAMETER(LRCC=LRC**LC, LRCI=LRC**LFC, LRCS=LRC**LS, LRCD=LRC**LD)
93           PARAMETER(LBCT=LBC**LT, LBCL=LBC**LL, LBCG=LBC**LG, LBCN=LBC**LN)
94           PARAMETER(LBCC=LBC**LC, LBCL=LBC**LFC, LBCL=LBC**LS, LBCL=LBC**LD)
95           PARAMETER(LBCU=LUK+LPH+LT+2, LBCV=LBCU+LSOLU)
96           PARAMETER(LOUPV=200+11*(LSOLU))
97           PARAMETER(LJI=LBD*LAN*LUK + LCG + (3*LNE+23*LFD*LUK+9)*LUM)
98           PARAMETER(LSCHR=18)
99

```

2.4 References

- Carslaw HS, and JC Jaeger. 1959. *Conduction of Heat in Solids*, trans., Oxford University Press, London.
- Celia MA, ET Bouloutas, and RL Zabra. 1990. "A general mass conservative numerical solution for the unsaturated flow equation." *Water Resources Research*, 26(7), 1483-1496.
- Chorley DW, and EO Frind. 1978. "An iterative quasi-three-dimensional finite element model for heterogeneous multiaquifer systems." *Water Resources Research*, 14(5), 943-952.
- Hantush MS, and CE Jacob. 1955. "Nonsteady radial flow in an infinite leaky aquifer." *Transactions American Geophysical Union*, 36, 95-100.
- Huyakorn PS, BG Jones, and PF Andersen. 1986. "Finite element algorithms for simulating three-dimensional groundwater flow and solute transport in multilayer systems." *Water Resources Research*, 22(3), 361-374.
- Moridis GL. 1995. Personal Communication. *Personal communication*.
- Moridis GL, and DL Reddell. 1991. "The Laplace transform finite difference method for simulation of flow through porous media." *Water Resources Research*, 27(8), 1873-1884.
- Neuman SP, and PA Witherspoon. 1969a. "Applicability of current theories of flow in leaky aquifers." *Water Resources Research*, 5, 817-829.
- Neuman SP, and PA Witherspoon. 1969b. "Theory of flow in a confined two-aquifer system." *Water Resources Research*, 5, 803-816.
- Neuman SP, and PA Witherspoon. 1972. "Field determination of the hydraulic properties of leaky multiple-aquifer systems." *Water Resources Research*, 8, 1284-1298.
- Ségol G. 1994. *Classic Groundwater Simulations: Proving and Improving Numerical Models*, trans., Prentice-Hall, Englewood Cliffs, New Jersey.
- Theis CV. 1935. "The relation between the lowering of the piezometric surface and the rate and duration of discharge of a well using groundwater storage." *Transaction American Geophysical Union*, 2, 519-524.

3.0 Mass Transport in Saturated Media

Two mass transport applications are solved with STOMP to introduce the simulator's capabilities in this area. One-dimensional transport in a uniform steady flow field is examined in Section 3.1. The patch source problem, involving a fixed concentration boundary condition used as source in a steady, uniform two-dimensional flow field, is solved in Section 3.2.

The governing equation for advection-dispersion in a saturated porous media is

$$\frac{\partial}{\partial t}(RC) + \frac{\partial}{\partial x_j}(q_j C) - \frac{\partial}{\partial x_i} \left(D_{ij} \frac{\partial C}{\partial x_j} \right) = Q \quad \text{for } i,j = 1,2,3$$

where C is the time (t) and space dependent (x) solute concentration, R is the retardation factor, q is the Darcy velocity, D is the dispersion tensor, and Q is a sink/source term.

The accuracy of the results obtained from numerical simulation of transport is usually affected by the values of the grid Courant Cr and Peclet Pe numbers. The Courant number controls the oscillations in the solution arising from the discretization of time derivative, and is defined as

$$Cr = \frac{v \Delta t}{\Delta x}$$

where Δt is the size of the time-step and Δx is the grid spacing.

The Peclet number is a measure of the ratio between the advective and the dispersive components of transport, and controls the oscillations in the solution due to the spatial discretization of the domain. The Peclet number is defined as

$$Pe = \frac{v \Delta x}{D}$$

Stability criteria for common numerical simulators require that $Cr \leq 1$, and $Pe \leq 2$ (Daus and Frind 1985).

3.1 One-Dimensional Transport in a Uniform Steady Flow Field

This test case illustrates transport of a solute within a steady state, uniform flow field. An initial square pulse of solute mass is instantaneously introduced into the flow field and transported downstream. The pulse undergoes advection, dispersion and molecular diffusion. An analytical solution by van Genuchten and Alves (1982) is used for comparison.

Problem Features: 3.1

- water operational mode
- nonreactive transport
- one dimensional
- saturated and confined
- heterogeneous and isotropic
- uniform Cartesian grid
- steady, uniform flow
- stability considerations

3.1.1 Problem Description and Parameters

The initial value problem discussed here was recommended by the Convection-Diffusion Forum during the VII International Conference on Computational Methods in Water Resources (Baptista et al. 1988), with the purpose of having a common comparison. The following numerical values for the problem dimensions and parameters are those suggested by the Forum. The one-dimensional domain extends from $0 < x < 12800$, the pore water velocity is 0.5 m/day, and the initial pulse is located at $1400 < x < 2600$. Grid spacing is specified as 200 m, time-steps are 96 days, and total simulation time is 9600 days. A dispersion coefficient of $50 \text{ m}^2/\text{day}$ is used, yielding a Peclet number $Pe = 2$. The Courant number for this simulation was $Cr = 0.24$.

An analytical solution given by van Genuchten and Alves (1982) is used for comparison with the simulated results. The analytical solution is modified to account for a translation of the initial pulse in the positive x -axis direction. Assuming the solute to be conservative, and given the initial and boundary conditions

$$C(x,0) = 0 \quad \text{for} \quad 0 \leq x \leq 1400 \text{ and } 2600 \leq x$$

$$C(x,0) = 1 \quad \text{for} \quad 1400 \leq x \leq 2600$$

$$C(0,t) = 0 \quad \text{for} \quad t > 0$$

$$\frac{\partial C}{\partial x}(\infty,t) = 0 \quad \text{for} \quad t > 0$$

the solution to the advection-dispersion equation is

$$C(x,t) = \frac{1}{2} \left\{ \operatorname{erfc} \left[\frac{x - x_2 - vt}{(4Dt)^{1/2}} \right] - \operatorname{erfc} \left[\frac{x - x_1 - vt}{(4Dt)^{1/2}} \right] \right\} \\ + \frac{1}{2} \exp \left(\frac{vx}{D} \right) \left\{ \operatorname{erfc} \left[\frac{x - x_2 - vt}{(4Dt)^{1/2}} \right] - \operatorname{erfc} \left[\frac{x - x_1 - vt}{(4Dt)^{1/2}} \right] \right\}$$

Equation 3.1-1

3.1.2 Simulation

A STOMP simulation was carried out using the parameters suggested for the reference problem outline above using the Patankar and TVD transport schemes at five different Courant numbers: 0.24, 0.12, 0.06, 0.03, and 0.015. For these simulations, decreasing Courant number implies shorter time steps. The simulations with a $Cr = 0.24$ used a time step of 96 days, whereas the simulations with a $Cr = 0.015$ used a time step of 6 days. Additional simulations were made for Peclet numbers of 0.2 and 20.0 using the Patankar and TVD transport schemes. All simulations are compared to analytical solution results.

All three simulations had a total duration of 9,600 days. Porous media and boundary conditions for the flow problem were chosen to establish a uniform velocity field with pore water velocity of 0.5 m/day (i.e., 0.25 m/day Darcy velocity). A uniform flow field was established by fixing the Darcy flow velocity on the west boundary with a Neumann type boundary, and maintaining a constant pressure above the gas pressure on the east boundary with a Dirichlet type boundary condition. Initial conditions for the solute concentration were specified to duplicate those in Equation 3.1-1 above. An example copy of the STOMP input file for the reference problem is presented in Exhibit 3.1-1, and a copy of the parameters file used to build the STOMP executable code is included in Exhibit 3.1-2.

3.1.3 Analysis

Simulation results compared against the analytical solution for the defined transport problem ($Pe = 2.0$) are shown in Figure 3.1-1 and Figure 3.1-2, respectively for the Patankar and TVD solution schemes, respectively. The Patankar scheme results show considerable numerical dispersion compared against the analytical result as evidence by the lower peak values and broader

distribution. Although symmetric the mass midpoint additionally lags the analytical solution. The solution results improve with decreasing Courant number but in a limited fashion. The TVD scheme results show marked improvement over the Patankar scheme compared against the analytical solution. Decreasing the Courant number improves the solution, but decreases below $Cr = 0.06$ do not yield significant changes.

Simulation results for $Pe = 0.2$ are shown against the analytical solution in Figure 3.1-3 and Figure 3.1-4, respectively, for the Patankar and TVD solution schemes. Both schemes show good agreement with the analytical solution for this diffusion dominated problem, however, the Patankar scheme shows slightly more numerical dispersion than the TVD scheme. The Patankar scheme additionally shows a slight time lag compared against the analytical solution. Because of the high dispersion in this problem some solute exits the physical domain via the west surface (i.e., against the flow field). Matching the analytical solution for this condition requires the use of the "Aqueous Volumetric Conc." type boundary condition on the west boundary instead of the Inflow type boundary condition, which neglects diffusion/dispersion across the boundary.

Simulation results for $Pe = 20.0$ are shown against the analytical solution in Figure 3.1-5 and Figure 3.1-6, respectively for the Patankar and TVD solution schemes. For this advection dominated problem the Patankar scheme yields more results compared against the analytical solution, showing considerable numerical dispersion. Although the overall solute mass balance remains accurate the solute distribution is poor. The TVD scheme shows marked improvement in tracking a sharp front, however, numerical dispersion does cause the solute distribution to be broader than the analytical solution.

3.1.4 Summary

One-dimensional transport simulations were compared to an analytical solution. The simulated results show more spreading of the solute due to numerical dispersion and a slight trailing of the peak in time for the Patankar scheme. The TVD scheme shows greater accuracy than the Patankar scheme across the range of Peclet numbers. Numerical dispersion becomes more important for simulations where the Peclet number is greater than about 2.

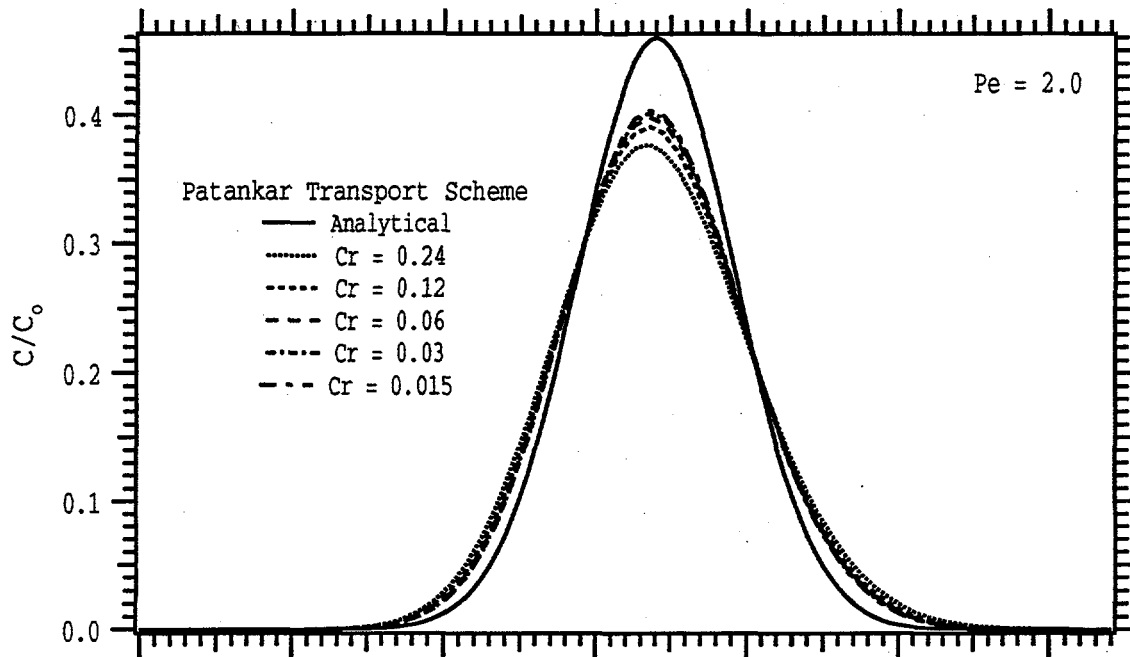


Figure 3.1-1. Concentration Profiles for the Analytical and Patankar Solution Scheme One-Dimensional Transport in a Uniform Steady Flow Field Problem ($Pe = 2.0$)

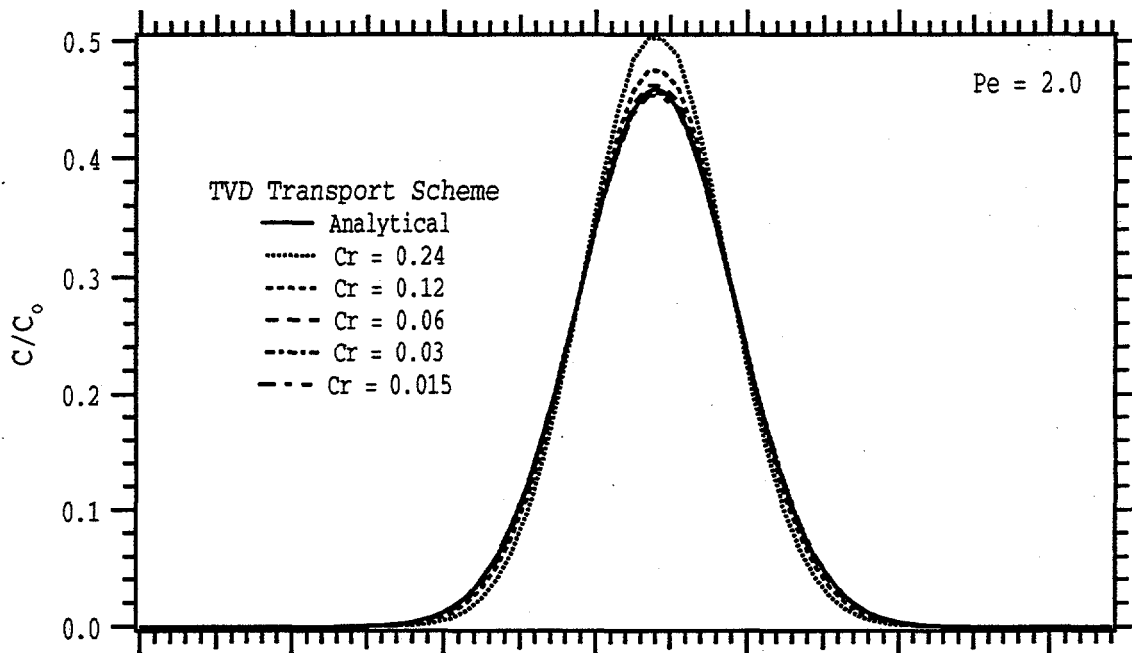


Figure 3.1-2. Concentration Profiles for the Analytical and TVD Solution Scheme One-Dimensional Transport in a Uniform Steady Flow Field Problem ($Pe = 2.0$)

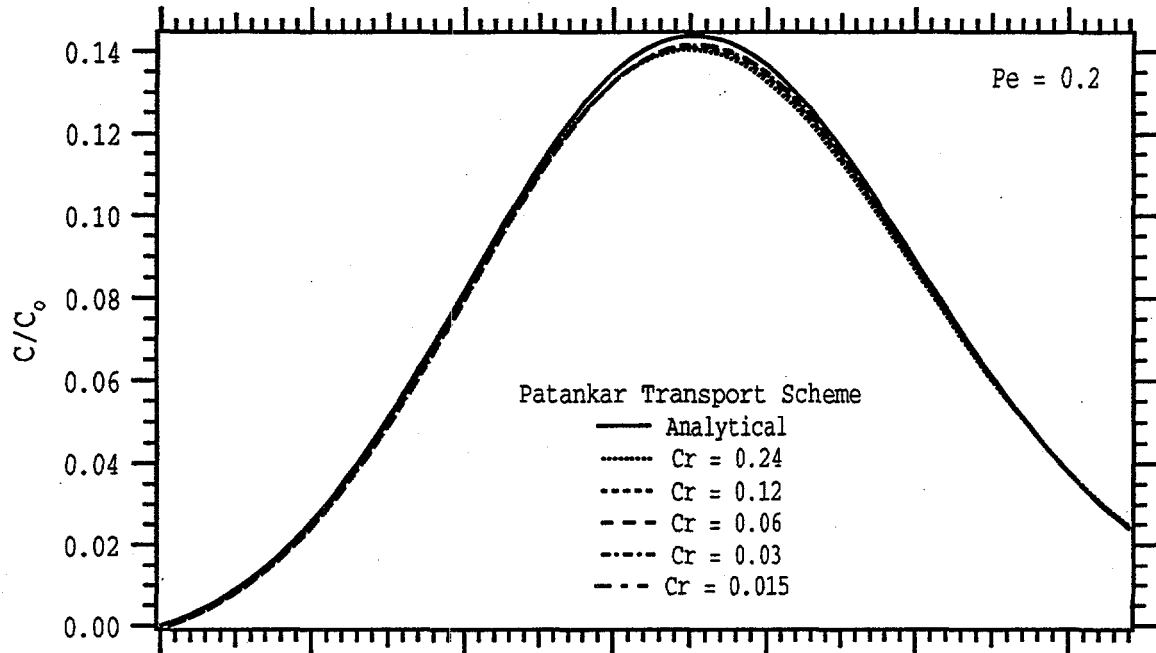


Figure 3.1-3. Concentration Profiles for the Analytical and Patankar Solution Scheme One-Dimensional Transport in a Uniform Steady Flow Field Problem ($Pe = 0.2$)

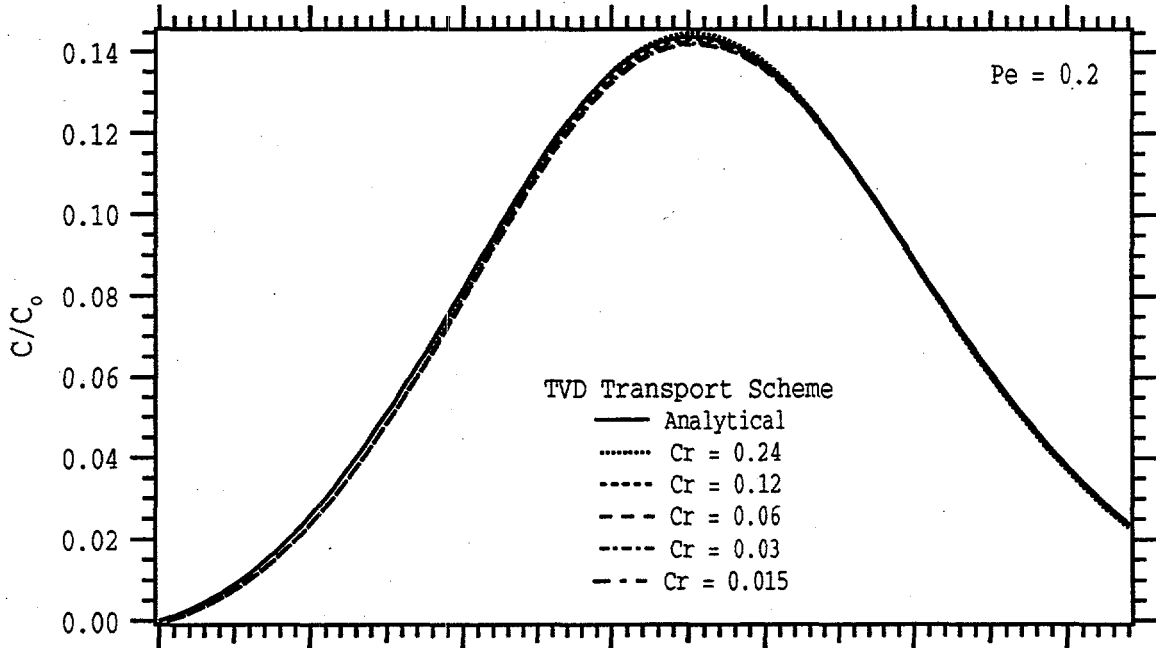


Figure 3.1-4. Concentration Profiles for the Analytical and TVD Solution Scheme One-Dimensional Transport in a Uniform Steady Flow Field Problem ($Pe = 0.2$)

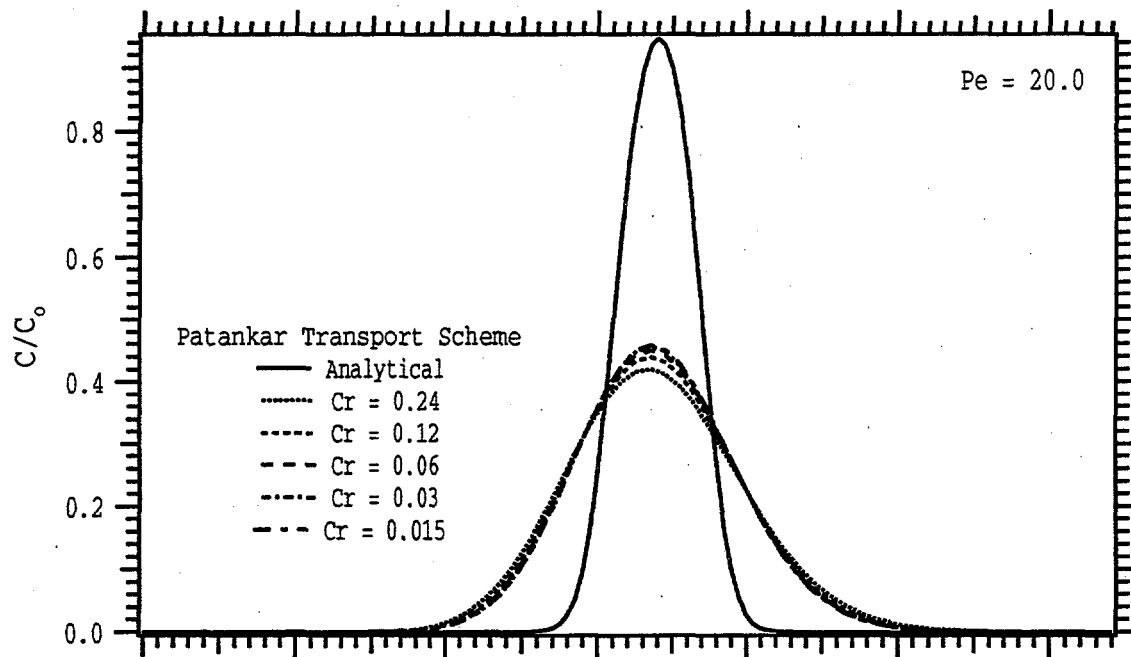


Figure 3.1-5. Concentration Profiles for the Analytical and Patankar Solution Scheme One-Dimensional Transport in a Uniform Steady Flow Field Problem ($Pe = 20.0$)

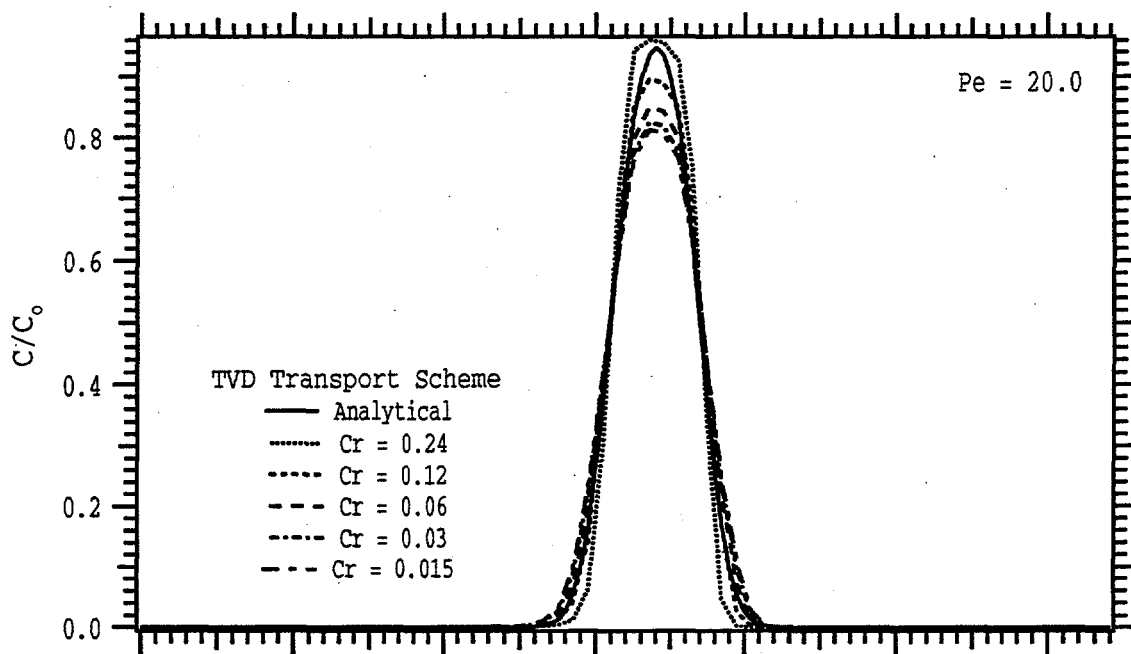


Figure 3.1-6. Concentration Profiles for the Analytical and TVD Solution Scheme One-Dimensional Transport in a Uniform Steady Flow Field Problem ($Pe = 20.0$)

Exhibit 3.1-1. STOMP Input File for 1D Transport in Uniform Steady Flow Problem

<u>Line</u>	<u>Input File</u>
1	#####
2	# STOMP APPLICATION GUIDE --- Case 3.1 #
3	# #
4	# 1D TRANSPORT IN A UNIFORM STEADY FLOW FIELD #
5	# #
6	# Showcased features: Non-reactive transport #
7	# Solute outflow boundaries #
8	# #
9	# Domain: One-dimensional, homogeneous, isotropic, #
10	# #
11	#####
12	
13	
14	
15	-Simulation Title Card
16	# -----
17	1,
18	1D transport verification, FB project, Forum Reference Problem.
19	NJ Aimo,
20	Pacific Northwest Laboratory,
21	August 1995,
22	4:00:00 PM PST,
23	1,
24	Case 3.1 --- Initial value problem, comparison to analytical solution
25	
26	
27	
28	-Solution Control Card
29	# -----
30	Normal,
31	Water w/TVD Transport,
32	1,
33	0,s,9600,d,96,d,96,d,1.,8,1.e-06,
34	1,day,1,day,10000,
35	0,
36	
37	
38	
39	-Grid Card
40	# -----
41	Cartesian,
42	100,1,1,
43	0,m,100@200,m,
44	0,m,1,m,
45	0,m,1,m,
46	
47	
48	
49	-Rock/Soil Zonation Card
50	# -----
51	1,
52	Sand,1,100,1,1,1,1,
53	
54	
55	

Exhibit 3.1-1. (Contd)

<u>Line</u>	<u>Input File</u>
56	
57	-Mechanical Properties Card
58	# -----
59	Sand,,,0.5,0.5,,,Millington and Quirk,
60	
61	
62	
63	-Hydraulic Properties Card
64	# -----
65	Sand,25000.,hc m/day,,,,,
66	
67	
68	
69	-Saturation Function Card
70	# -----
71	Sand,Nonhysteretic van Genuchten,0.015,1/cm,2.0,0.05,,
72	
73	
74	
75	-Aqueous Relative Permeability Card
76	# -----
77	Sand,Mualem,,
78	
79	
80	
81	-Solute/Fluid Interaction Card
82	# -----
83	1,
84	Sludge,Conventional,0.0,m^2/d,Continuous,1.0e+12,d,
85	0,
86	
87	
88	
89	-Solute/Porous Media Interaction Card
90	# -----
91	Sand,100.0,m,0.0,m,
92	Sludge,0,,,
93	
94	
95	
96	-Initial Conditions Card
97	# -----
98	Gas Pressure,Aqueous Pressure,
99	2,
100	Aqueous Pressure,102605.,Pa,-0.09794,1/m,,,,,1,100,1,1,1,1,
101	Solute Aqueous Volumetric,Sludge,1.,1/m^3,,,,,8,13,1,1,1,1,
102	
103	
104	
105	-Boundary Conditions Card
106	# -----
107	2,
108	West,Neumann,Aqueous Conc.,
109	1,1,1,1,1,1,1,
110	0.,hr,0.25,m/d,0.0,1/m^3,

Exhibit 3.1-1. (Contd)

<u>Line</u>	<u>Input File</u>
111	East,Dirichlet,Outflow,
112	100,100,1,1,1,1,1,
113	0.,hr,101425.,Pa,,,
114	
115	
116	
117	-Output Options Card
118	# -----
119	3,
120	13,1,1,
121	34,1,1,
122	35,1,1,
123	10,10,day,m,6,6,6,
124	2,
125	X Aqueous Vol,m/day,
126	Solute Aqueous Conc.,Sludge,1/m^3,
127	1,
128	9600,d,
129	2,
130	X Aqueous Vol,m/day,
131	Solute Aqueous Conc.,Sludge,1/m^3,

Exhibit 3.1-2. STOMP Parameters File for 1D Transport in Uniform Steady Flow Problem

<u>Line</u>	<u>Parameters File</u>
1	C-----C
2	C STOMP Parameter File
3	C-----C
4	C
5	C--- Number of lines of simulation notes
6	C Number of execution periods ---
7	C
8	PARAMETER(LNOTES=10, LEPD=10)
9	C
10	C--- Number of nodes in the x or r coordinate direction
11	C Number of nodes in the y or theta coordinate direction
12	C Number of nodes in the z coordinate direction
13	C Number of active nodes
14	C Number of active dimensions
15	C Minimum of (LFX*LFY, LFX*LPZ, LFY*LPZ) ---
16	C
17	PARAMETER(LFX=100, LFY=1, LPZ=1)
18	PARAMETER(LAN=100, LAD=1, LMNP=1)
19	C
20	C--- Energy equation switch (0 = off, 1 = on)
21	C Water mass equation switch (0 = off, 1 = on)
22	C Air mass equation switch (0 = off, 1 = on)
23	C VOC mass equation switch (0 = off, 1 = on)
24	C Solute transport equation switch (0 = off, 1 = on)
25	C Freezing conditions switch (0 = off, 1 = on) ---
26	C Dissolved salt transport equation switch (0 = off, 1 = on) ---
27	C Dissolved oil transport equation switch (0 = off, 1 = on) ---
28	C
29	PARAMETER(LT=0, LL=1, LG=0, LN=0, LC=1, LFC=0, LS=0, LD=0)
30	C
31	C--- Banded matrix linear equation solver switch (0 = off, 1 = on)
32	C Conjugate gradient linear equation solver switch (0 = off, 1 = on) ---
33	C
34	PARAMETER(LBD=1, LCG=0)
35	C
36	C--- Number of boundary condition surfaces
37	C Number of boundary condition times ---
38	C
39	PARAMETER(LBC=2, LBTM=1)
40	C
41	C--- Number of sources
42	C Number of source times ---
43	C
44	PARAMETER(LSR=1, LSTM=1)
45	C
46	C--- Number of rock/soil types
47	C Number of solutes
48	C
49	PARAMETER(LRC=1, LSOLU=1)
50	C
51	C--- Number of reference nodes
52	C Number of print times
53	C Number of integration surfaces ---
54	C
55	PARAMETER(LREF=10, LPTM=10, LSF=1)

Exhibit 3.1-2. (Contd)

<u>Line</u>	<u>Parameters File</u>
56	C
57	C--- Number saturation and relative permeability table entries.
58	C Number of hysteretic scanning paths
59	C Number of chemical reactions.
60	C
61	PARAMETER(LTBL=1, LPATH=3, LCHEM=1)
62	C--- Computed Parameters ---
63	C
64	PARAMETER(LUK=LT+LL+LG+LN+LS+LD, LPH=LL+LG+LN, LCMP=LL+LS+LD)
65	PARAMETER(LFXY=LFX*LFY, LPYZ=LFY*LPZ, LFZX=LPZ*LPX)
66	PARAMETER(LFD=LPX*LPY*LPZ)
67	PARAMETER(LNE=(LUK*LUK*(7*LFD-2*LFXY-2*LPYZ-2*LPZX)**LUM)
68	PARAMETER(LHBW=LUK*LMNP+LUK-1)
69	PARAMETER(LJA=LBD + LCG*LAN*LUK + LUM*LAN*LUK)
70	PARAMETER(LJB=(2*LAN*LUK)**LUM, LJC=LAN**LUM)
71	PARAMETER(LJD=LBD*(3*LHBW+1) + LCG*LAN*LUK + LUM*6*LNE)
72	PARAMETER(LJE=LBD*LAN*LUK + LCG*((2*LAD+1)*LUK+2*LAD) + LUM)
73	PARAMETER(LJF=LAN*LUK)
74	PARAMETER(LJG=LBD*(3*LHBW+1) + LCG*LAN*LUK + LUM)
75	PARAMETER(LJH=LBD*LAN*LUK + LCG*(2*LAD+1) + LUM)
76	PARAMETER(LJJ=LBD*LAN*LUK + LCG + LUM)
77	PARAMETER(LSV=LUK+2, LSFV=2*LUK+1)
78	PARAMETER(LSX=(LPX+1)*LPY*LPZ)
79	PARAMETER(LSY=LPX*(LPY+1)*LPZ)
80	PARAMETER(LSZ=LPX*LPY*(LPZ+1))
81	PARAMETER(LFDT=LFD**LT, LFDL=LFD**LL, LFDG=LFD**LG, LFDN=LFD**LN)
82	PARAMETER(LFDC=LFD**LC, LFDI=LFD**LFC, LFDS=LFD**LS, LFDD=LFD**LD)
83	PARAMETER(LSXT=LSX**LT, LSXL=LSX**LL, LSXG=LSX**LG, LSXN=LSX**LN)
84	PARAMETER(LSXC=LSX**LC, LSXS=LSX**LS, LSXD=LSX**LD)
85	PARAMETER(LSYT=LSY**LT, LSYL=LSY**LL, LSYG=LSY**LG, LSYN=LSY**LN)
86	PARAMETER(LSYC=LSY**LC, LSYS=LSY**LS, LSYD=LSY**LD)
87	PARAMETER(LSZT=LSZ**LT, LSZL=LSZ**LL, LSZG=LSZ**LG, LSZN=LSZ**LN)
88	PARAMETER(LSZC=LSZ**LC, LSZS=LSZ**LS, LSZD=LSZ**LD)
89	PARAMETER(LRCT=LRC**LT, LRCL=LRC**LL, LRCG=LRC**LG, LRCN=LRC**LN)
90	PARAMETER(LRCC=LRC**LC, LRCL=LRC**LFC, LRCS=LRC**LS, LRCD=LRC**LD)
91	PARAMETER(LBCT=LBC**LT, LBCL=LBC**LL, LBCG=LBC**LG, LBCN=LBC**LN)
92	PARAMETER(LBCC=LBC**LC, LBCL=LBC**LFC, LBCL=LBC**LS, LBCL=LBC**LD)
93	PARAMETER(LBCU=LUK+LPH+LT+2, LBCV=LBCU+LSOLU)
94	PARAMETER(LOUPV=200+11*(LSOLU))
95	PARAMETER(LJI=LBD*LAN*LUK + LCG + (3*LNE+23*LFD*LUK+9)*LUM)
96	PARAMETER(LSCHR=18)
97	

3.2 The Patch Source

The patch source problem was used by Daus and Frind (1985) as a test problem for a finite element Galerkin transport code, while an analytical solution was given by Cleary and Unga (1978). In this problem a fixed concentration boundary condition is used as source in a steady, uniform two-dimensional flow field. Results from STOMP simulations are compared to Cleary and Unga's analytical solution.

Problem Features: 3.2

- Water operational mode
- transport in uniform-steady flow field
- two dimensional (xy)
- uniform Cartesian grid
- saturated flow
- confined aquifer
- heterogeneous and isotropic
- Dirichlet solute boundaries
- outflow solute boundaries

3.2.1 Problem Description and Parameters

The patch source problem exemplifies transport undergoing longitudinal and transverse dispersion within a uniform steady flow field in an plan view aquifer. The governing equation for advective-dispersive transport introduced in Section 3.1 is applicable to this problem as well.

The problem domain is rectangular, with the x -axis oriented parallel to the direction of flow, and has dimensions of 200 by 40 arbitrary length units. A solute line-source is located on the upstream boundary (at $x = 0$) from $y = 0$ to $y = 6$. Figure 3.2-1 shows a schematic of the problem domain. Outflow boundary conditions exist everywhere else around the domain. The initial tracer concentration in the domain is zero. Stated mathematically these conditions are:

$$C(x,y,0) = 0$$

$$C(0,y,t) = 1 \quad \text{for} \quad 0 \leq y \leq 6 \quad \text{and} \quad t > 0$$

$$\frac{\partial C}{\partial y} = 0 \quad \text{for} \quad 0 \leq x \leq 200 \quad \text{at} \quad y = 0, 40$$

$$\frac{\partial C}{\partial x} = 0 \quad \text{for} \quad 6 \leq y \leq 40, \quad \text{at} \quad x = 0$$

$$\frac{\partial C}{\partial x} = 0 \quad \text{for} \quad 0 \leq y \leq 40, \quad \text{at} \quad x = 200.$$

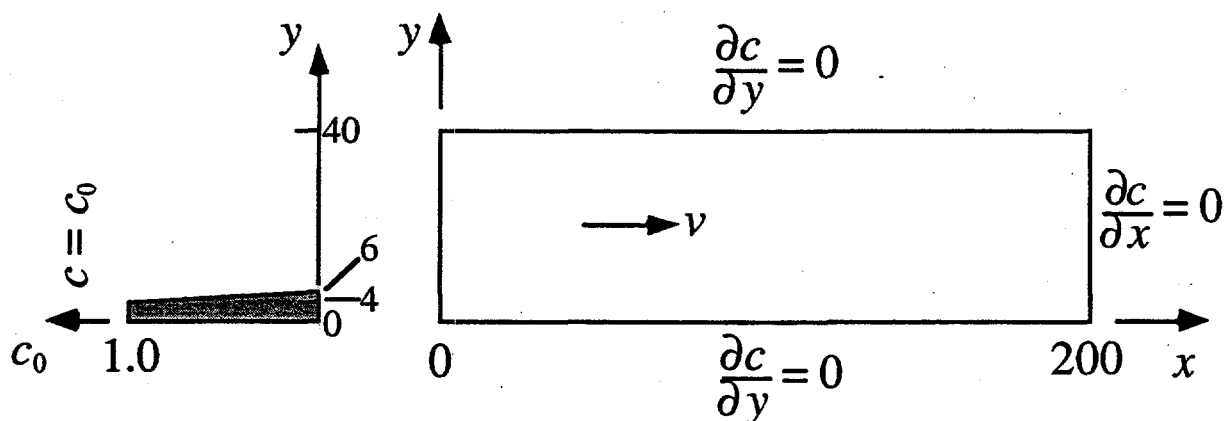


Figure 3.2-1. Daus and Frind's Representation of the Patch-Source Problem with Dirichlet Boundary Conditions (Adapted from Daus and Frind (1985))

3.2.2 Simulation

The simulated domain is overlain with a uniform square grid, with grid spacing of 2 length units (meters). The resulting grid has 100 blocks in the x -direction and 20 blocks in the y -direction for a total of 2000 blocks.

The hydraulic parameters and flow boundary conditions were chosen to yield a uniform seepage velocity of 0.1 (m/day) in a fully saturated and confined aquifer (see Exhibit 3.2-1). Generic values for the saturation-pressure relationship and solute fluid interaction parameters were used. Dispersivity values were chosen so that the resulting longitudinal and transverse dispersion coefficients each had values of 0.1 (m^2/day). A Dirichlet transport boundary condition was applied to the y -axis to simulate the required line source. A Cauchy boundary condition was not used because the available analytical solution was derived for a Dirichlet boundary condition.

The simulation was run using STOMP's TVD transport option (refer to Section 3.1) for 800 time units (days) with time steps of 4 units. The resulting Courant and Peclet numbers were $Cu = 0.02$ and $Pe = 2$. Output was requested for the following times: 160, 480, and 800 days. A copy of the STOMP input file for this problem is presented in Exhibit 3.2-1 and a copy of the STOMP parameters file used to build the needed STOMP executable code for this problem is shown in Exhibit 3.2-2.

3.2.3 Analysis

A plot showing a comparison of STOMP's predictions and the analytical solution of Cleary and Ungs is shown in Figure 3.2-2. The plot presents longitudinal concentration profiles at $y = 1$ along the x -direction (i.e. directly downstream from the source) for three different times. For all three times, STOMP's TVD transport predictions show a good match with the analytical solution, especially at the leading edge of the plume.

Concentration profiles in the transverse direction are presented in Figure 3.2-3 for $x = 41$. Comparison of STOMP's predictions and the analytical solution for show adequate agreement. Overall, transverse profiles exhibit slightly steeper fronts.

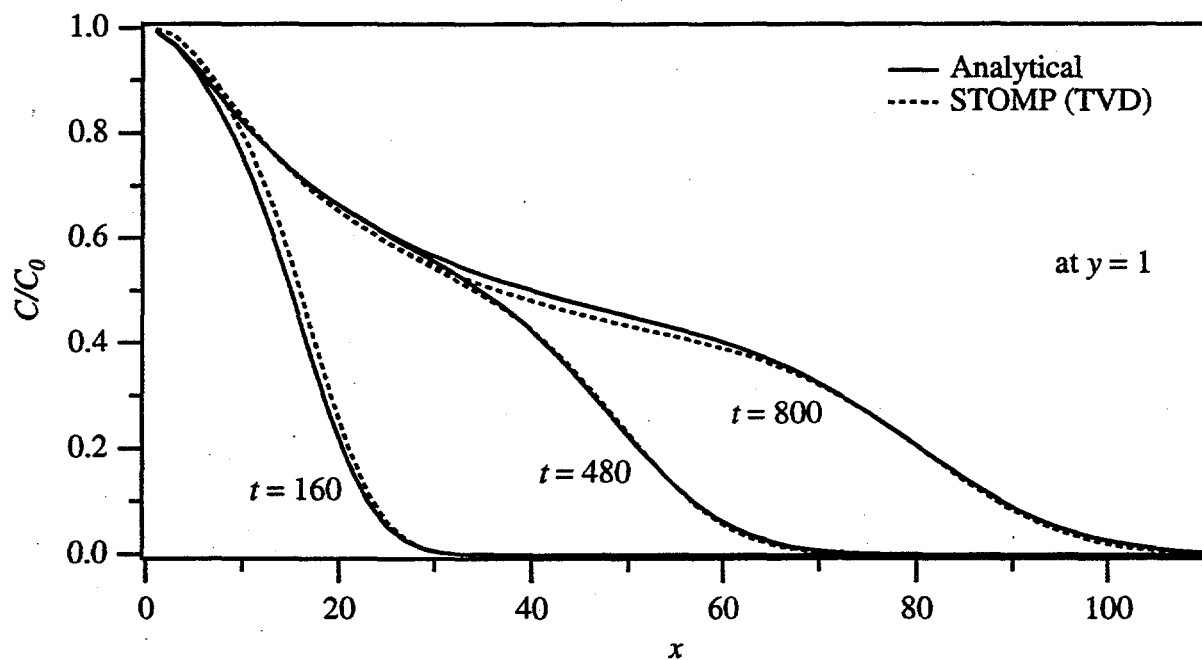


Figure 3.2-2. Longitudinal Concentration Profiles at $y = 1$ Along the x -Direction for the Patch Source Problem

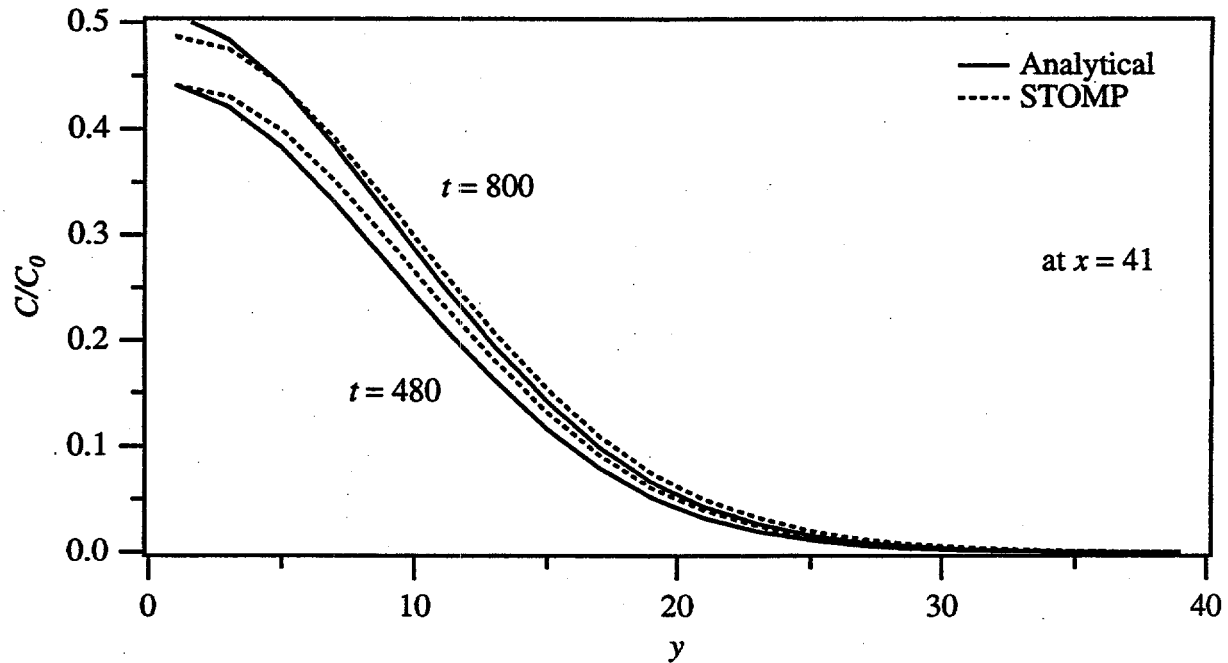


Figure 3.2-3. Transverse Concentration Profiles at $x = 41$ Along the y -Direction for the Patch Source Problem

3.2.4 Summary

Two-dimensional transport in a steady uniform flow field was simulated using STOMP's TVD option. The results were compared to an analytical solution for different times. Profiles of concentration along the longitudinal and transverse flow directions were presented. The comparison showed a very good agreement between STOMP predictions and analytical results. A slight "flattening" of the plume was observed in the transverse direction, while preserving the steep front. Mass balance was preserved.

Exhibit 3.2-1. STOMP Input File for Patch Source Problem

<u>Line</u>	<u>Input File</u>
1	#####
2	# STOMP APPLICATION GUIDE --- Case 3.2 #
3	# #
4	# THE PATCH SOURCE (Segol 1994, p.86-94) #
5	# #
6	# Showcased features: 2D Transport #
7	# #
8	# Domain: Rectangular domain with uniform grid spacing #
9	# #
10	#####
11	
12	
13	~Simulation Title Card
14	1,
15	THE PATCH SOURCE (Segol 1994, p.86-94)
16	NJ Aimo,
17	Pacific Northwest Laboratory,
18	June 1995,
19	4:00:00 PM PST;
20	4,
21	Case 3.2 --- STOMP Applications Guide
22	Domain: Two-dimensional rectangular confined aquifer, 200 by 40 units.
23	Solute source on left boundary, y=1 to 6, uniform x-velocity,
24	zero y-velocity.
25	
26	
27	~Solution Control Card
28	Normal,
29	Water w/TVD Transport,
30	1, Number of Simulation periods
31	0.,day,800.,day,4.,day,4.,day,1.,24,1.E-6,
32	1,day,1,day,100000, Max. machine times
33	0, Variables to average
34	
35	
36	~Grid Card
37	Uniform Cartesian,
38	100,20,1,
39	2.0,m,
40	2.0,m,
41	2.0,m,
42	
43	
44	~Rock/Soil Zonation Card
45	1,
46	AQFR1,1,100,1,20,1,1,
47	
48	
49	~Mechanical Properties Card
50	AQFR1,2.65E+06,g/m^3,0.30,0.30,1.E-05,1/m, Millington and Quirk,
51	
52	
53	~Hydraulic Properties Card
54	AQFR1,6.0003,hc m/day,0.,hc m/day,,,
55	

Exhibit 3.2-1. (Contd)

<u>Line</u>	<u>Input File</u>
56	
57	
58	-Saturation Function Card
59	AQFR1,Nonhysteretic van Genuchten,.133,1/cm,1.88,0.268,,
60	
61	
62	-Aqueous Relative Permeability Card
63	AQFR1,Mualem,,
64	
65	
66	-Solute/Fluid Interaction Card
67	1,
68	SOL1,Conventional Tortuosity Model,1.E-09,m^2/s,Continuous,1.E+20,yr,
69	0,
70	
71	
72	-Solute/Porous Media Interaction Card
73	AQFR1,1.,m,1.,m,
74	SOL1,0.,m^3/g,
75	
76	
77	-Initial Conditions Card
78	Gas Pressure, Aqueous Pressure,
79	1,
80	Aqueous Pressure,6.0979352E+05,Pa,-48.9676,1/m,,,,,1,100,1,20,1,1,
81	
82	
83	-Boundary Conditions Card
84	3,
85	West,Dirichlet Aqueous,Aqueous Conc.,
86	1,1,1,3,1,1,1,
87	0.0,day,6.0979352E+05,Pa,1.0,1/m^3,
88	West,Dirichlet Aqueous,,
89	1,1,4,20,1,1,1,
90	0.0,day,6.0979352E+05,Pa,,,
91	East,Dirichlet Aqueous,Outflow Solute,
92	100,100,1,20,1,1,1,
93	0.0,day,6.E+05,Pa,,,
94	
95	
96	-Output Control Card
97	3,
98	2,1,1,
99	50,1,1,
100	50,10,1,
101	1,1,day,m,4,8,8,
102	4,
103	Aqueous Saturation,,
104	Aqueous Pressure,Pa,
105	X Aqueous Volumetric Flux,m/day,
106	Solute Aqueous Conc.,SOL1,1/m^3,
107	3,
108	160.,day,
109	480.,day,
110	800.,day,

Exhibit 3.2-1. (Contd)

<u>Line</u>	<u>Input File</u>
111	1,
112	Solute Aqueous Conc., SOL1, 1/m ³ ,
113	

Exhibit 3.2-2. STOMP Parameters File for Patch Source Problem

<u>Line</u>	<u>Parameters File</u>
1	C-----C
2	C STOMP Parameter File
3	C-----C
4	C
5	C--- Number of lines of simulation notes
6	C Number of execution periods ---
7	C
8	PARAMETER(LNOTES=5, LEPD=1)
9	C
10	C--- Number of nodes in the x or r coordinate direction
11	C Number of nodes in the y or theta coordinate direction
12	C Number of nodes in the z coordinate direction
13	C Number of active nodes
14	C Number of active dimensions
15	C Minimum of (LFX*LFY, LFX*LFZ, LFY*LFZ) ---
16	C
17	PARAMETER(LFX=100, LFY=20, LFZ=1)
18	
19	PARAMETER(LAN=2000, LAD=2, LMNP=20)
20	C
21	C--- Energy equation switch (0 = off, 1 = on)
22	C Water mass equation switch (0 = off, 1 = on)
23	C Air mass equation switch (0 = off, 1 = on)
24	C VOC mass equation switch (0 = off, 1 = on)
25	C Solute transport equation switch (0 = off, 1 = on)
26	C Freezing conditions switch (0 = off, 1 = on) ---
27	C Dissolved salt transport equation switch (0 = off, 1 = on) ---
28	C Dissolved oil transport equation switch (0 = off, 1 = on) ---
29	C
30	PARAMETER(LT=0, LL=1, LG=0, LN=0, LC=1, LFC=0, LS=0, LD=0)
31	C
32	C--- Banded matrix linear equation solver switch (0 = off, 1 = on)
33	C Conjugate gradient linear equation solver switch (0 = off, 1 = on) ---
34	C Unsymmetric-pattern multifrontal package switch (0 = off, 1 = on) ---
35	C
36	PARAMETER(LBD=1, LCG=0, LUM=0)
37	C
38	C--- Number of boundary condition surfaces
39	C Number of boundary condition times ---
40	C
41	PARAMETER(LBC=80, LBTM=1)
42	C
43	C--- Number of sources
44	C Number of source times ---
45	C
46	PARAMETER(LSR=1, LSTM=1)
47	C
48	C--- Number of rock/soil types
49	C Number of solutes
50	C
51	PARAMETER(LRC=1, LSOLU=1)
52	C
53	C--- Number of reference nodes
54	C Number of print times
55	C Number of integration surfaces ---

Exhibit 3.2-2. (Contd)

<u>Line</u>	<u>Parameters File</u>
56	C
57	PARAMETER(LREF=5, LPTM=3, LSF=1)
58	C
59	C--- Number saturation and relative permeability table entries
60	C Number of hysteretic scanning paths
61	C Number of chemical reactions
62	C
63	PARAMETER(LTBL=10, LPATH=3, LCHEM=1)
64	C
65	C--- Computed Parameters ---
66	C
67	PARAMETER(LUK=LT+LL+LG+LN+LS+LD, LPH=LL+LG+LN, LCMP=2)
68	PARAMETER(LFXY=LFX*LFY, LFYZ=LFY*LFZ, LFZX=LFZ*LFX)
69	PARAMETER(LFD=LFX*LFY*LFZ)
70	PARAMETER(LNE=(LUK*LUK*(7*LFD-2*LFXY-2*LFYZ-2*LFZX))*LUM)
71	PARAMETER(LHBW=LUK*LMNP+LUK-1)
72	PARAMETER(LJA=LBD + LCG*LAN*LUK + LUM*LAN*LUK)
73	PARAMETER(LJB=(2*LAN*LUK)**LUM, LJC=LAN**LUM)
74	PARAMETER(LJD=LBD*(3*LHBW+1) + LCG*LAN*LUK + LUM*6*LNE)
75	PARAMETER(LJE=LBD*LAN*LUK + LCG*((2*LAD+1)*LUK+2*LAD) + LUM)
76	PARAMETER(LJF=LAN*LUK)
77	PARAMETER(LJG=LBD*(3*LHBW+1) + LCG*LAN*LUK + LUM)
78	PARAMETER(LJH=LBD*LAN*LUK + LCG*(2*LAD+1) + LUM)
79	PARAMETER(LJJ=LBD*LAN*LUK + LCG + LUM)
80	PARAMETER(LSV=LUK+2, LSFV=2*LUK+1)
81	PARAMETER(LSX=(LFX+1)*LFY*LFZ)
82	PARAMETER(LSY=LFX*(LFY+1)*LFZ)
83	PARAMETER(LSZ=LFX*LFY*(LFZ+1))
84	PARAMETER(LFDT=LFD**LT, LFDL=LFD**LL, LFDG=LFD**LG, LFDN=LFD**LN)
85	PARAMETER(LFDC=LFD**LC, LFDI=LFD**LFC, LFDS=LFD**LS, LFDD=LFD**LD)
86	PARAMETER(LSXT=LSX**LT, LSXL=LSX**LL, LSXG=LSX**LG, LSXN=LSX**LN)
87	PARAMETER(LSXC=LSX**LC, LSXS=LSX**LS, LSXD=LSX**LD)
88	PARAMETER(LSYT=LSY**LT, LSYL=LSY**LL, LSYG=LSY**LG, LSYN=LSY**LN)
89	PARAMETER(LSYC=LSY**LC, LSYS=LSY**LS, LSYD=LSY**LD)
90	PARAMETER(LSZT=LSZ**LT, LSZL=LSZ**LL, LSZG=LSZ**LG, LSZN=LSZ**LN)
91	PARAMETER(LSZC=LSZ**LC, LSZS=LSZ**LS, LSZD=LSZ**LD)
92	PARAMETER(LRCT=LRC**LT, LRCL=LRC**LL, LRCC=LRC**LG, LRCN=LRC**LN)
93	PARAMETER(LRCC=LRC**LC, LRCL=LRC**LFC, LRCS=LRC**LS, LRCD=LRC**LD)
94	PARAMETER(LBCT=LBC**LT, LBCL=LBC**LL, LBCG=LBC**LG, LBCN=LBC**LN)
95	PARAMETER(LBCC=LBC**LC, LBCI=LBC**LFC, LBCC=LBC**LS, LBCC=LBC**LD)
96	PARAMETER(LBCU=LUK+LPH+LT+2, LBCV=LBCU+LSOLU)
97	PARAMETER(LOUPV=200+11*(LSOLU))
98	PARAMETER(LJI=LBD*LAN*LUK + LCG + (3*LNE+23*LFD*LUK+9)*LUM)
99	PARAMETER(LSCHR=18)
100	

3.3 References

Baptista A, P Gresho, and E Adams. "Reference Problems for the Convection-Diffusion Forum," 1988. *VII International Conference on Computational Methods in Water Resources*, Cambridge, Massachusetts.

Cleary RW, and MJ Unga. 1978. *Groundwater Pollution and Hydrology*. Report 78-WR-15, Department of Civil Engineering, Princeton University, Princeton, New Jersey.

Daus AD, and EO Frind. 1985. "An alternating direction Galerkin technique for simulation of contaminant transport in complex groundwater systems." *Water Resources Research*, 21(5), 653-664.

Mualem Y. 1976. "A new model for predicting the hydraulic conductivity of unsaturated porous media." *Water Resources Research*, 12(3), 513-522.

van Genuchten MT, and WJ Alves. 1982. *Analytical Solutions of the One-Dimensional Convective-Dispersive Solute Transport Equation*. ARS Technical Bulletin 1661, USDA.

4.0 Salt-Water Intrusion and Density-Driven Flow

Salt-water intrusion is the classic problem for a density-dependent ground-water hydrology case. In this section two classic problems are tackled: Henry's Problem, which describes the advance of a diffused salt-water wedge in a confined aquifer initially filled with fresh water, and Elder's Problem, which is an example of complex natural convection suggested by Voss and Souza (1987) as an exercise to test the accuracy of models in representing fluid flow driven purely by density differences.

4.1 Henry's Problem (Salt Water Intrusion)

Henry's problem addresses the steady-state solution of a diffused salt-water wedge within a confined aquifer balanced against a flowing fresh-water field.

Fresh water enters the confined aquifer at a constant rate from a hypothetical inland boundary and discharges into a hypothetical coastal boundary. Salt water from the costal boundary advances and mixes against the discharging fresh water. Because both the inland and costal boundary conditions are invariant a steady-state condition is reached, which balances the intruding sea-water wedge against the fresh-water flow field. Henry (1964a; 1964b) published an analytical solution to this problem in a U.S. Geological Survey publication, and the problem has henceforth become a classical test for numerical simulators with solute dependent density capabilities. Unfortunately, no other numerical method has been able to successful in duplicating Henry's solution, which accordingly resulted in some doubt about its validity. Ségol (1994) revisited Henry's solution and noted several discrepancies in the published solution. Ségol's revisited solution to this classical problem shows close agreement with the numerical solution of Voss and Souza (1987). Comparisons for this application problem will be made against the revisited solution of Ségol (1994).

Problem Features: 4.1

- Water-Salt operational mode
- two dimensional
- saturated flow
- confined aquifer
- heterogeneous and anisotropic
- uniform cartesian grid
- variable density and viscosity

4.1.1 Problem Description and Parameters

Henry's problem involves a two-dimensional rectangular domain with no flow conditions along the top and bottom boundaries to simulate a confined aquifer of infinitesimal width, as shown in Figure 4.1-1. This problem description follows that developed by Voss and Souza

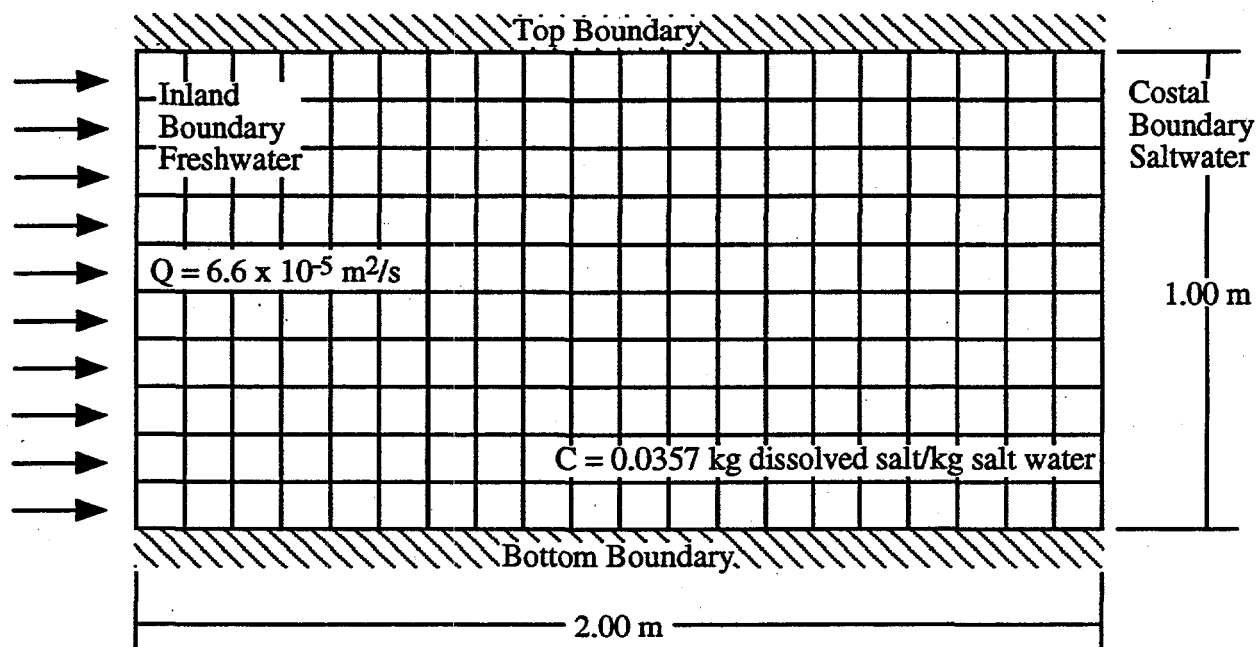


Figure 4.1-1. Henry's Problem and Computational Grid

(1987) from Henry's original formulation. The rectangular domain has dimensions of 2 m in the horizontal direction and 1 m in the vertical direction, which is aligned with the gravitational vector. The computational grid comprises 200 square nodes of uniform size. A constant fresh-water flux (Neumann condition) is imposed on the inland (west) boundary; whereas, a hydrostatic pressure boundary (hydraulic gradient condition) of salt water is imposed on the costal (east) boundary. Parameters used in this simulation are given in Table 4.1-1 and are consistent with the nondimensional parameters chosen by Henry (1964a; 1964b). Initially the aquifer was filled with freshwater under hydrostatic conditions. The pressure boundary conditions on the costal boundary were hydrostatic conditions for sea water. The STOMP input and parameters files for this application problem are shown in Exhibit 4.1-1 and Exhibit 4.1-2, respectively.

4.1.2 Simulation

Henry's problem was solved with the STOMP simulator by executing from fresh-water hydrostatic conditions in the aquifer until steady-state conditions were reached. A total simulation time period of 1000 yr was chosen to assure steady-state conditions had been reached. The time step acceleration factor of 1.25 allows the user to over specify the time required to reach steady-state conditions without excessive execution time costs. As the simulation approaches steady-state

Table 4.1-1. Parameters for Henry's Problem

Parameter Description	Value
Intrinsic Permeability	$1.020408 \times 10^{-9} \text{ m}^2$
Salt-Water Density	$\rho_\ell^s = \rho_\ell^w + 0.6829 C_\ell^s$
Salt-Water Viscosity	$1.0176 \times 10^{-3} \text{ Pa s}$
Sea-Water Concentration	0.0357 kg dissolved salt / kg sea water
Porosity	0.35
Dispersivity α_L, α_T	0.0 m
Salt Diffusion Coefficient	$18.8571 \times 10^{-6} \text{ m}^2/\text{s}$
Fresh-Water Inflow	$6.6 \times 10^{-5} \text{ m/s}$
Grid Spacing	0.1 m

conditions the number of Newton-Raphson iterations will diminish to one and all of the output variables will become invariant with time. Steady-state conditions for this problem were achieved roughly after 1 day of simulation time. The relatively small initial time step of 1 s was chosen to prevent convergence failures during the first time step. No convergence failures were noted during the entire simulation.

Two modifications were made to the source coding of the STOMP simulator to execute this application. Both modifications involved the computation of salt-water properties. Salt-water density in the STOMP simulator is normally computed using the function of Leijnse (1992), according to Equation 4.1-1. For this application this function was replaced with the one specified by Henry, as shown in Equation 4.1-2. The variation in salt-water viscosity was ignored in Henry's problem, therefore the expression for salt-water viscosity was modified from the function of Leijnse (1992), according to Equation 4.1-3 to that shown in Equation 4.1-4.

$$\rho_\ell^s = \rho_\ell^w \exp(0.7 \omega_\ell^s)$$

Equation 4.1-1

$$\rho_\ell^s = \rho_\ell^w + 0.6829 C_\ell^s$$

Equation 4.1-2

$$\mu_{\ell}^s = \mu_{\ell}^w \left[1.0 + 1.85 \omega_{\ell}^s + 4.1 (\omega_{\ell}^s)^2 + 44.5 (\omega_{\ell}^s)^3 \right]$$

Equation 4.1-3

$$\mu_{\ell}^s = \mu_{\ell}^w$$

Equation 4.1-4

4.1.3 Analysis

STOMP simulation results for the steady-state solution to Henry's problem in terms of isochlor contours is shown in Figure 4.1-2 as solid lines. For comparison, results from Ségol's analytical solution of Henry's problem are shown in Figure 4.1-2 as dashed lines. The STOMP numerical and analytical solution of Ségol appear to be in close agreement. Ségol has noted that the analytical solution is inaccurate in the high and low concentration regions, with small but non-negligible over- and undershoots. Both Henry and Ségol comment on these inaccuracies and attribute them to truncations of the Fourier series used to approximate the analytical solution. For comparison purposes, STOMP simulation results for Henry's problem using Leijnse's salt-water density and viscosity functions (the standard STOMP functions for brines) is shown in Figure 4.1-3 as solid lines, against the analytical solution of Ségol, shown as dashed lines. This numerical solution also appears to be close agreement with the analytical solution.

4.1.4 Summary

This application was chosen to demonstrate the coupled flow and transport capabilities of the STOMP simulator. Although these capabilities have been specifically written for salt-water brines other solutes could be considered by changing the algorithms for computing the brine properties (e.g., density and viscosity). The core capabilities of the STOMP simulator only address coupled flow and transport for solutes which are soluble in the aqueous phase (i.e., gas-phase solubility is neglected and coupled flow and transport is not available for the operational modes involving NAPL. Solution of Henry's problem has been rather elusive until the recent work of Ségol (1994), which provides an excellent review of previous numerical solutions and a complete discussion and analysis of Henry's analytical solution.

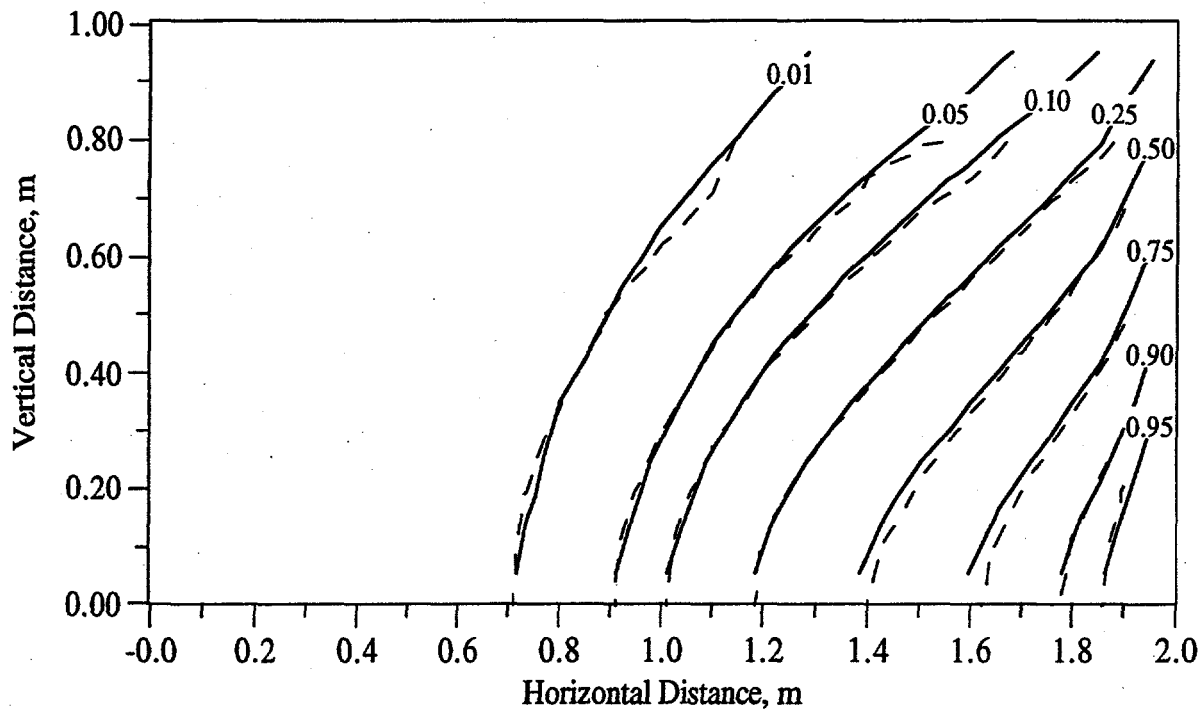


Figure 4.1-2. Steady-State Concentration Distribution from the STOMP Solution (Solid Lines) with Henry's Salt-Water Density and Viscosity Functions and from the Ségol Analytical Solution (Dashed Lines)

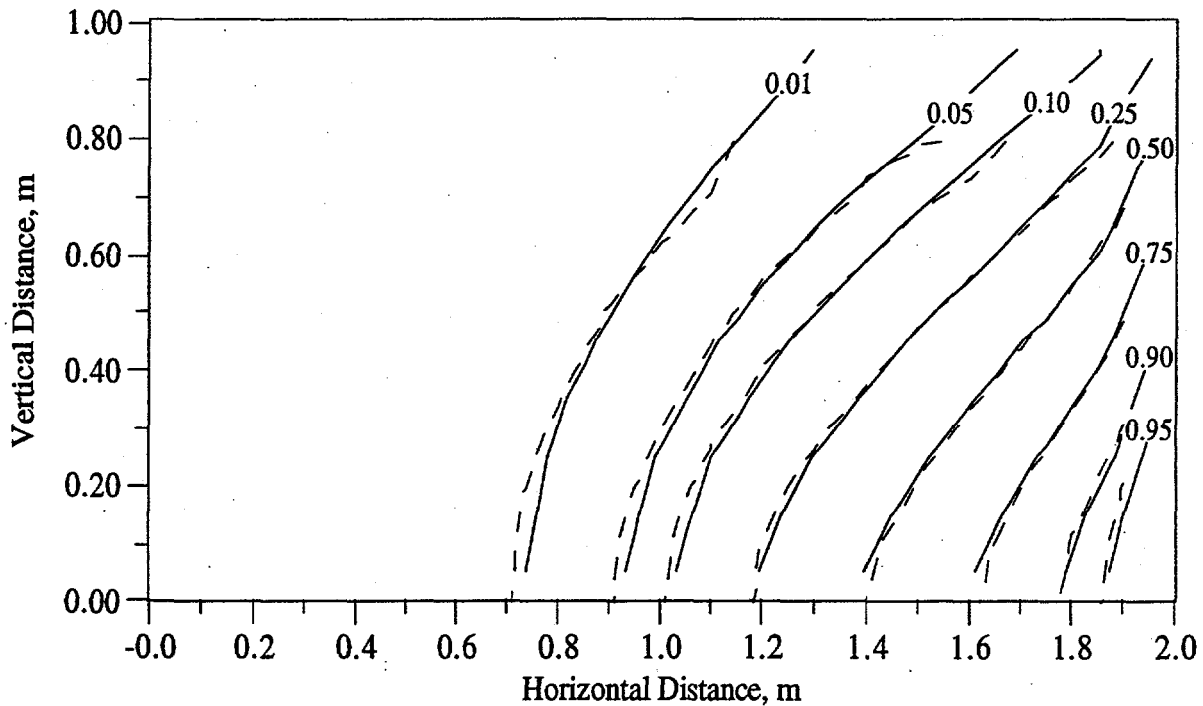


Figure 4.1-3. Steady-State Concentration Distribution from the STOMP Solution (Solid Lines) with Leijnse's Salt-Water Density and Viscosity Functions and from the Ségol Analytical Solution (Dashed Lines)

Exhibit 4.1-1. STOMP Input File for Henry's Problem

<u>Line</u>	<u>Input File</u>
1	-Simulation Title Card
2	1,
3	Henry's Problem for Salt Water Intrusion,
4	MD White,
5	Pacific Northwest Laboratory,
6	August 9 1995,
7	8:30:00 AM PDT,
8	1,
9	STOMP Application Guide Problem 4.1
10	
11	-Solution Control Card
12	Normal,
13	Water-Salt,
14	1,
15	0.0,yr,1.e+3,yr,1,s,1.e+3,yr,1.25,8,1.e-6,
16	1,hr,1,hr,1000,
17	0,
18	
19	-Grid Card
20	Uniform Cartesian,
21	20,1,10,
22	10,cm,
23	10,cm,
24	10,cm,
25	
26	-Rock/Soil Zonation Card
27	1,
28	Geologic Media,1,20,1,1,1,10,
29	
30	-Mechanical Properties Card
31	Geologic Media,,,0.35,0.35,,,Constant Diffusion,1.0,
32	
33	-Hydraulic Properties Card
34	Geologic Media,1.020408e-9,m^2,,,1.020408e-9,m^2,
35	
36	-Saturation Function Card
37	Geologic Media,Nonhysteretic van Genuchten,0.2,1/cm,1.8,0.0,,
38	
39	-Aqueous Relative Permeability Card
40	Geologic Media,Mualem,,
41	
42	-Salt Transport Card
43	Constant Diffusion,18.86e-6,m^2/s,
44	Geologic Media,0.0,m,0.0,m,
45	
46	-Initial Conditions Card
47	Gas Pressure, Aqueous Pressure,
48	1,
49	Aqueous Pressure,121325.,Pa,,,,,-9793.5331,1/m,1,20,1,1,1,10,
50	
51	-Boundary Conditions Card
52	2,
53	West,Neumann,Aqueous Conc.,
54	1,1,1,1,1,10,1,
55	0,yr,6.6e-5,m/s,0.0,kg/m^3,

Exhibit 4.1-1. (Contd)

<u>Line</u>	<u>Input File</u>
56	East,Hydraulic Gradient,Aqueous Conc.,
57	20,20,1,1,1,10,1,
58	0,yr,121557.98,Pa,36.5921,kg/m ³ ,
59	
60	-Output Control Card
61	4,
62	20,1,1,
63	20,1,3,
64	20,1,6,
65	20,1,10,
66	1,1,yr,m,,,,
67	4,
68	Salt Aqueous Concentration,kg/m ³ ,
69	Aqueous Pressure,Pa,
70	Aqueous Saturation,,
71	X Aqueous Volumetric Flux,m/s,
72	0,
73	4,
74	Salt Aqueous Concentration,kg/m ³ ,
75	Aqueous Density,kg/m ³ ,
76	Aqueous Pressure,Pa,
77	Aqueous Saturation,,
78	

Exhibit 4.1-2. STOMP Parameters File for Henry's Problem

<u>Line</u>	<u>Parameters File</u>
1	C-----C
2	C STOMP Parameter File
3	C-----C
4	C
5	C--- Number of lines of simulation notes
6	C Number of execution periods ---
7	C
8	PARAMETER(LNOTES=1, LEPD=1)
9	C
10	C--- Number of nodes in the x or r coordinate direction
11	C Number of nodes in the y or theta coordinate direction
12	C Number of nodes in the z coordinate direction
13	C Number of active nodes
14	C Number of active dimensions
15	C Minimum of (LFX*LFY, LFX*LFZ, LFY*LFZ) ---
16	C
17	PARAMETER(LFX=20, LFY=1, LFZ=10)
18	PARAMETER(LAN=200, LAD=2, LMNP=10)
19	C
20	C--- Energy equation switch (0 = off, 1 = on)
21	C Water mass equation switch (0 = off, 1 = on)
22	C Air mass equation switch (0 = off, 1 = on)
23	C VOC mass equation switch (0 = off, 1 = on)
24	C Solute transport equation switch (0 = off, 1 = on)
25	C Freezing conditions switch (0 = off, 1 = on) ---
26	C Dissolved salt transport equation switch (0 = off, 1 = on) ---
27	C Dissolved oil transport equation switch (0 = off, 1 = on) ---
28	C
29	PARAMETER(LT=0, LL=1, LG=0, LN=0, LC=0, LFC=0, LS=1, LD=0)
30	C
31	C--- Banded matrix linear equation solver switch (0 = off, 1 = on)
32	C Conjugate gradient linear equation solver switch (0 = off, 1 = on) ---
33	C Unsymmetric-pattern multifrontal package switch (0 = off, 1 = on) ---
34	C
35	PARAMETER(LBD=1, LCG=0, LUM=0)
36	C
37	C--- Number of boundary condition surfaces
38	C Number of boundary condition times ---
39	C
40	PARAMETER(LBC=20, LBTM=1)
41	C
42	C--- Number of sources
43	C Number of source times ---
44	C
45	PARAMETER(LSR=1, LSTM=1)
46	C
47	C--- Number of rock/soil types
48	C Number of solutes
49	C
50	PARAMETER(LRC=1, LSOLU=1)
51	C
52	C--- Number of reference nodes
53	C Number of print times
54	C Number of integration surfaces ---
55	C

Exhibit 4.1-2. (Contd)

<u>Line</u>	<u>Parameters File</u>
56	PARAMETER(LREF=4, LPTM=1, LSF=1)
57	C
58	C--- Number saturation and relative permeability table entries
59	C Number of hysteretic scanning paths
60	C Number of chemical reactions
61	C
62	PARAMETER(LTBL=1, LPATH=3, LCHEM=1)
63	C
64	C--- Computed Parameters ---
65	C
66	PARAMETER(LUK=LT+LL+LG+LN+LS+LD, LPH=LL+LG+LN, LCMP=LL+LS+LD)
67	PARAMETER(LFX=LFX*LFY, LFY=LFY*LPZ, LPZX=LPZ*LPX)
68	PARAMETER(LFD=LFX*LFY*LPZ)
69	PARAMETER(LNE=(LUK*LUK*(7*LFD-2*LFX-2*LFY-2*LPZ))*LUM)
70	PARAMETER(LHBW=LUK*LMNP+LUK-1)
71	PARAMETER(LJA=LBD + LCG*LAN*LUK + LUM*LAN*LUK)
72	PARAMETER(LJB=(2*LAN*LUK)**LUM, LJC=LAN**LUM)
73	PARAMETER(LJD=LBD*(3*LHBW+1) + LCG*LAN*LUK + LUM*6*LNE)
74	PARAMETER(LJE=LBD*LAN*LUK + LCG*((2*LAD+1)*LUK+2*LAD) + LUM)
75	PARAMETER(LJF=LAN*LUK)
76	PARAMETER(LJG=LBD*(3*LHBW+1) + LCG*LAN*LUK + LUM)
77	PARAMETER(LJH=LBD*LAN*LUK + LCG*(2*LAD+1) + LUM)
78	PARAMETER(LJJ=LBD*LAN*LUK + LCG + LUM)
79	PARAMETER(LSV=LUK+2, LSFV=2*LUK+1)
80	PARAMETER(LSX=(LFX+1)*LFY*LPZ)
81	PARAMETER(LSY=LFX*(LFY+1)*LPZ)
82	PARAMETER(LSZ=LFX*LFY*(LPZ+1))
83	PARAMETER(LFDT=LFD**LT, LFDL=LFD**LL, LFDG=LFD**LG, LFDN=LFD**LN)
84	PARAMETER(LFDC=LFD**LC, LFDI=LFD**LFC, LFDS=LFD**LS, LFDD=LFD**LD)
85	PARAMETER(LSXT=LSX**LT, LSXL=LSX**LL, LSXG=LSX**LG, LSXN=LSX**LN)
86	PARAMETER(LSXC=LSX**LC, LSXS=LSX**LS, LSXD=LSX**LD)
87	PARAMETER(LSYT=LSY**LT, LSYL=LSY**LL, LSYG=LSY**LG, LSYN=LSY**LN)
88	PARAMETER(LSYC=LSY**LC, LSYS=LSY**LS, LSYD=LSY**LD)
89	PARAMETER(LSZT=LSZ**LT, LSZL=LSZ**LL, LSZG=LSZ**LG, LSZN=LSZ**LN)
90	PARAMETER(LSZC=LSZ**LC, LSZS=LSZ**LS, LSZD=LSZ**LD)
91	PARAMETER(LRCT=LRC**LT, LRCL=LRC**LL, LRCG=LRC**LG, LRCN=LRC**LN)
92	PARAMETER(LRCC=LRC**LC, LRCL=LRC**LFC, LRCS=LRC**LS, LRCD=LRC**LD)
93	PARAMETER(LBCT=LBC**LT, LBCL=LBC**LL, LBCL=LBC**LG, LBCN=LBC**LN)
94	PARAMETER(LBCC=LBC**LC, LBCL=LBC**LFC, LBCL=LBC**LS, LBCL=LBC**LD)
95	PARAMETER(LBCU=LUK+LPH+LT+2, LBCV=LBCU+LSOLU)
96	PARAMETER(LOUPV=200+11*(LSOLU))
97	PARAMETER(LJI=LBD*LAN*LUK + LCG + (3*LNE+23*LFD*LUK+9)*LUM)
98	PARAMETER(LSCHR=18)
99	

4.2 Elder's Problem (Density Driven Flow)

The original problem described by Elder (1967) addresses transient thermal convection in porous media. Elder considered a two-dimensional rectangular enclosure filled with porous media. The bottom surface was heated over a segment of its horizontal extent and the remaining walls were held at constant temperature conditions. All surfaces of the enclosure were considered to be impermeable to fluid flow and thermally conducting. Isothermal and hydrostatic initial conditions are assumed. Elder showed generally close agreement between laboratory observations and the numerical solutions. This application problem involves the solution of an analogous problem to Elder's problem, which was first formulated by Voss and Souza (1987) as a verification exercise for numerical simulators to represent bulk fluid flow driven only by density differences. Density-driven advection in Elder's problem occurs thermally; whereas the Voss and Souza formulation involves coupled flow and solute transport, where aqueous phase density is dependent on the solute concentration. Either Elder's original thermally-driven density problem or Voss and Souza solute-driven density problem could have been selected for inclusion in this application guide. The latter was chosen as an additional coupled flow and solute transport problem.

Problem Features: 4.2

- Water-Salt operational mode
- two dimensional (xz)
- saturated flow
- confined aquifer
- heterogeneous and isotropic
- uniform Cartesian grid
- density-driven flow
- salt transport

4.2.1 Problem Description and Parameters

Voss and Souza version of Elder's problem involves a two-dimensional rectangular domain (600 m width, 150 m height) with no flow conditions, as shown in Figure 4.2-1. Boundary surfaces are considered impermeable to fluid flow, but permeable to solute diffusion. Solute enters the initially pure water through diffusion over a portion of the upper boundary surface by imposing saturated solute conditions on this surface. The lower boundary surface is maintained at zero solute concentration. The two vertical walls are considered totally impermeable. Solute which diffuses through the upper boundary increases the density of the aqueous phase, thus beginning the circulation process. The computational domain used for this application followed that of Voss and Souza, consisting of 44 uniform horizontal nodes and 25 uniform vertical nodes for a total of 1100 nodes. Saturated conditions were maintained by fixing the aqueous pressure at the corners of the top boundary to 1bar above atmospheric pressure (i.e., the gas pressure). Parameters used in this simulation are given in Table 4.2-1 and are consistent with the nondimensional parameters

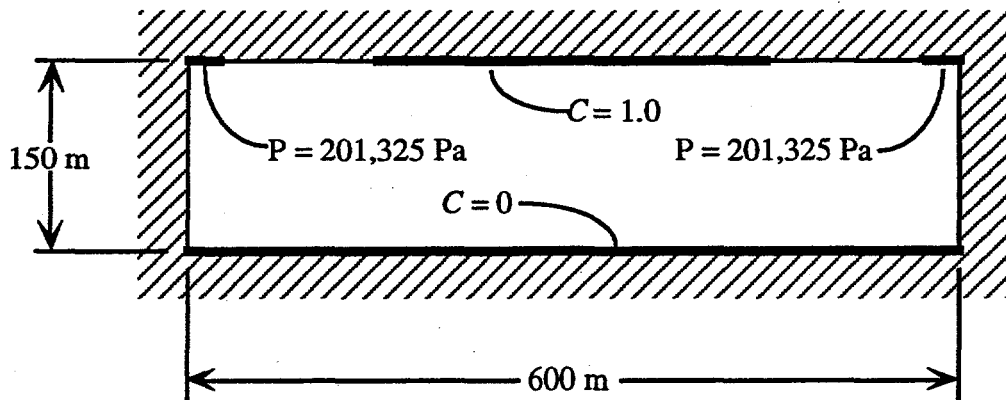


Figure 4.2-1. Schematic Definition for Elder's Problem

chosen by Voss and Souza. The STOMP input and parameters files for this application problem are shown in Exhibit 4.2-1 and Exhibit 4.2-2, respectively.

4.2.2 Simulation

Elder's problem was solved with the STOMP simulator as a transient problem using uniform time steps of 1/12 yr, starting from hydrostatic and zero solute concentration initial conditions. Plot files were generated at selected time periods (1yr, 2yr, 4yr, 10yr, 15yr, and 20-yr). No convergence failures occurred during the simulation, therefore the uniform time stepping was maintained and the time step acceleration factor was not used. Hydrostatic initial conditions were established by specifying an aqueous pressure gradient in the vertical direction on the Initial Conditions Card that matched the boundary pressures specified in the upper corners of the domain. Solute concentrations along the bottom boundary surface were maintained at zero, and those along the center half of the upper surface were maintained at solute saturated conditions (i.e., 0.2605 kg solute/kg solution or 312.6 kg solute/m³ solution at 1200 kg/m³).

Two modifications were made to the source coding of the STOMP simulator to execute this application. Both modifications involved the computation of aqueous phase properties. Aqueous-phase density as a function of solute concentration in the STOMP simulator is normally computed using the function of Leinjse (1992), according to Equation 4.2-1. For this application this function was replaced with the one specified by Voss and Souza, shown in Equation 4.2-2. The variation in aqueous-phase viscosity with solute concentration was ignored in Elder's problem,

Table 4.2-1. Parameters for Elder's Problem

Parameter Description	Value
Intrinsic Permeability	$4.845 \times 10^{-13} \text{ m}^2$
Fresh-Water Density	1000 kg/m^3
Salt-Water Density	$\rho_\ell^S = \rho_\ell^W + 200 \left(\frac{\omega_\ell^S}{0.2605} \right) \text{ kg/m}^3$
Salt-Water Viscosity	$1.0 \times 10^{-3} \text{ Pa s}$
Sea-Water Concentration	Concentration $0.0357 \text{ kg dissolved salt / kg sea water}$
Porosity	0.1
Dispersivity α_L, α_T	0.0 m
Salt Diffusion Coefficient	$3.565 \times 10^{-6} \text{ m}^2/\text{s}$
Horizontal Grid Spacing	13.636 m
Vertical Grid Spacing	6.0 m
Time Step	0.08333 yr

therefore the expression for aqueous-phase viscosity was modified from the function of Leijnse (1992), according to Equation 4.2-3 to that shown in Equation 4.2-4.

$$\rho_\ell^S = \rho_\ell^W \exp(0.7 \omega_\ell^S)$$

Equation 4.2-1

$$\rho_\ell^S = \rho_\ell^W + 200 \left(\frac{\omega_\ell^S}{0.2605} \right)$$

Equation 4.2-2

$$\mu_\ell^S = \mu_\ell^W \left[1.0 + 1.85 \omega_\ell^S + 4.1 (\omega_\ell^S)^2 + 44.5 (\omega_\ell^S)^3 \right]$$

Equation 4.2-3

$$\mu_{\ell}^S = 1.0 \times 10^{-3}$$

Equation 4.2-4

4.2.3 Analysis

Simulation results using the aqueous-phase property relations shown in Equation 4.2-2 and Equation 4.2-4 are shown in Figure 4.2-2 through Figure 4.2-4, respectively, for time equal to 2, 4, and 10 years. Solute concentration in these figures represents the fractional saturation concentrations, where saturated conditions are 0.2605 kg solute/kg aqueous solution. For visualization the vertical incomplete source small eddies form near the ends of the boundary source for solute. These eddies scale has been doubled for these plots. Elder's results at the corresponding times are shown in Figure 4.2-5 through Figure 4.2-7. The flow fields that evolve during Elder's problem comprise a series of transient vortices, which cause the concentration plumes to descend in a complex manner. At first the solute transport is dominated by diffusion from the boundary source. Because of the advect away the solute, which in turn increases the diffusion rate of solute from the boundary source. The compounding growth of the eddies near the end of the boundary source also induce eddies to form beneath the middle region of boundary source. Elder noted that this evolution of flow patterns was observed both in the laboratory and in the numerical simulations.

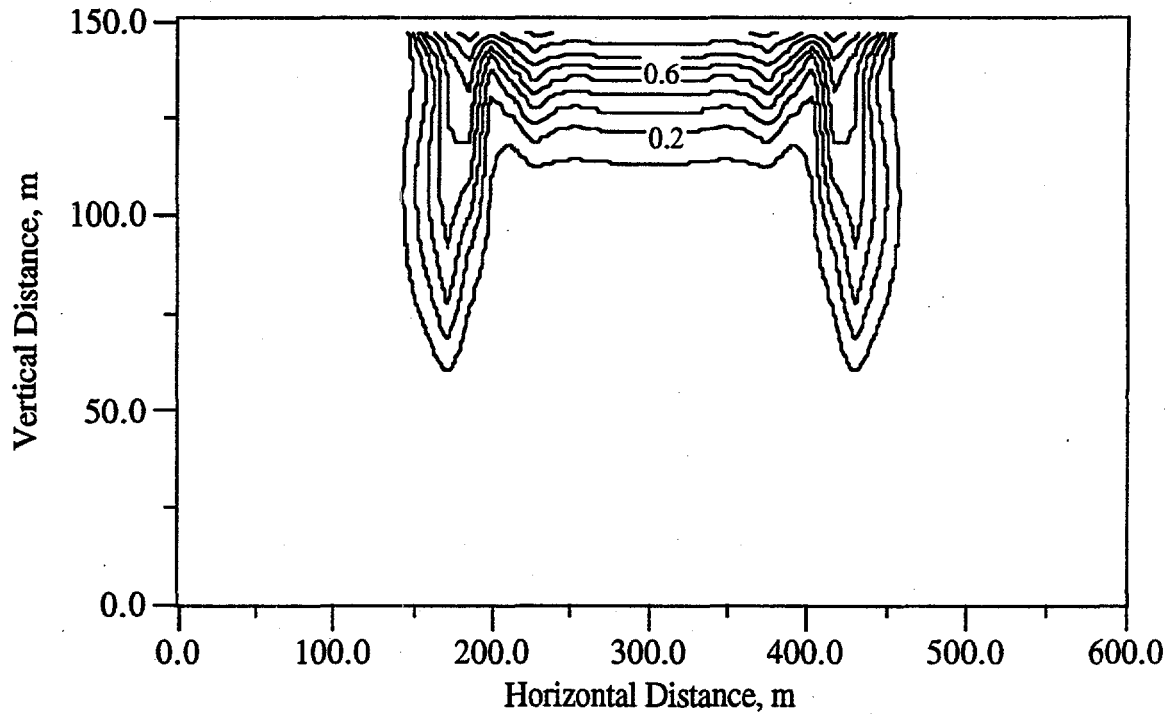


Figure 4.2-2. Contours of Solute Concentration at 2 yr (STOMP Results with Voss and Souza Aqueous Property Functions)

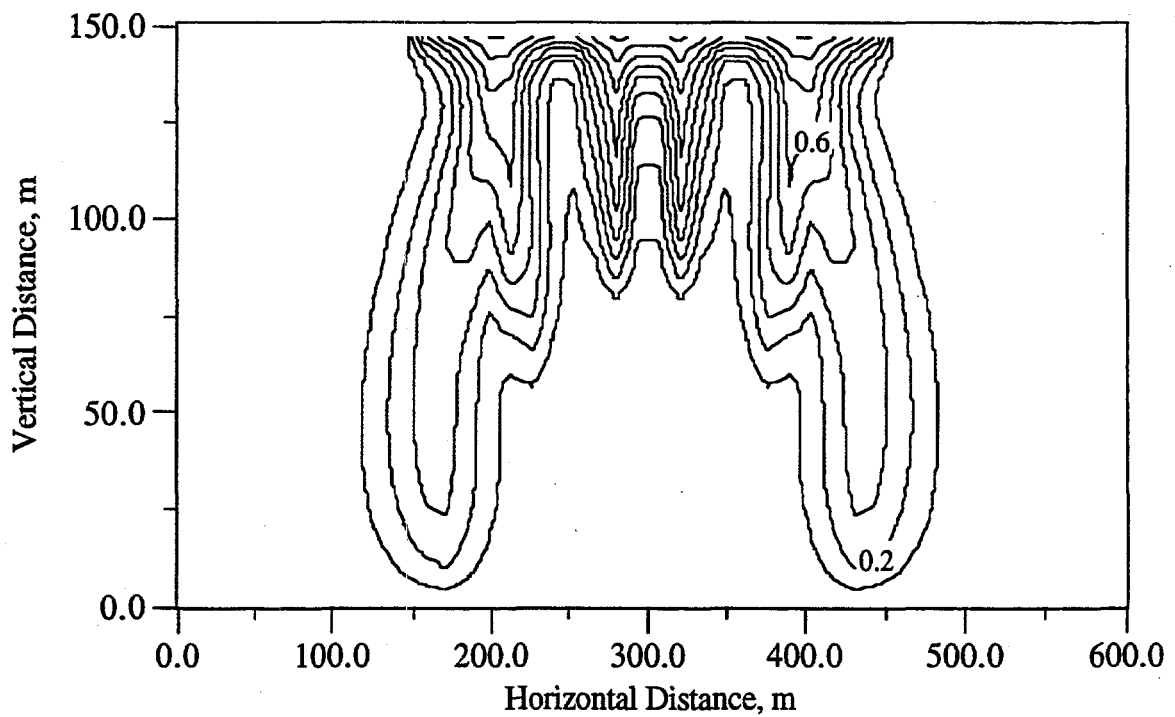


Figure 4.2-3. Contours of Solute Concentration at 4 yr (STOMP Results with Voss and Souza Aqueous Property Functions)

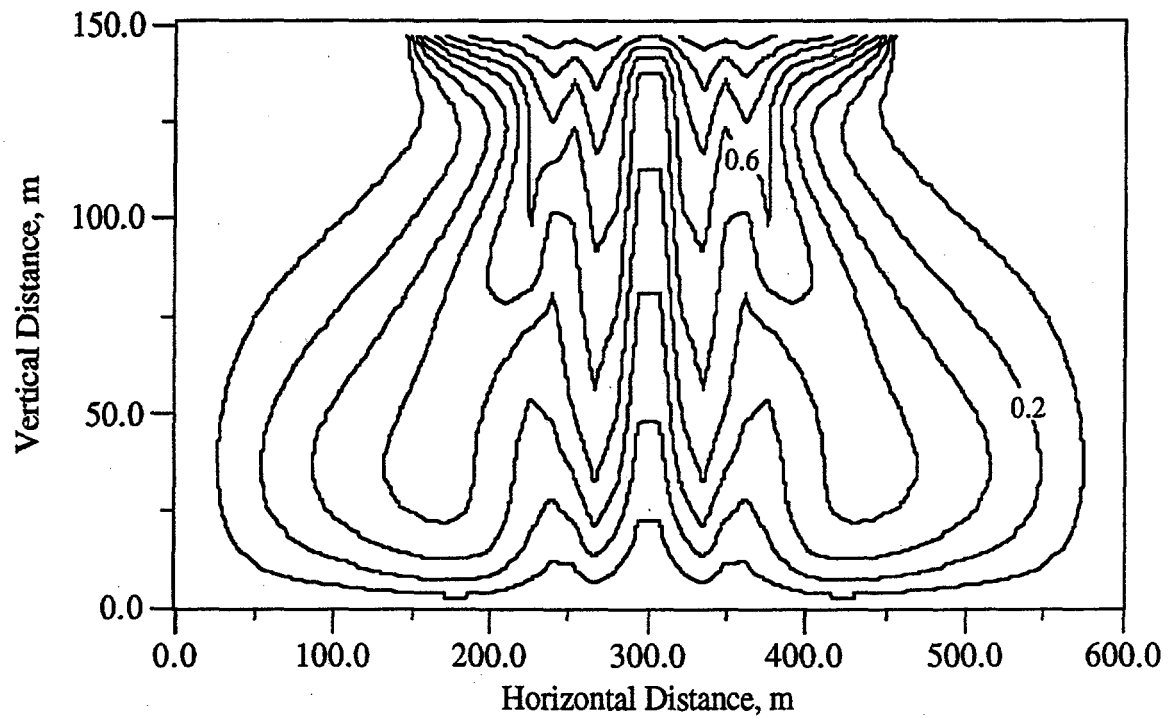


Figure 4.2-4. Contours of Solute Concentration at 10 yr (STOMP Results with Voss and Souza Aqueous Property Functions)

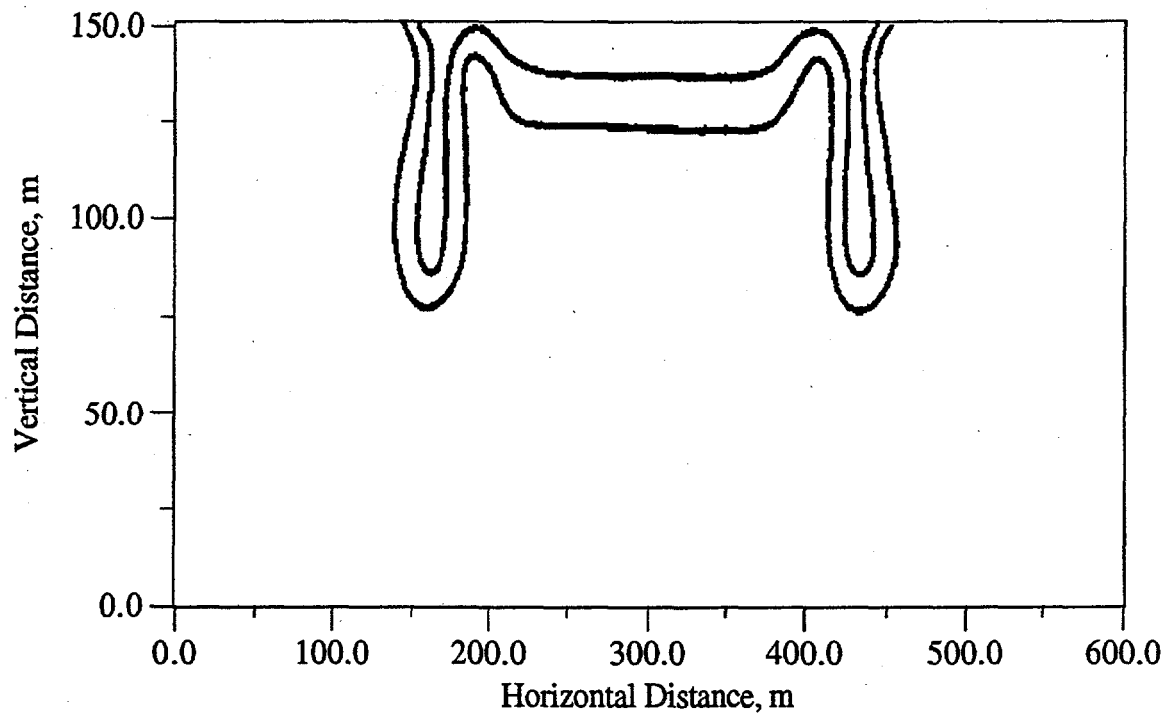


Figure 4.2-5. Contours of 0.2 and 0.6 Solute Concentration at 2 yr Results from Elder's Analogous Thermal Problem

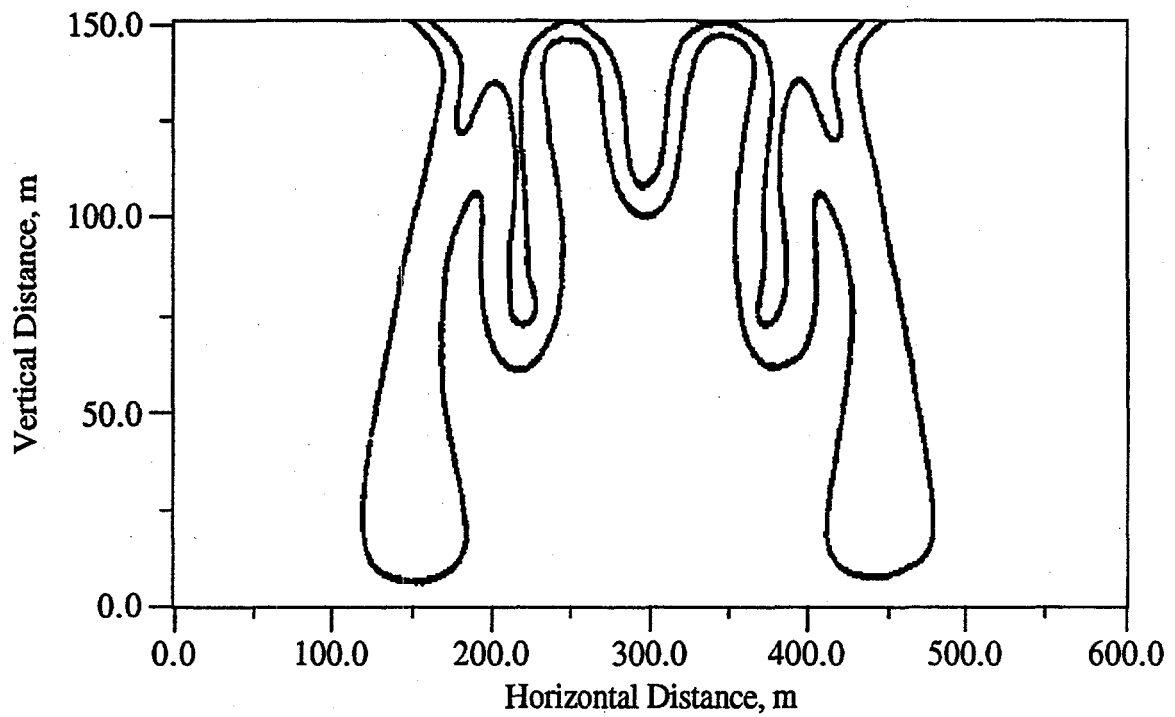


Figure 4.2-6. Contours of 0.2 and 0.6 Solute Concentration at 4 yr Results from Elder's Analogous Thermal Problem

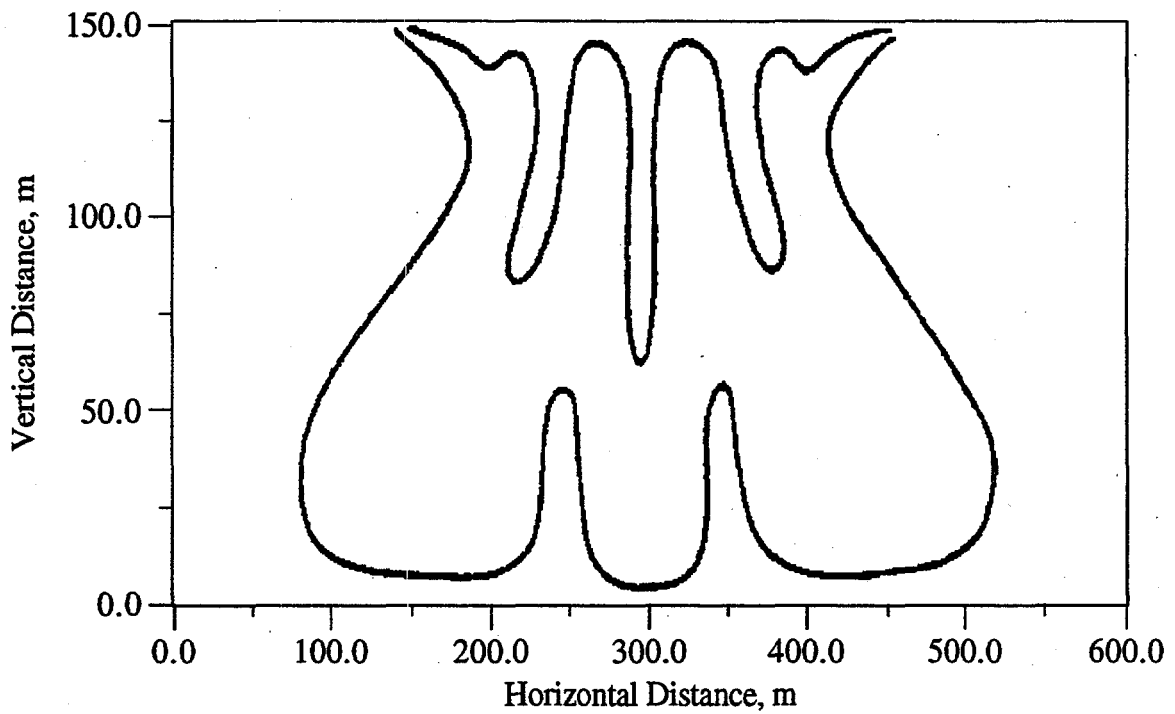


Figure 4.2-7. Contours of 0.2 and 0.6 Solute Concentration at 10 yr Results from Elder's Analogous Thermal Problem

The STOMP solute transport results generally agree with Elder's results in terms of the concentration plume extent and shape. The STOMP simulation preserves the symmetry of the problem, but two descending concentration lobes appear in the center portion of the plumes compared with the single lobe observed in the results of Elder and Voss and Souza. Differences in plume structure may be attributed to the computational domain. Elder's finite-difference based numerical solution used a finer mesh than that of the STOMP simulation; whereas, Voss and Souza used a finite-element based solution with 1170 nodes and 1100 elements. For comparison purposes, STOMP simulation results for Elder's problem using Leijnse's salt-water density and viscosity functions (the standard STOMP functions for brines) are shown in Figure 4.2-.8 through Figure 4.2-10 against those using the property functions of Voss and Souza. The Leijnse's salt-water viscosity function gives aqueous-phase viscosities at saturated conditions which are nearly double that for pure water. The affect of increased viscosity with salt concentration can be seen in Figure 4.2-.8 through Figure 4.2-10; where the descending solute plumes are delayed and more uniform. The increased uniformity stems from the decreased vortex velocities because of the increased resistance to flow with viscosity.

4.2.4 Summary

This application problem was chosen to demonstrate the accuracy of the STOMP simulator in representing bulk fluid flow driven purely by fluid density differences. This problem along with Henry's problem comprise two of the three problems suggested by Voss and Souza for verifying variable-density simulators. The close agreement between the STOMP generated results and those of Elder and Voss and Souza lends confidence in the capability for the simulator model coupled flow and solute transport.

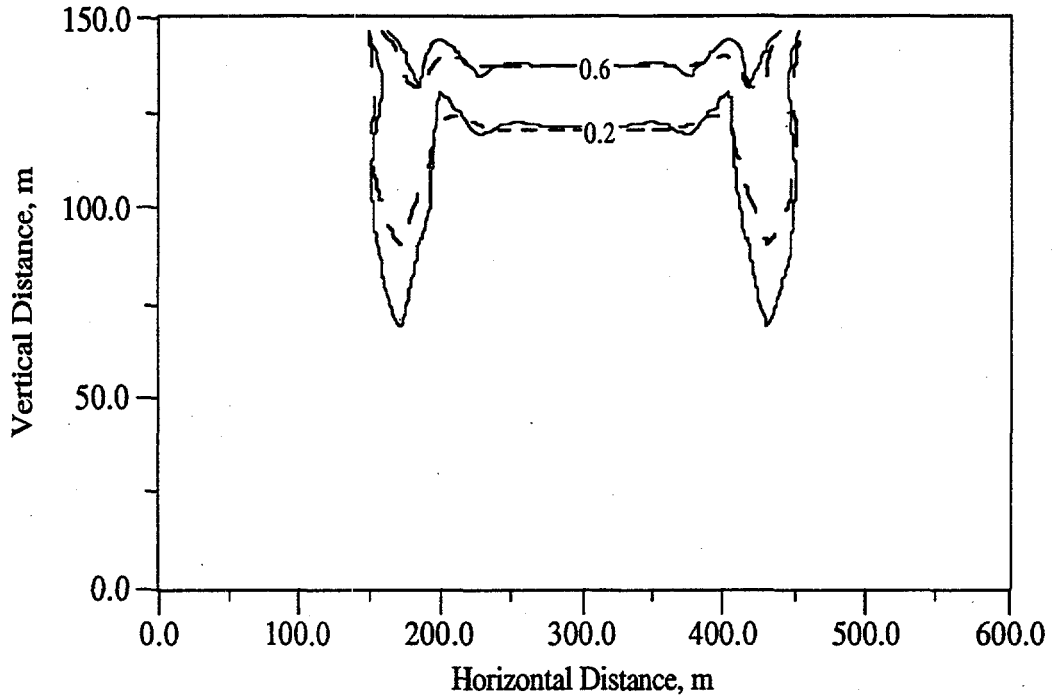


Figure 4.2-8. Contours of 0.2 and 0.6 Solute Concentration at 2 yr (Solid Lines- STOMP with Voss and Souza Aqueous Property Functions, Dashed Lines- STOMP with Leinjse Aqueous Property Functions)

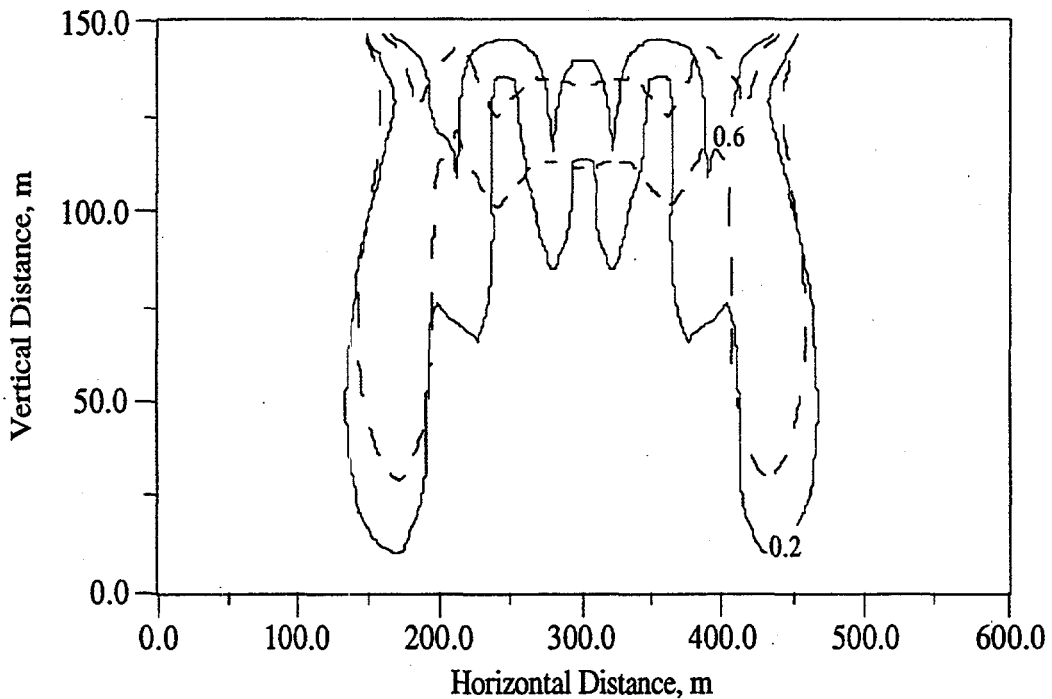


Figure 4.2-9. Contours of 0.2 and 0.6 Solute Concentration at 4 yr (Solid Lines- STOMP Results with Voss and Souza Aqueous Property Functions, Dashed Lines- STOMP Results with Leinjse Aqueous Property Functions)

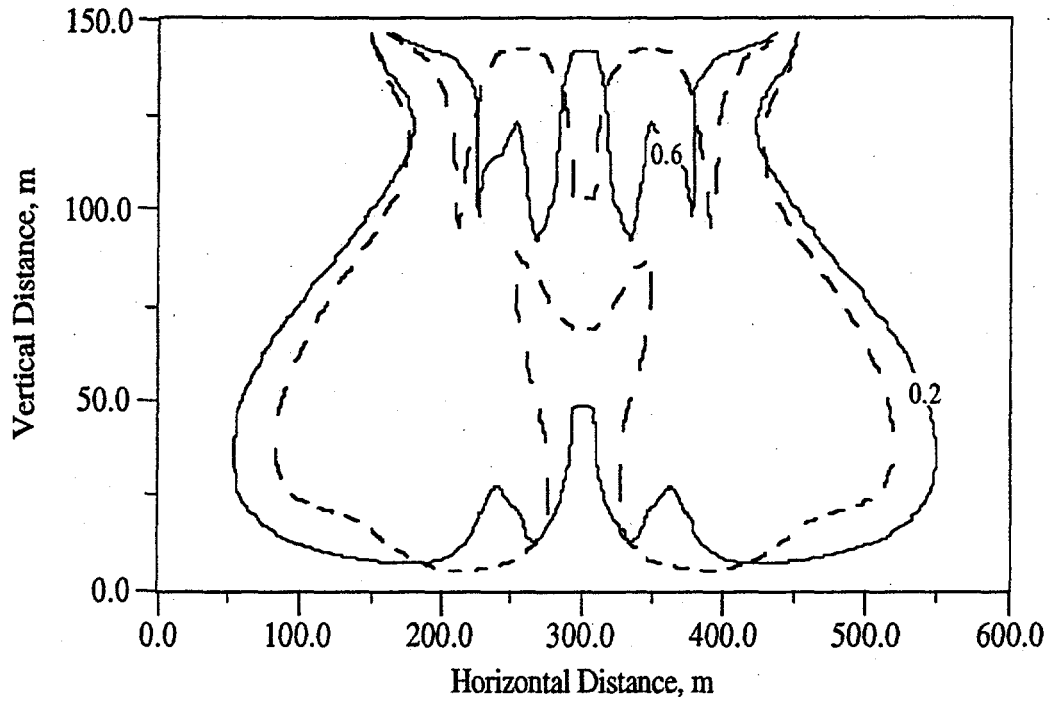


Figure 4.2-10. Contours of 0.2 and 0.6 Solute Concentration at 10 yr (Solid Lines- STOMP Results with Voss and Souza Aqueous Property Functions, Dashed Lines- STOMP Results with Leinjse Aqueous Property Functions)

Exhibit 4.2-1. STOMP Input File for Elder's Problem

<u>Line</u>	<u>Input File</u>
1	-Simulation Title Card
2	1,
3	Elder's Problem,
4	MD White,
5	Pacific Northwest Laboratory,
6	September 21 1995,
7	10:00:00 AM PDT,
8	1,
9	STOMP Application Guide Problem 4.2
10	
11	-Solution Control Card
12	Normal,
13	Water-Salt,
14	1,
15	0,yr,20,yr,0.08333333,yr,0.08333333,yr,1.25,8,1.e-6,
16	1,hr,1,hr,1000,
17	0,
18	
19	-Grid Card
20	Uniform Cartesian,
21	44,1,25,
22	13.636363,m,
23	1,m,
24	6.0,m,
25	
26	-Rock/Soil Zonation Card
27	1,
28	Geologic Media,1,44,1,1,1,25,
29	
30	-Mechanical Properties Card
31	Geologic Media,,,0.1,0.1,1.e-9,1/m,Constant Diffusion,1.0,
32	
33	-Hydraulic Properties Card
34	Geologic Media,4.845e-13,m^2,,,4.845e-13,m^2,
35	
36	-Saturation Function Card
37	Geologic Media,Nonhysteretic van Genuchten,0.2,1/cm,1.8,0.0,,
38	
39	-Aqueous Relative Permeability Card
40	Geologic Media,Mualem,,
41	
42	-Salt Transport Card
43	Constant Diffusion,3.565e-6,m^2/s,
44	Geologic Media,0.0,m,0.0,m,
45	
46	-Initial Conditions Card
47	Gas Pressure, Aqueous Pressure,
48	1,
49	Aqueous Pressure,1643395.0,Pa,,,,,-9810.0,1/m,1,44,1,1,1,25,
50	
51	-Boundary Conditions Card
52	4,
53	Bottom,Zero Flux,Aqueous Conc.,
54	1,44,1,1,1,1,1,
55	0,yr,,,0.0,kg/m^3,

Exhibit 4.2-1. (Contd)

<u>Line</u>	<u>Input File</u>
56	Top,Zero Flux,Aqueous Conc.,
57	12,33,1,1,25,25,1,
58	0,yr,,,312.6,kg/m^3,
59	Top,Dirichlet,Zero Flux,
60	1,1,1,1,25,25,1,
61	0,yr,201325,Pa,,,
62	Top,Dirichlet,Zero Flux,
63	44,44,1,1,25,25,1,
64	0,yr,201325,Pa,,,
65	
66	-Output Control Card
67	4,
68	22,1,25,
69	22,1,1,
70	1,1,25,
71	44,1,25,
72	1,1,yr,m,,,,
73	4,
74	Salt Aqueous Concentration,kg/m^3,
75	Aqueous Density,kg/m^3,
76	Aqueous Pressure,Pa,
77	Aqueous Saturation,,
78	5,
79	1,yr,
80	2,yr,
81	4,yr,
82	10,yr,
83	15,yr,
84	4,
85	Salt Aqueous Concentration,kg/m^3,
86	Aqueous Density,kg/m^3,
87	Aqueous Pressure,Pa,
88	Aqueous Saturation,,
89	

Exhibit 4.2-2. STOMP Parameters File for Elder's Problem

<u>Line</u>	<u>Parameters File</u>
1	C-----C
2	C STOMP Parameter File
3	C-----C
4	C
5	C--- Number of lines of simulation notes
6	C Number of execution periods ---
7	C
8	PARAMETER(LNOTES=1, LEPD=1)
9	C
10	C--- Number of nodes in the x or r coordinate direction
11	C Number of nodes in the y or theta coordinate direction
12	C Number of nodes in the z coordinate direction
13	C Number of active nodes
14	C Number of active dimensions
15	C Minimum of (LFX*LFY, LFX*LFZ, LFY*LFZ) ---
16	C
17	PARAMETER(LFX=44, LFY=1, LFZ=25)
18	PARAMETER(LAN=1100, LAD=2, LMNP=25)
19	C
20	C--- Energy equation switch (0 = off, 1 = on)
21	C Water mass equation switch (0 = off, 1 = on)
22	C Air mass equation switch (0 = off, 1 = on)
23	C VOC mass equation switch (0 = off, 1 = on)
24	C Solute transport equation switch (0 = off, 1 = on)
25	C Freezing conditions switch (0 = off, 1 = on) ---
26	C Dissolved salt transport equation switch (0 = off, 1 = on) ---
27	C Dissolved oil transport equation switch (0 = off, 1 = on) ---
28	C
29	PARAMETER(LT=0, LL=1, LG=0, LN=0, LC=0, LFC=0, LS=1, LD=0)
30	C
31	C--- Banded matrix linear equation solver switch (0 = off, 1 = on)
32	C Conjugate gradient linear equation solver switch (0 = off, 1 = on) ---
33	C Unsymmetric-pattern multifrontal package switch (0 = off, 1 = on) ---
34	C
35	PARAMETER(LBD=1, LCG=0, LUM=0)
36	C
37	C--- Number of boundary condition surfaces
38	C Number of boundary condition times ---
39	C
40	PARAMETER(LBC=68, LBTM=1)
41	C
42	C--- Number of sources
43	C Number of source times ---
44	C
45	PARAMETER(LSR=1, LSTM=1)
46	C
47	C--- Number of rock/soil types
48	C Number of solutes
49	C
50	PARAMETER(LRC=1, LSOLU=1)
51	C
52	C--- Number of reference nodes
53	C Number of print times
54	C Number of integration surfaces ---
55	C

Exhibit 4.2-2. (Contd)

<u>Line</u>	<u>Parameters File</u>
56	PARAMETER(LREF=4, LPTM=5, LSF=1)
57	C
58	C--- Number saturation and relative permeability table entries
59	C Number of hysteretic scanning paths
60	C Number of chemical reactions
61	C
62	PARAMETER(LTBL=1, LPATH=3, LCHEM=1)
63	C
64	C--- Computed Parameters ---
65	C
66	PARAMETER(LUK=LT+LL+LG+LN+LS+LD, LPH=LL+LG+LN, LCMP=LL+LS+LD)
67	PARAMETER(LFXY=LFX*LFY, LPYZ=LFY*LPZ, LFZX=LFZ*LFX)
68	PARAMETER(LFD=LFX*LFY*LPZ)
69	PARAMETER(LNE=(LUK*LUK*(7*LFD-2*LFXY-2*LPYZ-2*LFZX))*LUM)
70	PARAMETER(LHBW=LUK*LMNP+LUK-1)
71	PARAMETER(LJA=LBD + LCG*LAN*LUK + LUM*LAN*LUK)
72	PARAMETER(LJB=(2*LAN*LUK)**LUM, LJC=LAN**LUM)
73	PARAMETER(LJD=LBD*(3*LHBW+1) + LCG*LAN*LUK + LUM*6*LNE)
74	PARAMETER(LJE=LBD*LAN*LUK + LCG*((2*LAD+1)*LUK+2*LAD) + LUM)
75	PARAMETER(LJF=LAN*LUK)
76	PARAMETER(LJG=LBD*(3*LHBW+1) + LCG*LAN*LUK + LUM)
77	PARAMETER(LJH=LBD*LAN*LUK + LCG*(2*LAD+1) + LUM)
78	PARAMETER(LJJ=LBD*LAN*LUK + LCG + LUM)
79	PARAMETER(LSV=LUK+2, LSFV=2*LUK+1)
80	PARAMETER(LSX=(LFX+1)*LFY*LPZ)
81	PARAMETER(LSY=LFX*(LFY+1)*LPZ)
82	PARAMETER(LSZ=LFX*LFY*(LPZ+1))
83	PARAMETER(LFDT=LFD**LT, LFDL=LFD**LL, LFDG=LFD**LG, LFDN=LFD**LN)
84	PARAMETER(LFDC=LFD**LC, LFDI=LFD**LFC, LFDS=LFD**LS, LFDD=LFD**LD)
85	PARAMETER(LSXT=LSX**LT, LSXL=LSX**LL, LSXG=LSX**LG, LSXN=LSX**LN)
86	PARAMETER(LSXC=LSX**LC, LSXS=LSX**LS, LSXD=LSX**LD)
87	PARAMETER(LSYT=LSY**LT, LSYL=LSY**LL, LSYG=LSY**LG, LSYN=LSY**LN)
88	PARAMETER(LSYC=LSY**LC, LSYS=LSY**LS, LSYD=LSY**LD)
89	PARAMETER(LSZT=LSZ**LT, LSZL=LSZ**LL, LSZG=LSZ**LG, LSZN=LSZ**LN)
90	PARAMETER(LSZC=LSZ**LC, LSZS=LSZ**LS, LSZD=LSZ**LD)
91	PARAMETER(LRCT=LRC**LT, LRCL=LRC**LL, LRCG=LRC**LG, LRCN=LRC**LN)
92	PARAMETER(LRCC=LRC**LC, LRCL=LRC**LFC, LRCS=LRC**LS, LRCD=LRC**LD)
93	PARAMETER(LBCT=LBC**LT, LBCL=LBC**LL, LBCG=LBC**LG, LBCN=LBC**LN)
94	PARAMETER(LBCC=LBC**LC, LBCL=LBC**LFC, LBCC=LBC**LS, LBCC=LBC**LD)
95	PARAMETER(LBCU=LUK+LPH+LT+2, LBCV=LBCU+LSOLU)
96	PARAMETER(LOUPV=200+11*(LSOLU))
97	PARAMETER(LJI=LBD*LAN*LUK + LCG + (3*LNE+23*LFD*LUK+9)*LUM)
98	PARAMETER(LSCHR=18)
99	

4.3 References

- Elder JW. 1967. "Transient convection in a porous medium." *Journal of Fluid Mechanics*, 27(3), 609-623.
- Henry HR. 1964a. *Effects of Dispersion on Salt Encroachment in Coastal Aquifers*. Water-Supply Paper 1613-C, Sea Water in Coastal Aquifers: C71-84, U.S. Geological Survey.
- Henry HR. 1964b. *Interfaces between salt water and fresh water in coastal aquifers*. Water-Supply Paper 1613-C, Sea Water in Coastal Aquifers: C35-70, U.S. Geological Survey.
- Leijnse A. 1992. *Three-Dimensional Modeling of Coupled Flow and Transport in Porous Media*, Ph.D., University of Notre Dame, Notre Dame, Indiana.
- Ségol G. 1994. *Classic Groundwater Simulations: Proving and Improving Numerical Models*, trans., Prentice-Hall, Englewood Cliffs, New Jersey.
- Voss CI, and WR Souza. 1987. "Variable density flow and solute transport simulation of regional aquifers containing a narrow freshwater-saltwater transition zone." *Water Resources Research*, 23(10), 1851-1866.

5.0 Flow and Transport in Unsaturated Porous Media

Unsaturated, or variably saturated, flow is concerned with the motion of water in a porous medium in which the pore space also contains air in gas phase. Traditionally, the two-phase flow problem involving air and water is reduced to a single-phase problem using the assumption that the air phase is at constant atmospheric pressure. In this section, STOMP solutions to several classical problems that treat unsaturated flow in this manner are presented. One case is presented (Section 5.3) that contrasts a solution for the constant atmospheric pressure assumption with one obtained by modeling air and water explicitly as a two-phase system. More practical application examples are provided in Sections 5.2 and 5.4, which illustrate the use of the STOMP simulator in analysis of a underground waste storage tank leak and in vapor phase transport of radon from ground water to a residential basement space.

5.1 Haverkamp et al.'s Infiltration Experiments

Ségol (1994) introduced Haverkamp et al.'s (1977) infiltration experiments with the following information:

Problem Features: 5.1

- Water operational mode
- one dimensional (z)
- unsaturated infiltration
- dry initial conditions
- heterogeneous, isotropic
- uniform Cartesian grid
- tabular function input
- comparison with published solutions

Haverkamp et al. (1977) investigated experimentally the infiltration of water into a uniform laboratory-scale soil column, and used the results of these experiments to evaluate six discrete approximations of Richards' equation. Hills et al. (1989), in turn, used Haverkamp et al.'s problem definition and results to test alternative pressure-based and moisture content-based formulation for infiltration, with the ultimate objective of developing an algorithm capable of handling infiltration into very dry soils.

In this problem, we use the STOMP simulator to solve for the infiltration in Haverkamp et al.'s (1977) experiments, and compare the results to the experimental data provided by Ségol (1994).

5.1.1 Problem Description and Parameters

This problem concerns the simulation of infiltration of water into a uniform laboratory-scale soil column reported by Haverkamp et al. (1977). Hills et al. (1989) used Haverkamp et al.'s problem definition and results to test alternative pressure-based and moisture-content-based

formulations for infiltration, with the ultimate objective being the development of an algorithm capable of addressing infiltration into very dry soils.

The soil column modeled is 70 cm high, with an initial condition of uniform moisture content equal to 0.10, or a pressure equal to -61.5 cm tension head. A constant flux of 13.69 cm/hr is applied at the top of the column during the experiment while the base of the column is maintained at the initial moisture content value.

Haverkamp et al. provided analytical expressions of the pressure, moisture content, and hydraulic conductivity relationships for the soil in the column (sand), which were obtained by a least-squares fit through all the data points. These expressions are written as

$$\theta(\psi) = \frac{\alpha(\theta_s - \theta_r)}{\alpha + |\psi|^\beta} + \theta_r$$

Equation 5.1-1

$$K(\psi) = K_s \frac{A}{A + |\psi|^\gamma}$$

Equation 5.1-2

where K_s is the saturated hydraulic conductivity (34 cm/hr in this case), θ_r is the residual moisture content (0.075), and θ_s is the saturated moisture content (0.287). The coefficients have values $A = 1.175 \times 10^6$, $\alpha = 1.611 \times 10^6$, $\beta = 3.96$, and $\gamma = 4.74$. The STOMP simulator does not include the Haverkamp et al. (1977) expressions in Equation 5.1-1 and Equation 5.1-2. To specify these constitutive relations, we use the tabular feature in STOMP. The expressions in Equation 5.1-1 and Equation 5.1-2 were evaluated over a range of data values to generate a table that was included in the STOMP input file for this problem. STOMP would then linearly interpolate from the values in this table to determine needed values of pressure, saturation, or hydraulic conductivity.

Hills et al. (1989) contrasted a number of simulation test cases involving various algorithms (one-step, pressure-head, moisture-content), nodal spacings, and time increments. The two test cases akin to STOMP's algorithm (pressure-based) that we duplicate in this effort are Test Cases 3 and 6. Case 3 calls for a 1.0 cm nodal spacing and 0.005 day time increment, while Test

Case 6 involved a 5.0 cm nodal spacing and 0.020 day time increment. The full input parameter description is provided in Table 5.1-1 for these simulations.

The STOMP input file for Test Case 3 is shown in Exhibit 5.1-1, and for Test Case 6 in Exhibit 5.1-2. A single STOMP parameters file (Exhibit 5.1-3) was sized to the larger case (3) and used for both cases.

Table 5.1-1. Input Parameters for the Haverkamp et al. Infiltration Experiment Problem

Domain	Vertical column of depth 100 cm, containing homogeneous sand
Porosity	
Saturated Moisture Content θ_s	0.287
Residual Moisture Content θ_r	0.075
Aqueous saturation	
Tabular input of Haverkamp et al. (1977)	Equation (5.1-1)
Parameters for Equation (5.1-1):	
α	1.611×10^6
β	3.96
Aqueous permeability, k_r	
Saturated permeability (K_s), cm/hr	34
Tabular input of Haverkamp et al. (1977)	Equation (5.1-2)
Parameters for Equation (5.1-2):	
A	1.175×10^6
γ	4.74
Boundary conditions	Constant flux of 13.69 cm/hr at the top surface. Constant moisture content of 0.10 or pressure head of -61.5 cm at the base.
Initial saturation	0.10 throughout.
Grid characteristics	One-dimensional uniform finite-difference grid with 70 blocks (case 3) or 14 blocks (case 6).
Nodal spacing, Δz	1.0 cm (case 3) or 5 cm (case 6).
Time increment, Δt	5.0×10^{-4} day (case 3) or 2.0×10^{-2} day (case 6).

5.1.2 Simulations

The solutions obtained using the STOMP simulator for test cases 3 and 6 are displayed in Figure 5.1-1, along with the computational results reported in Ségol (1994) attributable to a personal communication from Hills (Ségol 1994) for the same test cases. Hills et al. (1989) was searching for a optimum algorithm to deal with infiltration into very dry soils, so we expect that STOMP, designed as a multiphase code and not specifically optimized for such conditions, will perform less efficiently than the results reported by Hills et al. (1989). Figure 5.1-1 reflects this.

5.1.3 Analysis

In Case 3, STOMP performed nearly as well as Hills et al.'s solution, with only a slightly less sharp infiltration front. In Case 6, STOMP shows obviously less adequate results. In judging STOMP's performance, bear in mind that Case 3 uses 1.0 cm grid spacing and 0.012 hr time increments, but Case 6 is much more severe with 5 cm time increments and 0.5 hr. In other words, case 6 demands the infiltration front be solved for in a single time step with only 14 grid nodes. Therefore, if greater accuracy were demanded, less severe time and spatial discretization would be necessary for the STOMP simulator.

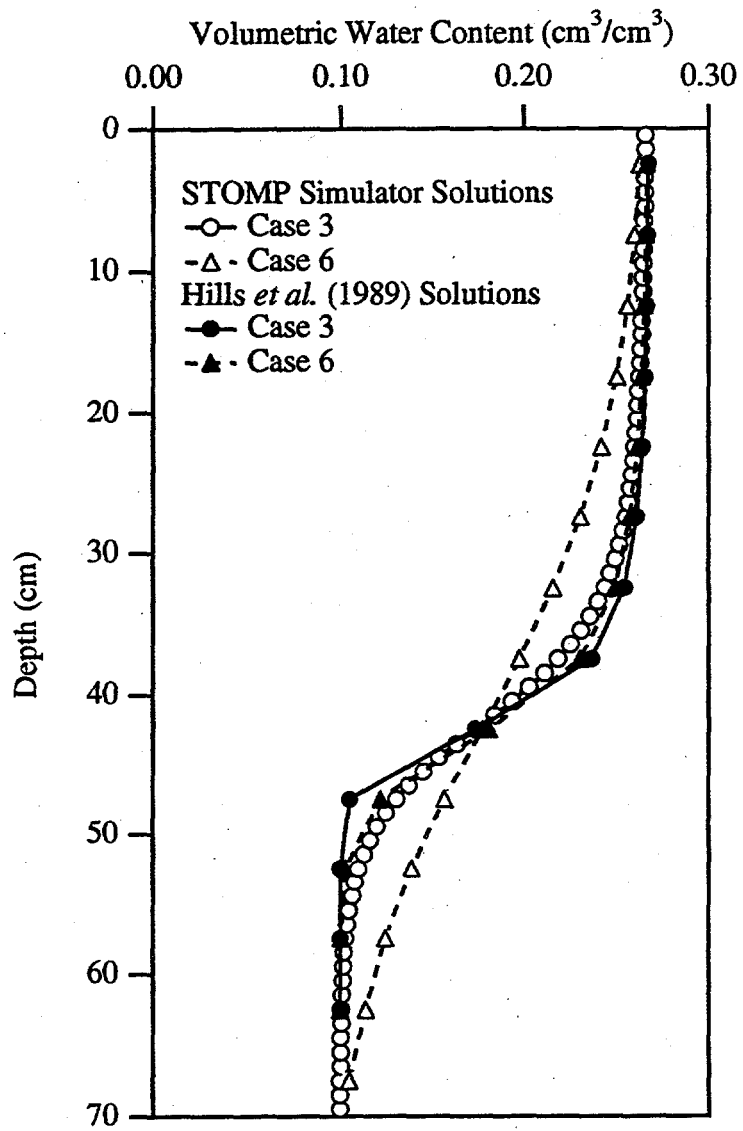


Figure 5.1-1. Comparison of STOMP and Hills et al. Solutions to the Haverkamp et al. Infiltration Problem

Exhibit 5.1-1. STOMP Input File for Haverkamp et al.'s Infiltration Experiment - Case 3

<u>Line</u>	<u>Input File</u>
1	-Simulation Title Card
2	1,
3	Haverkamp et al.'s Infiltration Experiments <Test Case 3>,
4	W. E. Nichols,
5	Pacific Northwest Laboratory,
6	September 1 1995,
7	1:30:00 PM PDT,
8	3,
9	Simulation of infiltration following Haverkamp, Vauclin, Touma, Wierenga, and
10	Vachaud, "A Comparison of Numerical Simulation Models for One-Dimensional
11	Infiltration," Soil Sci. J. Am., 41:285-294, 1977. The Water mode is used.
12	
13	-Solution Control Card
14	Normal,
15	Water,
16	1,
17	0.0,hr,0.5,hr,0.005,day,0.005,day,1.1,8,1.0e-6,
18	1.0,hr,1.0,hr,100,
19	1,
20	Aqueous Relative Permeability,Geometric,
21	
22	-Grid Card
23	Uniform Cartesian,
24	1,1,70,
25	1.0,cm,
26	1.0,cm,
27	1.0,cm,
28	
29	-Rock/Soil Zonation Card
30	1,
31	Sand,1,1,1,1,1,70,
32	
33	-Mechanical Properties Card
34	Sand,,,0.287,0.287,,,
35	
36	-Hydraulic Properties Card
37	Sand,,,,,34,hc cm/hr,
38	
39	-Saturation Function Card
40	Sand,Tabular,28,
41	0.1,cm,1,
42	1,cm,0.99999954,
43	5,cm,0.99973139,
44	10,cm,0.99584179,
45	16,cm,0.97404972,
46	20,cm,0.94019083,
47	24,cm,0.88660008,
48	26,cm,0.85273806,
49	28,cm,0.81508485,
50	30,cm,0.77470758,
51	32,cm,0.73283084,
52	33,cm,0.71172015,
53	34,cm,0.69069223,
54	36,cm,0.64941392,
55	38,cm,0.60991315,

Exhibit 5.1-1. (Contd)

<u>Line</u>	<u>Input File</u>
56	40, cm, 0.57286002,
57	42, cm, 0.53867726,
58	44, cm, 0.50756937,
59	46, cm, 0.47956669,
60	50, cm, 0.43240839,
61	55, cm, 0.38783491,
62	60, cm, 0.35567031,
63	65, cm, 0.33251134,
64	75, cm, 0.30347337,
65	100, cm, 0.27535923,
66	500, cm, 0.26134845,
67	1000, cm, 0.26132561,
68	10000, cm, 0.26132404,
69	
70	-Aqueous Relative Permeability Card
71	Sand, Tabular, 28,
72	1, 1,
73	0.99999954, 0.99999915,
74	0.99973139, 0.99825289,
75	0.99584179, 0.95532021,
76	0.97404972, 0.69734952,
77	0.94019083, 0.4444818,
78	0.88660008, 0.25214657,
79	0.85273806, 0.18746012,
80	0.81508485, 0.13968957,
81	0.77470758, 0.10480905,
82	0.73283084, 0.07937937,
83	0.71172015, 0.06935323,
84	0.69069223, 0.06075824,
85	0.64941392, 0.04701641,
86	0.60991315, 0.03677816,
87	0.57286002, 0.02907107,
88	0.53867726, 0.02320803,
89	0.50756937, 0.01870137,
90	0.47956669, 0.01520242,
91	0.43240839, 0.0102903,
92	0.38783491, 0.00657437,
93	0.35567031, 0.00436217,
94	0.33251134, 0.00298902,
95	0.30347337, 0.0015191,
96	0.27535923, 0.00038893,
97	0.26134845, 1.892E-07,
98	0.26132561, 7.0801E-09,
99	0.26132404, 1.2884E-13,
100	
101	-Initial Conditions Card
102	Gas Pressure, Aqueous Saturation,
103	2,
104	Gas Pressure, 101325.0, Pa, 0.0, 1/m, 0.0, 1/m, 0.0, 1/m, 1, 1, 1, 1, 1, 70,
105	Aqueous Saturation, 0.34843, , 0.0, 1/cm, 0.0, 1/cm, 0.0, 1/cm, 1, 1, 1, 1, 1, 70,
106	
107	-Boundary Conditions Card
108	2,
109	Top, Neumann Aqueous,
110	1, 1, 1, 1, 70, 70, 1,

Exhibit 5.1-1. (Contd)

<u>Line</u>	<u>Input File</u>
111	0.0,hr,-13.69,cm/hr,
112	Bottom,Dirichlet Aqueous,
113	1,1,1,1,1,1,1,
114	0.0,hr,95301.98569,Pa,
115	
116	-Output Control Card
117	3,
118	1,1,70,
119	1,1,60,
120	1,1,50,
121	1,1,hr,cm,3,5,5,
122	4,
123	Aqueous Pressure,Pa,
124	Aqueous Saturation,,
125	Aqueous Moisture Content,,
126	Aqueous Relative Permeability,,
127	1,
128	0.50,hr,
129	1,
130	Aqueous Moisture Content,,
131	

Exhibit 5.1-2. STOMP Input File for Haverkamp et al.'s Infiltration Experiments - Case 6

<u>Line</u>	<u>Input File</u>
1	-Simulation Title Card
2	1,
3	Haverkamp et al.'s Infiltration Experiments <TEST CASE 6>,
4	W. E. Nichols,
5	Pacific Northwest Laboratory,
6	September 1 1995,
7	1:30:00 PM PDT,
8	3,
9	Simulation of infiltration following Haverkamp, Vauclin, Touma, Wierenga, and
10	Vachaud, "A Comparison of Numerical Simulation Models for One-Dimensional
11	Infiltration," Soil Sci. J. Am., 41:285-294, 1977. The Water mode is used.
12	
13	-Solution Control Card
14	Normal,
15	Water,
16	1,
17	0.0,hr,0.5,hr,0.02,day,0.02,day,1.1,8,1.0e-6,
18	1.0,hr,1.0,hr,100,
19	1,
20	Aqueous Relative Permeability,Geometric,
21	
22	-Grid Card
23	Uniform Cartesian,
24	1,1,14,
25	1.0,cm,
26	1.0,cm,
27	5.0,cm,
28	
29	-Rock/Soil Zonation Card
30	1,
31	Sand,1,1,1,1,1,14,
32	
33	-Mechanical Properties Card
34	Sand,,,0.287,0.287,,,
35	
36	-Hydraulic Properties Card
37	Sand,,,,,34,hc cm/hr,
38	
39	-Saturation Function Card
40	Sand,Tabular,28,
41	0.1,cm,1,
42	1,cm,0.99999954,
43	5,cm,0.99973139,
44	10,cm,0.99584179,
45	16,cm,0.97404972,
46	20,cm,0.94019083,
47	24,cm,0.88660008,
48	26,cm,0.85273806,
49	28,cm,0.81508485,
50	30,cm,0.77470758,
51	32,cm,0.73283084,
52	33,cm,0.71172015,
53	34,cm,0.69069223,
54	36,cm,0.64941392,
55	38,cm,0.60991315,

Exhibit 5.1-2. (Contd)

<u>Line</u>	<u>Input File</u>
56	40, cm, 0.57286002,
57	42, cm, 0.53867726,
58	44, cm, 0.50756937,
59	46, cm, 0.47956669,
60	50, cm, 0.43240839,
61	55, cm, 0.38783491,
62	60, cm, 0.35567031,
63	65, cm, 0.33251134,
64	75, cm, 0.30347337,
65	100, cm, 0.27535923,
66	500, cm, 0.26134845,
67	1000, cm, 0.26132561,
68	10000, cm, 0.26132404,
69	
70	-Aqueous Relative Permeability Card
71	Sand, Tabular, 28,
72	1, 1,
73	0.99999954, 0.99999915,
74	0.99973139, 0.99825289,
75	0.99584179, 0.95532021,
76	0.97404972, 0.69734952,
77	0.94019083, 0.4444818,
78	0.88660008, 0.25214657,
79	0.85273806, 0.18746012,
80	0.81508485, 0.13968957,
81	0.77470758, 0.10480905,
82	0.73283084, 0.07937937,
83	0.71172015, 0.06935323,
84	0.69069223, 0.06075824,
85	0.64941392, 0.04701641,
86	0.60991315, 0.03677816,
87	0.57286002, 0.02907107,
88	0.53867726, 0.02320803,
89	0.50756937, 0.01870137,
90	0.47956669, 0.01520242,
91	0.43240839, 0.0102903,
92	0.38783491, 0.00657437,
93	0.35567031, 0.00436217,
94	0.33251134, 0.00298902,
95	0.30347337, 0.0015191,
96	0.27535923, 0.00038893,
97	0.26134845, 1.892E-07,
98	0.26132561, 7.0801E-09,
99	0.26132404, 1.2884E-13,
100	
101	-Initial Conditions Card
102	Gas Pressure, Aqueous Saturation,
103	2,
104	Gas Pressure, 101325.0, Pa, 0.0, 1/m, 0.0, 1/m, 0.0, 1/m, 1, 1, 1, 1, 1, 14,
105	Aqueous Saturation, 0.34843, , 0.0, 1/cm, 0.0, 1/cm, 0.0, 1/cm, 1, 1, 1, 1, 1, 14,
106	
107	-Boundary Conditions Card
108	2,
109	Top, Neumann Aqueous,
110	1, 1, 1, 1, 14, 14, 1,

Exhibit 5.1-2. (Contd)

<u>Line</u>	<u>Input File</u>
111	0.0,hr,-13.69,cm/hr,
112	Bottom,Dirichlet Aqueous,
113	1,1,1,1,1,1,1,
114	0.0,hr,95301.98569,Pa,
115	
116	-Output Control Card
117	3,
118	1,1,14,
119	1,1,13,
120	1,1,12,
121	1,1,hr,cm,3,5,5,
122	4,
123	Aqueous Pressure,Pa,
124	Aqueous Saturation,,
125	Aqueous Moisture Content,,
126	Aqueous Relative Permeability,,
127	1,
128	0.50,hr,
129	1,
130	Aqueous Moisture Content,,
131	

Exhibit 5.1-3. STOMP Parameters File for Haverkamp et al.'s Infiltration Experiments

<u>Line</u>	<u>Parameters File</u>
1	C-----C
2	C STOMP Parameter File
3	C STOMP Application Guide Case 5.1
4	C-----C
5	C
6	C--- Number of lines of simulation notes
7	C Number of execution periods ---
8	C
9	PARAMETER(LNOTES=10, LEPD=10)
10	C
11	C--- Number of nodes in the x or r coordinate direction
12	C Number of nodes in the y or theta coordinate direction
13	C Number of nodes in the z coordinate direction
14	C Number of active nodes
15	C Number of active dimensions
16	C Minimum of (LFX*LFY, LFX*LFZ, LFY*LFZ) ---
17	C
18	PARAMETER(LFX=1, LFY=1, LFZ=70)
19	PARAMETER(LAN=70, LAD=1, LMNP=1)
20	C
21	C--- Energy equation switch (0 = off, 1 = on)
22	C Water mass equation switch (0 = off, 1 = on)
23	C Air mass equation switch (0 = off, 1 = on)
24	C VOC mass equation switch (0 = off, 1 = on)
25	C Solute transport equation switch (0 = off, 1 = on)
26	C Freezing conditions switch (0 = off, 1 = on) ---
27	C Dissolved salt transport equation switch (0 = off, 1 = on) ---
28	C Dissolved oil transport equation switch (0 = off, 1 = on) ---
29	C
30	PARAMETER(LT=0, LL=1, LG=0, LN=0, LC=0, LFC=0, LS=0, LD=0)
31	C
32	C--- Banded matrix linear equation solver switch (0 = off, 1 = on)
33	C Conjugate gradient linear equation solver switch (0 = off, 1 = on) ---
34	C Unsymmetric-pattern multifrontal package switch (0 = off, 1 = on) ---
35	C
36	PARAMETER(LBD=1, LCG=0, LUM=0)
37	C
38	C--- Number of boundary condition surfaces
39	C Number of boundary condition times ---
40	C
41	PARAMETER(LBC=2, LBTM=1)
42	C
43	C--- Number of sources
44	C Number of source times ---
45	C
46	PARAMETER(LSR=1, LSTM=1)
47	C
48	C--- Number of rock/soil types
49	C Number of solutes
50	C
51	PARAMETER(LRC=1, LSOLU=1)
52	C
53	C--- Number of reference nodes
54	C Number of print times
55	C Number of integration surfaces ---

Exhibit 5.1-3. (Contd)

<u>Line</u>	<u>Parameters File</u>
56	C
57	PARAMETER(LREF=10, LPTM=10, LSF=10)
58	C
59	C--- Number saturation and relative permeability table entries
60	C Number of hysteretic scanning paths
61	C Number of chemical reactions
62	C
63	PARAMETER(LTBL=56, LPATH=3, LCHEM=1)
64	C
65	C--- Computed Parameters ---
66	C
67	PARAMETER(LUK=LT+LL+LG+LN+LS+LD, LPH=LL+LG+LN, LCMP=LL+LS+LD)
68	PARAMETER(LFXY=LFX*LFY, LFYZ=LFY*LFZ, LFZX=LFZ*LFX)
69	PARAMETER(LFD=LFX*LFY*LFZ)
70	PARAMETER(LNE=(LUK*LUK*(7*LFD-2*LFXY-2*LFYZ-2*LFZX))**LUM)
71	PARAMETER(LHBW=LUK*LMNP+LUK-1)
72	PARAMETER(LJA=LBD + LCG*LAN*LUK + LUM*LAN*LUK)
73	PARAMETER(LJB=(2*LAN*LUK)**LUM, LJC=LAN**LUM)
74	PARAMETER(LJD=LBD*(3*LHBW+1) + LCG*LAN*LUK + LUM*6*LNE)
75	PARAMETER(LJE=LBD*LAN*LUK + LCG*((2*LAD+1)*LUK+2*LAD) + LUM)
76	PARAMETER(LJF=LAN*LUK)
77	PARAMETER(LJG=LBD*(3*LHBW+1) + LCG*LAN*LUK + LUM)
78	PARAMETER(LJH=LBD*LAN*LUK + LCG*(2*LAD+1) + LUM)
79	PARAMETER(LJJ=LBD*LAN*LUK + LCG + LUM)
80	PARAMETER(LSV=LUK+2, LSFV=2*LUK+1)
81	PARAMETER(LSX=(LFX+1)*LFY*LFZ)
82	PARAMETER(LSY=LFX*(LFY+1)*LFZ)
83	PARAMETER(LSZ=LFX*LFY*(LFZ+1))
84	PARAMETER(LFDT=LFD**LT, LFDL=LFD**LL, LFDG=LFD**LG, LFDN=LFD**LN)
85	PARAMETER(LFDC=LFD**LC, LFDI=LFD**LFC, LFDS=LFD**LS, LFDD=LFD**LD)
86	PARAMETER(LSXT=LSX**LT, LSXL=LSX**LL, LSXG=LSX**LG, LSXN=LSX**LN)
87	PARAMETER(LSXC=LSX**LC, LSXS=LSX**LS, LSXD=LSX**LD)
88	PARAMETER(LSYT=LSY**LT, LSYL=LSY**LL, LSYG=LSY**LG, LSYN=LSY**LN)
89	PARAMETER(LSYC=LSY**LC, LSYS=LSY**LS, LSYD=LSY**LD)
90	PARAMETER(LSZT=LSZ**LT, LSZL=LSZ**LL, LSZG=LSZ**LG, LSZN=LSZ**LN)
91	PARAMETER(LSZC=LSZ**LC, LSZS=LSZ**LS, LSZD=LSZ**LD)
92	PARAMETER(LRCT=LRC**LT, LRCL=LRC**LL, LRCG=LRC**LG, LRCN=LRC**LN)
93	PARAMETER(LRCC=LRC**LC, LRCL=LRC**LFC, LRCS=LRC**LS, LRCD=LRC**LD)
94	PARAMETER(LBCT=LBC**LT, LBCL=LBC**LL, LBCG=LBC**LG, LBCN=LBC**LN)
95	PARAMETER(LBCC=LBC**LC, LBCI=LBC**LFC, LBCC=LBC**LS, LBCC=LBC**LD)
96	PARAMETER(LBCU=LUK+LPH+LT+2, LBCV=LBCU+LSOLU)
97	PARAMETER(LOUPV=200+11*(LSOLU))
98	PARAMETER(LJI=LBD*LAN*LUK + LCG + (3*LNE+23*LFD*LUK+9)*LUM)
99	PARAMETER(LSCHR=18)
100	

5.2 Tank Leak Simulation

This problem illustrates a hypothetical but practical case. The bottom of a liquid storage tank sits at ground level above a sandy soil. The tank is a repository for liquid waste and has been leaking for a long time. On a certain day ($t = 0$) a new waste/solute is introduced to the tank, at which point it

begins to leak into the underlying soil. The sandy soil contains isolated lenses of either clay or gravel, and the water table below has a gradient from west to east. The development of the resulting contaminant plume is simulated here.

Problem Features: 5.2

- two dimensional (xz)
- dilute species transport
- steady, nonuniform flow field
- variable saturation
- unconfined aquifer
- heterogeneous, isotropic
- uniform Cartesian grid
- hydraulic gradient boundaries

5.2.1 Problem Description and Parameters

The simulated domain is a two dimensional $x - z$ (vertical) cross-section, 100 m long and 15 m high. Two lenses, one clay and one gravel lie within the sandy unconfined aquifer directly below the tank. The clay lens is 20 m long and 1 m thick, while the gravel lens is 15 m long and 1 m thick. The water table is below the lenses at approximately 12 m below ground surface, and has a left-to-right gradient of 0.005. Figure 5.2-1 shows a schematic of the problem. Values for the porous media parameters for the three soil types are given in Table 5.2-1. The van Genuchten (1980) function was used to describe the pressure-saturation behavior for all three soil types, while the saturation-permeability function is determined via Mualem's (1976) relation. All three soils are considered isotropic. The tank has been leaking for a number of years at a constant rate of 20 l/day, resulting in a steady-state flow field.

5.2.2 Simulation

Discretization of the problem domain was achieved with a uniform grid with block size of 1 m by 0.25 m, which resulted in 12,000 nodes (200 by 60). Three material types are defined for the sand matrix, and the clay and gravel lenses. The complete simulation for this problem involves two steps. The first step requires that a steady flow field be established, The second step simulates the transient transport of the contaminant within the steady flow field. The tank leak was simulated via a Neumann boundary condition with a flux of 0.02 m/day, while the sloping water table was implemented with STOMP's Hydraulic Gradient boundary condition.

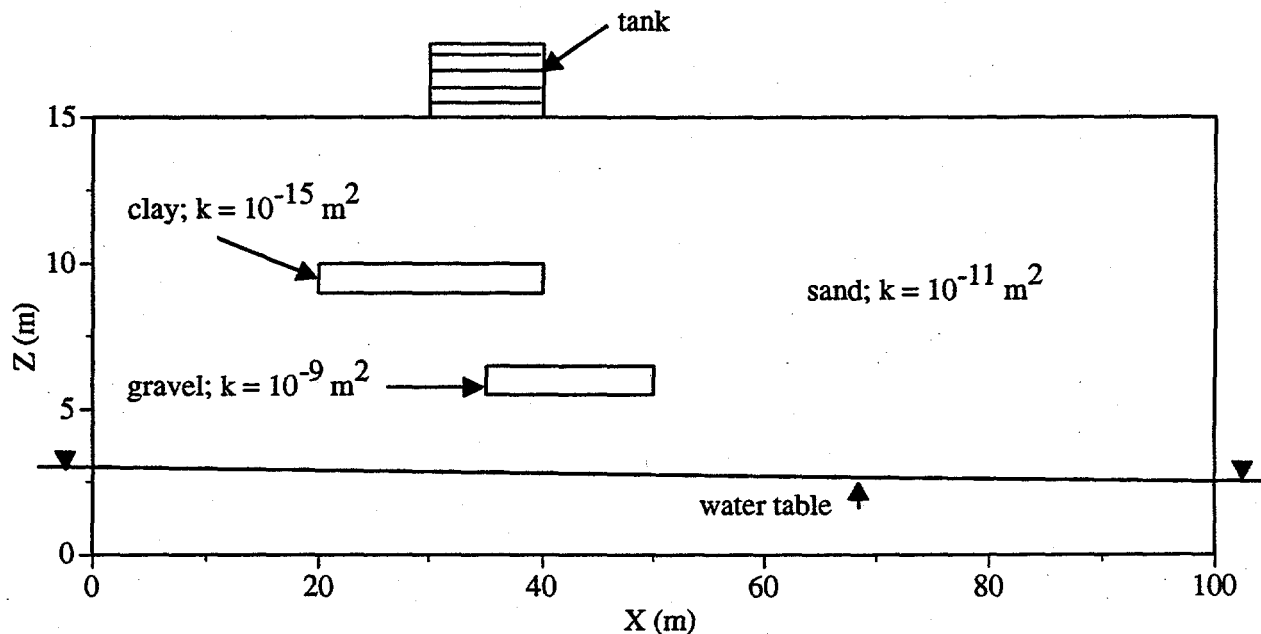


Figure 5.2-1. Tank Leak Simulation Domain Schematic

The transport simulation was performed for a Peclet (Pe) number of 2, which yielded a longitudinal dispersivity value of 0.5 m. A transverse dispersivity value of 1/10th the longitudinal value was used. The simulation was run for 5 years, with output requested at 1, 2 and 5 years. A copy of the STOMP input files for this problem are presented in Exhibit 5.2-1 and Exhibit 5.2-2, and a copy of the 'parameters' file used to build the STOMP executable is shown in Exhibit 5.2-3.

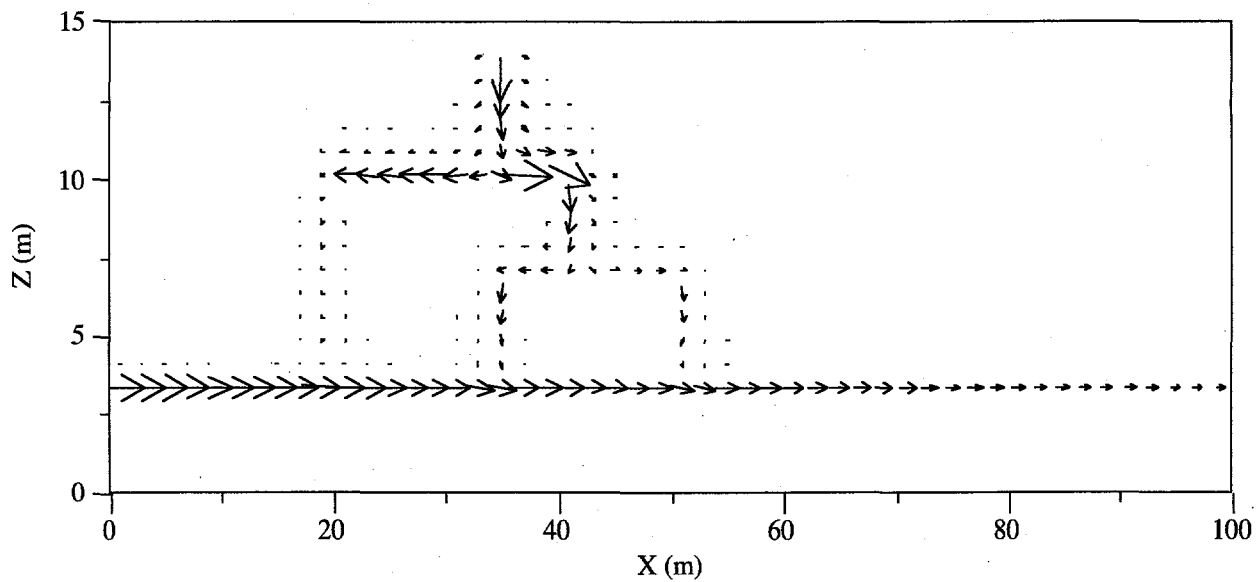
5.2.3 Analysis

The resulting flow field and water content distribution are shown in Figure 5.2-2 and Figure 5.2-3, respectively. Figure 5.2-3 shows leakage from the tank being diverted around both the clay and gravel lenses. The water diversion on top of the clay layer is a direct result of the low permeability of the clay, while the diversion on top of the gravel lens can be attributed to the capillary barrier effect between the gravel and the sand. The water pressures immediately adjacent to the gravel are not large enough to allow for significant amounts of water to enter the large pores in the gravel.

Table 5.2-1. Input Parameters for the Tank Leak Simulation

Parameters	Sand	Clay	Gravel
Domain	Rectangular area 100 m by 15 m, xz alignment, of sand with a lense of sand and a lense of clay (see Figure 5.4-1)		
Porosity			
Saturated Moisture Content θ_s	0.3	0.3	0.3
Residual Moisture Content θ_r	0.0	0.0	0.0
Aqueous saturation			
Function: <u>van Genuchten (1980)</u>			
Fitting Parameter α , cm^{-1}	0.015	0.005	1.0
Fitting Parameter n	2.0	1.5	1.5
Fitting Parameter $m = 1-1/n$	0.5	0.3334	0.3334
Aqueous permeability, k_z			
Saturated permeability (K_s), cm/day	1.0×10^{-11}	1.0×10^{-15}	1.0×10^{-9}
Function: <u>Mualem (1976) with van Genuchten (1980)</u>			
Transport			
Dispersivity (Longitudinal)	0.5	0.5	0.5
Dispersivity (Transverse)	0.05	0.05	0.05
Boundary conditions	Hydraulic gradient boundaries on east and west faces, 0.2 m/day constant infiltration into top boundary.		
Initial saturation	Obtained by simulation of Step I (refer to Exhibit 5.4-1)		
Grid characteristics	One-dimensional uniform finite-difference 200x60 grid, total of 12,000 blocks.		
Nodal spacing, Δx , Δz	1 m uniform horizontal, 0.25 m uniform vertical		
Time increment, Δt	$\Delta t \leq 5$ yr (Step I), $\Delta t \leq 0.1$ yr (Step II)		

Shown in Figure 5.2-4 is the contaminant distribution after 2 years, while Figure 5.2-5 shows the distribution after 5 years. The contaminant leaches from the tank and eventually reaches the water table where it is transported down gradient. Note the contaminant is already moving down-gradient within the capillary zone above the water table.



→ = 1.600e-02

Figure 5.2-2. Flow Field Predicted by STOMP for Tank Leak Simulation

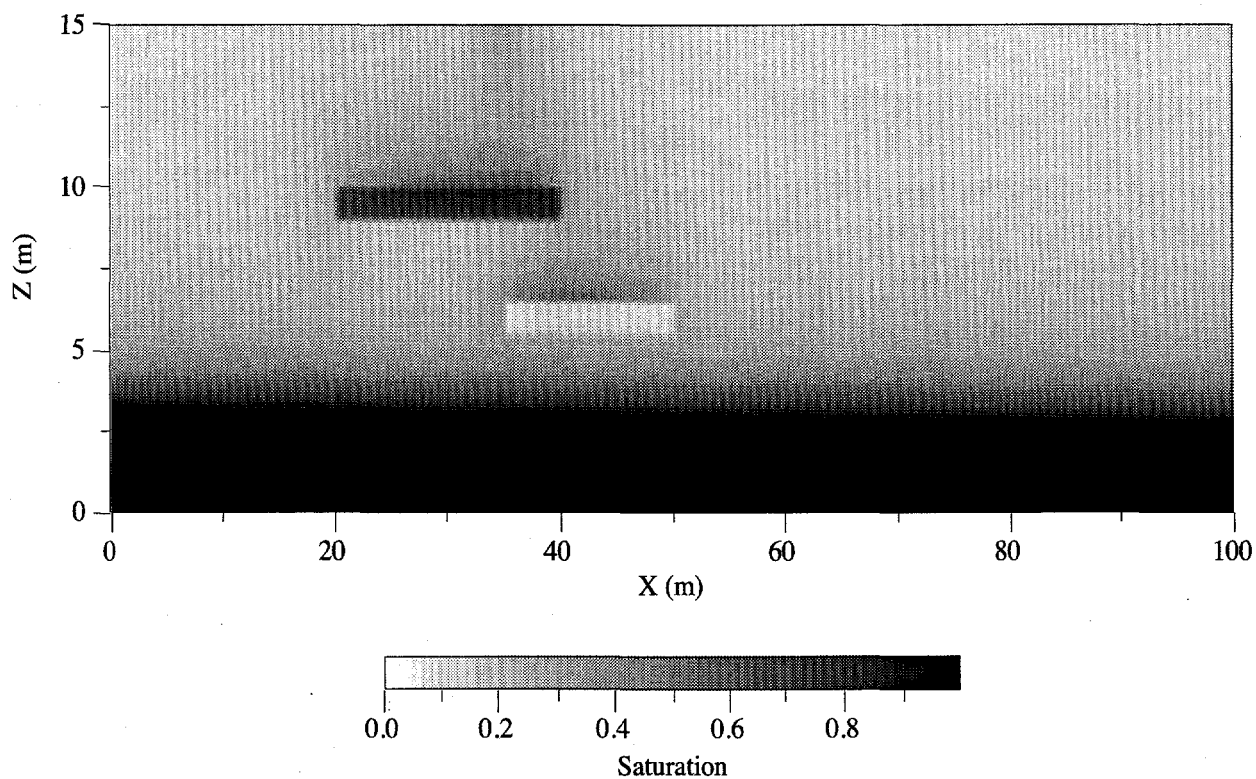


Figure 5.2-3. Water Content Distribution, Showing Leakage From the Tank Being Diverted Around Both the Clay and Gravel Lenses

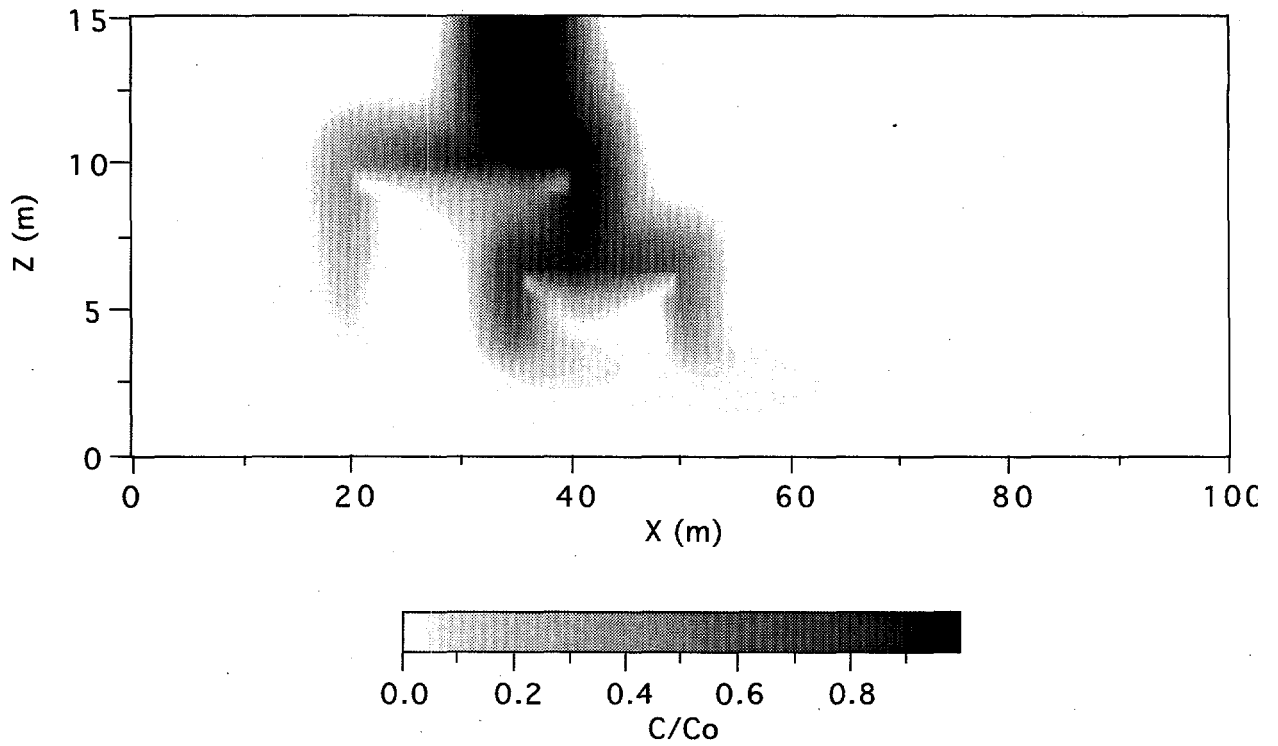


Figure 5.2-4. Contaminant Distribution at $t = 2$ yr for Tank Leak Simulation

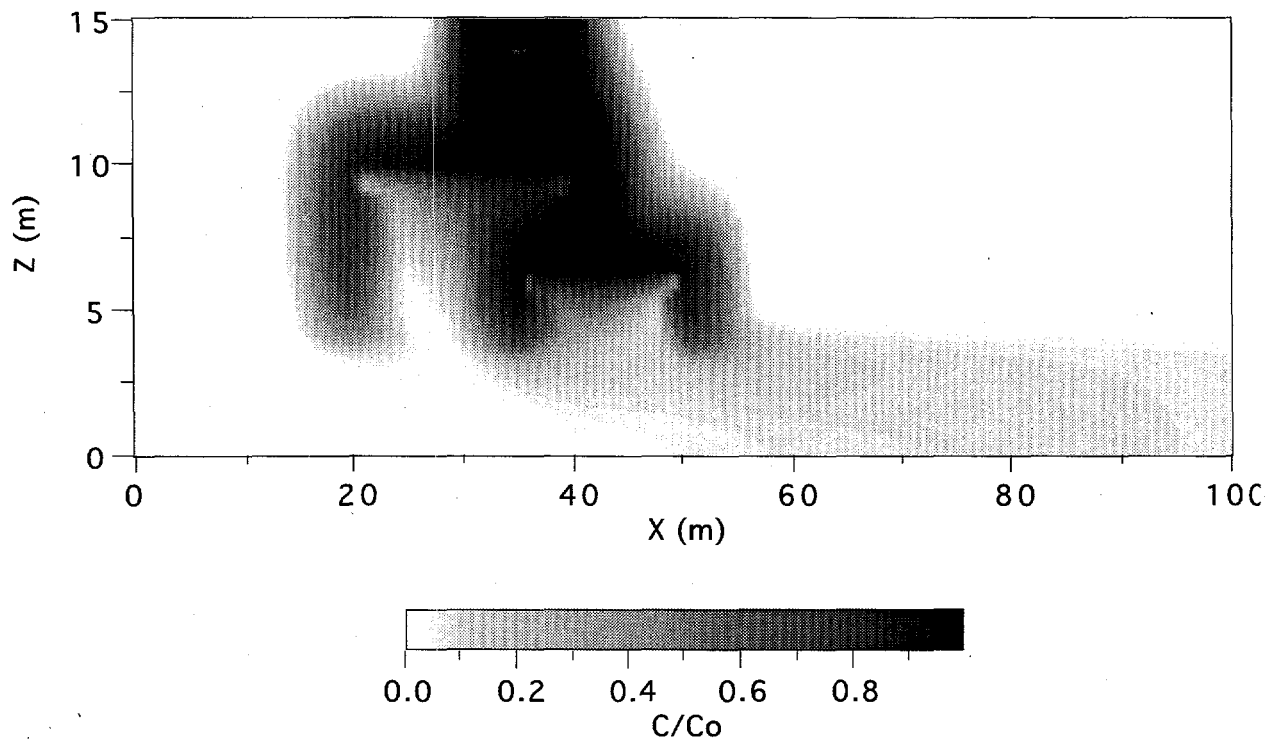


Figure 5.2-5. Contaminant Distribution at $t = 5$ yr for Tank Leak Simulation

5.2.4 Summary

A realistic problem consisting of transport in a heterogeneous, variably saturated aquifer is simulated. The flow field is non-uniform and is at steady-state. The contaminant source is a point source. The results show the effects contrasting unsaturated properties have on transport, as well as transport down-gradient within the capillary zone of the water table.

Exhibit 5.2-1. STOMP Input File for Tank Leak Simulation, Step I

<u>Line</u>	<u>Input File</u>
1	#####
2	# STOMP APPLICATION GUIDE --- Case 5.2 Achieve Initial Conditions (I.C.'s) #
3	#
4	# 2D TRANSPORT IN A HETEROGENEOUS UNSATURATED FLOW FIELD #
5	#
6	# Showcased features: Non-reactive transport #
7	# Solute outflow boundaries #
8	#
9	# Domain: Two-dimensional, heterogeneous, variably saturated #
10	#
11	#####
12	
13	
14	~Simulation Title Card
15	# -----
16	1,
17	Tank leak simulation,
18	M.Oostrom/Nino Aimo,
19	Pacific Northwest Laboratory,
20	December/January 1994,
21	13:00 PM PDT,
22	1,
23	Simulation to establish flow field,
24	
25	
26	--Solution Control Card
27	# -----
28	Normal,
29	Water w/Transport,
30	1,
31	0,hr,200,yr,1,s,5,yr,1.25,8,1.e-06,
32	1,day,1,day,10000,
33	0,
34	
35	
36	--Grid Card
37	# -----
38	Cartesian,
39	200,1,60,
40	0,m,200@0.5,m,
41	0,m,1,m,
42	0,m,60@0.25,m,
43	
44	
45	--Rock/Soil Zonation Card
46	# -----
47	3,
48	Sand,1,200,1,1,1,60,
49	Clay,41,80,1,1,37,40,
50	Gravel,71,100,1,1,23,26,
51	
52	
53	--Mechanical Properties Card
54	# -----
55	Sand,,,0.3,0.3,,,Millington and Quirk,

Exhibit 5.2-1. (Contd)

<u>Line</u>	<u>Input File</u>
56	Clay,,,0.3,0.3,,,Millington and Quirk,
57	Gravel,,,0.3,0.3,,,Millington and Quirk,
58	
59	
60	~Hydraulic Properties Card
61	# -----
62	Sand,1.0e-11,m^2,,,1.0e-11,m^2,
63	Clay,1.0e-15,m^2,,,1.0e-15,m^2,
64	Gravel,1.0e-9,m^2,,,1.0e-9,m^2,
65	
66	
67	~Saturation Function Card
68	# -----
69	Sand,Nonhysteretic van Genuchten,0.015,1/cm,2.0,0.05,,
70	Clay,Nonhysteretic van Genuchten,0.005,1/cm,1.5,0.2,,
71	Gravel,Nonhysteretic van Genuchten,1.0,1/cm,1.5,0.0,,
72	
73	
74	~Aqueous Relative Permeability Card
75	# -----
76	Sand,Mualem,,
77	Clay,Mualem,,
78	Gravel,Mualem,,
79	
80	
81	~Gas Relative Permeability Card
82	# -----
83	Sand,Mualem,,
84	Clay,Mualem,,
85	Gravel,Mualem,,
86	
87	
88	~Solute/Fluid Interaction Card
89	# -----
90	1,
91	Sludge,Conventional,1.0e-9,m^2/s,,1.0e+12,d,
92	0,
93	
94	
95	~Solute/Porous Media Interaction Card
96	# -----
97	Sand,0.5,m,0.05,m,
98	Sludge,0,,
99	Clay,0.5,m,0.05,m,
100	Sludge,0,,
101	Gravel,0.5,m,0.05,m,
102	Sludge,0,,
103	
104	
105	~Initial Conditions Card
106	# -----
107	Gas Pressure, Aqueous Pressure,
108	1,
109	Aqueous Pressure,130704.31,Pa,-50.,1/m,,, -9789.24,1/m,1,200,1,1,1,60,
110	

Exhibit 5.2-1. (Contd)

<u>Line</u>	<u>Input File</u>
111	
112	-Boundary Conditions Card
113	# -----
114	3,
115	Top,Neumann,Sludge Aqueous Conc.,
116	70,71,1,1,60,60,1,
117	0,hr,-0.02,m/day,1.0,1/m^3,
118	West,Hydraulic Gradient,Sludge Outflow,
119	1,1,1,1,1,60,1,
120	0,hr,130704.31,Pa,,,
121	East,Hydraulic Gradient,Sludge Outflow,
122	200,200,1,1,1,60,1,
123	0,hr,125704.31,Pa,,,
124	
125	
126	-Output Options Card
127	# -----
128	4,
129	70,1,60,
130	70,1,59,
131	60,1,59,
132	80,1,59,
133	1,1,yr,m,6,4,6,
134	2,
135	XNC Aqueous Vol,m/day,
136	ZNC Aqueous Vol,m/day,
137	1,
138	5,yr,
139	3,
140	XNC Aqueous Vol,m/day,
141	ZNC Aqueous Vol,m/day,
142	Aqueous Saturation,,
143	

Exhibit 5.2-2. STOMP Input File for Tank Leak Simulation, Step II

<u>Line</u>	<u>Input File</u>
1	#####
2	# STOMP APPLICATION GUIDE --- Case 5.2 Restart from I.C's #
3	# #
4	# 2D TRANSPORT IN A HETEROGENEOUS UNSATURATED FLOW FIELD #
5	# #
6	# Showcased features: Non-reactive transport #
7	# Solute outflow boundaries #
8	# #
9	# Domain: Two-dimensional, heterogeneous, variably saturated #
10	# #
11	#####
12	
13	
14	-Simulation Title Card
15	# -----
16	1,
17	Tank leak simulation,
18	M.Oostrom/Nino Aimo,
19	Pacific Northwest Laboratory,
20	December/January 1994,
21	13:00 PM PDT,
22	1,
23	Transport part of problem, Restart from I.C's.
24	
25	
26	-Solution Control Card
27	# -----
28	Restart,
29	Water w/Transport,
30	1,
31	0,hr,5,yr,1,s,0.1,yr,1.25,8,1.e-06,
32	1,day,1,day,10000,
33	0,
34	
35	
36	-Grid Card
37	# -----
38	Cartesian,
39	200,1,60,
40	0,m,200@0.5,m,
41	0,m,1,m,
42	0,m,60@0.25,m,
43	
44	
45	-Inactive Domain Card
46	# -----
47	1,
48	61,80,1,1,57,60,
49	
50	
51	-Rock/Soil Zonation Card
52	# -----
53	3,
54	Sand,1,200,1,1,1,60,
55	Clay,41,80,1,1,37,40,

Exhibit 5.2-2. (Contd)

<u>Line</u>	<u>Input File</u>
56	Gravel,71,100,1,1,23,26,
57	
58	
59	-Mechanical Properties Card
60	# -----
61	Sand,,,0.3,0.3,,,Millington and Quirk,
62	Clay,,,0.3,0.3,,,Millington and Quirk,
63	Gravel,,,0.3,0.3,,,Millington and Quirk,
64	-Hydraulic Properties Card
65	# -----
66	Sand,1.0e-11,m^2,,,1.0e-11,m^2,
67	Clay,1.0e-15,m^2,,,1.0e-15,m^2,
68	Gravel,1.0e-9,m^2,,,1.0e-9,m^2,
69	
70	
71	-Saturation Function Card
72	# -----
73	Sand,Nonhysteretic van Genuchten,0.015,1/cm,2.0,0.05,,
74	Clay,Nonhysteretic van Genuchten,0.005,1/cm,1.5,0.2,,
75	Gravel,Nonhysteretic van Genuchten,1.0,1/cm,1.5,0.0,,
76	
77	
78	-Aqueous Relative Permeability Card
79	# -----
80	Sand,Mualem,,
81	Clay,Mualem,,
82	Gravel,Mualem,,
83	
84	
85	-Gas Relative Permeability Card
86	# -----
87	Sand,Mualem,,
88	Clay,Mualem,,
89	Gravel,Mualem,,
90	
91	
92	-Solute/Fluid Interaction Card
93	# -----
94	1,
95	Sludge,Conventional,1.0e-9,m^2/s,,1.0e+12,d,
96	0,
97	
98	
99	-Solute/Porous Media Interaction Card
100	# -----
101	Sand,0.5,m,0.05,m,
102	Sludge,0,,
103	Clay,0.5,m,0.05,m,
104	Sludge,0,,
105	Gravel,0.5,m,0.05,m,
106	Sludge,0,,
107	
108	
109	-Initial Conditions Card
110	# -----

Exhibit 5.2-2. (Contd)

<u>Line</u>	<u>Input File</u>
111	
112	
113	-Boundary Conditions Card
114	# -----
115	3,
116	Top,Neumann,Sludge Aqueous Conc.,
117	70,71,1,1,56,56,1,
118	0,hr,-0.02,m/day,1.0,1/m^3,
119	West,Hydraulic Gradient,Sludge Outflow,
120	1,1,1,1,1,60,1,
121	0,hr,130704.31,Pa,,,
122	East,Hydraulic Gradient,Sludge Outflow,
123	200,200,1,1,1,60,1,
124	0,hr,125704.31,Pa,,,
125	
126	-Output Options Card
127	# -----
128	4,
129	70,1,56,
130	70,1,38,
131	120,1,12,
132	196,1,6,
133	1,1,yr,m,6,4,6,
134	1,
135	Solute Conc. Aqueous,Sludge,1/m^3,
136	3,
137	1,yr,
138	2,yr,
139	5,yr,
140	4,
141	Aqueous Saturation,,
142	Aqueous Gauge Pressure,m wh,
143	XNC Aqueous Vol,m/day,
144	ZNC Aqueous Vol,m/day,
145	

Exhibit 5.2-3. STOMP Parameters File for Tank Leak Simulation

<u>Line</u>	<u>Parameters File</u>
1	C-----C
2	C STOMP Parameter File
3	C-----C
4	C
5	C--- Number of lines of simulation notes
6	C Number of execution periods ---
7	C
8	PARAMETER(LNOTES=1, LEPD=1)
9	C
10	C--- Number of nodes in the x or r coordinate direction
11	C Number of nodes in the y or theta coordinate direction
12	C Number of nodes in the z coordinate direction
13	C Number of active nodes
14	C Number of active dimensions
15	C Minimum of (LFX*LFY, LFX*LFZ, LFY*LFZ) ---
16	C
17	PARAMETER(LFX=200, LFY=1, LFZ=60)
18	PARAMETER(LAN=12000, LAD=2, LMNP=60)
19	C
20	C--- Energy equation switch (0 = off, 1 = on)
21	C Water mass equation switch (0 = off, 1 = on)
22	C Air mass equation switch (0 = off, 1 = on)
23	C VOC mass equation switch (0 = off, 1 = on)
24	C Solute transport equation switch (0 = off, 1 = on)
25	C Freezing conditions switch (0 = off, 1 = on) ---
26	C Dissolved salt transport equation switch (0 = off, 1 = on) ---
27	C Dissolved oil transport equation switch (0 = off, 1 = on) ---
28	C
29	PARAMETER(LT=0, LL=1, LG=0, LN=0, LC=1, LFC=0, LS=0, LD=0)
30	C
31	C--- Banded matrix linear equation solver switch (0 = off, 1 = on)
32	C Conjugate gradient linear equation solver switch (0 = off, 1 = on) ---
33	C Unsymmetric-pattern multifrontal package switch (0 = off, 1 = on) ---
34	C
35	PARAMETER(LBD=1, LCG=0, LUM=0)
36	C
37	C--- Number of boundary condition surfaces
38	C Number of boundary condition times ---
39	C
40	PARAMETER(LBC=122, LBTM=1)
41	C
42	C--- Number of sources
43	C Number of source times ---
44	C
45	PARAMETER(LSR=1, LSTM=1)
46	C
47	C--- Number of rock/soil types
48	C Number of solutes
49	C
50	PARAMETER(LRC=3, LSOLU=1)
51	C
52	C--- Number of reference nodes
53	C Number of print times
54	C Number of integration surfaces ---
55	C

Exhibit 5.2-3. (Contd)

<u>Line</u>	<u>Parameters File</u>
56	PARAMETER(LREF=4, LPTM=3, LSF=1)
57	C
58	C--- Number saturation and relative permeability table entries
59	C Number of hysteretic scanning paths
60	C Number of chemical reactions
61	C
62	PARAMETER(LTBL=1, LPATH=7, LCHEM=1)
63	C
64	C--- Computed Parameters ---
65	C
66	PARAMETER(LUK=LT+LL+LG+LN+LS+LD, LPH=LL+LG+LN, LCMP=LL+LS+LD)
67	PARAMETER(LFX=LFX*LFY, LFYZ=LFY*LFZ, LFZX=LFZ*LFX)
68	PARAMETER(LFD=LFX*LFY*LFZ)
69	PARAMETER(LNE=(LUK*LUK*(7*LFD-2*LFX-2*LFY-2*LFZ))*LUM)
70	PARAMETER(LHBW=LUK*LMNP+LUK-1)
71	PARAMETER(LJA=LBD + LCG*LAN*LUK + LUM*LAN*LUK)
72	PARAMETER(LJB=(2*LAN*LUK)**LUM, LJC=LAN**LUM)
73	PARAMETER(LJD=LBD*(3*LHBW+1) + LCG*LAN*LUK + LUM*6*LNE)
74	PARAMETER(LJE=LBD*LAN*LUK + LCG*((2*LAD+1)*LUK+2*LAD) + LUM)
75	PARAMETER(LJF=LAN*LUK)
76	PARAMETER(LJG=LBD*(3*LHBW+1) + LCG*LAN*LUK + LUM)
77	PARAMETER(LJH=LBD*LAN*LUK + LCG*(2*LAD+1) + LUM)
78	PARAMETER(LJJ=LBD*LAN*LUK + LCG + LUM)
79	PARAMETER(LSV=LUK+2, LSFV=2*LUK+1)
80	PARAMETER(LSX=(LFX+1)*LFY*LFZ)
81	PARAMETER(LSY=LFX*(LFY+1)*LFZ)
82	PARAMETER(LSZ=LFX*LFY*(LFZ+1))
83	PARAMETER(LFDT=LFD**LT, LFDL=LFD**LL, LFDG=LFD**LG, LFDN=LFD**LN)
84	PARAMETER(LFDC=LFD**LC, LFDI=LFD**LFC, LFDS=LFD**LS, LFDD=LFD**LD)
85	PARAMETER(LSXT=LSX**LT, LSXL=LSX**LL, LSXG=LSX**LG, LSXN=LSX**LN)
86	PARAMETER(LSXC=LSX**LC, LSXS=LSX**LS, LSXD=LSX**LD)
87	PARAMETER(LSYT=LSY**LT, LSYL=LSY**LL, LSYG=LSY**LG, LSYN=LSY**LN)
88	PARAMETER(LSYC=LSY**LC, LSYS=LSY**LS, LSYD=LSY**LD)
89	PARAMETER(LSZT=LSZ**LT, LSZL=LSZ**LL, LSZG=LSZ**LG, LSZN=LSZ**LN)
90	PARAMETER(LSZC=LSZ**LC, LSZS=LSZ**LS, LSZD=LSZ**LD)
91	PARAMETER(LRCT=LRC**LT, LRCL=LRC**LL, LRCG=LRC**LG, LRCN=LRC**LN)
92	PARAMETER(LRCC=LRC**LC, LRCI=LRC**LFC, LRCS=LRC**LS, LRCD=LRC**LD)
93	PARAMETER(LBCT=LBC**LT, LBCL=LBC**LL, LBCG=LBC**LG, LBCN=LBC**LN)
94	PARAMETER(LBCC=LBC**LC, LBCI=LBC**LFC, LBCC=LBC**LS, LBCC=LBC**LD)
95	PARAMETER(LBCU=LUK+LPH+LT+2, LBCV=LBCU+LSOLU)
96	PARAMETER(LOUPV=200+11*(LSOLU))
97	PARAMETER(LJI=LBD*LAN*LUK + LCG + (3*LNE+23*LFD*LUK+9)*LUM)
98	PARAMETER(LSCHR=18)
99	

5.3 Two-Phase, One-Dimensional Infiltration

Touma and Vauclin (1986) demonstrated, both experimentally and numerically, the effects of air flow on water infiltration in a 93.5-cm column of soil. Touma and Vauclin applied three types of boundary conditions to the top of the soil column: 1) positive time-constant liquid head, 2) positive time-constant aqueous-phase liquid flux less than the saturated soil hydraulic conductivity, and 3) positive time-constant aqueous-phase liquid flux greater than the saturated hydraulic conductivity. In this section, the positive time-constant aqueous-phase liquid head (referred to as ponded infiltration) simulations of Touma and Vauclin (1986) are repeated using STOMP to demonstrate the impact of air flow on water infiltration rates and compare solutions with the previously published experimental and numerical results. Two cases are described: a column open to air flow at the base, and a column closed at the base so that air must flow out the top of the column as it is displaced by infiltrating water.

Problem Features: 5.3

- Water and Water-Air modes
- one dimensional (z)
- unsaturated infiltration
- single- and two-phase flow
- homogeneous, isotropic
- uniform Cartesian grid
- van Genuchten function
- tabular permeability input
- comparison to published experimental data and numerical solution

5.3.1 Problem Domain and Input Parameters

The problem domain is a column of soil of height $L = 93.5$ cm for which hydraulic properties were experimentally determined by Touma and Vauclin (1986). Input parameters are summarized in Table 5.3-1. The experimental data for the relationship between capillary pressure head and water content were statistically fit by Touma and Vauclin (1986) with the van Genuchten (1980) analytical expression shown in Figure 5.3-1(a). Touma and Vauclin fitted analytical expressions to the experimental data to describe aqueous and gas relative permeability relationships (functions specified in Table 5.3-1). Because the expressions used by Touma and Vauclin were not available in STOMP, the tabular option was used to specify the relative permeabilities using 33 points generated from Touma and Vauclin's expressions. The relationships between aqueous and gas relative permeability and aqueous saturation are shown in Figure 5.3-1(b). No distinction was made between drainage and infiltration in this expression (i.e., hysteresis was not modeled).

The first case is for an open column, which represents the traditional single-phase solution for water infiltration neglecting air-flow effects. The STOMP input file for this problem is provided in Exhibit 5.3-1. The Water operational mode (Mode 1) is used in this solution. The top

Table 5.3-1. Input Parameters for the Touma and Vauclin (1986) Infiltration Problems

Domain	Vertical column of depth 93.5 cm
Porosity	Saturated Moisture Content $\theta_s = 0.312$ Residual Moisture Content $\theta_r = 0.0265$
Aqueous saturation	Function: <u>van Genuchten</u> (1980) Fitting Parameter $\alpha = 0.044 \text{ cm}^{-1}$ Fitting Parameter $n = 2.2$
Aqueous permeability, k_a	Saturated permeability: 15.4 cm/hr Relative permeability function: Tabular, with 33 points computed from analytical expression fitted to experimental data by Touma and Vauclin (1986): $k_{rs} = A_w \theta_w^B$ where $A_w = 1176.2012$ $B_w = 6.07$
Gas permeability, k_g	Function: Tabular, with 33 points computed from analytical expression fitted to experimental data by Touma and Vauclin (1986): $k_{rs} = \frac{A_a}{A_a + \psi^{B_a}}$ where $A_a = 3.86 \times 10^{-5}$ $B_a = -2.4$
Boundary conditions	Aqueous boundaries: ponded condition equivalent to a constant hydraulic head of 2.3 cm at top of the column and base held constant at initial saturation. Gas boundaries: constant atmospheric pressure (101,325 Pa) at top of column, and either constant 101,325 Pa or zero-flux for base of column.
Initial saturation	Reached by draining the saturated column to the static equilibrium corresponding to a piezometric level at 120 cm below the surface (top) of the column.
Grid characteristics	One-dimensional uniform finite-difference grid with 94 blocks.
Nodal spacing, Δz	1 cm
Time increment, Δt	1 s

boundary is specified as a Dirichlet condition equivalent to a constant hydraulic head of 2.3 cm while the lower boundary is specified as a Dirichlet condition equal to the initial condition (Exhibit 5.3-1, Boundary Conditions Card, lines 84-91). Touma and Vauclin (1986) specified that the initial condition of the soil column was reached by draining the saturated column to the static

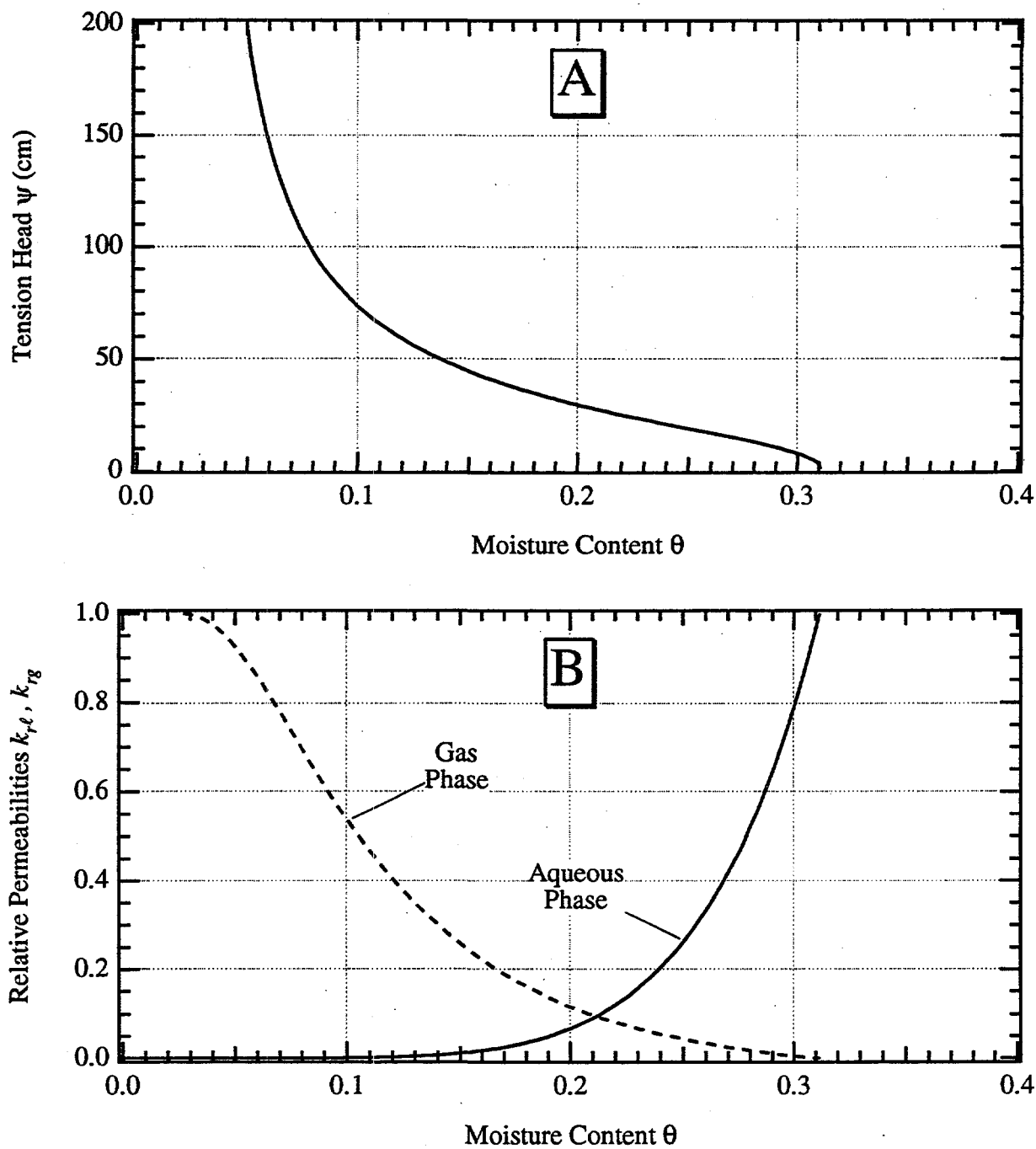


Figure 5.3-1. Moisture Retention and Relative Permeability Functions for the Two Phase, One Dimensional Infiltration Problem: A) Relationship Between Volumetric Moisture Content and Tension Head, B) Relationship Between Volumetric Water Content and Aqueous and Gas Relative Permeabilities

equilibrium corresponding to a piezometric level at 120 cm below the top of the column. The initial hydrologic conditions are specified as a uniform gas pressure of 101,325 Pa and an aqueous pressure that is computed directly from the van Genuchten relation for a zero hydraulic gradient (pressure head and elevation head equal throughout). Examine the actual input card (Exhibit 5.3-1, Initial Conditions Card, lines 78-82) to see how the input condition is specified using the gradient feature of the Initial Conditions card. The STOMP parameters file used for this simulation is shown in Exhibit 5.3-2.

The second simulation includes the effects of air flow in the column. The Water-Air mode (mode 2) is used and the gas boundary conditions are defined to address this issue. Exhibit 5.3-3 shows the STOMP input file for this simulation. Note that the STOMP parameters file shown in Exhibit 5.3-2 for the open column problem can be used for the bounded column problem with one modification (changing air mass equation switch, parameter LG, from 0 to 1 in line 30 of Exhibit 5.3-2). A longer time is simulated than for the open column case (1.2 hour rather than 0.4 hour) because the inclusion of air flow slows the wetting front greatly, as reported by Touma and Vauclin (1986). Touma and Vauclin also reported that the air-entry pressure was estimated to be 14 cm for this problem. Hence, the gas pressure at the upper boundary is specified as the pressure equivalent of the liquid pressure boundary (2.3 cm) plus the air-entry pressure (14.0 cm), or 101,550.25 Pa (Exhibit 5.3-3, Boundary Conditions card, lines 122-129).

5.3.2 Simulations

The aqueous moisture content profiles for the open-column case, which represents traditional single-phase infiltration models, are depicted in Figure 5.3-2. The aqueous moisture content profiles for the bounded-column case are depicted in Figure 5.3-2. Comparing the two figures, we observe as Touma and Vauclin (1986) reported that the rate of advance of the wetting front is drastically reduced when air cannot escape. Notice also the reduction in the maximum saturation of the water content profiles from $0.312 \text{ cm}^3/\text{cm}^3$ in the open-column case to approximately $0.27 \text{ cm}^3/\text{cm}^3$ in the bounded-column case, an effect caused by the flow of escaping air. Finally, we note that the wetting fronts shown in Figure 5.3-2 for the bounded-column case are less steep than for the open-column case shown in Figure 5.3-2.

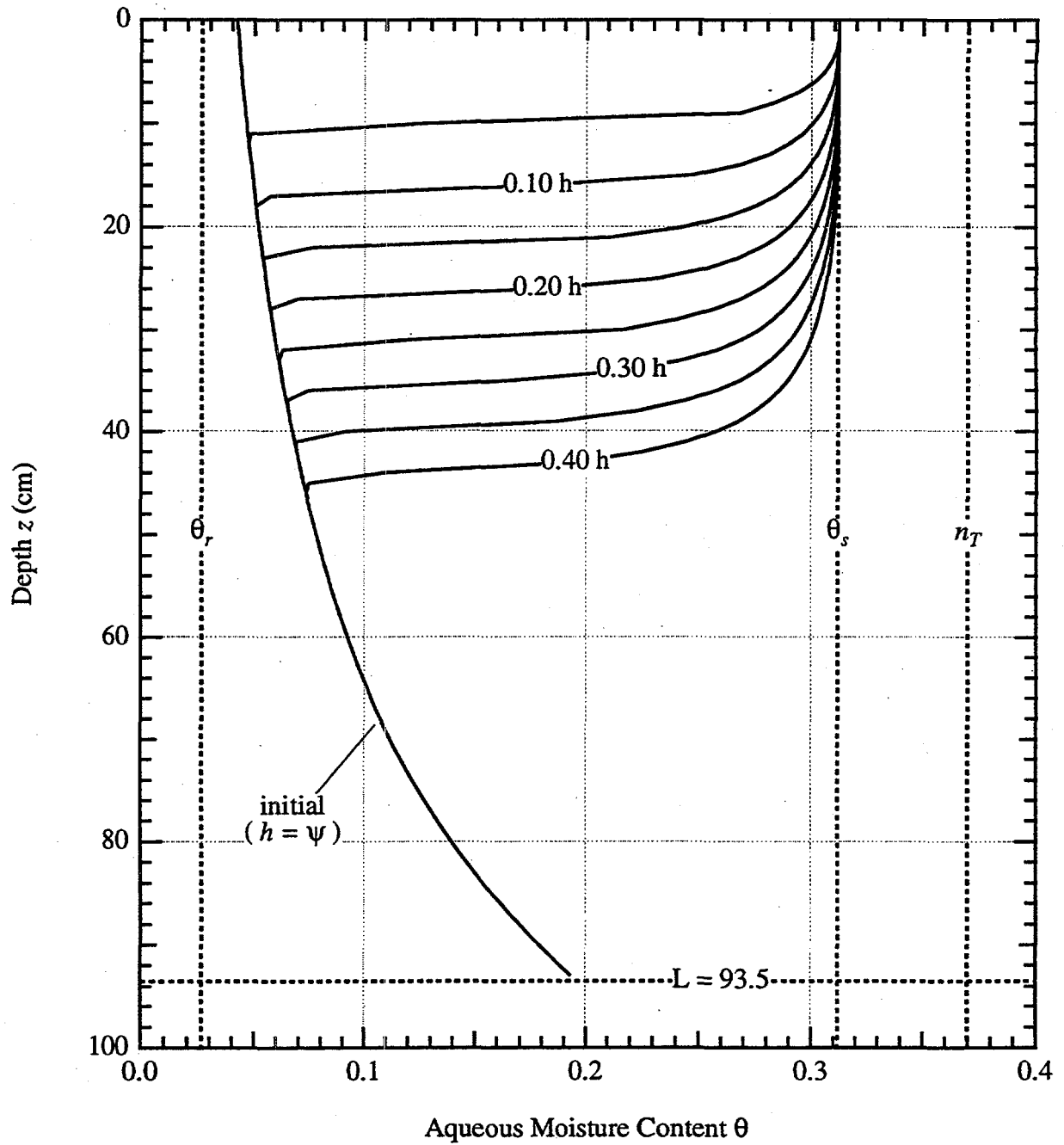


Figure 5.3-2. Aqueous Moisture Content Profiles Predicted by STOMP for Ponded Infiltration in the One-Dimensional, Two-Phase Infiltration Problem: Open Column

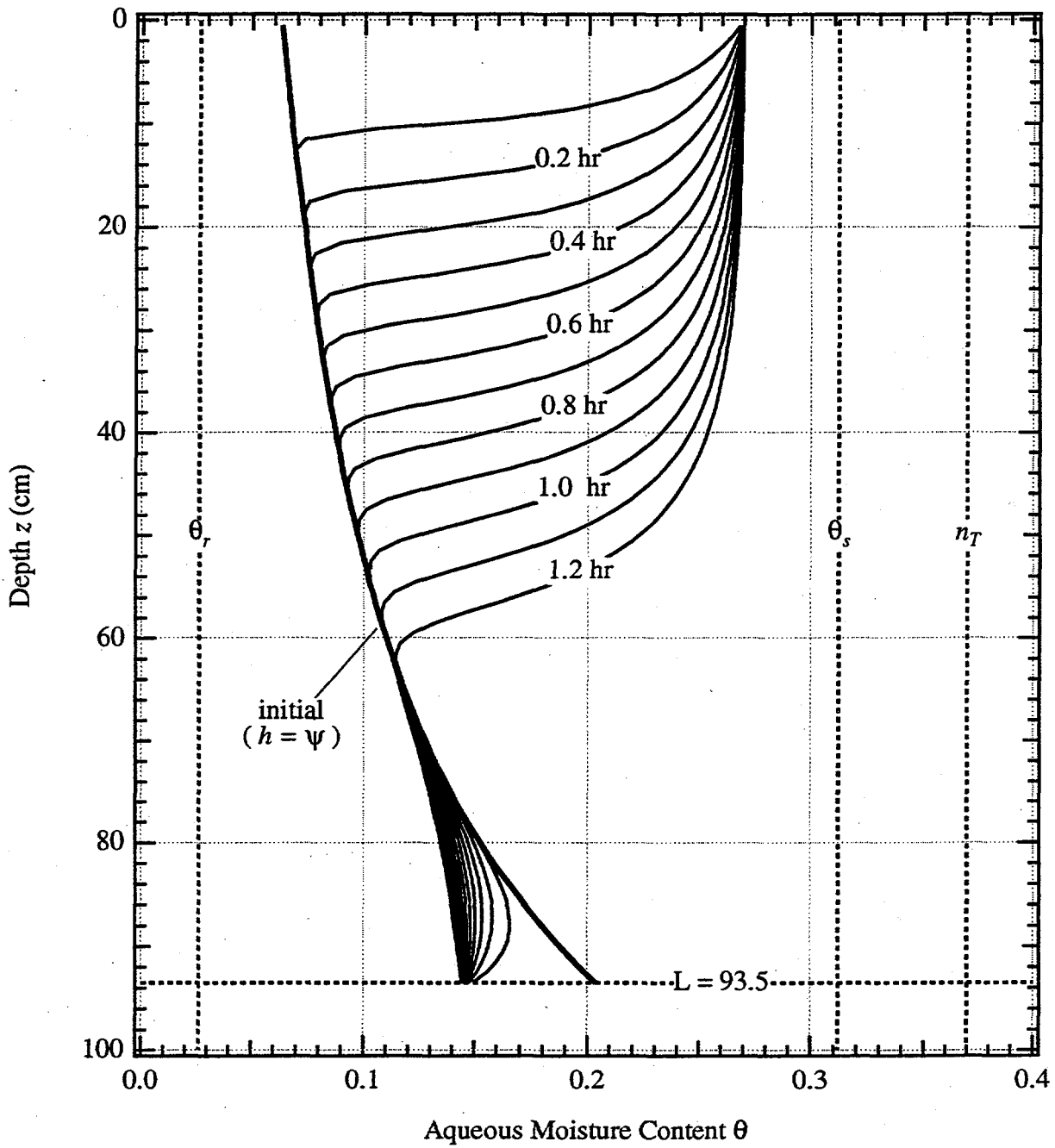


Figure 5.3-3. Aqueous Moisture Content Profiles Predicted by STOMP for Poned Infiltration in the One-Dimensional, Two-Phase Infiltration Problem: Bounded Column

5.3.3 Analysis

Comparing with graphical results reported in Touma and Vauclin (1986) and repeated here as Figure 5.3-4, we observe qualitatively that STOMP appears to predict a slightly slower infiltration front advance in the open column than Touma and Vauclin did (at $t = 1.20$ h, Touma and Vauclin show a furthest advance of approximately 50 cm, while STOMP is roughly 0.45 cm). STOMP predicted similar infiltration rates for the bounded column case. Touma and Vauclin did not report the reduction in saturation at the base of the column in the bounded column case due to gas pressure increase that STOMP shows in Figure 5.3-3.

5.3.4 Summary

Solutions for one-dimensional (vertical) infiltration in open and bounded columns were simulated, and the difference in wetting fronts with respect to time shown. The results obtained for these cases using STOMP are compared favorably with the experimental and numerically simulated results reported in Touma and Vauclin (1986) and the numerical solution obtained with MSTs by Nichols and White (1993).

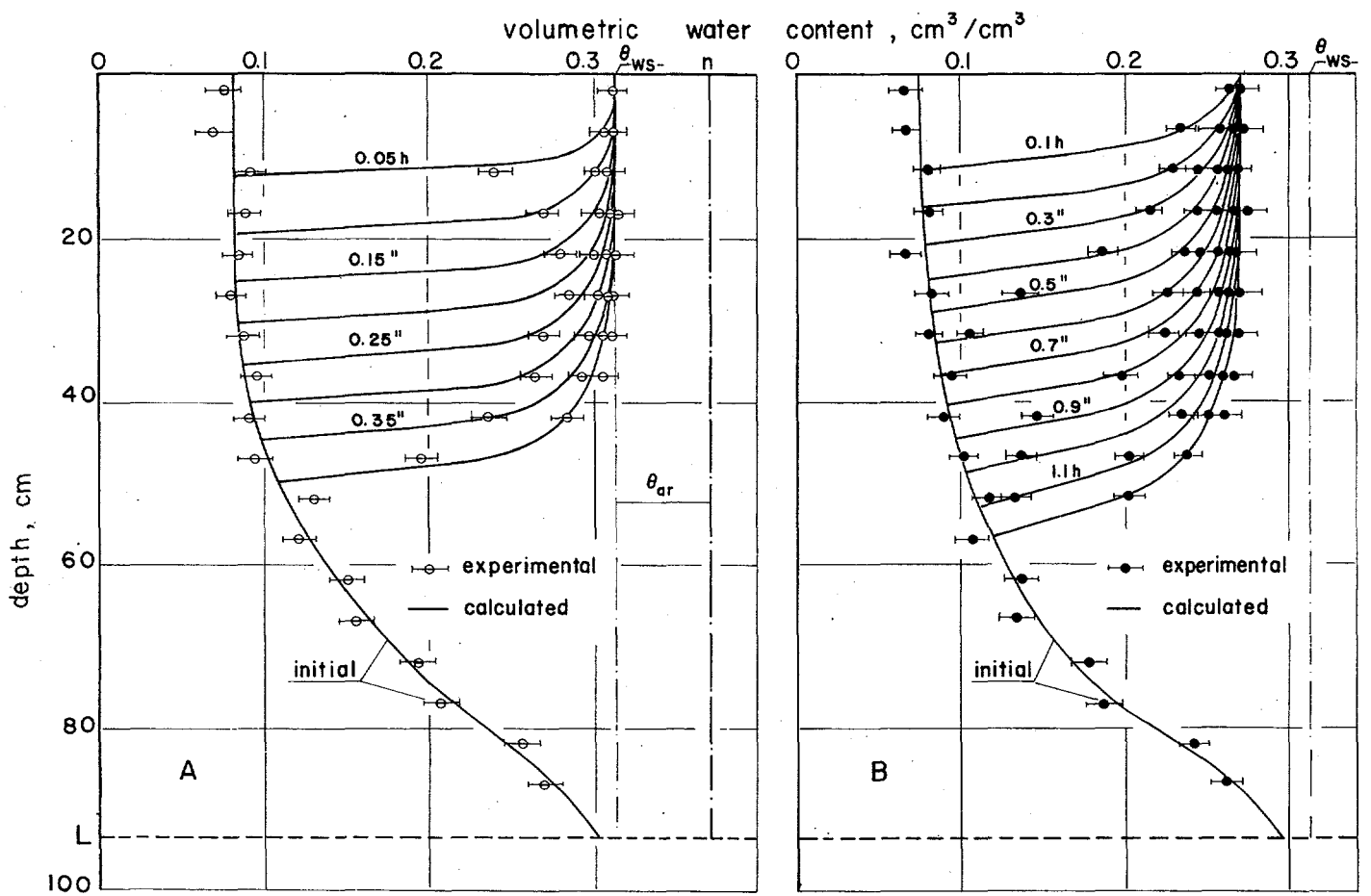


Figure 5.3-4. Pondered infiltration: water content profiles in the open (a) and bounded (b) columns. Horizontal bars represent experimental uncertainties (SOURCE: Touma and Vauclin (1986))

Exhibit 5.3-1. STOMP Input File for Two-Phase Infiltration Problem: Open Column

<u>Line</u>	<u>Input File</u>
1	-Simulation Title Card
2	1,
3	Touma & Vauclin (1986) 1D Poned Boundary Infiltration in Open Column,
4	W. E. Nichols,
5	Pacific Northwest Laboratory,
6	August 10 1995,
7	4:15:00 PM PDT,
8	3,
9	Simulation of infiltration in an open column after numerical and experimental
10	results reported in Touma and Vauclin (1986). Initial conditions are computed
11	from the zero-hydraulic-gradient condition. The Water mode is used.
12	
13	-Solution Control Card
14	Normal,
15	Water,
16	1,
17	0.0,hr,0.40,hr,1.0,s,1.0,s,1.5,8,1.0e-6,
18	1.0,hr,1.0,hr,2000,
19	1,
20	Aqueous Relative Permeability,Geometric,
21	
22	-Grid Card
23	Uniform Cartesian,
24	1,1,94,
25	1.0,cm,
26	1.0,cm,
27	1.0,cm,
28	
29	-Rock/Soil Zonation Card
30	1,
31	Sand,1,1,1,1,1,94,
32	
33	-Mechanical Properties Card
34	Sand,2650.0,kg/m ³ ,0.370,0.312,,,
35	
36	-Hydraulic Properties Card
37	Sand,,,,,4.2778e-3,hc cm/s,
38	
39	-Saturation Function Card
40	Sand,Nonhysteretic van Genuchten,0.044,1/cm,2.2,0.0,,
41	
42	-Aqueous Relative Permeability Card
43	Sand,Tabular,33,
44	3.5026E-09,3.1593E-07,
45	0.01225919,6.7082E-07,
46	0.02977233,1.7099E-06,
47	0.04728546,3.8458E-06,
48	0.0647986,7.8611E-06,
49	0.08231173,1.4901E-05,
50	0.117338,4.5067E-05,
51	0.15236427,0.00011488,
52	0.18739054,0.00025837,
53	0.22241681,0.00052812,
54	0.25744308,0.00100111,
55	0.29246935,0.0017854,

Exhibit 5.3-1. (Contd)

<u>Line</u>	<u>Input File</u>
56	0.32749562,0.00302769,
57	0.36252189,0.00492173,
58	0.39754816,0.00771754,
59	0.43257443,0.01173155,
60	0.4676007,0.01735761,
61	0.50262697,0.02507879,
62	0.53765324,0.03548017,
63	0.57267951,0.04926245,
64	0.60770578,0.06725641,
65	0.64273205,0.09043837,
66	0.67775832,0.11994642,
67	0.71278459,0.15709761,
68	0.74781086,0.20340604,
69	0.78283713,0.26060184,
70	0.8178634,0.330651,
71	0.85288967,0.41577624,
72	0.88791594,0.51847864,
73	0.92294221,0.64156028,
74	0.95796848,0.78814774,
75	0.99299475,0.96171657,
76	1,1,
77	
78	-Initial Conditions Card
79	Gas Pressure,Aqueous Pressure,
80	2,
81	Gas Pressure,101325.0,Pa,0.0,1/m,0.0,1/m,0.0,1/m,1,1,1,1,1,94,
82	Aqueous Pressure,98729.71741,Pa,0.0,1/cm,0.0,1/cm,-97.935192,1/cm,1,1,1,1,1,94,
83	
84	-Boundary Conditions Card
85	2,
86	Top,Dirichlet Aqueous,
87	1,1,1,1,94,94,1,
88	0.0,hr,101550.25,Pa,
89	Bottom,Dirichlet Aqueous,
90	1,1,1,1,1,1,1,
91	0.0,hr,98778.685,Pa,
92	
93	-Output Control Card
94	1,
95	1,1,94,
96	1,1,hr,cm,3,5,5,
97	4,
98	Aqueous Pressure,Pa,
99	Aqueous Saturation,,
100	Aqueous Moisture Content,,
101	Aqueous Relative Permeability,,
102	9,
103	0.00,hr,
104	0.05,hr,
105	0.10,hr,
106	0.15,hr,
107	0.20,hr,
108	0.25,hr,
109	0.30,hr,
110	0.35,hr,

Exhibit 5.3-1. (Contd)

<u>Line</u>	<u>Input File</u>
111	0.40,hr,
112	3,
113	Aqueous Pressure,Pa,
114	Aqueous Saturation,,
115	Aqueous Moisture Content,,
116	

Exhibit 5.3-2. STOMP Parameters File for Two-Phase Infiltration Problem: Open Column

<u>Line</u>	<u>Parameters File</u>
1	C-----C
2	C STOMP Parameter File
3	C Touma and Vauclin Problems (Application Guide Section 5.5)
4	C-----C
5	C
6	C--- Number of lines of simulation notes
7	C Number of execution periods ---
8	C
9	PARAMETER(LNOTES=10, LEPD=10)
10	C
11	C--- Number of nodes in the x or r coordinate direction
12	C Number of nodes in the y or theta coordinate direction
13	C Number of nodes in the z coordinate direction
14	C Number of active nodes
15	C Number of active dimensions
16	C Minimum of (LFX*LFY, LFX*LFZ, LFY*LFZ) ---
17	C
18	PARAMETER(LFX=1, LFY=1, LFZ=94)
19	PARAMETER(LAN=94, LAD=1, LMNP=1)
20	C
21	C--- Energy equation switch (0 = off, 1 = on)
22	C Water mass equation switch (0 = off, 1 = on)
23	C Air mass equation switch (0 = off, 1 = on)
24	C VOC mass equation switch (0 = off, 1 = on)
25	C Solute transport equation switch (0 = off, 1 = on)
26	C Freezing conditions switch (0 = off, 1 = on) ---
27	C Dissolved salt transport equation switch (0 = off, 1 = on) ---
28	C Dissolved oil transport equation switch (0 = off, 1 = on) ---
29	C
30	PARAMETER(LT=0, LL=1, LG=0, LN=0, LC=0, LFC=0, LS=0, LD=0)
31	C
32	C--- Banded matrix linear equation solver switch (0 = off, 1 = on)
33	C Conjugate gradient linear equation solver switch (0 = off, 1 = on) ---
34	C Unsymmetric-pattern multifrontal package switch (0 = off, 1 = on) ---
35	C
36	PARAMETER(LBD=1, LCG=0, LUM=0)
37	C
38	C--- Number of boundary condition surfaces
39	C Number of boundary condition times ---
40	C
41	PARAMETER(LBC=2, LBTM=1)
42	C
43	C--- Number of sources
44	C Number of source times ---
45	C
46	PARAMETER(LSR=1, LSTM=1)
47	C
48	C--- Number of rock/soil types
49	C Number of solutes
50	C
51	PARAMETER(LRC=1, LSOLU=1)
52	C
53	C--- Number of reference nodes
54	C Number of print times
55	C Number of integration surfaces ---

Exhibit 5.3-2. (Contd)

<u>Line</u>	<u>Parameters File</u>
56	C
57	PARAMETER(LREF=10, LPTM=13, LSF=10)
58	C
59	C--- Number saturation and relative permeability table entries
60	C Number of hysteretic scanning paths
61	C Number of chemical reactions
62	C
63	PARAMETER(LTBL=66, LPATH=3, LCHEM=1)
64	C
65	C--- Computed Parameters ---
66	C
67	PARAMETER(LUK=LT+LL+LG+LN+LS+LD, LPH=LL+LG+LN, LCMP=LL+LS+LD)
68	PARAMETER(LFX=LFX*LFY, LFY=LFY*LFZ, LFZX=LFZ*LFX)
69	PARAMETER(LFD=LFX*LFY*LFZ)
70	PARAMETER(LNE=(LUK*LUK*(7*LFD-2*LFX-2*LFY-2*LFZ))*LUM)
71	PARAMETER(LHBW=LUK*LMNP+LUK-1)
72	PARAMETER(LJA=LBD + LCG*LAN*LUK + LUM*LAN*LUK)
73	PARAMETER(LJB=(2*LAN*LUK)**LUM, LJC=LAN**LUM)
74	PARAMETER(LJD=LBD*(3*LHBW+1) + LCG*LAN*LUK + LUM*6*LNE)
75	PARAMETER(LJE=LBD*LAN*LUK + LCG*((2*LAD+1)*LUK+2*LAD) + LUM)
76	PARAMETER(LJF=LAN*LUK)
77	PARAMETER(LJG=LBD*(3*LHBW+1) + LCG*LAN*LUK + LUM)
78	PARAMETER(LJH=LBD*LAN*LUK + LCG*(2*LAD+1) + LUM)
79	PARAMETER(LJJ=LBD*LAN*LUK + LCG + LUM)
80	PARAMETER(LSV=LUK+2, LSFV=2*LUK+1)
81	PARAMETER(LSX=(LFX+1)*LFY*LFZ)
82	PARAMETER(LSY=LFX*(LFY+1)*LFZ)
83	PARAMETER(LSZ=LFX*LFY*(LFZ+1))
84	PARAMETER(LFDT=LFD**LT, LFDL=LFD**LL, LFDG=LFD**LG, LFDN=LFD**LN)
85	PARAMETER(LFDC=LFD**LC, LFDI=LFD**LFC, LFDS=LFD**LS, LFDD=LFD**LD)
86	PARAMETER(LSXT=LSX**LT, LSXL=LSX**LL, LSXG=LSX**LG, LSXN=LSX**LN)
87	PARAMETER(LSXC=LSX**LC, LSXS=LSX**LS, LSXD=LSX**LD)
88	PARAMETER(LSYT=LSY**LT, LSYL=LSY**LL, LSYG=LSY**LG, LSYN=LSY**LN)
89	PARAMETER(LSYC=LSY**LC, LSYS=LSY**LS, LSYD=LSY**LD)
90	PARAMETER(LSZT=LSZ**LT, LSZL=LSZ**LL, LSZG=LSZ**LG, LSZN=LSZ**LN)
91	PARAMETER(LSZC=LSZ**LC, LSZS=LSZ**LS, LSZD=LSZ**LD)
92	PARAMETER(LRCT=LRC**LT, LRCL=LRC**LL, LRCG=LRC**LG, LRCN=LRC**LN)
93	PARAMETER(LRCC=LRC**LC, LRCL=LRC**LFC, LRCS=LRC**LS, LRCD=LRC**LD)
94	PARAMETER(LBCT=LBC**LT, LBCL=LBC**LL, LBCG=LBC**LG, LBCN=LBC**LN)
95	PARAMETER(LBCC=LBC**LC, LBCI=LBC**LFC, LBCS=LBC**LS, LBCL=LBC**LD)
96	PARAMETER(LBCU=LUK+LPH+LT+2, LBCV=LBCU+LSOLU)
97	PARAMETER(LOUPV=200+11*(LSOLU))
98	PARAMETER(LJI=LBD*LAN*LUK + LCG + (3*LNE+23*LFD*LUK+9)*LUM)
99	PARAMETER(LSCHR=18)
100	

Exhibit 5.3-3. STOMP Input File for Two-Phase Infiltration Problem: Bounded Column

<u>Line</u>	<u>Input File</u>
1	~Simulation Title Card
2	1,
3	Touma & Vauclin (1986) 1D Poned Boundary Infiltration in Bounded Column,
4	W. E. Nichols,
5	Pacific Northwest Laboratory,
6	August 17 1995,
7	12:15:00 AM PDT,
8	3,
9	Simulation of infiltration in a bounded column after numerical and experimental
10	results reported in Touma and Vauclin (1986). Initial conditions are computed
11	from the zero-hydraulic-gradient condition. The Water-Air mode is used.
12	
13	~Solution Control Card
14	Normal,
15	Water-Air,
16	1,
17	0.0,hr,1.20,hr,1.0,s,1.0,s,1.5,8,1.0e-6,
18	2.,hr,2.,hr,5000,
19	Zero,
20	Zero,
21	1,
22	Aqueous Relative Permeability,Geometric,
23	
24	~Grid Card
25	Uniform Cartesian,
26	1,1,94,
27	1.0,cm,
28	1.0,cm,
29	1.0,cm,
30	
31	~Rock/Soil Zonation Card
32	1,
33	Sand,1,1,1,1,1,94,
34	
35	~Mechanical Properties Card
36	Sand,2650.0,kg/m^3,0.370,0.312,,,
37	
38	~Hydraulic Properties Card
39	Sand,,,,,4.2778e-3,hc cm/s,
40	
41	~Saturation Function Card
42	Sand,Nonhysteretic van Genuchten,0.044,1/cm,2.2,0.08494,,
43	
44	~Aqueous Relative Permeability Card
45	Sand,Tabular,33,
46	3.5026E-09,3.1593E-07,
47	0.01225919,6.7082E-07,
48	0.02977233,1.7099E-06,
49	0.04728546,3.8458E-06,
50	0.0647986,7.8611E-06,
51	0.08231173,1.4901E-05,
52	0.117338,4.5067E-05,
53	0.15236427,0.00011488,
54	0.18739054,0.00025837,
55	0.22241681,0.00052812,

Exhibit 5.3-3. (Contd)

<u>Line</u>	<u>Input File</u>
56	0.25744308,0.00100111,
57	0.29246935,0.0017854,
58	0.32749562,0.00302769,
59	0.36252189,0.00492173,
60	0.39754816,0.00771754,
61	0.43257443,0.01173155,
62	0.4676007,0.01735761,
63	0.50262697,0.02507879,
64	0.53765324,0.03548017,
65	0.57267951,0.04926245,
66	0.60770578,0.06725641,
67	0.64273205,0.09043837,
68	0.67775832,0.11994642,
69	0.71278459,0.15709761,
70	0.74781086,0.20340604,
71	0.78283713,0.26060184,
72	0.8178634,0.330651,
73	0.85288967,0.41577624,
74	0.88791594,0.51847864,
75	0.92294221,0.64156028,
76	0.95796848,0.78814774,
77	0.99299475,0.96171657,
78	1,1,
79	
80	-Gas Relative Permeability Card
81	Sand,Tabular,33,
82	1,1,
83	0.98774081,0.99999139,
84	0.97022767,0.99994918,
85	0.95271454,0.99987151,
86	0.9352014,0.99975797,
87	0.91768827,0.99960795,
88	0.882662,0.99919528,
89	0.84763573,0.99862545,
90	0.81260946,0.99788751,
91	0.77758319,0.99696733,
92	0.74255692,0.99584706,
93	0.70753065,0.99450437,
94	0.67250438,0.99291148,
95	0.63747811,0.99103385,
96	0.60245184,0.98882835,
97	0.56742557,0.98624081,
98	0.5323993,0.98320258,
99	0.49737303,0.97962579,
100	0.46234676,0.9753964,
101	0.42732049,0.97036419,
102	0.39229422,0.96432763,
103	0.35726795,0.95701052,
104	0.32224168,0.94802483,
105	0.28721541,0.93680881,
106	0.25218914,0.92251973,
107	0.21716287,0.90383668,
108	0.1821366,0.87857318,
109	0.14711033,0.84284783,
110	0.11208406,0.78910152,

Exhibit 5.3-3. (Contd)

<u>Line</u>	<u>Input File</u>
111	0.07705779,0.70059708,
112	0.04203152,0.53266493,
113	0.00700525,0.13244732,
114	0,0,
115	
116	-Initial Conditions Card
117	Gas Pressure,Aqueous Pressure,
118	2,
119	Gas Pressure,101325.0,Pa,0.0,1/m,0.0,1/m,0.0,1/m,1,1,1,1,1,94,
120	Aqueous Pressure,98729.71741,Pa,0.0,1/cm,0.0,1/cm,-97.935192,1/cm,1,1,1,1,1,94,
121	
122	-Boundary Conditions Card
123	2,
124	Top,Dirichlet Aqueous,Dirichlet Gas,
125	1,1,1,1,94,94,1,
126	0.0,hr,101550.25,Pa,,102921.343630,Pa,,
127	Bottom,Dirichlet Aqueous,Zero Flux Gas,
128	1,1,1,1,1,1,1,
129	0.0,hr,98778.685,Pa,,,,,
130	
131	-Output Control Card
132	1,
133	1,1,94,
134	1,1,hr,cm,3,5,5,
135	4,
136	Gas Pressure,Pa,
137	Aqueous Pressure,Pa,
138	Aqueous Saturation,,
139	Aqueous Relative Permeability,,
140	13,
141	0.00,hr,
142	0.10,hr,
143	0.20,hr,
144	0.30,hr,
145	0.40,hr,
146	0.50,hr,
147	0.60,hr,
148	0.70,hr,
149	0.80,hr,
150	0.90,hr,
151	1.00,hr,
152	1.10,hr,
153	1.20,hr,
154	5,
155	Gas Pressure,Pa,
156	Aqueous Pressure,Pa,
157	Aqueous Saturation,,
158	Aqueous Moisture Content,,
159	Aqueous Relative Permeability,,
160	
161	-Surface Flux Card
162	1,
163	Aqueous Volumetric Flux,m ³ /s,m ³ ,Top,1,1,1,1,94,94,

5.4 Radon Vapor Transport into Dwellings

Investigators (e.g., Narasimhan et al. (1990)) have shown that subsurface air advection patterns can significantly affect radon entry into buildings. Nero (1989) reports that when structures are located on soils with large intrinsic permeabilities, extraordinarily high indoor radon

concentrations can occur even when the radium content of the soil is low. Other researchers have documented high radon activity in ground water. The combination of these two factors poses an interesting question of whether degassing of radon from ground water may contribute to indoor radon levels, especially when the structures are slightly under pressurized with respect to atmospheric conditions. In previous modeling efforts, the source of radon is assumed to be from evenly distributed radon-producing radium in the soil (e.g., Holford et al. (1993)); no consideration was given to ground water as a potential source of radon.

Problem Features: 5.4

- Water-Air operational mode
- vapor-phase transport
- two dimensional
- variable saturation
- homogeneous, isotropic
- nonuniform Cartesian grid
- van Genuchten expression
- solute gas source

To investigate whether the radon that partitions from ground water to soil gas can contribute to indoor radon levels, multiphase flow models need to be used that consider interphase mass partitioning. Predictive tools that only consider a subset of the governing transport mechanisms will likely result in inaccurate predictions. In this example, the distribution of radon under a structure is predicted for two different intrinsic permeabilities. The production of radon from decaying radium in the solid phase is ignored for illustrative purposes. The radon in the unsaturated regions of the subsurface is assumed to be transported from the ground water. The structures are assumed to have a slight under pressure relative to atmospheric conditions, which causes advective air fluxes in the subsurface. Under appropriate conditions, the flux of radon into structures can result in concentrations above the suggested Environmental Protection Agency action limit of 148 Bq/m^3 , when ground water is considered to be the only radon source.

5.4.1 Problem Description and Parameters

For the applications in this section, the mass conservation equations for air and water are solved simultaneously, assuming isothermal conditions. The radon transport equation, which accounts for advection, diffusion/dispersion, retardation, production and decay, is solved sequentially using the computed water and gas velocity fields as inputs. For unsaturated conditions, radon is transported in the water and gas phase. The concentration in the air phase is related through the concentration in the water phase by a temperature-dependent distribution

coefficient. The constitutive relations for fluid-phase saturations and relative permeabilities follow those described by van Genuchten (1980) and include expressions for the gas phase.

In the example, steady-state subsurface radon concentration profiles and indoor radon concentrations are computed for two-dimensional scenarios. The conceptual model, similar to the one used by Tsang and Narasimhan (1992), is depicted in Figure 5.4-1. The ground water table lies 10 m below the land surface and 8 m below the 10-m-wide basement floor. The plane of symmetry is at $x = 0$ m. A constant atmospheric pressure is assumed at the land surface, and the basement has a constant 5 Pa under pressure. This configuration forces air to move from the land surface into the subsurface and flow into the basement. The soil is assumed to not generate any radon; the only source of radon is the ground water with a radon concentration of 11.1 kBq/m^3 .

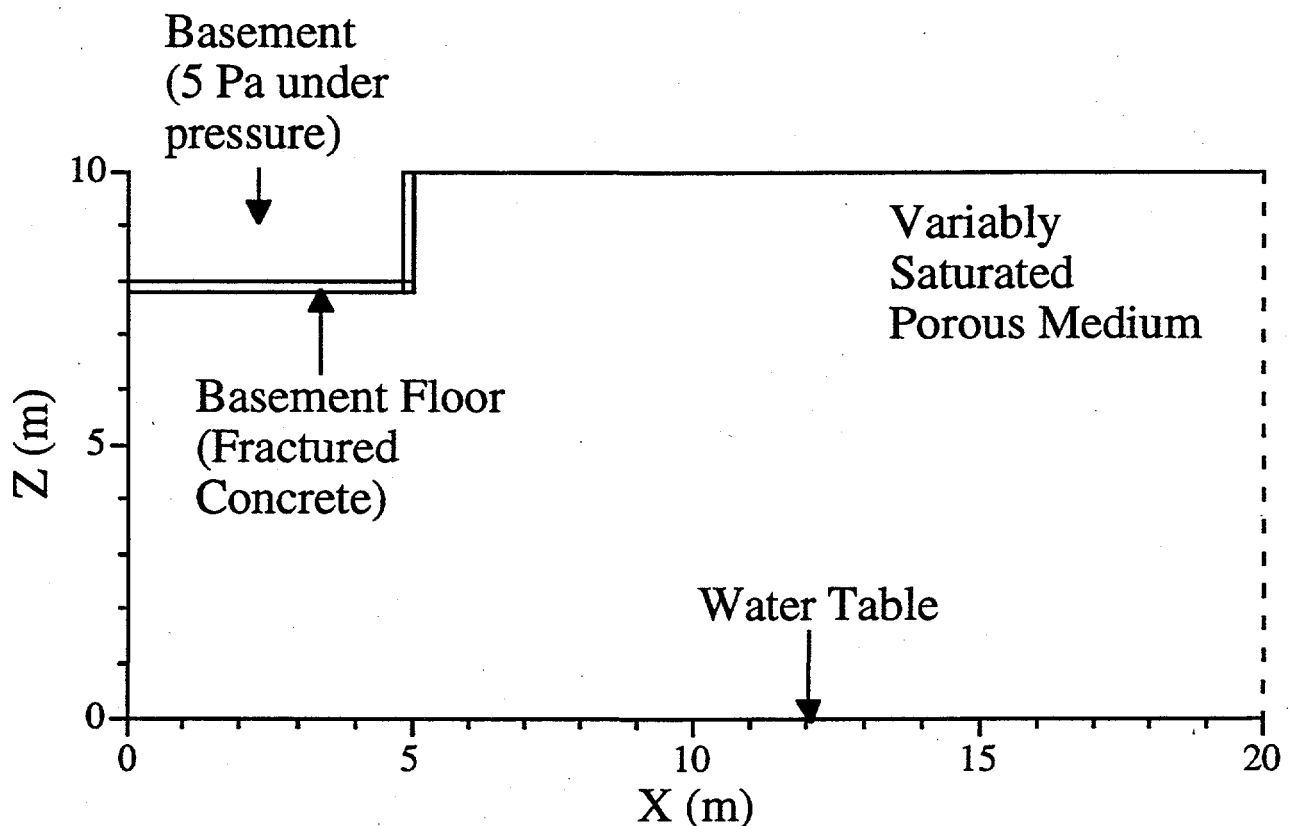


Figure 5.4-1. Radon Concentration Profiles for Porous Medium Permeability of (a) 10^{-10} m^2 and (b) 10^{-11} m^2

5.4.2 Simulations

The simulations are conducted using a total of 900 nodes (30 x 30). The grid is more refined near the basement of the dwelling. The radon was allowed to be transported through either advection by gradients in the gaseous phase or by molecular diffusion. For the simulations shown in this example, it is assumed that a fractured concrete foundation is present with one 0.5 cm crack per meter. To model cracks accurately, equations representing the continuum approach (Nitao, (1988)) have been implemented in the code. The STOMP input and parameters file are shown in Exhibit 5.4-1 and Exhibit 5.4-2, respectively.

5.4.3 Analysis

In Figure 5.4-2(a) and Figure 5.4-2(b), the subsurface radon concentration profiles are shown for a permeability of 10^{-11} and 10^{-10} m², respectively. For the lower permeability (i.e., equivalent to a medium sand), only a slight increase in the radon concentrations is predicted near the plane of symmetry. For the higher permeability (i.e., equivalent to a very coarse sand), significant amounts of radon are drawn into the dwelling. The concentration profiles shown in Figure 5.4-2(a) results in a indoor radon concentration of 8.2 Bq/m³, assuming a ventilation rate of 0.1/hr. The situation depicted in Figure 5.4-2(b) yields an indoor radon concentration of 394 Bq/m³, for the same ventilation rate. These results show that in relatively high permeable soils, sufficient amounts of radon may be transported into dwellings from the ground water, if the water table depth is 10 m or less from the land surface.

5.4.4 Summary

Our simulations suggest that radon degassing from ground water may contribute to indoor radon concentrations. This may have important implications for regions where the aquifer that underlies dwellings passes through geologic materials high in radium content and the subsurface materials overlying the aquifer is composed of very coarse sands and gravels, such as is common in many fast flowing alluvial deposits. The degassing of radon from ground water may help to explain how some dwellings may have high indoor radon concentrations when the radium content of the underlying geologic strata is low.

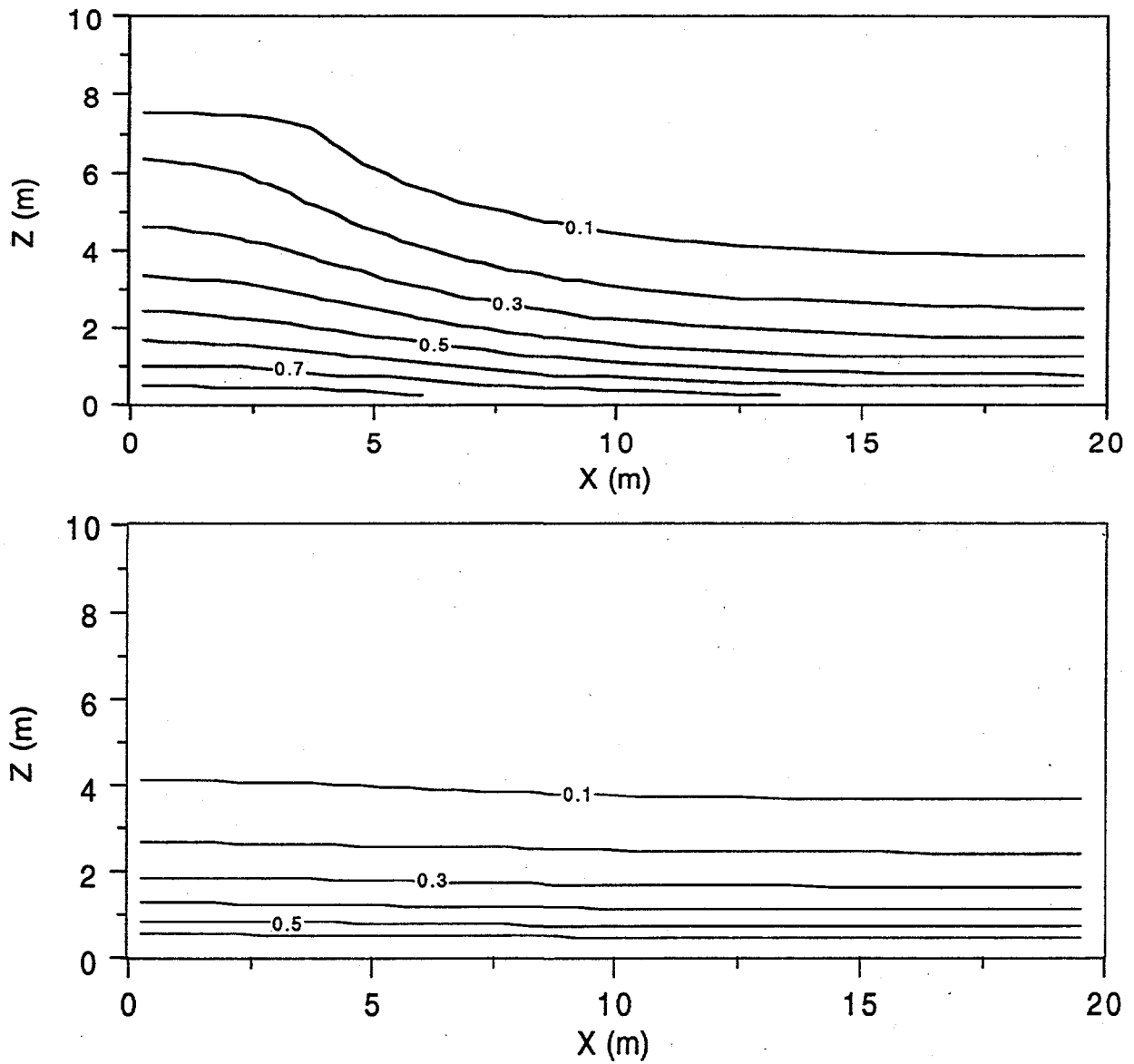


Figure 5.4-2. Radon Concentration Profiles for Porous Medium Permeability of (a) 10^{-10} m^2 and (b) 10^{-11} m^2 .

Exhibit 5.4-1. STOMP Input File for Vapor Transport of Radon Into Dwellings Problem

<u>Line</u>	<u>Input File</u>
1	# -----
2	-Simulation Title Card
3	# -----
4	1,
5	Radon flow and transport (2D),
6	M.Oostrom,
7	Pacific Northwest Laboratory,
8	December/January 1994,
9	13:00 PM PDT,
10	1,
11	2d radon tranport, diffusion/advection,
12	# -----
13	-Solution Control Card
14	# -----
15	Normal,
16	Water-Air w/Transport,
17	1,
18	0,hr,200,d,60,s,5,d,1.25,8,1.e-06,
19	1,day,1,day,10000,
20	Variable Aqueous Phase Diffusion,
21	Variable Gas Phase Diffusion,
22	0,
23	# -----
24	-Grid Card
25	# -----
26	Cartesian,
27	30,1,30,
28	0,m,20@0.5,m,10@1.,m,
29	0,m,1,m,
30	0,m,14@0.5,m,2@0.3,m,1@0.2,m,4@0.05,m,7@0.25,m,2@0.125,m,
31	# -----
32	-Inactive Domain Card
33	# -----
34	1,
35	1,10,1,1,22,30,
36	# -----
37	-Rock/Soil Zonation Card
38	# -----
39	1,
40	Sand,1,30,1,1,1,30,
41	Fractured Concrete,1,10,1,1,20,21,
42	Gravel,1,10,1,1,18,19,
43	# -----
44	-Mechanical Properties Card
45	# -----
46	Sand,,,0.4,0.4,,,Millington and Quirk,,,
47	Fractured Concrete,,,0.25,0.25,0.01,0.01,,,Millington and Quirk,
48	Gravel,,,0.4,0.4,,,Millington and Quirk,
49	# -----
50	-Hydraulic Properties Card
51	# -----
52	Sand,4.e-11,m^2,,,4.e-11,m^2,
53	Fractured Concrete,4.4e-16,m^2,,,4.4e-16,m^2,1.0e-6,m^2,,,1.0e-6,m^2,
54	Gravel,1.0e-8,m^2,,,1.0e-8,m^2,
55	# -----

Exhibit 5.4-1. (Contd)

<u>Line</u>	<u>Input File</u>
56	-Saturation Function Card
57	# -----
58	Sand,Nonhysteretic van Genuchten,.146,1/cm,2.5,0.0,,
59	Fractured Concrete,Nonhysteretic van
60	Genuchten,.146,1/cm,2.5,0.0,14.0,1/m,2.5,0.0,,,
61	Gravel,Nonhysteretic van Genuchten,.146,1/cm,2.5,0.0,,
62	# -----
63	-Aqueous Relative Permeability Card
64	# -----
65	Sand,Mualem,,
66	Fractured Concrete,Mualem,,,
67	Gravel,Mualem,,
68	# -----
69	-Gas Relative Permeability Card
70	# -----
71	Sand,Mualem,,
72	Fractured Concrete,Mualem,,,
73	Gravel,Mualem,,
74	# -----
75	-Solute/Fluid Interaction Card
76	# -----
77	1,
78	Radon,1.0e-9,m^2/s,1.0e-5,m^2/s,Constant,4.12,,Continuous,3.8,d,
79	0,
80	# -----
81	-Solute/Porous Media Interaction Card
82	# -----
83	Sand,0.0,m,0.0,m,
84	Radon,0,,
85	Gravel,0.0,m,0.0,m,
86	Radon,0,,
87	Concrete,0.0,m,0.0,m,
88	Radon,0,,
89	Fractured Concrete,0.0,m,0.0,m,
90	Radon,0,,
91	# -----
92	-Initial Conditions Card
93	# -----
94	Gas Pressure,Aqueous Pressure,
95	4,
96	Aqueous Pressure,96654.454,Pa,,,,,-9793.54,1/m,1,30,1,1,1,30,
97	Gas Pressure,101439.21,Pa,,,,,-11.7137,1/m,1,30,1,1,1,30,
98	Temperature,20,C,,,,,1,30,1,1,1,30,
99	Solute Aqueous Volumetric,Radon,0,1/m^3,,,,,1,30,1,1,1,30,
100	# -----
101	-Boundary Conditions Card
102	# -----
103	3,
104	Top,Zero Flux,Dirichlet,Radon Gas Conc.,
105	1,10,1,1,21,21,1,
106	0,hr,,,,,101343.43,Pa,1.0,0.0,1/m^3,
107	Top,Zero Flux,Dirichlet,Radon Gas Conc.,
108	11,30,1,1,30,30,1,
109	0,hr,,,,,101325.,Pa,1.0,0.0,1/m^3,
110	Bottom,Dirichlet,Dirichlet,Radon Gas Conc.,

Exhibit 5.4-1. (Contd)

<u>Line</u>	<u>Input File</u>
111	1,30,1,1,1,1,1,
112	0,hr,100325,Pa,,101442.185,Pa,1.0,1.0,1/m^3,
113	# -----
114	-Output Options Card
115	# -----
116	4,
117	20,1,1,
118	20,1,5,
119	20,1,10,
120	5,1,21,
121	1,1,day,m,6,6,6,
122	3,
123	X Gas Vol,m/day,
124	Z Gas Vol,m/day,
125	Solute Gas Conc,Radon,1/m^3,
126	1,
127	200,d,
128	3,
129	X Gas Vol,m/day,
130	Z Gas Vol,m/day,
131	Solute Gas Conc,Radon,1/m^3,
132	# -----
133	-Surface Flux Card
134	# -----
135	1,
136	Solute Flux,Radon,, ,Top,1,10,1,1,21,21,
137	

Exhibit 5.4-2. STOMP Parameters File for Vapor Transport of Radon Problem

<u>Line</u>	<u>Parameters File</u>
1	C-----C
2	C STOMP Parameter File
3	C-----C
4	C
5	C--- Number of lines of simulation notes
6	C Number of execution periods ---
7	C
8	PARAMETER(LNOTES=10, LEPD=10)
9	C
10	C--- Number of nodes in the x or r coordinate direction
11	C Number of nodes in the y or theta coordinate direction
12	C Number of nodes in the z coordinate direction
13	C Number of active nodes
14	C Number of active dimensions
15	C Minimum of (LFX*LFY, LFX*LFZ, LFY*LFZ) ---
16	C
17	PARAMETER(LFX=30, LFY=1, LFZ=30)
18	PARAMETER(LAN=810, LAD=2, LMNP=30)
19	C
20	C--- Energy equation switch (0 = off, 1 = on)
21	C Water mass equation switch (0 = off, 1 = on)
22	C Air mass equation switch (0 = off, 1 = on)
23	C VOC mass equation switch (0 = off, 1 = on)
24	C Solute transport equation switch (0 = off, 1 = on)
25	C Freezing conditions switch (0 = off, 1 = on) ---
26	C Dissolved salt transport equation switch (0 = off, 1 = on) ---
27	C Dissolved oil transport equation switch (0 = off, 1 = on) ---
28	C
29	PARAMETER(LT=0, LL=1, LG=1, LN=0, LC=1, LFC=0, LS=0, LD=0)
30	C
31	C--- Banded matrix linear equation solver switch (0 = off, 1 = on)
32	C Conjugate gradient linear equation solver switch (0 = off, 1 = on) ---
33	C Unsymmetric-pattern multifrontal package switch (0 = off, 1 = on) ---
34	C
35	PARAMETER(LBD=1, LCG=0, LUM=0)
36	C
37	C--- Number of boundary condition surfaces
38	C Number of boundary condition times ---
39	C
40	PARAMETER(LBC=60, LBTM=50)
41	C
42	C--- Number of sources
43	C Number of source times ---
44	C
45	PARAMETER(LSR=900, LSTM=10)
46	C
47	C--- Number of rock/soil types
48	C Number of solutes
49	C
50	PARAMETER(LRC=3, LSOLU=1)
51	C
52	C--- Number of reference nodes
53	C Number of print times
54	C Number of integration surfaces ---
55	C

Exhibit 5.4-2. (Contd)

<u>Line</u>	<u>Parameters File</u>
56	PARAMETER(LREF=5, LPTM=1, LSF=10)
57	C
58	C--- Number saturation and relative permeability table entries
59	C Number of hysteretic scanning paths
60	C Number of chemical reactions
61	C
62	PARAMETER(LTBL=1, LPATH=3, LCHEM=1)
63	C
64	C--- Computed Parameters ---
65	C
66	PARAMETER(LUK=LT+LL+LG+LN+LS+LD, LPH=LL+LG+LN, LCMP=LL+LS+LD)
67	PARAMETER(LFX=LFX*LFY, LFYZ=LFY*LFZ, LFZX=LFZ*LFX)
68	PARAMETER(LFD=LFX*LFY*LFZ)
69	PARAMETER(LNE=(LUK*LUK*(7*LFD-2*LFX-2*LFYZ-2*LFZX))**LUM)
70	PARAMETER(LHBW=LUK*LMNP+LUK-1)
71	PARAMETER(LJA=LBD + LCG*LAN*LUK + LUM*LAN*LUK)
72	PARAMETER(LJB=(2*LAN*LUK)**LUM, LJC=LAN**LUM)
73	PARAMETER(LJD=LBD*(3*LHBW+1) + LCG*LAN*LUK + LUM*6*LNE)
74	PARAMETER(LJE=LBD*LAN*LUK + LCG*((2*LAD+1)*LUK+2*LAD) + LUM)
75	PARAMETER(LJF=LAN*LUK)
76	PARAMETER(LJG=LBD*(3*LHBW+1) + LCG*LAN*LUK + LUM)
77	PARAMETER(LJH=LBD*LAN*LUK + LCG*(2*LAD+1) + LUM)
78	PARAMETER(LJJ=LBD*LAN*LUK + LCG + LUM)
79	PARAMETER(LSV=LUK+2, LSFV=2*LUK+1)
80	PARAMETER(LSX=(LFX+1)*LFY*LFZ)
81	PARAMETER(LSY=LFX*(LFY+1)*LFZ)
82	PARAMETER(LSZ=LFX*LFY*(LFZ+1))
83	PARAMETER(LFDT=LFD**LT, LFDL=LFD**LL, LFDG=LFD**LG, LFDN=LFD**LN)
84	PARAMETER(LFDC=LFD**LC, LFDI=LFD**LFC, LFDS=LFD**LS, LFDD=LFD**LD)
85	PARAMETER(LSXT=LSX**LT, LSXL=LSX**LL, LSXG=LSX**LG, LSXN=LSX**LN)
86	PARAMETER(LSXC=LSX**LC, LSXS=LSX**LS, LSXD=LSX**LD)
87	PARAMETER(LSYT=LSY**LT, LSYL=LSY**LL, LSYG=LSY**LG, LSYN=LSY**LN)
88	PARAMETER(LSYC=LSY**LC, LSYS=LSY**LS, LSYD=LSY**LD)
89	PARAMETER(LSZT=LSZ**LT, LSZL=LSZ**LL, LSZG=LSZ**LG, LSZN=LSZ**LN)
90	PARAMETER(LSZC=LSZ**LC, LSZS=LSZ**LS, LSZD=LSZ**LD)
91	PARAMETER(LRCT=LRC**LT, LRCL=LRC**LL, LRCG=LRC**LG, LRCN=LRC**LN)
92	PARAMETER(LRCC=LRC**LC, LRCI=LRC**LFC, LRCS=LRC**LS, LRCD=LRC**LD)
93	PARAMETER(LBCT=LBC**LT, LBCL=LBC**LL, LBCG=LBC**LG, LBCN=LBC**LN)
94	PARAMETER(LBCC=LBC**LC, LBCI=LBC**LFC, LBCC=LBC**LS, LBCC=LBC**LD)
95	PARAMETER(LBCU=LUK+LPH+LT+2, LBCV=LBCU+LSOLU)
96	PARAMETER(LOUPV=200+11*(LSOLU))
97	PARAMETER(LJI=LBD*LAN*LUK + LCG + (3*LNE+23*LFD*LUK+9)*LUM)
97	PARAMETER(LSCHR=18)
99	

5.5 References

- Haverkamp R, M Vauclin, J Touma, PJ Wierenga, and G Vachaud. 1977. "Comparison of numerical simulation models for one-dimensional infiltration." *Soil Science Society of America Journal*, 41, 285-294.
- Hills RG, I Porro, DB Hudson, and PJ Wierenga. 1989. "Modeling one-dimensional infiltration into very dry soils. 1. model development and evaluation." *Water Resources Research*, 25(6), 1259-1269.
- Holford DJ, SD Schery, JL Wilson, and FM Phillips. 1993. "Modeling radon transport in dry, cracked soil." *Journal of Geophysical Research*, 98(B1), 567-580.
- Mualem Y. 1976. "A new model for predicting the hydraulic conductivity of unsaturated porous media." *Water Resources Research*, 12(3), 513-522.
- Narasimhan TN, YW Tsang, and HY Holman. 1990. "On the potential importance of transient air flow in advective radon entry into buildings." *Geophysical Research Letters*, 17, 821-824.
- Nero A. 1989. "Earth, air, radon and home." *Physics Today*, 42(4), 32-39.
- Nichols WE, and MD White. 1993. *MSTS: Multiphase Subsurface Transport Simulator User's Guide and Reference*, PNL-8637, Pacific Northwest Laboratory, Richland, Washington.
- Nitao JJ. 1988. *Numerical Modeling of the Thermal and Hydrological Environment Around a Nuclear Waste Package Using the Equivalent Continuum Approximation: Horizontal Emplacement*, Lawrence Berkeley National Laboratory, Berkeley, California.
- Ségol G. 1994. *Classic Groundwater Simulations: Proving and Improving Numerical Models*, Prentice-Hall, Englewood Cliffs, New Jersey.
- Touma J, and M Vauclin. 1986. "Experimental and numerical analysis of two-phase infiltration in a partially saturated soil." *Transport in Porous Media*, 27-55.
- Tsang YW, and TN Narasimhan. 1992. "Effects of periodic atmospheric pressure variation on radon entry into buildings." *Journal of Geophysical Research*, 97(B6), 9161-9170.
- van Genuchten MT. 1980. "A closed form equation for predicting the hydraulic conductivity of unsaturated soils." *Soil Science Society of America Journal*, 44, 982-998.

6.0 Mass and Energy Conservation Tests

Applications in this example are simple conservation checks that test the mass and energy conservation of the STOMP simulator for phase changes. The objective in each case is to demonstrate that the total quantity of mass and energy in a single, closed, adiabatic volume of partially saturated porous media node remains the same before and after a simulated phase change. Five cases are presented: evaporation and condensation (vaporization point: aqueous/gas), and freezing and thawing (fusion point: solid/aqueous), plus a simulation of flow from hot two-phase conditions used to test energy conservation.

6.1 Single Node Evaporation

The single node evaporation problem involves the evaporation of aqueous phase water within a closed adiabatic volume of partially saturated porous medium.

The evaporation process occurs through the addition of heat into the control volume. Sufficient heat is added to the system to desaturate the porous medium. Because the control volume surfaces are closed and adiabatic, the initial quantities of air and water mass will remain constant throughout the simulation. Upon desaturation of a node, STOMP switches the primary variable for the water mass conservation equation from the liquid pressure to the water-vapor mass fraction. This problem demonstrates this numerical transition from two-phase conditions to gas-phase-only conditions. The problem requires the coupled solution of the water mass, air mass, and energy conservation equations.

Problem Features: 6.1

- Water-Air-Energy operation mode
- liquid-vapor phase change
- single node
- variable saturation
- homogeneous, isotropic
- Cartesian grid
- van Genuchten function
- mass balance test

6.1.1 Problem Description and Parameters

This test problem involves a 10-m^3 cube of porous media, with a total porosity of 0.50, rock density of 2650 kg/m^3 , and specific heat of 1000 J/kg K . The initial gas pressure, liquid saturation, and temperature are 10^5 Pa (absolute), 0.01, and 90°C , respectively. A constant internal heat source of 2.0 MW was applied. All boundary surfaces are adiabatic, no-flow surfaces. The input file for the single-node-evaporation problem is shown in Exhibit 6.2-1.

6.1.2 Simulation

Simulation results in terms of the system temperature and liquid saturation are shown in Figure 6.1-1. The system begins at an initially fully saturated state, and liquid saturation declines with time to a completely desaturated state as water undergoes phase change with increasing temperature. The simulation is halted at 1875 seconds at a final temperature of 363.9°C, which is slightly below the critical temperature for water.

6.1.3 Analysis (Mass Balance Check)

This problem concerns a closed system in which mass must be conserved while simulating a vaporization phase change. A mass balance check was performed, comparing the total mass of water in the cube represented by the single node at the initial conditions to the total mass of water at 1875 seconds, the end of the simulation. The total mass of water in the node (m_r^w) is the sum of

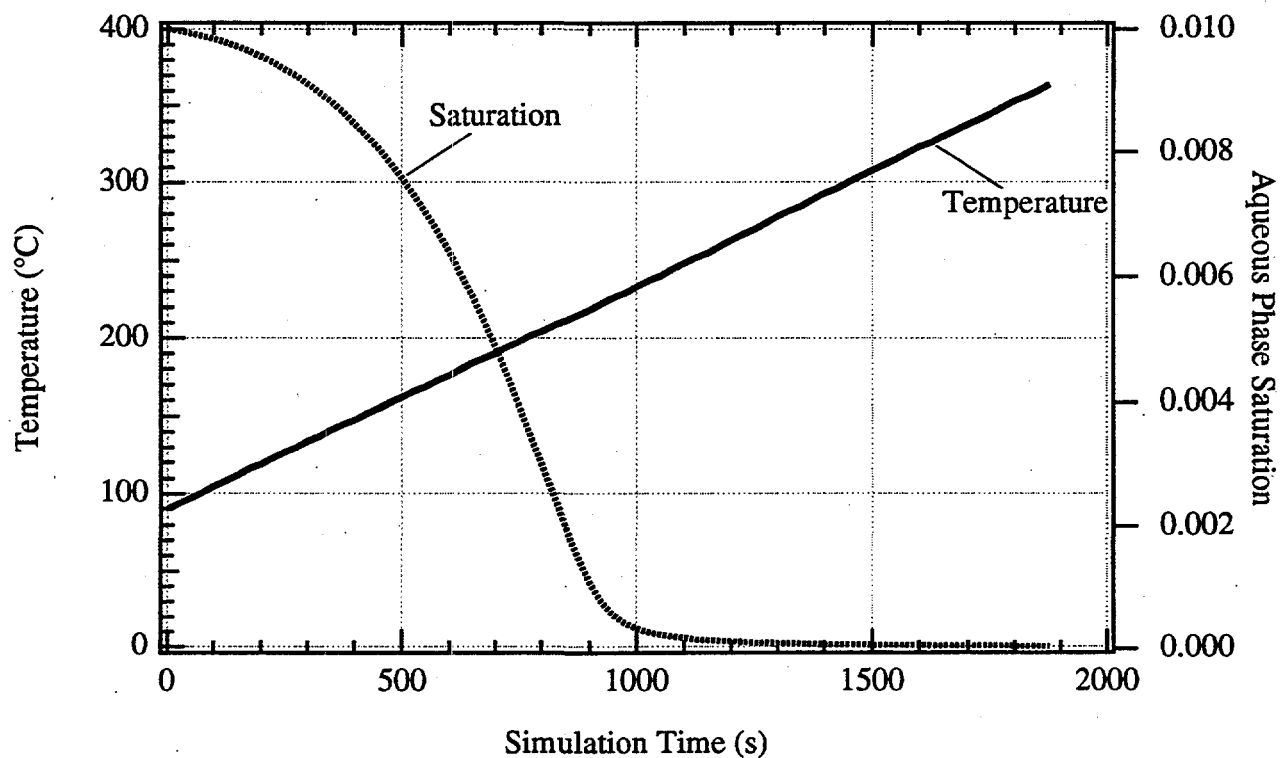


Figure 6.1-1. STOMP-Predicted Temperature and Aqueous-Phase Saturation Variation with Time for the Single Node Evaporation Problem

the water in the aqueous (m_l^w) and vapor (m_g^w) phases. The mass of water in the aqueous phase is given by

$$m_l^w = \eta_D V \rho_l = (n_T - n_D + s_l n_D) V \rho_l$$

Equation 6.1-1

and the mass of water in the gas phase by

$$m_g^w = (1 - s_l) n_D V x_l^w \rho_g$$

Equation 6.1-2

In mathematical terms, the total mass in the domain is the sum of the water in each phase:

$$m_T^w = m_l^w + m_g^w$$

Equation 6.1-3

The initial conditions were derived from the problem definition and the final conditions were obtained from the plot file generated by the STOMP code; both are shown in Table 6.1-1. Substituting the values from Table 6.1-1 into Equation 6.1-1, the total water mass in the aqueous phase at time zero (initial) is

$$\begin{aligned} m_l^w &= (n_T - n_D + s_l n_D) V \rho_l \\ &= [0.50 - 0.50 + (0.01)(0.50)] (10 \text{ m}^3) (965.12 \text{ kg/m}^3) \\ &= 48.256 \text{ kg} \end{aligned}$$

Equation 6.1-4

Substituting values from Table 6.1-1 into Equation 6.1-2, the water mass in the gas phase at time zero is

Table 6.1-1. Single Node Evaporation Problem Initial and Final Conditions

Variable	Units	Initial Conditions	Final Conditions
V	m^3	10.0	10.0
n_T	-	0.50	0.50
n_D	-	0.50	0.50
T	$^{\circ}\text{C}$	90.0	363.92
s_l	-	0.01	3.5284×10^{-5}
ρ_l	kg/m^3	965.12	473.58
ρ_g	kg/m^3	0.72078	10.348
x_l^*	-	0.57360	0.97059

$$\begin{aligned}
 m_g^w &= (1 - s_l) n_D V x_g^* \rho_g \\
 &= (1 - 0.01) (0.50) (10 \text{ m}^3) (0.57360) (0.72078 \text{ kg}/\text{m}^3) \\
 &= 2.04653 \text{ kg}
 \end{aligned}$$

Equation 6.1-5

Therefore, the total water mass in the node at time zero is 50.303 kg. When the simulation is completed, the temperature is 363.92°C and the water mass in the aqueous phase is

$$\begin{aligned}
 m_l^w &= (n_T - n_D + s_l n_D) V \rho_l \\
 &= [0.50 - 0.50 + (3.5284 \times 10^{-5}) (0.50)] (10 \text{ m}^3) (473.58 \text{ kg}/\text{m}^3) \\
 &= 0.08355 \text{ kg}
 \end{aligned}$$

Equation 6.1-6

(i.e., there is essentially no water mass in the aqueous phase) and the water mass in the gas phase is

$$\begin{aligned}
 m_g^w &= (1 - s_l) n_D V x_g^* \rho_g \\
 &= (1 - 3.5284 \times 10^{-5}) (0.50) (10 \text{ m}^3) (0.97059) (10.348 \text{ kg}/\text{m}^3) \\
 &= 50.217 \text{ kg}
 \end{aligned}$$

Equation 6.1-7

These two values sum to a total water mass in the node at final conditions of 50.300kg. The mass difference between initial and final conditions is therefore $50.303 - 50.300 = 0.003$ kg, or 0.006%.

6.1.4 Summary

This problem represents an internal consistency check to confirm that mass was conserved during a phase change simulation. Error in mass balance was less than 0.01%. This problem was also reported in Nichols and White (1993) for the MSTS code; the MSTS code yielded a mass balance error of 0.10%.

Exhibit 6.1-1. STOMP Input File for Single Node Evaporation Problem

<u>Line</u>	<u>Input File</u>
1	-Simulation Title Card
2	1,
3	Single Node Evaporation Problem,
4	W.E. Nichols,
5	Pacific Northwest Laboratory,
6	July 19 1995,
7	11:14:00 AM PDT,
8	1,
9	Single Node Evaporation Problem to Test STOMP Mass and Energy Conservation
10	
11	-Solution Control Card
12	Normal,
13	Water-Air-Energy,
14	1,
15	0,s,1875,s,25,s,25,s,1.0,8,1.e-6,
16	1,hr,1,hr,100,
17	Zero,
18	Zero,
19	0,
20	
21	-Grid Card
22	Cartesian,
23	1,1,1,
24	0.0,m,2.1544,m,
25	0.0,m,2.1544,m,
26	0.0,m,2.1544,m,
27	
28	-Rock/Soil Zonation Card
29	1,
30	Generic Sand,1,1,1,1,1,1,
31	
32	-Mechanical Properties Card
33	Generic Sand,2650.0,kg/m^3,0.5,0.5,1.e-7,1/m,
34	
35	-Hydraulic Properties Card
36	Generic Sand,1.0e-14,m^2,1.0e-14,m^2,1.0e-14,m^2,
37	
38	-Thermal Properties Card
39	Generic Sand,Constant,2.10,W/m K,2.10,W/m K,2.10,W/m K,1000.0,J/kg K,
40	
41	-Saturation Function Card
42	Generic Sand,Nonhysteretic van Genuchten,0.5,1/m,2.0,0.0,,
43	
44	-Aqueous Relative Permeability Card
45	Generic Sand,Mualem,0.5,
46	
47	-Gas Relative Permeability Card
48	Generic Sand,Mualem,0.5,
49	
50	-Initial Conditions
51	Gas Pressure, Aqueous Saturation,
52	3,
53	Gas Pressure,1.0E+5,Pa,,1/m,,1/m,,1/m,1,1,1,1,1,1,
54	Aqueous Saturation,0.01,,,1/m,,1/m,,1/m,1,1,1,1,1,1,
55	Temperature,90.0,C,,1/m,,1/m,,1/m,1,1,1,1,1,1,

Exhibit 6.1-1. (Contd)

<u>Line</u>	<u>Input File</u>
56	
57	-Source Card
58	1,
59	Power Density,1,1,1,1,1,1,1,
60	0,s,2.0E+5,W/m^3,
61	
62	-Output Control Card
63	1,
64	1,1,1,
65	1,1,s,m,3,3,5,
66	4,
67	Aqueous Pressure,,
68	Gas Pressure,,
69	Temperature,,
70	Aqueous Saturation,,
71	1,
72	1875,s,
73	10,
74	Aqueous Pressure,,
75	Gas Pressure,,
76	Temperature,,
77	Phase Condition,,
78	Aqueous Saturation,,
79	Gas Saturation,,
80	Gas Phase Water Mass Frac.,,
81	Aqueous Phase Water Mass Frac.,,
82	Aqueous Density,,
83	Gas Density,,
84	

6.2 Single Node Condensation

The single node condensation problem involves the condensation of water vapor within a closed adiabatic volume of porous medium initially desaturated. The condensation process occurs through the removal of heat from the control volume. Sufficient heat is removed from the system to cause condensation and partially saturate the porous medium. Because the control volume surfaces are closed and adiabatic, the initial quantities of air and water mass should remain constant throughout the simulation. Upon partial saturation of a desaturated node, STOMP switches the primary variable for the water mass conservation equation from the the water-vapor mass fraction to the aqueous pressure. This problem demonstrates this numerical transition from gas-phase-only conditions to two-phase conditions. The problem requires the coupled solution of the water mass, air mass, and energy conservation equations.

Problem Features: 6.2

- Water-Air-Energy operation mode
- vapor-liquid phase change
- single node
- variable saturation
- homogeneous, isotropic
- Cartesian grid
- van Genuchten function
- mass balance test

6.2.1 Problem Domain and Input Parameters

This problem involves a 10-m³ cube of porous media, with a total porosity of 0.50, rock density of 2650 kg/m³, and specific heat of 1000 J/kg K. The initial gas pressure, aqueous saturation, and temperature are 6.5 MPa (absolute), 0, and 280°C, respectively. A constant internal heat removal rate of -0.5 MW is applied. All boundary surfaces are adiabatic, no-flow surfaces. The STOMP input file is shown in Exhibit 6.2-1.

6.2.2 Simulation

Simulation results in terms of the system temperature and aqueous saturation are shown in Figure 6.2-1. The liquid saturation increases nonlinearly from zero (the initial condition) 0.0005 at the end of 7200 seconds when the final temperature of 12.0°C.

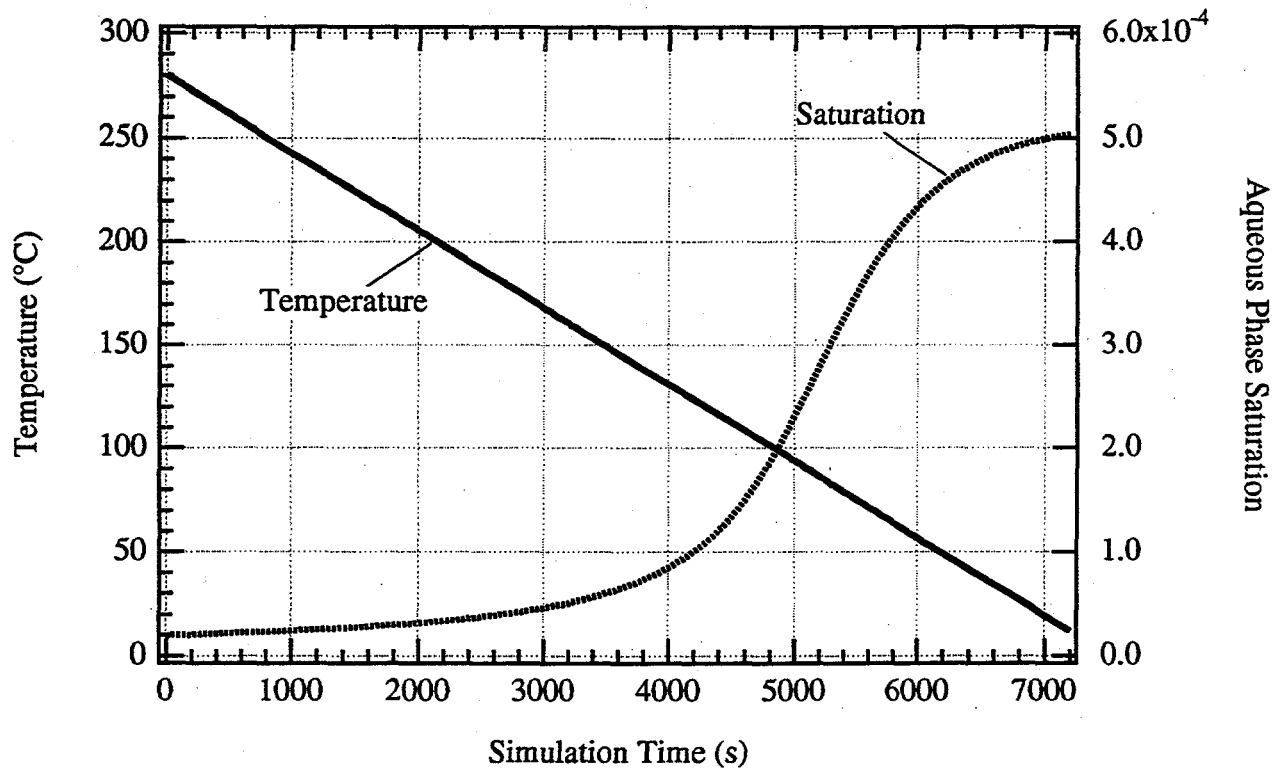


Figure 6.2-1. STOMP-Predicted Temperature and Aqueous Saturation Variation with Time for the Single Node Condensation Problem

6.2.3 Analysis (Mass Balance Check)

As for the single node evaporation problem, this problem concerns a closed system in which mass must be conserved. The mass balance check is repeated for the condensation problem using Equation 6.1-2 through Equation 6.1-4 with values from the single node condensation problem Table 6.2-1. For the initial conditions, the mass of water in the aqueous phase is computed as

$$\begin{aligned}
 m_l^w &= (n_T - n_D + s_l n_D) V \rho_l \\
 &= (0.50 - 0.50 + (0.0)(0.50))(10 \text{ m}^3)(751.46 \text{ kg/m}^3) \\
 &= 0.0 \text{ kg}
 \end{aligned}$$

Equation 6.2-1

(i.e., there is no water in the aqueous phase), while the water mass in the gas phase at time zero is

Table 6.2-1. Single Node Condensation Problem Initial and Final Conditions

Variable	Units	Initial Conditions	Final Conditions
V	m^3	10.0	10.0
n_T	-	0.50	0.50
n_D	-	0.50	0.50
T	$^{\circ}\text{C}$	280.00	12.032
s_l	-	0.0	0.00050357
ρ_l	kg/m^3	751.46	1001.2
ρ_g	kg/m^3	43.791	43.323
x_l^*	-	0.99836	0.99915

$$\begin{aligned}
 m_g^w &= (1 - s_l)n_D V x_l^* \rho_g \\
 &= (1 - 0.0)(0.50)(10 \text{ m}^3)(1.0)(43.791 \text{ kg}/\text{m}^3) \\
 &= 218.955 \text{ kg}
 \end{aligned}$$

Equation 6.2-2

Therefore, the total water mass at the start of the simulation period is 218.955 kg. At the end of the simulation (after 7200 seconds), the temperature is reduced to 12.0 °C and the water mass in the aqueous phase is

$$\begin{aligned}
 m_l^w &= (n_T - n_D + s_l n_D) V \rho_l \\
 &= [0.50 - 0.50 + (0.00050357)(0.50)](10 \text{ m}^3)(1001.2 \text{ kg}/\text{m}^3) \\
 &= 2.521 \text{ kg}
 \end{aligned}$$

Equation 6.2-3

while the water mass remaining in the gas phase is

$$\begin{aligned}
 m_g^w &= (1 - s_l) n_D V x_l^w \rho_g \\
 &= (1 - 0.00050357) (0.50) (10 \text{ m}^3) (0.99915) (43.323 \text{ kg/m}^3) \\
 &= 216.322 \text{ kg}
 \end{aligned}$$

Equation 6.2-4

Summing, the total water mass in the system at the end of the simulation is $2.521 + 216.322 = 218.843$ kg. The difference between initial and final mass is $218.955 - 218.843 = 0.122$ kg, which is 0.05% of the initial mass.

6.2.4 Summary

This problem represents an internal consistency check to confirm that mass was conserved during a phase change simulation (in this case, in the reverse direction of the phase change examined in the previous problem, Section 6.1). Error in mass balance was 0.05%. This problem was also reported in Nichols and White (1993) for the MSTS code; the MSTS code yielded a mass balance error of 0.71%.

Exhibit 6.2-1. STOMP Input File for Single Node Condensation Problem

<u>Line</u>	<u>Input File</u>
1	-Simulation Title Card
2	1,
3	Single Node Condensation Problem,
4	W.E. Nichols,
5	Pacific Northwest Laboratory,
6	July 19 1995,
7	12:50:00 PM PDT,
8	1,
9	Single Node Condensation Problem to Test STOMP Mass and Energy Conservation
10	
11	-Solution Control Card
12	Normal,
13	Water-Air-Energy,
14	1,
15	0,s,7200,s,25,s,25,s,1.1,8,1.e-6,
16	1,hr,1,hr,1000,
17	Zero,
18	Zero,
19	0,
20	
21	-Grid Card
22	Cartesian,
23	1,1,1,
24	0.0,m,2.1544,m,
25	0.0,m,2.1544,m,
26	0.0,m,2.1544,m,
27	
28	-Rock/Soil Zonation Card
29	1,
30	Generic Sand,1,1,1,1,1,1,
31	
32	-Mechanical Properties Card
33	Generic Sand,2650.0,kg/m ³ ,0.5,0.5,1.e-7,1/m,
34	
35	-Hydraulic Properties Card
36	Generic Sand,1.0e-14,m ² ,1.0e-14,m ² ,1.0e-14,m ² ,
37	
38	-Thermal Properties Card
39	Generic Sand,Constant,2.10,W/m K,2.10,W/m K,2.10,W/m K,1000.0,J/kg K,
40	
41	-Saturation Function Card
42	Generic Sand,Nonhysteretic van Genuchten,0.5,1/m,2.0,0.0,,
43	
44	-Aqueous Relative Permeability Card
45	Generic Sand,Mualem,0.5,
46	
47	-Gas Relative Permeability Card
48	Generic Sand,Mualem,0.5,
49	
50	-Initial Conditions Card
51	Gas Pressure,Aqueous Saturation,
52	3,
53	Gas Pressure,7.0E+6,Pa,,1/m,,1/m,,1/m,1,1,1,1,1,1,
54	Temperature,280.0,C,,1/m,,1/m,,1/m,1,1,1,1,1,1,
55	Aqueous Saturation,0.0,,,1/m,,1/m,,1/m,1,1,1,1,1,1,

Exhibit 6.2-1. (Contd)

<u>Line</u>	<u>Input File</u>
56	
57	--Source Card
58	1,
59	Power Density,1,1,1,1,1,1,1,
60	0,s,-5.0E+4,W/m^3,
61	
62	--Output Control Card
63	1,
64	1,1,1,
65	1,1,s,m,3,5,5,
66	4,
67	Aqueous Pressure,,
68	Gas Pressure,,
69	Temperature,,
70	Aqueous Saturation,,
71	1,
72	7200,s,
73	10,
74	Aqueous Pressure,,
75	Gas Pressure,,
76	Temperature,,
77	Phase Condition,,
78	Aqueous Saturation,,
79	Gas Saturation,,
80	Gas Phase Water Mass Frac.,,
81	Aqueous Phase Water Mass Frac.,,
82	Aqueous Density,,
83	Gas Density,,
84	

6.3 Single Node Freezing

The single node freezing problem involves the fusion of initially unfrozen, aqueous phase water within a closed adiabatic volume of porous medium. The fusion process occurs through the removal of heat from the control volume. Sufficient heat is removed from the system to cause the formation of ice in the porous

medium. Because the control volume surfaces are closed and adiabatic, the initial quantities of air and water mass should remain constant throughout the simulation. This problem demonstrates this numerical transition from two-phase (aqueous/gas) conditions to three-phase (ice/aqueous/gas) conditions. The problem requires the coupled solution of the water mass, air mass, and energy conservation equations with the Ice Option.

Problem Features: 6.3

- Water-Air-Energy operation mode
- liquid-solid (ice) phase change
- single node
- variable saturation
- homogeneous, isotropic
- Cartesian grid
- van Genuchten function
- mass balance test

6.3.1 Problem Domain and Input Parameters

This problem involves a 10-m³ cube of porous media, with a total porosity of 0.50, rock density of 2650 kg/m³, and specific heat of 1000 J/kg K. The initial gas pressure, aqueous saturation, and temperature are 1.5 MPa, 0.30, and 10°C, respectively. A constant internal heat removal rate of -0.5 MW is applied for 30 minutes. All boundary surfaces are adiabatic, no-flow surfaces. The STOMP input file is shown in Exhibit 6.3-1.

6.3.2 Simulation

Simulation results in terms of the system temperature, aqueous saturation, and ice saturation are shown in Figure 6.3-1. Aqueous saturation is nearly constant as the temperature is decreased linearly from 10°C to the freezing point. As freezing commences, the temperature remains constant during the phase change (see Figure 6.3-1), while aqueous saturation decreases and ice saturation increases (i.e., water mass undergoes phase change from aqueous to ice phase). After nearly all of the water mass has been frozen, the temperature begins to decrease again with no significant change in phase saturations, until the end of the 30 minute simulated time when the final temperature is -12.3°C. Table 6.3-1 lists the values of parameters necessary to perform the mass balance check for this problem at initial and final conditions. These values were obtained from the plot files generated by STOMP using the STOMP input file shown in Exhibit 6.3-1 (initial

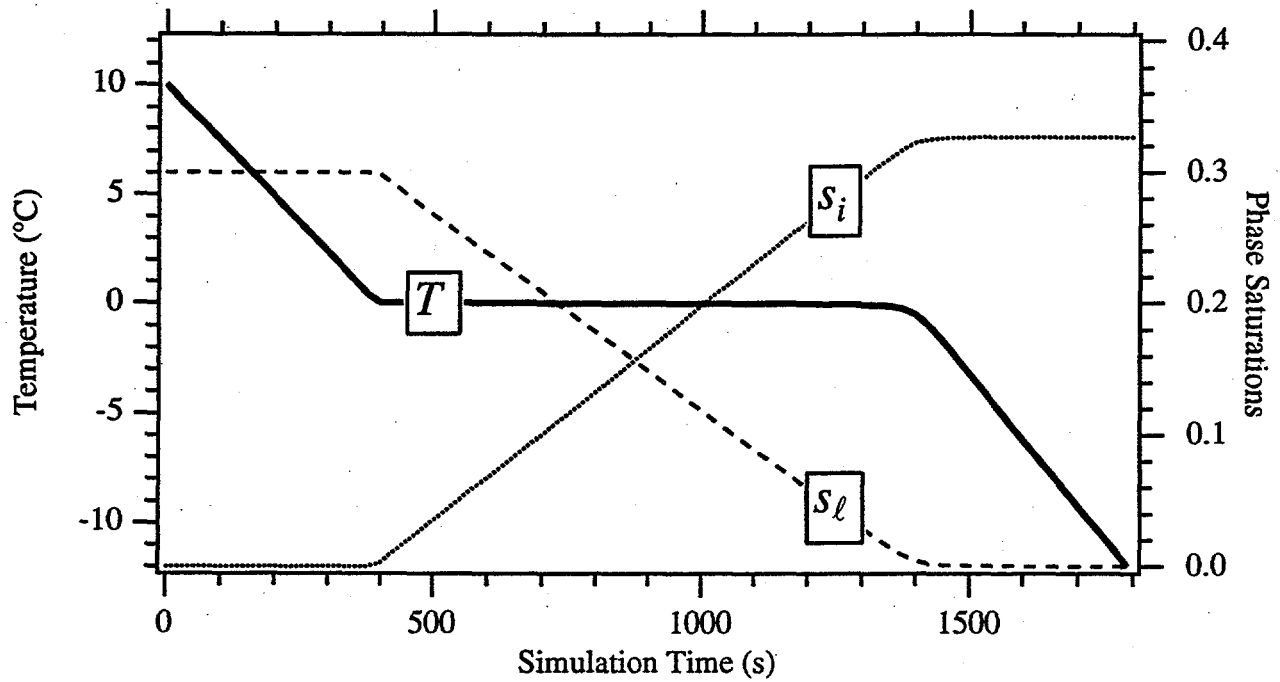


Figure 6.3-1. STOMP Predicted Temperature and Saturation Change with Time for the Single Node Freezing Problem

Table 6.3-1. Single Node Freezing Problem Initial and Final Conditions

Variable	Units	Initial Conditions	Final Conditions
V	m^3	10.0	10.0
n_T	-	0.50	0.50
n_D	-	0.50	0.50
T	$^{\circ}C$	10.000	-12.297
s_i	-	0.00	0.32640
s_l	-	0.30	0.00017647
ρ_i	kg/m^3	-	918.71
ρ_l	kg/m^3	1000.5	997.77
ρ_s	kg/m^3	18.453	19.332
x_r^*	-	0.99964	0.99965

conditions obtained by repeating the simulation with the "Initial" rather than "Normal" execution mode).

6.3.3 Analysis (Mass Balance Check)

As for the previous single node phase-change problems, this problem concerns a closed system in which mass must be conserved. The mass of water in the ice phase is computed as

$$m_i^w = s_i n_D V \rho_i$$

Equation 6.3-1

while in aqueous phase the mass of water is given by

$$m_l^w = \eta_D V \rho_l = (n_T - n_D + s_l n_D) V \rho_l$$

Equation 6.3-2

and the mass of water in gas phase is

$$m_g^w = (1 - s_l - s_i) n_D V x_l^w \rho_g$$

Equation 6.3-3

and of course, the summation of the above mass terms for each phase is the total water mass in the system:

$$m_T^w = m_i^w + m_l^w + m_g^w$$

Equation 6.3-4

For the initial conditions, there is no ice phase because the temperature is well above freezing (10°C), so $s_i = 0$. Initial water mass in aqueous phase is

$$\begin{aligned}
 m_l^w &= (n_T - n_D + s_l n_D) V \rho_l \\
 &= [0.50 - 0.50 + (0.30)(0.50)] (10 \text{ m}^3) (1000.5 \text{ kg/m}^3) \\
 &= 1500.75 \text{ kg}
 \end{aligned}$$

Equation 6.3-5

and the initial water mass in gas phase is

$$\begin{aligned}
 m_g^w &= (1 - s_l - s_i) n_D V x_l^w \rho_g \\
 &= (1 - 0.30 - 0.00) (0.50) (10 \text{ m}^3) (0.99964) (18.453 \text{ kg/m}^3) \\
 &= 64.5623 \text{ kg}
 \end{aligned}$$

Equation 6.3-6

Thus, the total water mass for the initial conditions is $0 \text{ kg} + 1500.75 \text{ kg} + 64.56 \text{ kg} = 1565.31 \text{ kg}$.

At the end of the 1-hour simulation, nearly all of the aqueous phase water has been frozen into ice phase at temperature -12.3°C . The water mass in ice phase is

$$\begin{aligned}
 m_i^w &= s_i n_D V \rho_i \\
 &= (0.32640) (0.50) (10 \text{ m}^3) (918.71 \text{ kg/m}^3) \\
 &= 1499.33 \text{ kg}
 \end{aligned}$$

Equation 6.3-7

The remainder of aqueous phase water has mass

$$\begin{aligned}
 m_l^w &= (n_T - n_D + s_l n_D) V \rho_l \\
 &= [0.50 - 0.50 + (0.00017647)(0.50)] (10 \text{ m}^3) (997.77 \text{ kg/m}^3) \\
 &= 0.88038 \text{ kg}
 \end{aligned}$$

Equation 6.3-8

and the final gas water phase is

$$\begin{aligned}
 m_g^w &= (1 - s_l - s_i) n_D V x_l^w \rho_g \\
 &= (1 - 0.00017647 - 0.32640) (0.50) (10 \text{ m}^3) (0.99965) (19.332 \text{ kg/m}^3) \\
 &= 65.07034 \text{ kg}
 \end{aligned}$$

Equation 6.3-9

The total water mass at the end of the simulated time is $1499.33 \text{ kg} + 0.88 \text{ kg} + 65.07 \text{ kg} = 1565.28 \text{ kg}$. The difference in total water mass computed for initial and final conditions, $1565.31 \text{ kg} - 1565.28 \text{ kg} = 0.03 \text{ kg}$, represents a mass balance error of only 0.0019%.

6.3.4 Summary

This problem represents an internal consistency check to confirm that mass was conserved during a phase change simulation that involved soil water freezing phenomena. Error in mass balance was shown to be less than 0.002%.

Exhibit 6.3-1. STOMP Input File for Single Node Freezing Problem

<u>Line</u>	<u>Input File</u>
1	-Simulation Title Card
2	1,
3	Single Node Freezing Problem,
4	W.E. Nichols,
5	Pacific Northwest Laboratory,
6	July 27 1995,
7	9:40:00 AM PDT,
8	1,
9	Single Node Freezing Problem to Test STOMP Mass and Energy Conservation
10	
11	-Solution Control Card
12	Normal,
13	Water-Air-Ice-Energy,
14	1,
15	0,s,1800,s,25,s,25,s,1.1,8,1.e-6,
16	1,hr,1,hr,1000,
17	Zero,
18	Zero,
19	0,
20	
21	-Grid Card
22	Cartesian,
23	1,1,1,
24	0.0,m,2.1544,m,
25	0.0,m,2.1544,m,
26	0.0,m,2.1544,m,
27	
28	-Rock/Soil Zonation Card
29	1,
30	Generic Sand,1,1,1,1,1,1,
31	
32	-Mechanical Properties Card
33	Generic Sand,2650.0,kg/m^3,0.5,0.5,1.e-7,1/m,
34	
35	-Hydraulic Properties Card
36	Generic Sand,1.0e-14,m^2,1.0e-14,m^2,1.0e-14,m^2,
37	
38	-Thermal Properties Card
39	Generic Sand,Parallel,2.10,W/m K,2.10,W/m K,2.10,W/m K,1000.0,J/kg K,
40	
41	-Saturation Function Card
42	Generic Sand,Nonhysteretic van Genuchten,0.5,1/m,2.0,0.0,1.0,2.36,0.5,
43	
44	-Aqueous Relative Permeability Card
45	Generic Sand,Mualem,0.5,
46	
47	-Gas Relative Permeability Card
48	Generic Sand,Mualem,0.5,
49	
50	-Initial Conditions Card
51	Gas Pressure,Apparent Aqueous Saturation,Temperature,
52	3,
53	Gas Pressure,1.5E+6,Pa,,1/m,,1/m,,1/m,1,1,1,1,1,1,
54	Temperature,10.0,C,,1/m,,1/m,,1/m,1,1,1,1,1,1,
55	Apparent Aqueous Saturation,0.3,,1/m,,1/m,,1/m,1,1,1,1,1,1,

Exhibit 6.3-1. (Contd)

<u>Line</u>	<u>Input File</u>
56	
57	-Source Card
58	1,
59	Power Density,1,1,1,1,1,1,1,
60	0,s,-5.0E+4,W/m^3,
61	
62	-Output Control Card
63	1,
64	1,1,1,
65	1,1,s,m,3,5,5,
66	3,
67	Temperature,,
68	Ice Saturation,,
69	Aqueous Saturation,,
70	1,
71	1800,s,
72	12,
73	Aqueous Pressure,,
74	Gas Pressure,,
75	Temperature,,
76	Phase Condition,,
77	Ice Saturation,,
78	Aqueous Saturation,,
79	Gas Saturation,,
80	Gas Water Mass Fraction,,
81	Aqueous Water Mass Fraction,,
82	Ice Density,,
83	Aqueous Density,,
84	Gas Density,,
85	

6.4 Single Node Thawing

The single node thawing problem involves the melting of ice within a closed adiabatic volume of porous medium initially desaturated. The thawing process occurs through the removal of heat from the control volume.

Sufficient heat is removed from the system to cause

melting and partially saturate the porous medium. Because the control volume surfaces are closed and adiabatic, the initial quantities of air and water mass should remain constant throughout the simulation. This problem demonstrates this numerical transition from frozen to unfrozen conditions. The problem requires the coupled solution of the water mass, air mass, and energy conservation equations with the Frozen Water Option.

Problem Features: 6.4

- Water-Air-Energy operation mode
- solid (ice)-liquid phase change
- single node
- variable saturation
- homogeneous, isotropic
- Cartesian grid
- van Genuchten function
- mass balance test

6.4.1 Problem Domain and Input Parameters

This problem involves a 10-m³ cube of porous media, with a total porosity of 0.50, rock density of 2650 kg/m³, and specific heat of 1000 J/kg K. The initial gas pressure, aqueous saturation, ice saturation, and temperature are 1.5 MPa, 0.0001, 0.40, and -10°C, respectively. A constant internal heat addition rate of 0.5 MW is applied for 30 minutes. All boundary surfaces are adiabatic, no-flow surfaces. The STOMP input file is shown in Exhibit 6.4-1.

6.4.2 Simulation

Simulation results in terms of the system temperature, aqueous saturation, and ice saturation are illustrated in Figure 6.4-1. Aqueous saturation is nearly constant as the temperature is increased linearly from 10°C to the freezing point. As thawing commences, the temperature remains constant with time during the phase change (see Figure 6.4-1), while aqueous saturation decreases and ice saturation increases (i.e., water mass undergoes phase change from aqueous to ice phase). After nearly all of the water mass has been frozen, the temperature begins to decrease again with no significant change in phase saturations, until the end of the 1 hour simulated time when the final temperature is 10.0°C. Table 6.4-1 lists the values of parameters necessary to perform the mass balance check for this problem at initial and final conditions. These values were obtained from the plot files generated by STOMP using the STOMP input file shown in

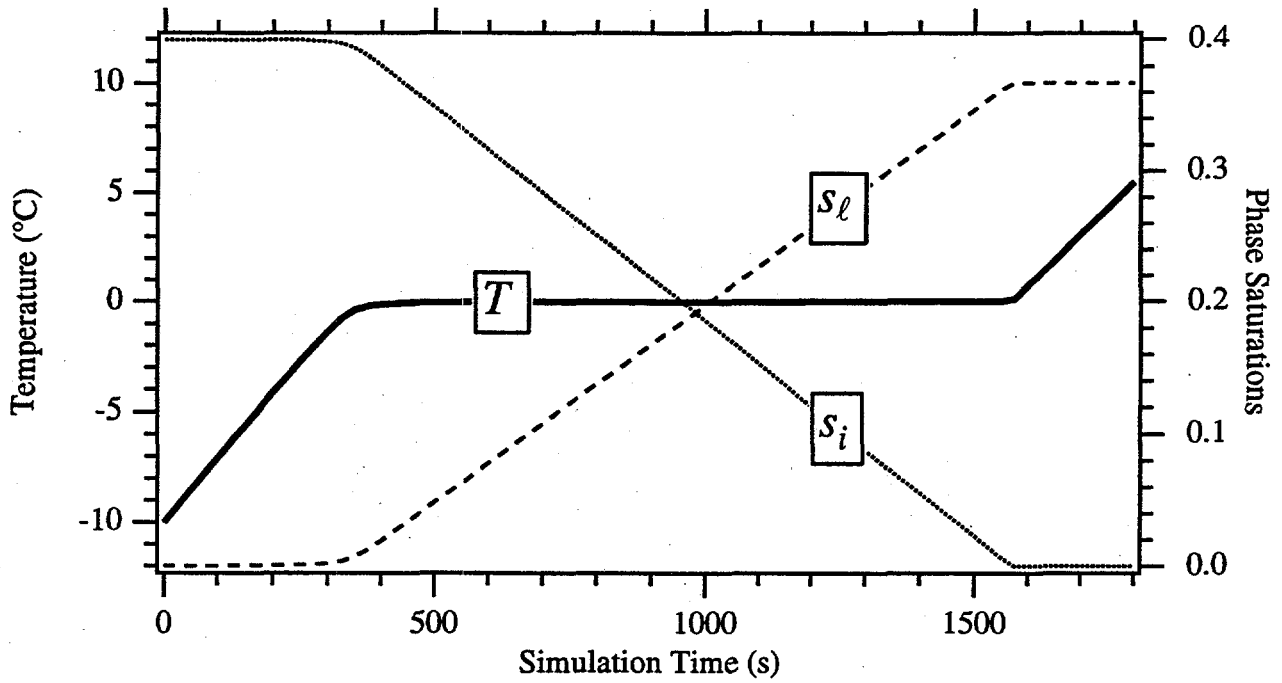


Figure 6.4-1. STOMP Predicted Temperature and Phase Change with Time for the Single Node Thawing Problem

Table 6.4-1. Single Node Freezing Problem Initial and Final Conditions

Variable	Units	Initial Conditions	Final Conditions
V	m^3	10.0	10.0
n_T	-	0.50	0.50
n_D	-	0.50	0.50
T	$^{\circ}C$	-10.000	5.4545
s_i	-	0.39973	0.00000
s_l	-	0.00026696	0.36726
ρ_i	kg/m^3	918.38	-
ρ_l	kg/m^3	998.39	1000.5
ρ_g	kg/m^3	14.563	13.663
x_l^*	-	0.99974	0.99974

Exhibit 6.4-1 (initial conditions obtained by repeating the simulation with the "Initial" rather than "Normal" execution mode).

6.4.3 Analysis (Mass Balance Check)

Mass is conserved within the closed volume of this problem. The expressions for water mass in each phase and mass balance are the same as for those for the preceeding Single Node Freezing Problem (Section 6.3), expressed in Equation 6.3-1 through Equation 6.3-4. For this problem, we calculate the mass balance as follows.

At the start of the 30-minute simulation, most of the water mass is in ice phase, and the mass of water in ice is

$$\begin{aligned} m_i^w &= s_i n_D V \rho_i \\ &= (0.39973)(0.50)(10 \text{ m}^3)(918.38 \text{ kg/m}^3) \\ &= 1835.52 \text{ kg} \end{aligned}$$

Equation 6.4-1

The small amount of aqueous phase water has mass

$$\begin{aligned} m_l^w &= (n_T - n_D + s_l n_D) V \rho_l \\ &= [0.50 - 0.50 + (0.00026696)(0.50)](10 \text{ m}^3)(998.39 \text{ kg/m}^3) \\ &= 1.33265 \text{ kg} \end{aligned}$$

Equation 6.4-2

and the initial gas water phase is

$$\begin{aligned} m_g^w &= (1 - s_l - s_i) n_D V x_l^w \rho_g \\ &= (1 - 0.00026696 - 0.39973)(0.50)(10 \text{ m}^3)(0.99974)(14.563 \text{ kg/m}^3) \\ &= 43.6779 \text{ kg} \end{aligned}$$

Equation 6.4-3

And the sum of these three phase masses yields a total of 1880.53 kg of water.

After 30 minutes of heating, the temperature has risen to 5.5°C and ice is no longer present in the system. ($s_i = 0$). Final water mass in aqueous phase at this time is

$$\begin{aligned} m_l^w &= (n_T - n_D + s_l n_D) V \rho_l \\ &= [0.50 - 0.50 + (0.36726)(0.50)] (10 \text{ m}^3) (1000.5 \text{ kg/m}^3) \\ &= 1837.22 \text{ kg} \end{aligned}$$

Equation 6.4-4

and the final water mass in gas phase is

$$\begin{aligned} m_g^w &= (1 - s_l - s_i) n_D V x_l^w \rho_g \\ &= (1 - 0.36726 - 0.00) (0.50) (10 \text{ m}^3) (0.99974) (13.663 \text{ kg/m}^3) \\ &= 43.2144 \text{ kg} \end{aligned}$$

Equation 6.4-5

Thus, the total water mass for the initial conditions is 1880.43 kg. The difference in total water mass computed for initial and final conditions, 1880.53 kg - 1880.43 kg = 0.10 kg, represents a mass balance error of 0.0053%.

6.4.4 Summary

This problem represents an internal consistency check to confirm that mass was conserved during a phase change simulation involving freezing phenomena (in this case, the reverse of the phase change examined in the previous problem, Section 6.3). Error in mass balance was less than 0.006%.

Exhibit 6.4-1. STOMP Input File for Single Node Thawing Problem

<u>Line</u>	<u>Input File</u>
1	-Simulation Title Card
2	1,
3	Single Node Thawing Problem,
4	W.E. Nichols,
5	Pacific Northwest Laboratory,
6	August 1 1995,
7	9:25:00 AM PDT,
8	1,
9	Single Node Thawing Problem to Test STOMP Mass and Energy Conservation
10	
11	-Solution Control Card
12	Normal,
13	Water-Air-Ice-Energy,
14	1,
15	0,s,1800,s,25,s,25,s,1.1,8,1.e-6,
16	1,hr,1,hr,1000,
17	Zero,
18	Zero,
19	0,
20	
21	-Grid Card
22	Cartesian,
23	1,1,1,
24	0.0,m,2.1544,m,
25	0.0,m,2.1544,m,
26	0.0,m,2.1544,m,
27	
28	-Rock/Soil Zonation Card
29	1,
30	Generic Sand,1,1,1,1,1,1,
31	
32	-Mechanical Properties Card
33	Generic Sand,2650.0,kg/m^3,0.5,0.5,1.e-7,1/m,
34	
35	-Hydraulic Properties Card
36	Generic Sand,1.0e-14,m^2,1.0e-14,m^2,1.0e-14,m^2,
37	
38	-Thermal Properties Card
39	Generic Sand,Parallel,2.10,W/m K,2.10,W/m K,2.10,W/m K,1000.0,J/kg K,
40	
41	-Saturation Function Card
42	Generic Sand,Nonhysteretic van Genuchten,0.5,1/m,2.0,0.0,1.0,2.36,0.5,
43	
44	-Aqueous Relative Permeability Card
45	Generic Sand,Mualem,0.5,
46	
47	-Gas Relative Permeability Card
48	Generic Sand,Mualem,0.5,
49	
50	-Initial Conditions Card
51	Gas Pressure,Apparent Aqueous Saturation,Temperature,
52	3,
53	Gas Pressure,1.1E+6,Pa,,1/m,,1/m,,1/m,1,1,1,1,1,1,
54	Temperature,-10.0,C,,1/m,,1/m,,1/m,1,1,1,1,1,1,
55	Apparent Aqueous Saturation,0.40,,,1/m,,1/m,,1/m,1,1,1,1,1,1,

Exhibit 6.4-1. (Contd)

<u>Line</u>	<u>Input File</u>
56	
57	-Source Card
58	1,
59	Power Density,1,1,1,1,1,1,1,
60	0,s,5.0E+4,W/m^3,
61	
62	-Output Control Card
63	1,
64	1,1,1,
65	1,1,s,m,3,5,5,
66	3,
67	Temperature,,
68	Ice Saturation,,
69	Aqueous Saturation,,
70	1,
71	1800,s,
72	12,
73	Aqueous Pressure,,
74	Gas Pressure,,
75	Temperature,,
76	Phase Condition,,
77	Ice Saturation,,
78	Aqueous Saturation,,
79	Gas Saturation,,
80	Gas Water Mass Fraction,,
81	Aqueous Water Mass Fraction,,
82	Ice Density,,
83	Aqueous Density,,
84	Gas Density,,
85	

6.5 Flow from Hot Two-Phase Conditions

Problem Features: 6.5

- Water-Air-Energy operation mode
- two-phase flow
- one dimensional (x)
- variable saturation
- homogeneous, isotropic
- Cartesian grid
- van Genuchten function
- energy conservation test

This problem is concerned with two-phase flow between two adjacent cubes of porous medium with sharply differing initial conditions. The problem starts with both nodes in two-phase conditions; however, one node is nearly saturated with relatively cool water and the other is nearly desaturated at an elevated temperature. The problem involves simulating imbibition and vaporization of the liquid water from relatively cool saturated conditions to hot dry conditions. The control volume surfaces surrounding the two nodes are adiabatic and impermeable to fluid flow. The problem proceeds until equilibrium conditions are reached. This simulation demonstrates the conservation of water mass, air mass, and thermal energy by the STOMP simulator for two-phase flow conditions. An energy balance error analysis is presented.

6.5.1 Problem Domain and Input Parameters

The problem involves two cubes of porous medium, both with porosity 0.50, volume 10 m^3 , and hydraulic conductivity $1.0 \times 10^{-14} \text{ m}^2$. The rock thermal conductivity, density, and specific heat are 2.10 W/m K , 2650 kg/m^3 , and 1000 J/kg K , respectively. The initial conditions for the first (west) cube are: gas pressure, $1.0 \times 10^5 \text{ Pa}$ (absolute); liquid saturation, 0.999; temperature, 99.5°C . For the second (east) cube, the initial conditions are: gas pressure, $9.9 \times 10^6 \text{ Pa}$ (absolute); liquid saturation, 0.001; temperature, 310.0°C . The input file used in this application is shown in Exhibit 6.5-1.

6.5.2 Simulation

The simulation performed with STOMP using the input file in Exhibit 6.5-1 yielded the final variable values reported in the "Final Conditions" columns of Table 6.5-1. Values in Table 6.5-1 were taken from the STOMP plot file generated during the simulation.

Table 6.5-1. Hot Two-Phase Flow Problem Initial and Final Conditions

Variable	Units	Initial Conditions		Final Conditions	
		West Node	East Node	West Node	East Node
c_s	J/kg K	1000.0	1000.0	1000.0	1000.0
n_T	m ³ /m ³	0.50	0.50	0.50	0.50
ρ_s	kg/m ³	2650.0	2650.0	2650.0	2650.0
ρ_l	kg/m ³	958.47	690.65	902.81	902.81
ρ_g	kg/m ³	0.59551	38.426	8.0980	8.0980
s_l	-	0.999	0.001	0.54789	0.54788
s_g	-	0.001	0.999	0.45211	0.45212
T	°C	99.5	310.0	164.87	164.87
u_l^w	kJ/kg	416.83	1387.1	696.00	696.00
u_g^w	kJ/kg	2505.91	2546.4	2572.39	2572.39
u_g^a	kJ/kg	266.39	421.96	313.89	313.89
x_g^w	-	0.97177	0.88704	0.42657	0.42657

6.5.3 Analysis (Energy Conservation Check)

Let q_i represent the thermal energy in computational node i ; q_i is the sum of the rock or soil internal energy, aqueous-phase-water internal energy, water-vapor internal energy, and air internal energy (the contribution from air dissolved in the aqueous phase is negligible):

$$q = (1 - n_T) c_s \rho_s T + s_l \rho_l n_D u_l^w + s_g \rho_g x_g^w n_D u_g^w + s_g \rho_g (1 - x_g^w) n_D u_g^a$$

Equation 6.5-1

The total energy in the problem domain at time t is the sum of all computational nodes, or Σq_i . Table 6.5-1 lists the values of all of the parameters required by Equation 6.5-1 for both initial and final conditions. All parameter values except the internal energies (u_l^w , u_g^w , u_g^a) were obtained from STOMP-generated "plot" files using the STOMP input file shown in Exhibit 6.5-1. The plot file for initial conditions was obtained by changing the Operational Mode Option in the input file

(Exhibit 6.5-1, line 13 in the Solution Control Card) from "Normal" to "Initial" and running STOMP again. The values for the internal energies of water in the aqueous and gas phases were obtained from steam tables (Table A.1, van Wylen and Sonntag (1985)). The values for the internal energy of air in the gas phase were obtained from a table of ideal gas integrals for air (van Wylen and Sonntag (1985), Table A.10).

Computing the total internal energy per unit volume for the west node at initial conditions:

$$\begin{aligned}
 q_{west}^{init} &= (1 - 0.50) \left(1000 \frac{\text{J}}{\text{kg K}} \right) \left(2650 \frac{\text{kg}}{\text{m}^3} \right) (372.65 \text{ K}) \\
 &+ (0.999) \left(958.47 \frac{\text{kg}}{\text{m}^3} \right) (0.50) \left(416,830 \frac{\text{J}}{\text{kg}} \right) \\
 &+ (0.001) \left(0.59551 \frac{\text{kg}}{\text{m}^3} \right) (0.97177) (0.50) \left(2,050,910 \frac{\text{J}}{\text{kg}} \right) \\
 &+ (0.001) \left(0.59551 \frac{\text{kg}}{\text{m}^3} \right) (1 - 0.97177) (0.50) \left(266,390 \frac{\text{J}}{\text{kg}} \right) \\
 &= 6.9332 \times 10^8 \text{ J/m}^3
 \end{aligned}$$

Equation 6.5-2

which, when multiplied by the node volume (10 m^3), yields the total node energy at time zero of $6.9332 \times 10^9 \text{ J}$. Repeating for the east node, we obtain

$$\begin{aligned}
 q_{east}^{init} &= (1 - 0.50) \left(1000 \frac{\text{kg}}{\text{kg K}} \right) \left(2650 \frac{\text{kg}}{\text{m}^3} \right) (583.15 \text{ K}) \\
 &+ (0.001) \left(690.65 \frac{\text{kg}}{\text{m}^3} \right) (0.50) \left(1,387,100 \frac{\text{J}}{\text{kg}} \right) \\
 &+ (0.999) \left(38.426 \frac{\text{kg}}{\text{m}^3} \right) (0.88704) (0.50) \left(2,546,400 \frac{\text{J}}{\text{kg}} \right) \\
 &+ (0.999) \left(38.426 \frac{\text{kg}}{\text{m}^3} \right) (1 - 0.88704) (0.50) \left(421,960 \frac{\text{J}}{\text{kg}} \right) \\
 &= 8.1742 \times 10^8 \text{ J/m}^3
 \end{aligned}$$

Equation 6.5-3

for which the total energy is therefore 8.4258×10^9 J. The total energy in the problem domain is the sum of these two nodes, or 15,107 MJ. For the final conditions, the two nodes are in equilibrium; hence only one calculation is necessary:

$$\begin{aligned}
 q^{final} &= (1 - 0.50) \left(1000 \frac{\text{kg}}{\text{kg K}} \right) \left(2650 \frac{\text{kg}}{\text{m}^3} \right) (438.02 \text{ K}) \\
 &+ (0.54789) \left(902.81 \frac{\text{kg}}{\text{m}^3} \right) (0.50) \left(696,000 \frac{\text{J}}{\text{kg}} \right) \\
 &+ (0.45211) \left(8.0980 \frac{\text{kg}}{\text{m}^3} \right) (0.42657) (0.50) \left(2,572,390 \frac{\text{J}}{\text{kg}} \right) \\
 &+ (0.45211) \left(8.0980 \frac{\text{kg}}{\text{m}^3} \right) (1 - 0.42657) (0.50) \left(313,890 \frac{\text{J}}{\text{kg}} \right) \\
 &= 7.5485 \times 10^8 \text{ J/m}^3
 \end{aligned}$$

Equation 6.5-4

This applies for both nodes, or a total volume of 20 m^3 ; hence the total energy in the system predicted by STOMP at the end of the simulation for equilibrium conditions is 15,097 MJ. The difference between the total energy in the domain at the beginning and at the end of the simulation (10 MJ) is the error introduced during the simulation by STOMP through numerical approximation, and is equal to 0.07% of the initial total energy.

6.5.4 Summary

This problem represents an internal consistency check to confirm energy conservation only. Error in the energy balance for this problem was 0.07%. This problem was also reported in Nichols and White (1993) for the MSTS code; the MSTS code yielded a energy balance error of 0.013%.

Exhibit 6.5-1. STOMP Input File for Hot Two-Phase Problem

<u>Line</u>	<u>Input File</u>
1	~Simulation Title Card
2	1,
3	Flow From Hot Two-Phase Conditions,
4	W.E. Nichols,
5	Pacific Northwest Laboratory,
6	July 26 1995,
7	10:35:00 AM PDT,
8	1,
9	Flow from hot two-phase conditions
10	
11	~Solution Control Card
12	Normal,
13	Water-Air-Energy,
14	1,
15	0,s,1.875E+8,s,10.0,s,1.875E+8,s,1.1,8,1.0e-6,
16	1,hr,1,hr,5000,
17	Zero,
18	Zero,
19	0,
20	
21	~Grid Card
22	Cartesian,
23	2,1,1,
24	0.0,m,2.15443,m,4.30887,m,
25	0.0,m,2.15443,m,
26	0.0,m,2.15443,m,
27	
28	~Rock/Soil Zonation Card
29	1,
30	Generic Sand,1,2,1,1,1,1,
31	
32	~Mechanical Properties Card
33	Generic Sand,2650.0,kg/m ³ ,0.5,0.5,1.e-7,1/m,
34	
35	~Hydraulic Properties Card
36	Generic Sand,1.0e-14,m ² ,1.0e-14,m ² ,1.0e-14,m ² ,
37	
38	~Thermal Properties Card
39	Generic Sand,Constant,2.10,W/m K,2.10,W/m K,2.10,W/m K,1000.0,J/kg K,
40	
41	~Saturation Function Card
42	Generic Sand,Nonhysteretic van Genuchten,0.5,1/m,2.0,0.0,,
43	
44	~Aqueous Relative Permeability Card
45	Generic Sand,Mualem,0.5,
46	
47	~Gas Relative Permeability Card
48	Generic Sand,Mualem,0.5,
49	
50	~Initial Conditions
51	Gas Pressure, Aqueous Saturation,
52	6,
53	Gas Pressure,1.0E+5,Pa,,1/m,,1/m,,1/m,1,1,1,1,1,1,
54	Gas Pressure,99.0E+5,Pa,,1/m,,1/m,,1/m,2,2,1,1,1,1,
55	Aqueous Saturation,0.999,,1/m,,1/m,,1/m,1,1,1,1,1,1,

Exhibit 6.5-1. (Contd)

<u>Line</u>	<u>Input File</u>
56	Aqueous Saturation,0.001,,,1/m,,1/m,,1/m,2,2,1,1,1,1,
57	Temperature,99.5,C,,1/m,,1/m,,1/m,1,1,1,1,1,1,
58	Temperature,310.0,C,,1/m,,1/m,,1/m,2,2,1,1,1,1,
59	
60	-Sources & Sinks
61	0,
62	
63	-Output Control Card
64	1,
65	1,1,1,
66	1,1,s,m,3,3,5,
67	4,
68	Aqueous Pressure,,
69	Gas Pressure,,
70	Temperature,,
71	Aqueous Saturation,,
72	1,
73	1.875E+8,s,
74	10,
75	Aqueous Pressure,,
76	Gas Pressure,,
77	Temperature,,
78	Phase Condition,,
79	Aqueous Saturation,,
80	Gas Saturation,,
81	Gas Phase Water Mass Frac,,,
82	Aqueous Phase Water Mass Frac,,,
83	Aqueous Density,,
84	Gas Density,,
85	

6.6 References

Nichols WE, and MD White. 1993. *MSTS: Multiphase Subsurface Transport Simulator User's Guide and Reference*. PNL-8637, Pacific Northwest Laboratory, Richland, Washington.

van Wylen G, and RE Sonntag. 1985. *Fundamentals of Classical Thermodynamics*, trans., Wiley, New York.

7.0 Heat Pipe Effect

The heat pipe problem is a classic test of a numerical simulator's ability to simulate countercurrent hydrothermal flow in geologic media. The problem typically consists of a heat source and a heat sink separated by a partially saturated porous media. Two specific heat pipe problems are solved and discussed in this Section; the first is the more common heat pipe involving evaporation of water into gas phase at the heat source and condensation into aqueous phase at the heat sink, with countercurrent flow and heat transfer between. The second problem is a heat pipe in a different temperature regime: between freezing and thawing conditions to demonstrate the ice phase capability of the STOMP simulator.

7.1 Evaporation / Condensation Heat Pipe

Hydrogeologic heat pipes have been shown to occur in partially saturated soils subjected to thermal gradients. For example, radial heat pipes have been created around the nuclear waste packages emplaced in variably saturated and fractured rock during the Engineering Barrier Design Test at the Yucca Mountain Exploratory Shaft Test Site (Buscheck and Nitao 1988). The general requirements for creating countercurrent hydrothermal (i.e., heat pipe) flow in geologic media are a heat source and heat sink separated by partially saturated porous media. The heat source causes pore water to evaporate, creating a locally elevated gas pressure and water vapor concentration. Evaporation of the pore water reduces the saturation near the heat source, which in turn elevates the local capillary pressure. The heat sink causes water vapor to condense, creating a locally reduced gas pressure and water vapor concentration. The condensing water vapor also increases the local saturation. The pressure and water vapor gradients in the gas phase produce a flow of water vapor and associated heat from the heat source to the heat sink. Conversely, the capillary draw created by the elevated capillary pressures near the heat sink produces flow of liquid water towards the heat source. This countercurrent flow of water vapor in the gas phase and liquid water in the aqueous phase yields a net flow of heat from the heat source to the heat sink. Because of the importance of heat pipe flow to the overall heat transfer of engineered geologic systems, the ability of the numerical simulator to accurately and efficiently predict these complex and multiple-phase flow

Problem Features: 7.1

- Water-Air-Energy operational mode
- countercurrent flow in two phases
- one dimensional (x)
- uniform Cartesian grid
- variable saturation
- homogeneous, isotropic
- Fatt and Klikoff functions

structures is imperative. The heat pipe problem chosen for solution is a modified version of the problem posed and solved by Udell and Fitch (1985).

7.1.1 Problem Description and Parameters

The heat pipe problem solved by Udell and Fitch involved a one-dimensional horizontal cylinder (2.25m in length) of porous media, which was assumed perfectly insulated on the sides, subjected to a constant heat flux (100W/m²) on one end, and maintained at a constant temperature (70°C) on the other end. The heat flux end of the cylinder was sealed and the constant temperature end was maintained under total-liquid saturation conditions. Initial conditions for the porous media were a total-liquid saturation of 0.7, a temperature of 70°C, and an absolute gas pressure of 101,330 Pa. Initial conditions and boundary conditions are listed for reference in Table 7.1-1.

The constitutive functions used in this problem differ slightly from those used by Udell and Fitch. The soil-moisture retention function was the van Genuchten relation modified to extend the curve below residual saturations as shown in Equation 7.1-1. This form allows the liquid saturation to drop below the residual saturation for high capillary pressures, as expected near the heat source. The aqueous- and gas-phase relative permeability functions were the Fatt and Klikoff relations and the effective thermal conductivity function followed the model of Somerton, refer to the STOMP Theory Guide (White and Oostrom 1996). Constants for the soil-moisture retention, relative permeability, and thermal conductivity constitutive functions and other physical properties are listed in Table 7.1-2. Gas and aqueous phase properties were computed as functions of temperature and pressure, refer to the STOMP Theory Guide (White and Oostrom 1996). The STOMP input file for this problem is shown in Exhibit 7.1-1.

$$s_l = \left[1 + (\alpha h_{gl})^n \right]^{-m} (1 - \bar{s}_m) + \bar{s}_m$$

Equation 7.1-1

where,

$$\bar{s}_m = \left(1 - \frac{\ln(h_{gl})}{\ln(h_{od})} \right) s_m$$

Equation 7.1-2

Table 7.1-1. Initial and Boundary Conditions for the Evaporation / Condensation Heat Pipe Problem

Property Description	Symbol	Property Value
<i>Initial Condition Parameter Values</i>		
Total Aqueous Saturation	s_l	0.7
Gas Pressure	p_g	101,330. Pa
Temperature	T	70.° C
<i>Heated Boundary Parameter Values</i>		
Aqueous Flux		0. m ³ /m ² s
Gas Flux		0. m ³ /m ² s
Energy Flux		100. W/m ²
<i>Saturated Boundary Parameter Values</i>		
Total Aqueous Saturation	s_l	1.
Gas Pressure	p_g	101,330. Pa
Temperature	T	70.° C

Table 7.1-2. Constitutive Function and Physical Parameters for the Evaporation / Condensation Heat Pipe Problem

Property Description	Symbol	Property Value
Dry Thermal Conductivity		0.582 W/m K
Wet Thermal Conductivity		1.130 W/m K
Intrinsic Permeability	k	1.0 x 10 ⁻¹² m ²
Porosity	n	0.4
Soil Grain Density	ρ_s	2650. kg/m ³
Soil Grain Specific Heat	c_s	700. J/kg K
Gas Tortuosity	τ	0.5
van Genuchten α Parameter	α	1.5631/m
van Genuchten n Parameter	n	5.4
Residual Saturation	θ_r	0.15

7.1.2 Simulation

Simulation results in terms of temperature, total-liquid saturation, and water vapor mass fraction, as a function of distance from the saturated boundary, are shown in Figure 7.1-1 through Figure 7.1-5, at times of 2, 5, 10, 50, and 876.6 days, respectively. After 2 days (Figure 7.1-1), the temperature on the heated boundary has risen to near 97°C and water has started to imbibe from the saturated boundary. Because the temperature on the heated boundary has not risen above the boiling point, the temperature profile has little influence on the total-liquid saturation profile. After 5 days (Figure 7.1-2), the temperature on the heated boundary has risen to the boiling point of 102°C and the elevated gas pressures are forcing the total-liquid saturation to fall. The gas phase near the heated boundary comprises nearly all water vapor with small amounts of noncondensibles. After 10 days (Figure 7.1-3), the trends established after 5 days continue to develop. The heated boundary temperature has risen slightly to 102.5°C and the liquid saturation continues to fall because of the elevated gas pressures forcing both liquid water and water vapor towards the saturated boundary. A portion of the temperature profile near the heated boundary remains nearly constant with a sharp decline near the 1.25 m point from the saturated boundary. Condensation of the water-vapor is occurring on the saturated boundary side of this point as evidenced by the slight

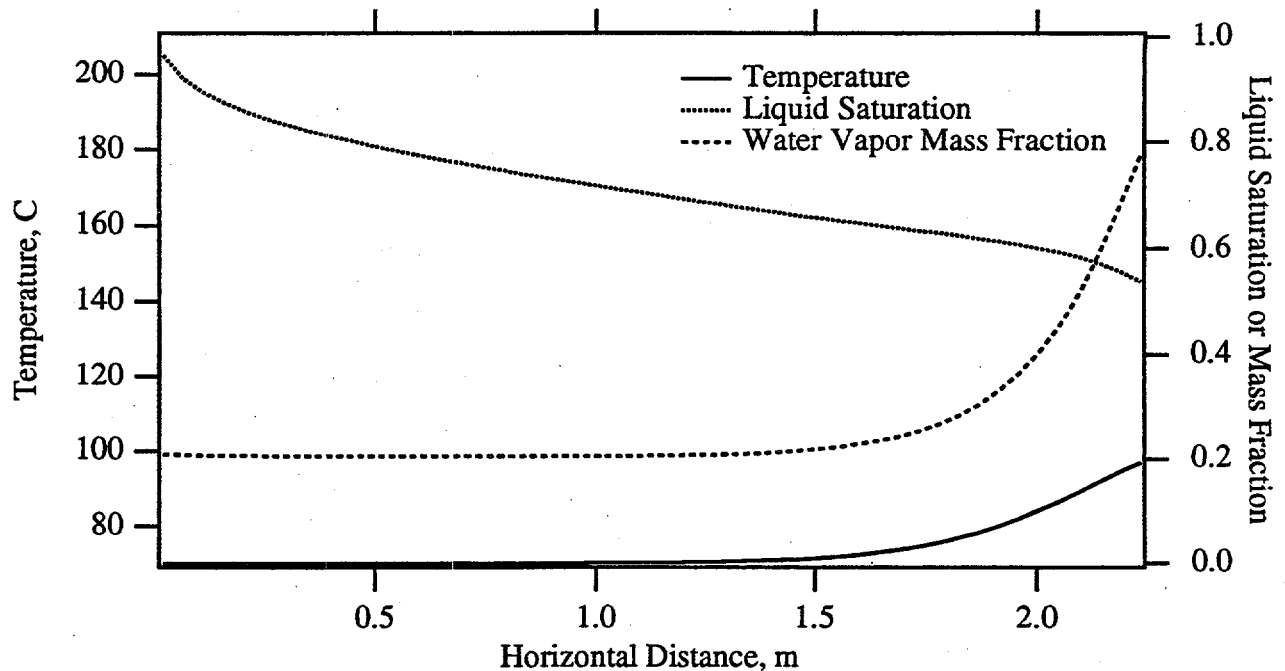


Figure 7.1-1. Temperature, Total-Liquid Saturation, and Water Vapor Mass Fraction Profiles Versus Distance from Saturated Boundary after 2 Days

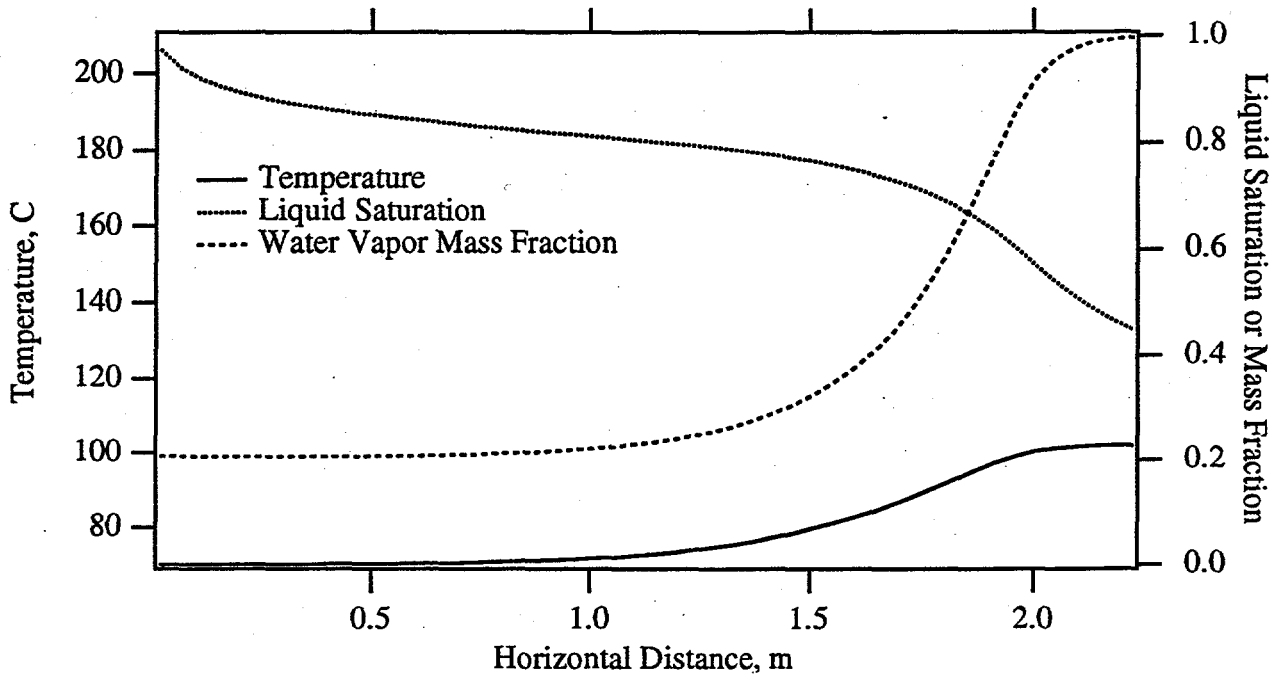


Figure 7.1-2. Temperature, Total-Liquid Saturation, and Water Vapor Mass Fraction Profiles Versus Distance from Saturated Boundary after 5 Days

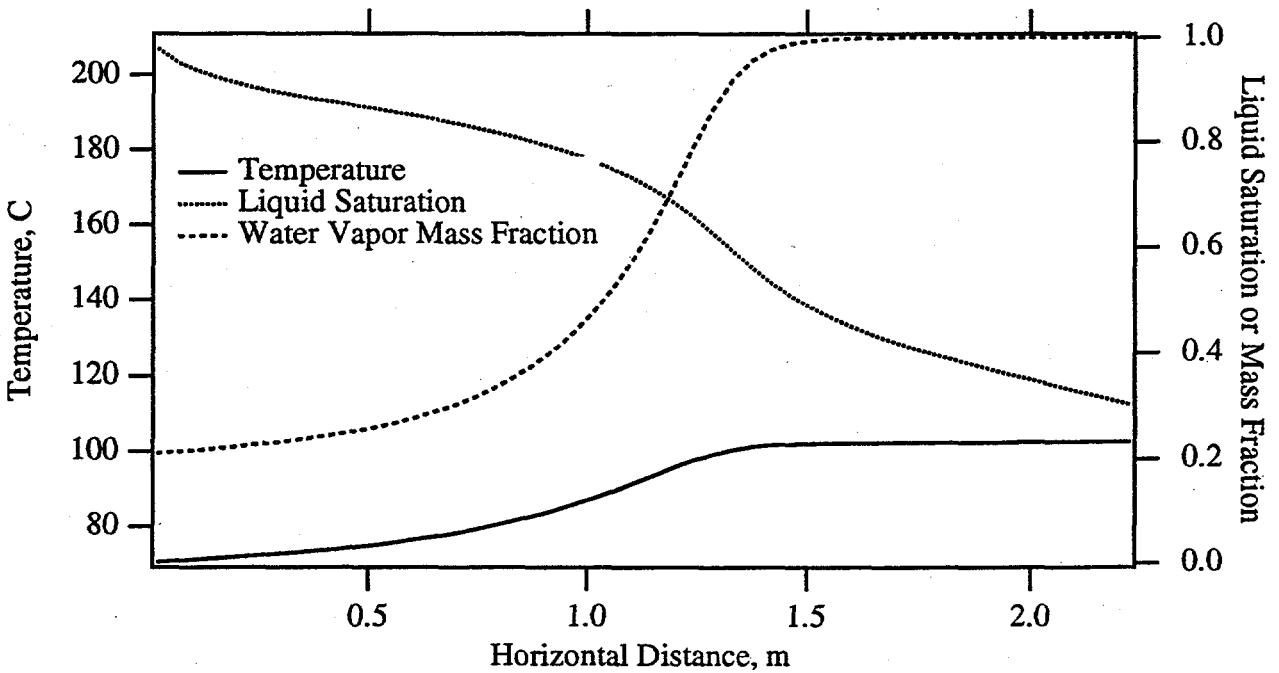


Figure 7.1-3. Temperature, Total-Liquid Saturation, and Water Vapor Mass Fraction Profiles Versus Distance from Saturated Boundary after 10 Days

bulge in the total-liquid saturation profile. After 50 days (Figure 7.1-4), conditions in the heat pipe are nearing steady-state conditions. The temperature profile has three distinct sections. Nearest the heat boundary the temperature profile is linear with distance indicating that the heat transfer is dominated by thermal conduction through the nearly dry soil. In the middle section of the heat pipe the temperature profile is constant indicating that heat transfer is occurring through countercurrent flow of gas and liquid with condensation and evaporation. The saturated boundary portion of the heat pipe shows combined conduction and advection-diffusion heat transfer. Steady-state conditions were reached after 876.6 days (Figure 7.1-5), using 94 time steps. The profiles resemble those at 50 days indicating that near steady-state conditions were reached after 50 days. The total liquid saturation profile near the heated boundary shows a marked decrease followed by a more gradual decrease with distance from the saturated boundary. All saturations in this region are below the residual saturation of 0.15 and are computed according to the saturation function extensions, refer to the STOMP Theory Guide (White and Oostrom 1996).

7.1.3 Analysis

The heat-pipe problem, which was solved using a semi-analytical approach by Udell and Fitch (1985), differs from the current problem in several aspects. First, the Udell and Fitch problem used constant physical properties, whereas the STOMP simulation included temperature and pressure dependent physical properties for the gas and aqueous phases. Second, nitrogen gas, instead of air, was used as the noncondensable in the Udell and Fitch problem. Third, the saturation-capillary function in the Udell and Fitch formulation used the Leverett function (Leverett 1941) without extensions below the residual saturation, whereas the STOMP simulation used a van Genuchten function which closely matched the Leverett function. In spite of these differences the results show good agreement between the solution of Udell and Fitch and the STOMP simulation for the steady-state conditions; the Udell and Fitch solution is valid only for the steady-state solution. Both results show temperature profiles with mixed conduction and advection/diffusion heat transport near the saturated boundary and nearly pure countercurrent gas and aqueous flow heat transport in the center portion of the heat pipe. The Udell and Fitch solution stops short of the dry-out region with the minimum saturation being the residual saturation level. The STOMP solution allows a region near the heated boundary to dry out, thus creating elevated temperatures, in comparison to the Udell and Fitch results.

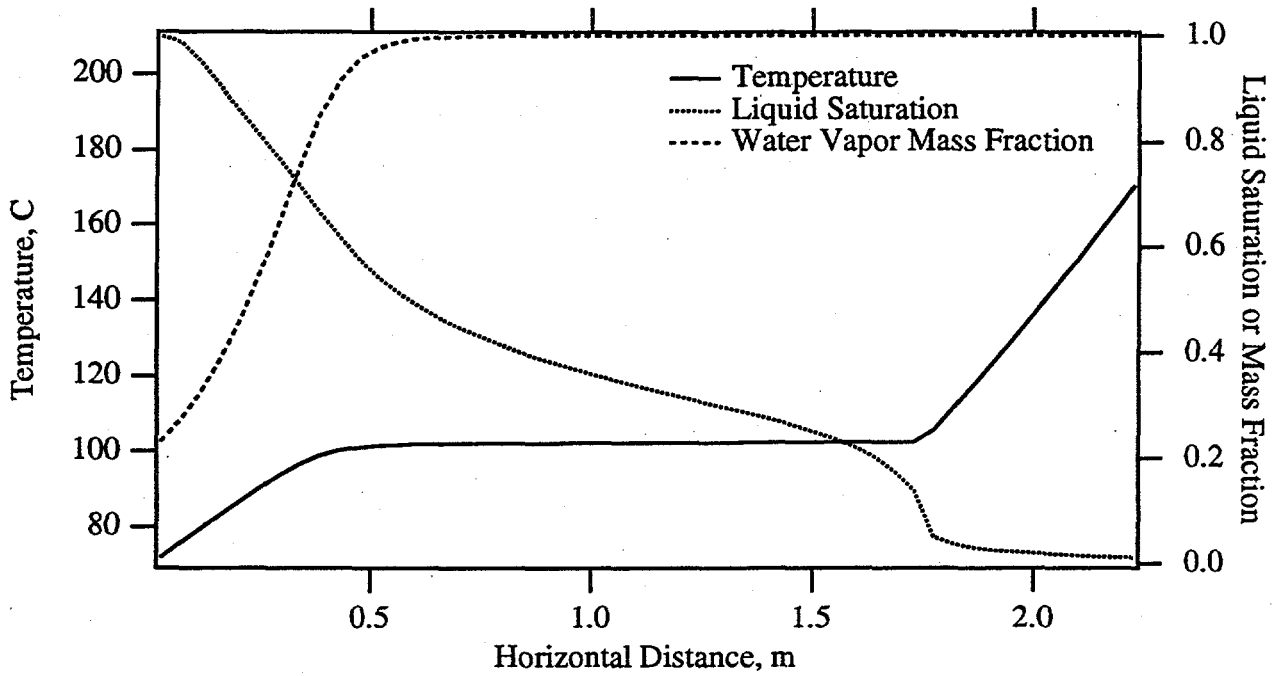


Figure 7.1-4. Temperature, Total-Liquid Saturation, and Water Vapor Mass Fraction Profiles Versus Distance from Saturated Boundary after 50 Days

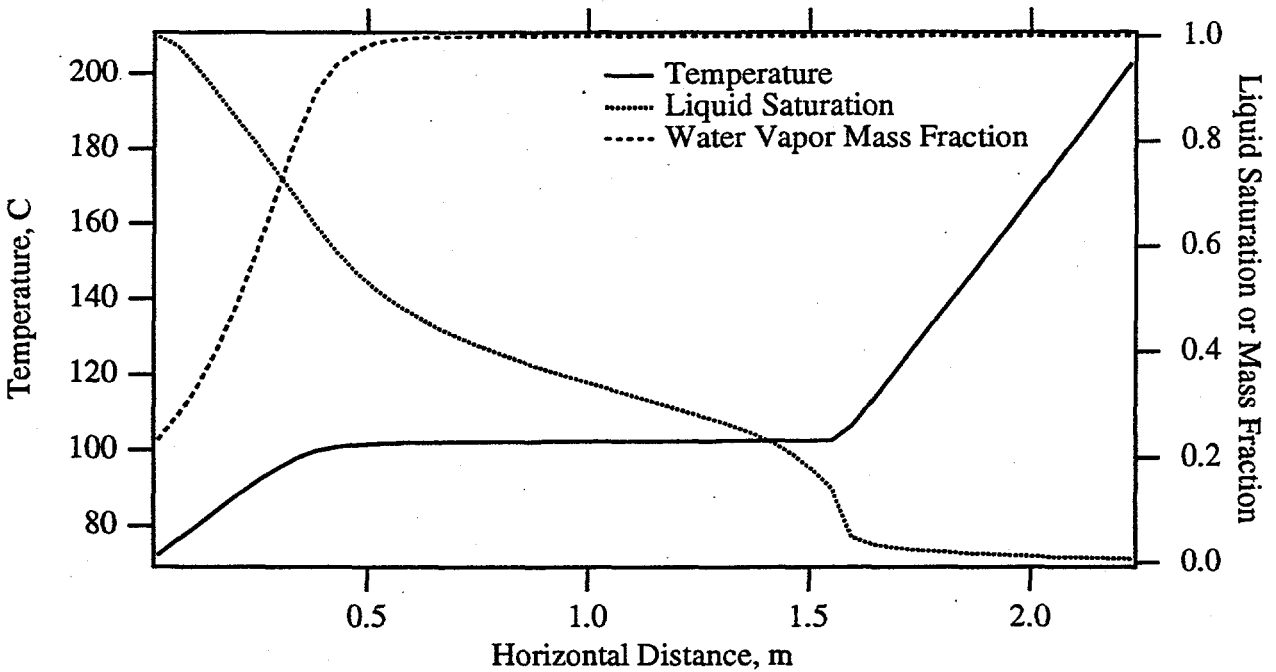


Figure 7.1-5. Temperature, Total-Liquid Saturation, and Water Vapor Mass Fraction Profiles Versus Distance from Saturated Boundary after 876.6 Days

7.1.4 Summary

The heat-pipe problem was selected as a classical problem because it represents a class of nonisothermal hydrologic systems which produce heat-pipe type conditions. Heat-pipe flows that develop in natural systems, however, are generally three-dimensional. A key component of these simulations is the use of a modified van Genuchten saturation function (Fayer and Simmons 1995) to represent soil moisture retention at all matric suctions. This modification retains the form of the original van Genuchten function in the wet range and transforms to an adsorption equation in the dry range. This approach allows the use of conventionally determined van Genuchten function parameters to obtain a reasonable representation in the high matric suction range, therefore allowing saturations to decrease below the residual saturation level. For nonisothermal conditions the residual saturation becomes solely a function fitting parameter and does not represent a lower saturation limit.

Exhibit 7.1-1. STOMP Input File for Evaporation/Condensation Heat Pipe Problem

<u>Line</u>	<u>Input File</u>
1	~Simulation Title Card
2	1,
3	Evaporation/Condensation Heat Pipe,
4	M.D. White,
5	Pacific Northwest Laboratory,
6	June 18 1994,
7	10:04 AM PDT,
8	4,
9	This application problem follows the heat-pipe problem solved
10	semi-analytically by Udell and Fitch. The soil moisture retention
11	function has been changed to a modified van Genuchten function to
12	allow saturations for all matric suctions.
13	
14	~Solution Control Card
15	Normal,
16	Water-Air-Energy,
17	1,
18	0,day,876.6,day,10,s,100,day,1.25,16,1.e-06,
19	1,day,1,day,1000,
20	Variable Aqueous Diffusion,
21	Variable Gas Diffusion,
22	0,
23	
24	~Grid Card
25	Uniform Cartesian,
26	50,1,1,
27	4.5,cm,
28	10.0,cm,
29	10.0,cm,
30	
31	~Rock/Soil Zonation Card
32	1,
33	Sand,1,50,1,1,1,1,
34	
35	~Mechanical Properties Card
36	Sand,2650,kg/m^3,0.4,0.4,,,Constant,0.5,0.5,
37	
38	~Hydraulic Properties Card
39	Sand,1.e-12,m^2,,,,,
40	
41	~Thermal Properties Card
42	Sand,Somerton,0.582,W/m K,,,,,1.13,W/m K,,,,,700,J/kg K,
43	
44	~Saturation Function Card
45	Sand,Nonhysteretic van Genuchten,1.563,1/m,5.4,0.15,,
46	
47	~Aqueous Relative Permeability Card
48	Sand,Fatt and Klikoff,
49	
50	~Gas Relative Permeability Card
51	Sand,Fatt and Klikoff,
52	
53	~Initial Conditions Card
54	Aqueous Saturation,Gas Pressure,
55	3,

Exhibit 7.1-1. (Contd)

<u>Line</u>	<u>Input File</u>
56	Aqueous Saturation,0.5,,,,,,,,1,50,1,1,1,1,
57	Gas Pressure,101330,Pa,,,,,,,,1,50,1,1,1,1,
58	Temperature,70.0,C,,,,,,,,1,50,1,1,1,1,
59	
60	-Boundary Conditions Card
61	2,
62	West,Dirichlet Energy,Dirichlet Aqueous,Dirichlet Gas,
63	1,1,1,1,1,1,1,
64	0,day,70,C,101330,Pa,,101330,Pa,1,
65	East,Neumann Energy,Zero Flux Aqueous,Zero Flux Gas,
66	50,50,1,1,1,1,1,
67	0,day,-100,W/m^2,,,,,,,,
68	
69	-Output Options Card
70	2,
71	1,1,1,
72	50,1,1,
73	1,1,day,m,5,5,5,
74	6,
75	Temperature,,
76	Aqueous saturation,,
77	Phase condition,,
78	Water gas mass frac,,,
79	Aqueous pressure,,
80	Gas pressure,,
81	4,
82	2,day,
83	5,day,
84	10,day,
85	50,day,
86	6,
87	Temperature,,
88	Aqueous saturation,,
89	Phase condition,,
90	Water gas mass frac,,,
91	Aqueous pressure,,
92	Gas pressure,,
93	

Exhibit 7.1-2. STOMP Parameters File for Evaporation/Condensation Heat Pipe Problem

```

Line   Parameters File
-----
1      C-----C
2      C      STOMP Parameter File
3      C-----C
4      C
5      C--- Number of lines of simulation notes
6      C      Number of execution periods ---
7      C
8      C      PARAMETER(LNOTES=4, LEPD=1)
9      C
10     C--- Number of nodes in the x or r coordinate direction
11     C      Number of nodes in the y or theta coordinate direction
12     C      Number of nodes in the z coordinate direction
13     C      Number of active nodes
14     C      Number of active dimensions
15     C      Minimum of (LFX*LFY, LFX*LFZ, LFY*LFZ) ---
16     C
17     C      PARAMETER(LFX=50, LFY=1, LFZ=1)
18     C      PARAMETER(LAN=50, LAD=1, LMNP=1)
19     C
20     C--- Energy equation switch (0 = off, 1 = on)
21     C      Water mass equation switch (0 = off, 1 = on)
22     C      Air mass equation switch (0 = off, 1 = on)
23     C      VOC mass equation switch (0 = off, 1 = on)
24     C      Solute transport equation switch (0 = off, 1 = on)
25     C      Freezing conditions switch (0 = off, 1 = on) ---
26     C      Dissolved salt transport equation switch (0 = off, 1 = on) ---
27     C      Dissolved oil transport equation switch (0 = off, 1 = on) ---
28     C
29     C      PARAMETER(LT=1, LL=1, LG=1, LN=0, LC=0, LFC=0, LS=1, LD=0)
30     C
31     C--- Banded matrix linear equation solver switch (0 = off, 1 = on)
32     C      Conjugate gradient linear equation solver switch (0 = off, 1 = on) ---
33     C      Unsymmetric-pattern multifrontal package switch (0 = off, 1 = on) ---
34     C
35     C      PARAMETER(LBD=1, LCG=0, LUM=0)
36     C
37     C--- Number of boundary condition surfaces
38     C      Number of boundary condition times ---
39     C
40     C      PARAMETER(LBC=2, LBTM=1)
41     C
42     C--- Number of sources
43     C      Number of source times ---
44     C
45     C      PARAMETER(LSR=1, LSTM=1)
46     C
47     C--- Number of rock/soil types
48     C      Number of solutes
49     C
50     C      PARAMETER(LRC=1, LSOLU=1)
51     C
52     C--- Number of reference nodes
53     C      Number of print times
54     C      Number of integration surfaces ---
55     C

```

Exhibit 7.1-2. (Contd)

<u>Line</u>	<u>Parameters File</u>
56	PARAMETER(LREF=2, LPTM=4, LSF=1)
57	C
58	C--- Number saturation and relative permeability table entries
59	C Number of hysteretic scanning paths
60	C Number of chemical reactions
61	C
62	PARAMETER(LTBL=1, LPATH=3, LCHEM=1)
63	C
64	C--- Computed Parameters ---
65	C
66	PARAMETER(LUK=LT+LL+LG+LN+LS+LD, LPH=LL+LG+LN, LCMP=LL+LS+LD)
67	PARAMETER(LFX=LFY*LFY, LFY=LFY*LFZ, LFZX=LFZ*LFX)
68	PARAMETER(LFD=LFX*LFY*LFZ)
69	PARAMETER(LNE=(LUK*LUK*(7*LFD-2*LFX-2*LFY-2*LFZ))**LUM)
70	PARAMETER(LHBW=LUK*LMNP+LUK-1)
71	PARAMETER(LJA=LBD + LCG*LAN*LUK + LUM*LAN*LUK)
72	PARAMETER(LJB=(2*LAN*LUK)**LUM, LJC=LAN**LUM)
73	PARAMETER(LJD=LBD*(3*LHBW+1) + LCG*LAN*LUK + LUM*6*LNE)
74	PARAMETER(LJE=LBD*LAN*LUK + LCG*(2*LAD+1)*LUK+2*LAD) + LUM)
75	PARAMETER(LJF=LAN*LUK)
76	PARAMETER(LJG=LED*(3*LHBW+1) + LCG*LAN*LUK + LUM)
77	PARAMETER(LJH=LBD*LAN*LUK + LCG*(2*LAD+1) + LUM)
78	PARAMETER(LJJ=LBD*LAN*LUK + LCG + LUM)
79	PARAMETER(LSV=LUK+2, LSFV=2*LUK+1)
80	PARAMETER(LSX=(LFX+1)*LFY*LFZ)
81	PARAMETER(LSY=LFX*(LFY+1)*LFZ)
82	PARAMETER(LSZ=LFX*LFY*(LFZ+1))
83	PARAMETER(LFDT=LFD**LT, LFDL=LFD**LL, LFDG=LFD**LG, LFDN=LFD**LN)
84	PARAMETER(LFDC=LFD**LC, LFDI=LFD**LFC, LFDS=LFD**LS, LFDD=LFD**LD)
85	PARAMETER(LSXT=LSX**LT, LSXL=LSX**LL, LSXG=LSX**LG, LSXN=LSX**LN)
86	PARAMETER(LSXC=LSX**LC, LSXS=LSX**LS, LSXD=LSX**LD)
87	PARAMETER(LSYT=LSY**LT, LSYL=LSY**LL, LSYG=LSY**LG, LSYN=LSY**LN)
88	PARAMETER(LSYC=LSY**LC, LSYS=LSY**LS, LSYD=LSY**LD)
89	PARAMETER(LSZT=LSZ**LT, LSZL=LSZ**LL, LSZG=LSZ**LG, LSZN=LSZ**LN)
90	PARAMETER(LSZC=LSZ**LC, LSZS=LSZ**LS, LSZD=LSZ**LD)
91	PARAMETER(LRCT=LRC**LT, LRCL=LRC**LL, LRCG=LRC**LG, LRCN=LRC**LN)
92	PARAMETER(LRCC=LRC**LC, LRCL=LRC**LFC, LRCS=LRC**LS, LRCD=LRC**LD)
93	PARAMETER(LBCT=LBC**LT, LBCL=LBC**LL, LBCG=LBC**LG, LBCN=LBC**LN)
94	PARAMETER(LBCC=LBC**LC, LBCI=LBC**LFC, LBCS=LBC**LS, LBCD=LBC**LD)
95	PARAMETER(LBCU=LUK+LPH+LT+2, LBCV=LBCU+LSOLU)
96	PARAMETER(LOUPV=200+11*(LSOLU))
97	PARAMETER(LJI=LBD*LAN*LUK + LCG + (3*LNE+23*LFD*LUK+9)*LUM)
98	PARAMETER(LSCHR=18)

7.2 Freezing / Thawing Heat Pipe

Frozen soil barriers, referred to as cryogenic barriers, have been proposed for temporarily containing plumes of radioactive and/or organic contamination within the subsurface environment. Predicting the effectiveness of cryogenic barriers and near-surface barriers in temperate or arctic

climates requires capabilities for numerically modeling subsurface flow and transport for freezing soil conditions. Field-scale experiments of frozen soil barriers require significant investments in refrigeration and monitoring equipment and time for planning and executing. Numerical modeling of cryogenic barrier systems with proven, physically based simulators can cut the requirements for field-scale testing, by providing mechanisms for appropriately scaling laboratory experiments to field applications. Critical components of a physically based simulator for freezing conditions are the constitutive relations for predicting liquid water and ice saturations and aqueous relative permeabilities as a function of temperature, interfacial pressure differences, and osmotic potential. This problem demonstrates the application of the STOMP simulator to a problem involving hydrothermal flow in a horizontal cylinder where one end of the cylinder is held below the freezing point.

Problem Features: 7.2

- Water-Air-Energy [Ice] operational mode
- Ice (frozen water) phase
- countercurrent flow in two phases
- one dimensional (x)
- uniform Cartesian grid
- variable saturation
- homogeneous, isotropic
- van Genuchten function
- Mualem function

7.2.1 Problem Description and Parameters

This problem follows the laboratory experiments of Jame (1977), where different temperature gradients were imposed across a radially insulated horizontal lucite tube (0.3 m in length and 0.1 m in diameter) filled with partially saturated porous media. Both ends of the tube were sealed to prevent water flow across these boundaries. Gas pressures were maintained at atmospheric conditions. The porous medium was a silica flour (dry bulk density of 1.335 g/cm^3) of which 72% passed a #325 sieve (0.044 mm). Initial conditions for the experiments were uniform temperatures and saturations along the tube length. Each experiment was initiated by lowering the temperature of the cool end below the freezing point and maintaining the temperature of the warm end at the initial temperature. During the course of the experiments, which each lasted 72 hr, constant temperature conditions were maintained at both ends of the tube. Initial conditions and boundary conditions are listed in Table 7.2-1.

Table 7.2-1. Initial and Boundary Conditions for Freezing/Thawing Heat Pipe Problem

Property Description	Symbol	Property Value
<i>Initial Condition Parameter Values</i>		
Total Aqueous Saturation	s_l	0.4203 (15.6% dry weight)
Gas Pressure	P_g	101,325. Pa
Temperature	T	20.°C
<i>Warm Boundary Parameter Values</i>		
Aqueous Flux		0. m ³ /m ² s
Gas Flux		0. m ³ /m ² s
Energy Flux		20. W/m ²
<i>Cold Boundary Parameter Values</i>		
Aqueous Flux		0. m ³ /m ² s
Gas Flux		0. m ³ /m ² s
Temperature	T	-10.°C

To numerically simulate these laboratory experiments, Jame and Norum (1980) used experimentally determined data to relate liquid water content as a function of temperature for freezing conditions. For the present application, van Genuchten moisture retention function parameters were estimated from grain size distribution data reported by Jame (1977) for the silica flour according to the technique by Mishra et al. (1989). These parameters were then used in the modified van Genuchten functions for soil-moisture retention and unfrozen water fraction (refer to the STOMP Theory Manual (White and Oostrom 1996), to compute the unfrozen water content as a function of temperature for freezing conditions for totally saturated conditions. The resulting function and associated van Genuchten parameters are compared against the experimental data of Jame (1977) in Figure 7.2-1. The method of Mishra et al. was additionally used to estimate a saturated soil hydraulic conductivity of 3.07×10^{-5} m/s, which compared well with the value of 3.45×10^{-5} m/s, extracted from the diffusivity data reported by Jame (1977). Aqueous- and gas-phase relative permeability were computed using the Mualem porosity distribution model. The effective thermal conductivity was computed using the de Vries model with all weight factors set equal to 1.0. Parameters for the soil-moisture retention, relative permeability, and key physical properties are listed in Table 7.2-2. Gas, aqueous, and ice properties were computed as functions

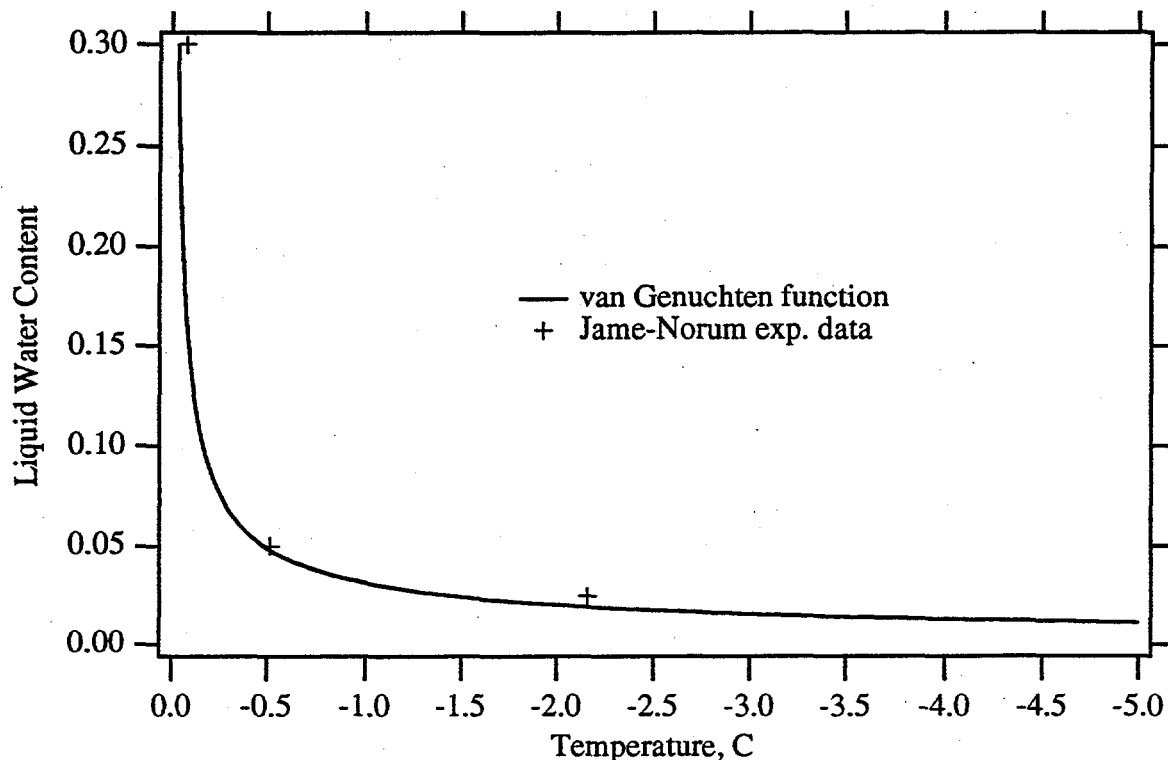


Figure 7.2-1. Unfrozen Water Content versus Temperature for the Freezing / Thawing Heat Pipe Problem

Table 7.2-2. Constitutive Function and Physical Parameters for Freezing / Thawing Heat Pipe Problem

Property Description	Symbol	Property Value
Soil Grain Thermal Conductivity	k	2.3 W/m K
de Vries Weight Factors		1.0
Hydraulic Conductivity	k	256. or 25.6 cm/day
Porosity	n	0.496
Soil Grain Density	ρ_s	2650. kg/m ³
Soil Grain Specific Heat	c_s	837. J/kg K
Gas Tortuosity		Millington & Quirk Model
van Genuchten α Parameter	α	0.279 1/m
van Genuchten n Parameter	n	1.64
Air-Water Scaling Factor		1.0
Ice-Water Scaling Factor		2.36
Residual Saturation	s_r	0.

of temperature and pressure, refer to the STOMP Theory Guide (White and Oostrom 1996) for specifics on these functions.

This application, actually involves two simulations which differ only in the hydraulic conductivity of the porous media. These simulations were generally designed to follow the experiments of Jame and Norum (1980), however the lack of complete information on the soil thermal conductivity characteristics no direct comparisons are possible between the experimental and numerical results. In both simulations a horizontal tube of soil at uniform liquid water content (15.6% dry weight) and temperature (+20C) was cooled on one end to -10 C and held at that temperature while the other end remained at +20C. Both simulations were executed over a 72-hr period using 233 nonuniform time steps. The first simulation used a saturated hydraulic conductivity of 256cm/day; whereas, the second used a reduced value of 25.6cm/day.

The STOMP input file for this application problem is shown in Exhibit 7.2-1. This simulation was executed with four execution periods as shown under the Solution Control Card input. This approach was used to control the maximum time step size during the transient portion of the simulation. For the first 6 hours of the simulation time steps were restricted to 5 minutes, followed by increases to 15, 30, and 60 minutes for the next 18, 12, and 36 hours, respectively. Under this time stepping scheme no nonconvergent time steps occurred. Because this problem only involved transport in the x-direction, hydraulic conductivities and thermal conductivities values for the y- and z-directions were not entered under the Hydraulic Properties Card and Thermal Properties Card, respectively. Formatting requirements, however, require the use of a comma delimiter for all entries, including null entries. To match the experimental variations in boundary conditions, time varying boundary conditions were applied on the cold boundary, as shown on the Boundary Condition Card for the West boundary surface. The temperature on the cold end varied linearly from 0 C to -5 C over the first 2 hours, then from -5 C to -10 C over the next 10 hours, and then was maintained at -10 C for the remainder of the simulation period. Specification of these boundary variations requires four boundary condition input lines. Requested output for these simulations differed between the Reference Nodes and Plot files. Output for the Reference Nodes was restricted to aqueous saturation, ice saturation, and temperature; where all output units were defaulted to Systemé Internationale units. Output for the Plot files, which were recorded at 1, 2, 6, 12, 24, and 72 hours, included the gas pressure, aqueous saturation, ice saturation, temperature, aqueous density in units of g/cm^3 , and ice density in units of g/cm^3 ; where all unspecified units were default to Systeme Internationale (SI) units. Time and length output appeared in units of hours and cm, respectively.

7.2.2 Simulation

Simulation results in terms of total moisture content and temperature as a function of distance from the cold boundary are shown in Figure 7.2-2 and Figure 7.2-3 for the soil with higher hydraulic conductivity (i.e., 256. cm/day). Total moisture content refers to the percent dry weight of total water (liquid and frozen) within the soil pore spaces. The results demonstrate the experimentally observed phenomena of freezing-induced redistribution of soil moisture. The zone of freezing acts as a strong sink for liquid water by effectively reducing the aqueous pressure, which induces liquid water to flow into the zone of freezing. Water vapor diffusion through the gas phase also occurs, but the quantities of redistributed water greatly exceed that which can be accounted for by water vapor diffusion. At each point in time, the freezing point isotherm (0°C) occurs in distance between the two points that bracket the abrupt change in total moisture content.

Total moisture content and temperature profiles for the simulation with the soil of lower hydraulic conductivity are shown in Figure 7.2-4 and Figure 7.2-5. These results differ markedly in the total moisture content profiles. The lower hydraulic conductivity of the soil inhibits the freezing-induced flow of liquid water to the freezing zone thus yielding lower total moisture contents near the cold end. Near the tube midpoint, however, the total moisture contents are greater than those for the higher permeability soil, thus producing a U-shaped profile. These U-shaped profiles have been observed experimentally (Dirksen and Miller 1966) and occur as the temperature profile approaches steady-state and the freezing front slows to a halt. As with the simulation results for higher permeability soil, the freezing point isotherm occurs within the sharp discontinuity in total moisture content.

7.2.3 Analysis

The freezing/thawing heat pipe problem was designed to model the experiments of Jame and Norum (1980). Whereas the results agree with the trends observed in terms of ice formation and moisture redistribution, the position of the freezing point along the heat pipe was in error by rough 1.5 cm. The ratio of thermal diffusivity to soil hydraulic conductivity and thermal conductivity function strongly influence the structure and profile of the ice along the heat pipe. The thermal conductivity of frozen soil is a function of the conductivities and volume fractions for the soil grains, liquid water, ice, and gas phase. The de Vries model for thermal conductivity also includes weighting factors as shown in Equation 7.2-1:

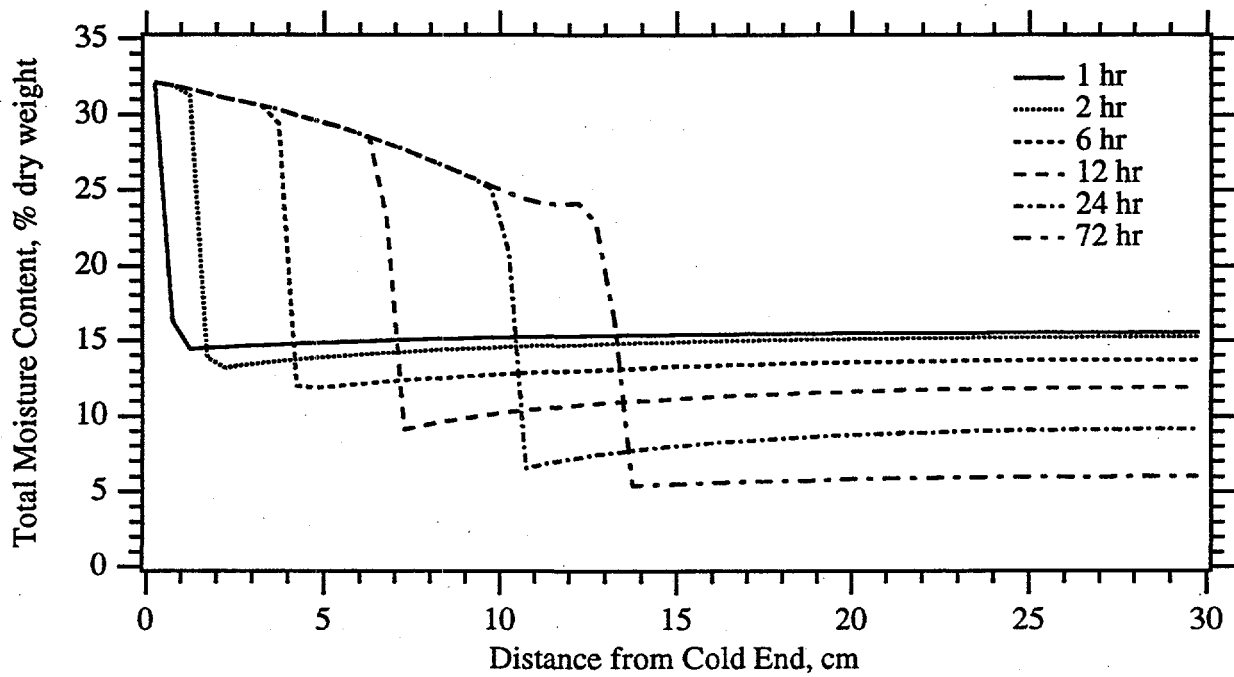


Figure 7.2-2. Total Moisture Content Versus Distance from the Cold Boundary for the High Conductivity Soil (256. cm/day)

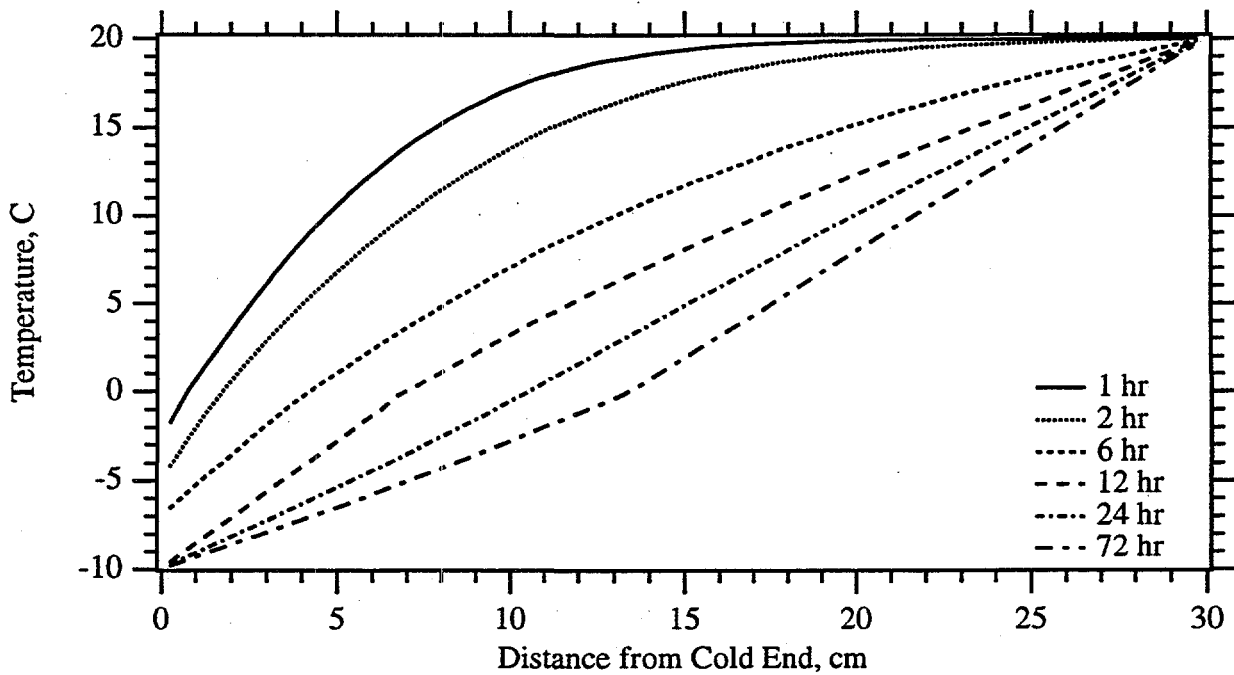


Figure 7.2-3. Temperature Versus Distance from the Cold Boundary for the High Conductivity Soil (256. cm/day)

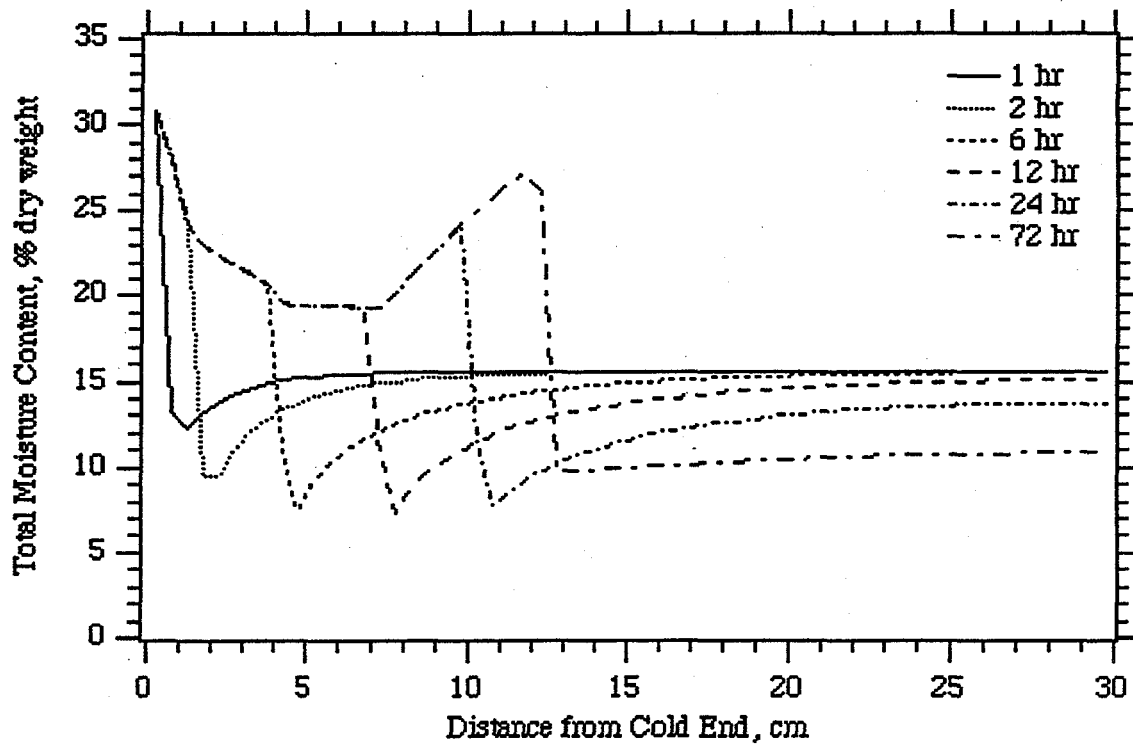


Figure 7.2-4. Total Moisture Content Versus Distance from the Cold Boundary for the Low Conductivity Soil (25.6 cm/day)

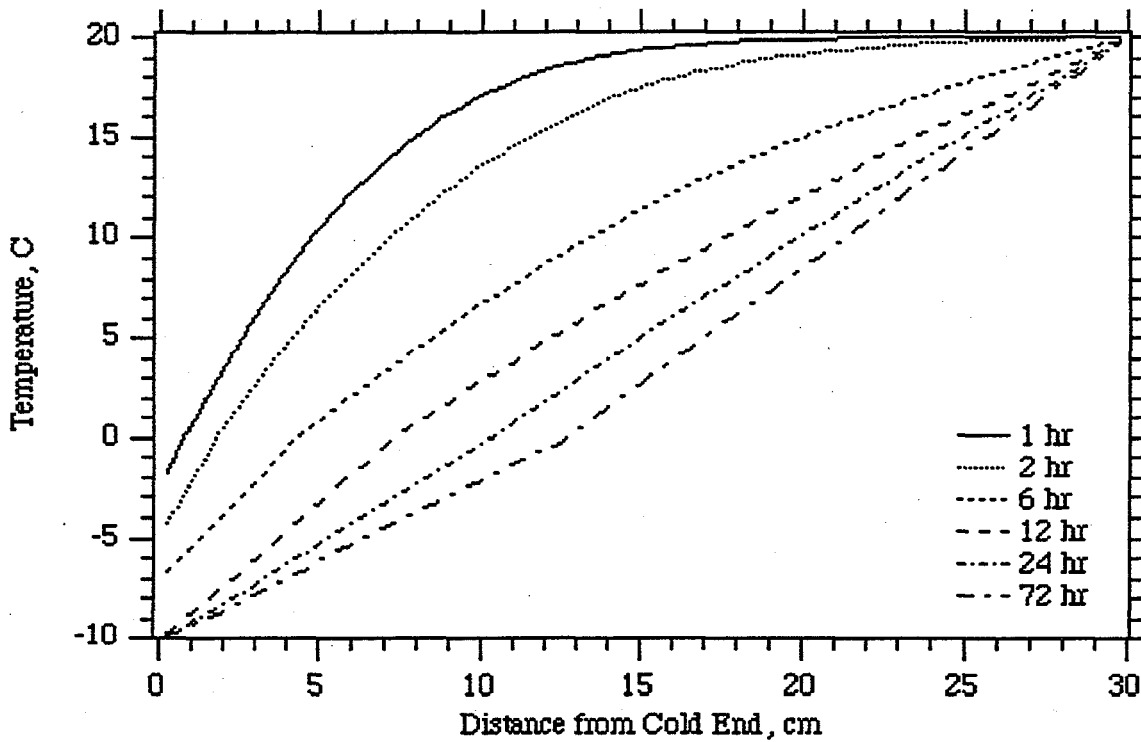


Figure 7.2-5. Temperature Versus Distance from the Cold Boundary for the Low Conductivity Soil (25.6 cm/day)

$$k_e = \frac{\sum_{n=s,l,g,i} w_n n_D s_n k_n}{\sum_{n=s,l,g,i} w_n n_D s_n}$$

Equation 7.2-1

The simulations shown for this application used unit weighting factors, which yielded only fair agreement with the thermal conductivity functions for unfrozen porous media reported by Jame and Norum (1980). The results from this study and application, therefore indicate the importance of accurately modeling the thermal conductivity function to the prediction of frozen barrier profiles.

7.2.4 Summary

This application was chosen to demonstrate the capabilities for the STOMP simulator to model frozen soil conditions. The constitutive functions for frozen soils in the STOMP simulator predict phase saturations and fluid-phase relative permeabilities for variably saturated air-water systems in porous media as a function of phase pressures, temperature, and salt concentrations. The current configuration of the simulator does not consider heaving phenomena. Although discussed in the STOMP Theory Guide (White and Oostrom 1996), the theory behind these constitutive functions is based on relating the scaled air-water capillary head to the aqueous saturation and the scaled ice-water capillary head to the unfrozen water fraction. This approach allows equilibrium saturations as a function of temperature, phase pressure, and solute concentration for different soils to be computed through conventional soil-moisture retention functions (e.g., van Genuchten and Brooks and Corey). Aqueous-phase relative permeability functions were derived for variably saturated, freezing conditions using inverse van Genuchten and Brooks and Corey moisture retention functions in conjunction with the Mualem and Burdine models for predicting the relative permeability from knowledge of the soil-moisture retention curve. These formulations have been shown (White 1995) to capture the essential features of moisture redistribution and ice formation observed experimentally. Further investigations and applications will be required, however, to determine whether the freezing-induced capillary draw forces predicted by the proposed formulations agree with experimental measurements for a variety of soils. Given the appropriateness of the proposed functions, the numerical simulations revealed that affective cryogenic barrier formation will be dependent on soil thermal and moisture-soil retention properties in addition to cooling rates and freezing front migration rates.

Exhibit 7.2-1. STOMP Input File for the Freezing/Thawing Heat Pipe Problem

<u>Line</u>	<u>Input File</u>
1	~Simulation Title Card
2	1,
3	Freezing/Thawing Heat Pipe,
4	Mark D. White,
5	Pacific Northwest Laboratory,
6	February 8 1995,
7	14:30 PM PST,
8	1,
9	Freezing/thawing heat pipe problem of Jame and Norum.
10	
11	~Solution Control Card
12	Normal,
13	Water-Air-Energy w/Ice,
14	4,
15	0,hr,6,hr,1,s,5,min,1.25,16,1.e-6,
16	6,hr,24,hr,5,min,15,min,1.25,16,1.e-6,
17	24,hr,36,hr,15,min,30,min,1.25,16,1.e-6,
18	36,hr,72,hr,30,min,60,min,1.25,16,1.e-6,
19	1,day,1,day,1000,
20	Variable Aqueous Diffusion,
21	Variable Gas Diffusion,
22	0,
23	
24	~Grid Card
25	Uniform Cartesian,
26	60,1,1,
27	0.5,cm,
28	8.8623,cm,
29	8.8623,cm,
30	
31	~Rock/Soil Zonation Card
32	1,
33	Silica Flour,1,60,1,1,1,1,
34	
35	~Mechanical Properties Card
36	Silica Flour,2.650,gm/cm ³ ,0.496,0.496,1.e-8,1/m,Millington and Quirk Tortuosity,
37	
38	~Hydraulic Properties Card
39	Silica Flour,256.,hc cm/day,,,,,
40	Silica Flour,25.6,hc cm/day,,,,,
41	
42	~Thermal Properties Card
43	Silica Flour,Parallel,2.3,W/m K,,,,,837.0,J/kg K,
44	
45	~Saturation Function
46	Silica Flour,Nonhysteretic van Genuchten,0.279,1/m,1.64,0.0,1.0,2.36,,
47	
48	~Aqueous Relative Permeability Card
49	Silica Flour,Mualem,,
50	
51	~Gas Relative Permeability Card
52	Silica Flour,Mualem,,
53	
54	~Initial Conditions Card
55	Gas Pressure,Apparent Aqueous Saturation,Temperature,

Exhibit 7.2-1. (Contd)

<u>Line</u>	<u>Input File</u>
56	3,
57	Gas Pressure,101325.0,Pa,,,,,,,,1,60,1,1,1,1,
58	Apparent Aqueous Saturation,0.4203,,,,,,,,1,60,1,1,1,1,
59	Temperature,20,C,,,,,,,,1,60,1,1,1,1,
60	
61	~Boundary Condition Card
62	2,
63	West,Dirichlet,Zero Flux,Zero Flux,
64	1,1,1,1,1,1,4,
65	0.0,hr,0.0,C,,,,,,,,
66	2.0,hr,-5.0,C,,,,,,,,
67	12.0,hr,-10.0,C,,,,,,,,
68	72.0,hr,-10.0,C,,,,,,,,
69	East,Dirichlet,Zero Flux,Zero Flux,Dirichlet,
70	60,60,1,1,1,1,1,
71	0.0,hr,20.0,C,,,,,101325.0,Pa,1.0,
72	
73	~Output Control Card
74	3,
75	1,1,1,
76	30,1,1,
77	60,1,1,
78	1,1,hr,cm,6,6,6,
79	5,
80	Aqueous Pressure,Pa,
81	Gas Pressure,Pa,
82	Aqueous Saturation,,
83	Ice Saturation,,
84	Temperature,,
85	5,
86	1.0,hr,
87	2.0,hr,
88	6.0,hr,
89	12.0,hr,
90	24.0,hr,
91	6,
92	Gas Pressure,,
93	Aqueous Saturation,,
94	Ice Saturation,,
95	Temperature,,
96	Aqueous Density,gm/cm^3,
97	Ice Density,gm/cm^3,
98	

Exhibit 7.2-2. STOMP Parameters File for the Freezing/Thawing Heat Pipe Problem

<u>Line</u>	<u>Parameters File</u>
1	C-----C
2	C STOMP Parameter File
3	C-----C
4	C
5	C--- Number of lines of simulation notes
6	C Number of execution periods ---
7	C
8	PARAMETER(LNOTES=1, LEPD=4)
9	C
10	C--- Number of nodes in the x or r coordinate direction
11	C Number of nodes in the y or theta coordinate direction
12	C Number of nodes in the z coordinate direction
13	C Number of active nodes
14	C Number of active dimensions
15	C Minimum of (LFX*LFY, LFX*LFZ, LPY*LPZ) ---
16	C
17	PARAMETER(LFX=60, LPY=1, LPZ=1)
18	PARAMETER(LAN=60, LAD=1, LMNP=1)
19	C
20	C--- Energy equation switch (0 = off, 1 = on)
21	C Water mass equation switch (0 = off, 1 = on)
22	C Air mass equation switch (0 = off, 1 = on)
23	C VOC mass equation switch (0 = off, 1 = on)
24	C Solute transport equation switch (0 = off, 1 = on)
25	C Freezing conditions switch (0 = off, 1 = on) ---
26	C Dissolved salt transport equation switch (0 = off, 1 = on) ---
27	C Dissolved oil transport equation switch (0 = off, 1 = on) ---
28	C
29	PARAMETER(LT=1, LL=1, LG=1, LN=0, LC=0, LFC=1, LS=1, LD=0)
30	C
31	C--- Banded matrix linear equation solver switch (0 = off, 1 = on)
32	C Conjugate gradient linear equation solver switch (0 = off, 1 = on) ---
33	C Unsymmetric-pattern multifrontal package switch (0 = off, 1 = on) ---
34	C
35	PARAMETER(LBD=1, LCG=0, LUM=0)
36	C
37	C--- Number of boundary condition surfaces
38	C Number of boundary condition times ---
39	C
40	PARAMETER(LBC=2, LBTM=4)
41	C
42	C--- Number of sources
43	C Number of source times ---
44	C
45	PARAMETER(LSR=1, LSTM=1)
46	C
47	C--- Number of rock/soil types
48	C Number of solutes
49	C
50	PARAMETER(LRC=1, LSOLU=1)
51	C
52	C--- Number of reference nodes
53	C Number of print times
54	C Number of integration surfaces ---
55	C

Exhibit 7.2-2. (Contd)

<u>Line</u>	<u>Parameters File</u>
56	PARAMETER(LREF=3, LPTM=5, LSF=1)
57	C
58	C--- Number saturation and relative permeability table entries
59	C Number of hysteretic scanning paths
60	C Number of chemical reactions
61	C
62	PARAMETER(LTBL=1, LPATH=3, LCHEM=1)
63	C
64	C--- Computed Parameters ---
65	C
66	PARAMETER(LUK=LT+LL+LG+LN+LS+LD, LPH=LL+LG+LN, LCPM=LL+LS+LD)
67	PARAMETER(LFX=LFY*LFY, LFYZ=LFY*LFZ, LFZX=LFZ*LFX)
68	PARAMETER(LFD=LFX*LFY*LFZ)
69	PARAMETER(LNE=(LUK*LUK*(7*LFD-2*LFX-2*LFY-2*LFZ))*LUM)
70	PARAMETER(LHBW=LUK*LMNP+LUK-1)
71	PARAMETER(LJA=LBD + LCG*LAN*LUK + LUM*LAN*LUK)
72	PARAMETER(LJB=(2*LAN*LUK)**LUM, LJC=LAN**LUM)
73	PARAMETER(LJD=LBD*(3*LHBW+1) + LCG*LAN*LUK + LUM*6*LNE)
74	PARAMETER(LJE=LBD*LAN*LUK + LCG*((2*LAD+1)*LUK+2*LAD) + LUM)
75	PARAMETER(LJF=LAN*LUK)
76	PARAMETER(LJG=LBD*(3*LHBW+1) + LCG*LAN*LUK + LUM)
77	PARAMETER(LJH=LBD*LAN*LUK + LCG*(2*LAD+1) + LUM)
78	PARAMETER(LJJ=LBD*LAN*LUK + LCG + LUM)
79	PARAMETER(LSV=LUK+2, LSFV=2*LUK+1)
80	PARAMETER(LSX=(LFX+1)*LFY*LFZ)
81	PARAMETER(LSY=LFX*(LFY+1)*LFZ)
82	PARAMETER(LSZ=LFX*LFY*(LFZ+1))
83	PARAMETER(LFDT=LFD**LT, LFDL=LFD**LL, LFDG=LFD**LG, LFDN=LFD**LN)
84	PARAMETER(LFDC=LFD**LC, LFDI=LFD**LFC, LFDS=LFD**LS, LFDD=LFD**LD)
85	PARAMETER(LSXT=LSX**LT, LSXL=LSX**LL, LSXG=LSX**LG, LSXN=LSX**LN)
86	PARAMETER(LSXC=LSX**LC, LSXS=LSX**LS, LSXD=LSX**LD)
87	PARAMETER(LSYT=LSY**LT, LSYL=LSY**LL, LSYG=LSY**LG, LSYN=LSY**LN)
88	PARAMETER(LSYC=LSY**LC, LSYS=LSY**LS, LSYD=LSY**LD)
89	PARAMETER(LSZT=LSZ**LT, LSZL=LSZ**LL, LSZG=LSZ**LG, LSZN=LSZ**LN)
90	PARAMETER(LSZC=LSZ**LC, LSZS=LSZ**LS, LSZD=LSZ**LD)
91	PARAMETER(LRCT=LRC**LT, LRCL=LRC**LL, LRCG=LRC**LG, LRCN=LRC**LN)
92	PARAMETER(LRCC=LRC**LC, LRCL=LRC**LFC, LRCS=LRC**LS, LRCD=LRC**LD)
93	PARAMETER(LBCT=LBC**LT, LBCL=LBC**LL, LBCG=LBC**LG, LBCN=LBC**LN)
94	PARAMETER(LBCC=LBC**LC, LBCI=LBC**LFC, LBCC=LBC**LS, LBCC=LBC**LD)
95	PARAMETER(LBCU=LUK+LPH+LT+2, LBCV=LBCU+LSOLU)
96	PARAMETER(LOUPV=200+11*(LSOLU))
97	PARAMETER(LJI=LBD*LAN*LUK + LCG + (3*LNE+23*LFD*LUK+9)*LUM)
98	PARAMETER(LSCHR=18)
99	

7.3 References

- Buscheck TA, and JJ Nitao. 1988. *Preliminary Scoping Calculations of Hydrothermal Flow in Variably Saturated, Fractured, Welded Tuff During the Engineering Barrier Design Test at the Yucca Mountain Exploratory Shaft Test Site*, UCID-21571, Lawrence Livermore National Laboratory, Livermore, California.
- Dirksen C, and RD Miller. 1966. "Closed-system freezing of unsaturated soil." *Soil Science Society of America Proceedings*, 30, 168-173.
- Fayer MJ, and CS Simmons. 1995. "Modified soil water retention function for all matric suctions." *Water Resources Research*, 31(5), 1233-1238.
- Jame YW. 1977. *Heat and Mass Transfer in Freezing Unsaturated Soil*, Ph.D., University of Saskatoon, Saskatoon.
- Jame YW, and DI Norum. 1980. "Heat and mass transfer in a freezing unsaturated porous medium." *Water Resources Research*, 16(4), 811-819.
- Leverett MC. 1941. "Capillary behavior in porous solids." *AIME Transactions*, 142-152.
- Mishra S, JC Parker, and N Singhal. 1989. "Estimation of soil hydraulic properties and their uncertainty from particle size distribution." *Journal of Hydrology*, 108, 1-18.
- Udell KS, and J. S. Fitch. 1985. "Heat and mass transfer in capillary porous media considering evaporation, condensation, and non-condensable gas effects," In Proceedings of 23rd ASME/AIChE National Heat Transfer Conference, Denver, Colorado.
- White MD. 1995. "Theory and numerical application of subsurface flow and transport for transient freezing conditions," In Proceedings of Fifteenth Annual American Geophysical Union Hydrology Days, Fort Collins, Colorado, 339-352.
- White MD, and M Oostrom. 1996. *STOMP Subsurface Transport Over Multiple Phases Theory Guide*, PNNL-11217, Pacific Northwest National Laboratory, Richland, Washington.

8.0 Nonaqueous Phase Liquid Flow and Transport

Ground-water contamination as a result of subsurface leakage or surface spills of immiscible organic liquids, such as solvents and hydrocarbon products, is a widespread problem in the industrialized world. Many organic liquids existing as a separate phase are in fact often slightly miscible with water and their solubility often exceeds the drinking water standards by orders of magnitude. To accurately describe the movement of such liquids in the subsurface, separate Nonaqueous Phase Liquid (NAPL), aqueous, and, in the case of volatile organic liquids, gas phase flow has to be considered. Three examples are presented in this chapter: the behavior of nonvolatile organic liquid spills in a hypothetical aquifer, infiltration and redistribution of Soltrol and carbon tetrachloride in one-dimensional laboratory columns, and an investigation of density-dependent gas advection of trichloroethylene (TCE) in a two-dimensional flow container.

8.1 Infiltration and Redistribution of Oil in a Hypothetical, Two-Dimensional Aquifer

The objective of this example is to investigate the effects of fluid density and viscosity on the movement of NAPLs after a spill in a partly saturated, hypothetical, aquifer. Infiltration and redistribution of a finite quantity of oil (7.5 m^3) in a vertical section are considered. STOMP generated results are compared with simulations conducted with the MOFAT code (Kaluarachchi and Parker 1989). The MOFAT simulations have been included in Ségol (1994).

Problem Features: 8.1

- Water-Oil operational mode
- VOC migration
- two-dimensional (xz)
- variable saturation
- uniform Cartesian grid
- homogeneous, isotropic media
- hydraulic gradient boundary
- Benchmark with MOFAT code

8.1.1 Problem Description and Parameters

The conceptual model is similar to the problem presented by Kaluarachchi and Parker (1989). The geometry of the flow domain, which has a hydraulic gradient of $2/23$, is shown in Figure 8.1-1. The problem domain is discretized into 750 cells (50×15). For the water phase, hydraulic gradient boundary conditions were imposed for the saturated zone on the west and east

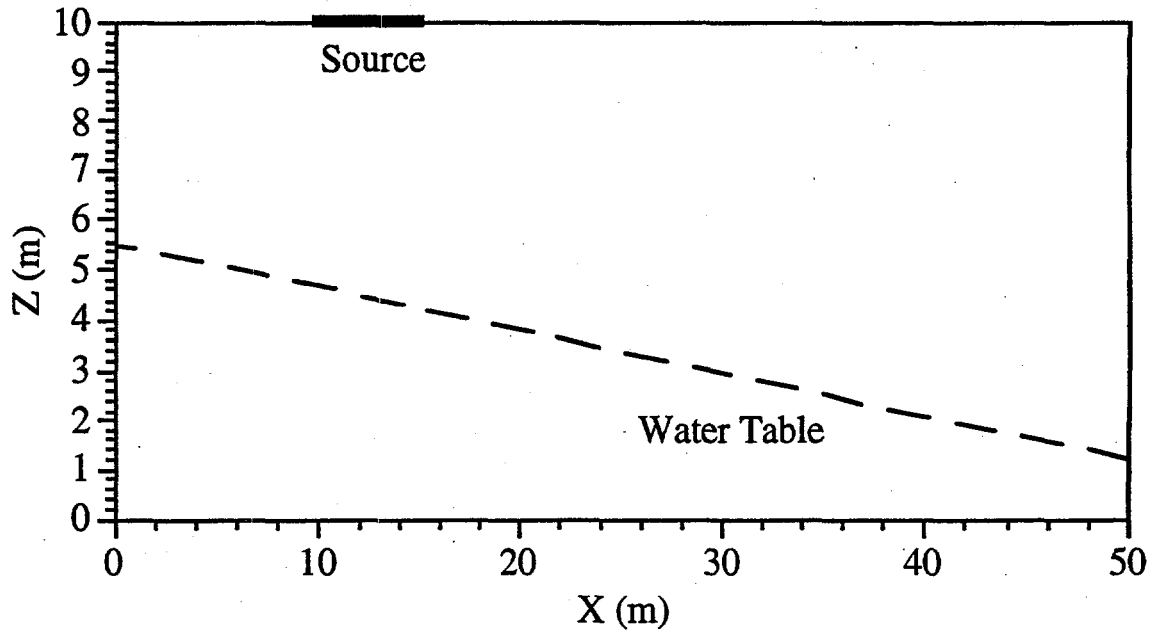


Figure 8.1-1. Conceptual Model of the Flow Domain

boundaries. Zero-flux boundaries were used on all other boundaries. A total of $7.5 \text{ m}^3/\text{m}$ oil was allowed to infiltrate the system from a 5-m-wide source area at the top boundary under a water equivalent oil head of 1 cm. No oil flow was permitted across any other boundary. Four cases (labeled A through D) are considered, involving variations in the oil density and viscosity (Table 8.1-1).

The simulations are performed using the van Genuchten-Mualem capillary pressure-saturation-relative permeability model with $\alpha = 0.007 \text{ 1/cm}$, $n = 2.1$, and $S_m = 0.02$. The fluid dependent scaling factors β_{ao} and β_{vo} are 1.8 and 2.25, respectively. The STOMP input file for the high oil density and viscosity case (case A) is shown in Exhibit 8.1-1.

8.1.2 Simulations

Simulation results for the Cases A through D are shown in Figure 8.1-2, Figure 8.1-3, Figure 8.1-4, and Figure 8.1-5, respectively. Each figure shows the results at 25, 50, and 100 days following the start of infiltration. The infiltration times for the Cases A through D were 4.25, 1.10, 5.86, and 1.47 days, respectively.

Table 8.1-1. NAPL Densities and Viscosities

Case	Density (kg/m ³)	Viscosity (Pa s)
A	1200	0.0020
B	1200	0.0005
C	800	0.0020
D	800	0.0005

The results show that, according to expectation, both DNAPL plumes (Case A and B) reach the bottom of the aquifer. Both LNAPL plumes (Case C and D) only partially penetrate the water table. The viscosity of the NAPL has a large influence on the movement of the plumes. The two low-viscosity plumes (Case B and D) move much faster in both the vadose and the saturated zone than the two high-viscosity plumes (Case A and C).

8.1.3 Analysis

The simulations were originally conducted with a grid identical to the 23x15 grid used by Kaluarachchi and Parker (1989). The flow domain defined by these authors was 23 m long in the horizontal, and 10 m in the vertical direction. In contrast with the MOFAT simulations, results with STOMP indicated that low-viscosity plumes reached the west and east boundaries somewhere between 50 and 100 days after initiation of the surface spill. The MOFAT simulations show that the plumes in all four cases remain easily within the two vertical boundaries. To allow for a longer simulation time, the horizontal dimension of the model was increased to 50 m. In addition, the source was moved 5 m to avoid interference of the NAPL plumes with the west boundaries.

Even after expansion of the computational domain, the differences between the STOMP- and MOFAT-generated plumes are significant. In general, the STOMP plumes move much faster than the MOFAT plumes. The reasons for the discrepancy between the results of both simulators were largely explained in a letter send by Kaluarachchi and Parker to the editor of Water Resources Research (Kaluarachchi and Parker (1994)). In that letter, the authors indicated that the results published in their 1989 paper were highly erroneous as a result of the usage of a split time derivative formulation. For two-phase flow, the split time derivate formulation has the form

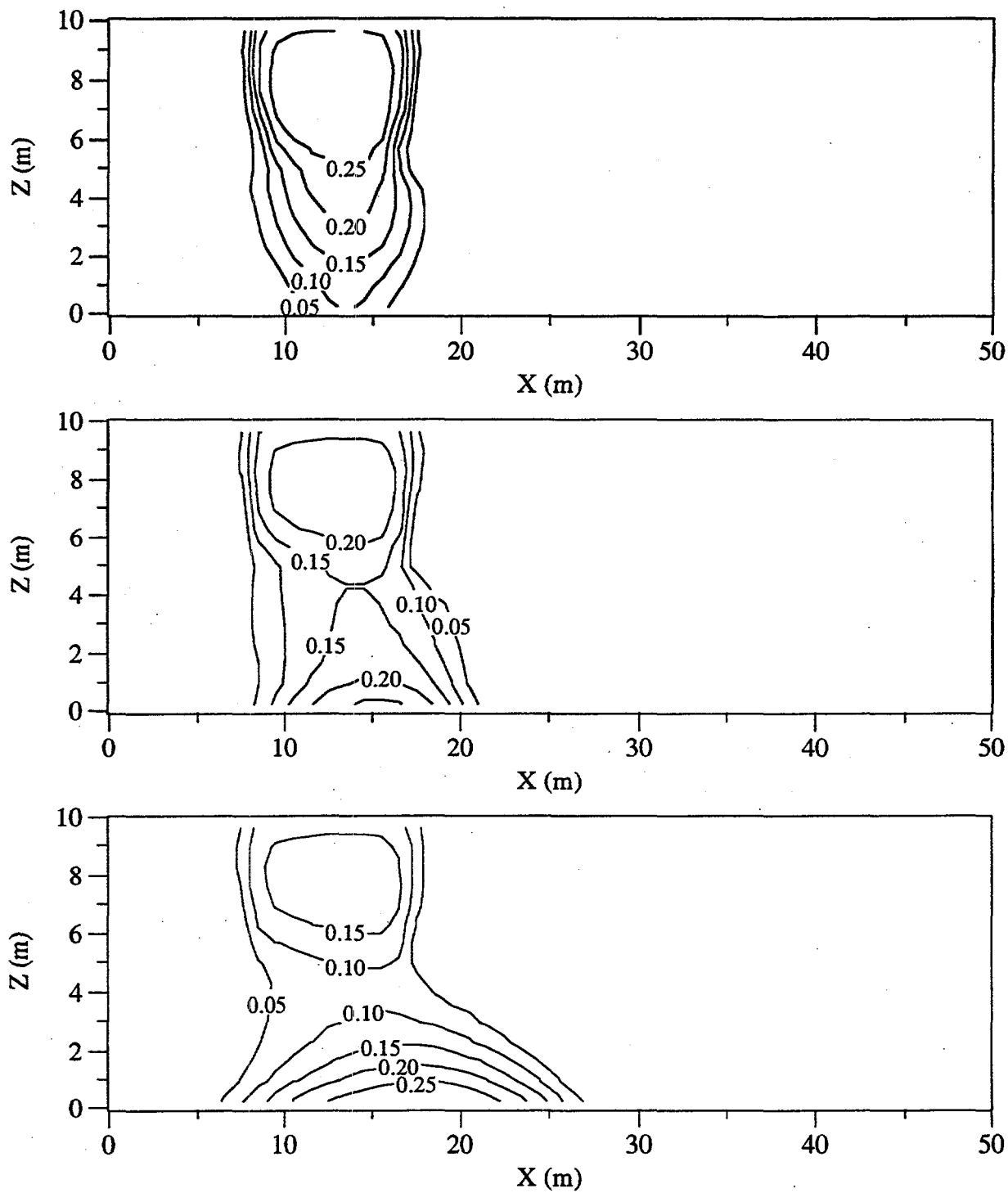


Figure 8.1-2. NAPL saturations for $\rho_n = 1200 \text{ kg/m}^3$, and $\mu_n = 0.002 \text{ Pa s}$ after (a) 25 days, (b) 50 days, and (c) 100 days

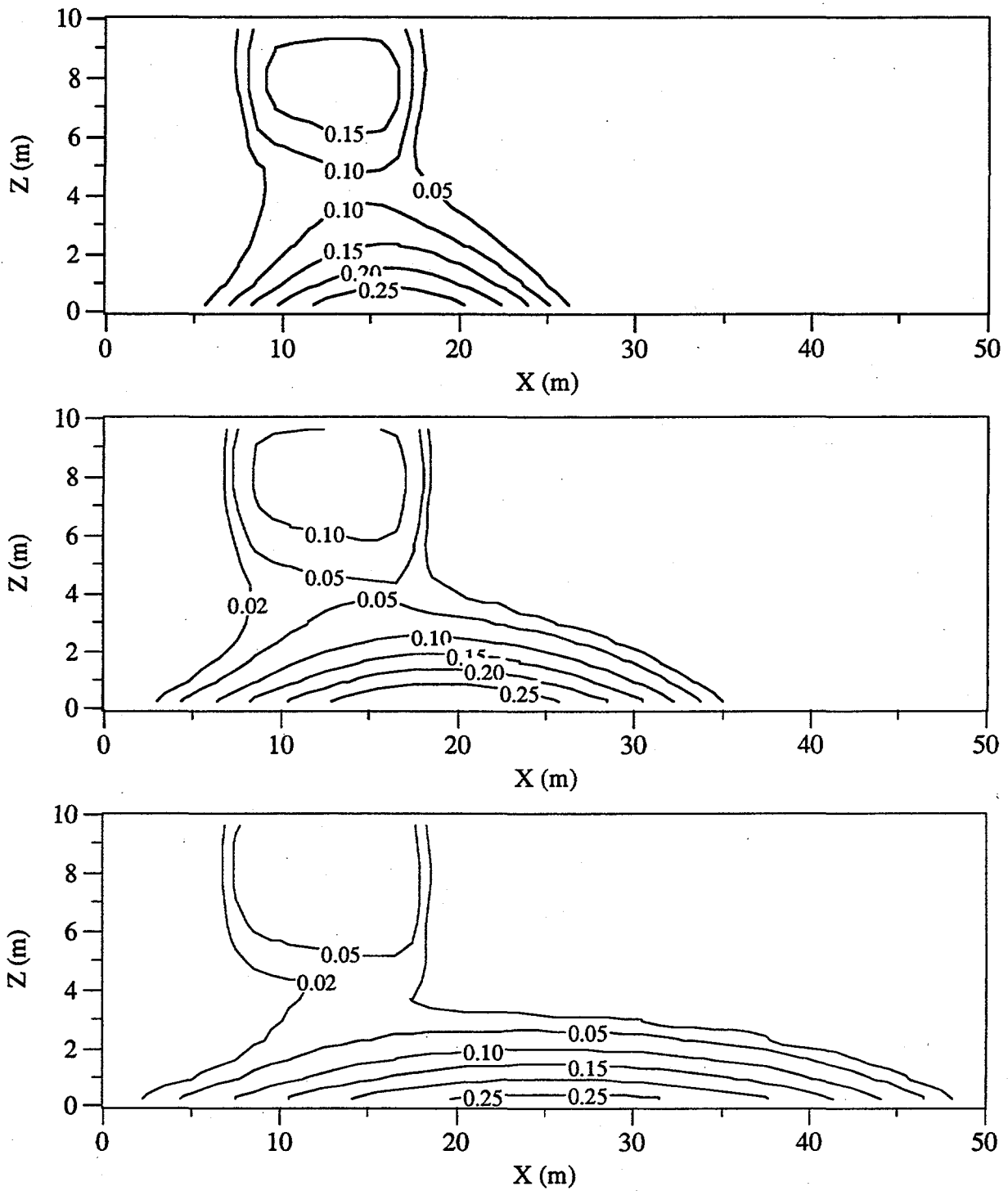


Figure 8.1-3. NAPL saturations for $\rho_n = 1200 \text{ kg/m}^3$, and $\mu_n = 0.0005 \text{ Pa s}$ after (a) 25 days, (b) 50 days, and (c) 100 days

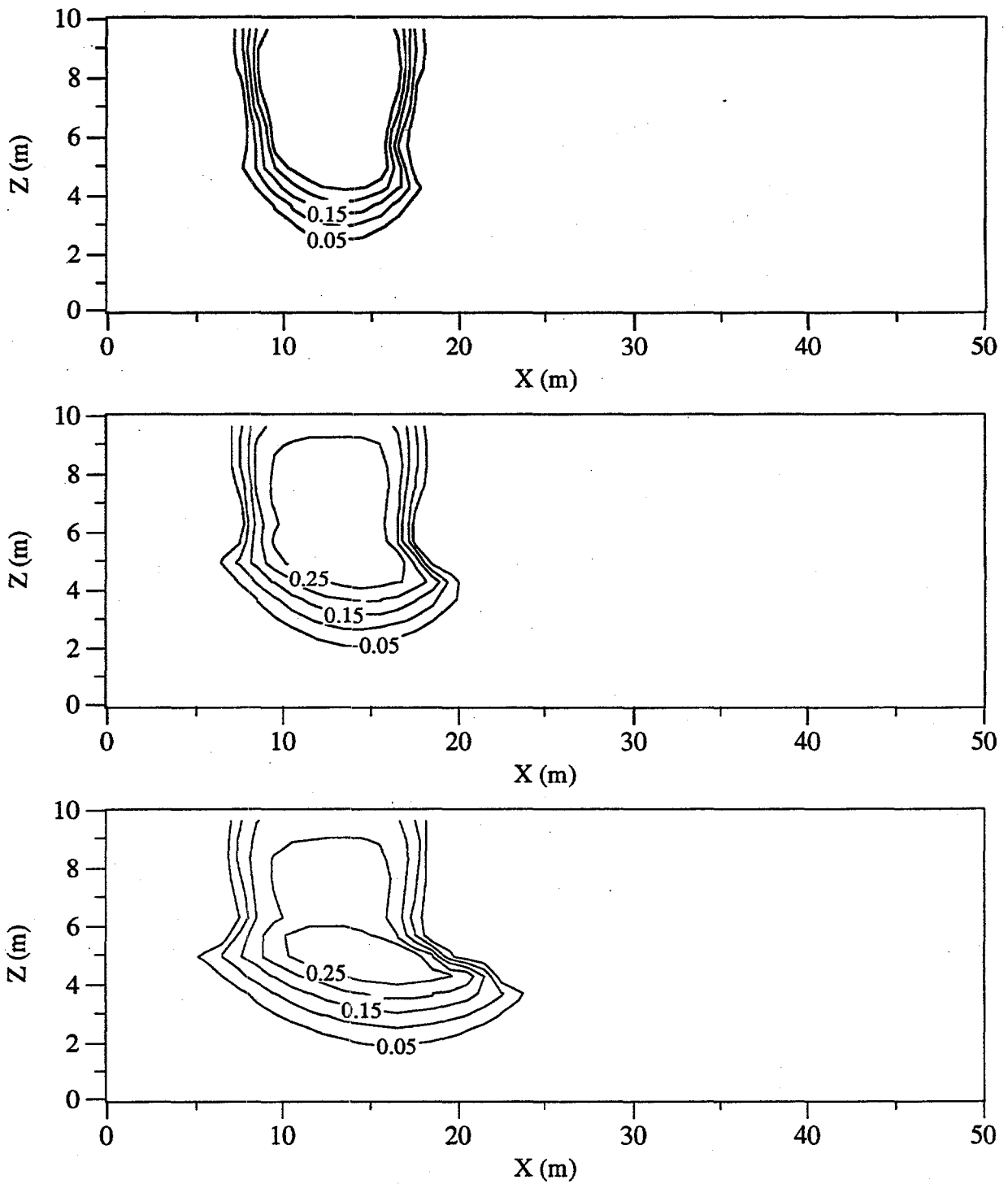


Figure 8.1-4. NAPL saturations for $\rho_n = 800 \text{ kg/m}^3$, and $\mu_n = 0.002 \text{ Pa s}$ after (a) 25 days, (b) 50 days, and (c) 100 days

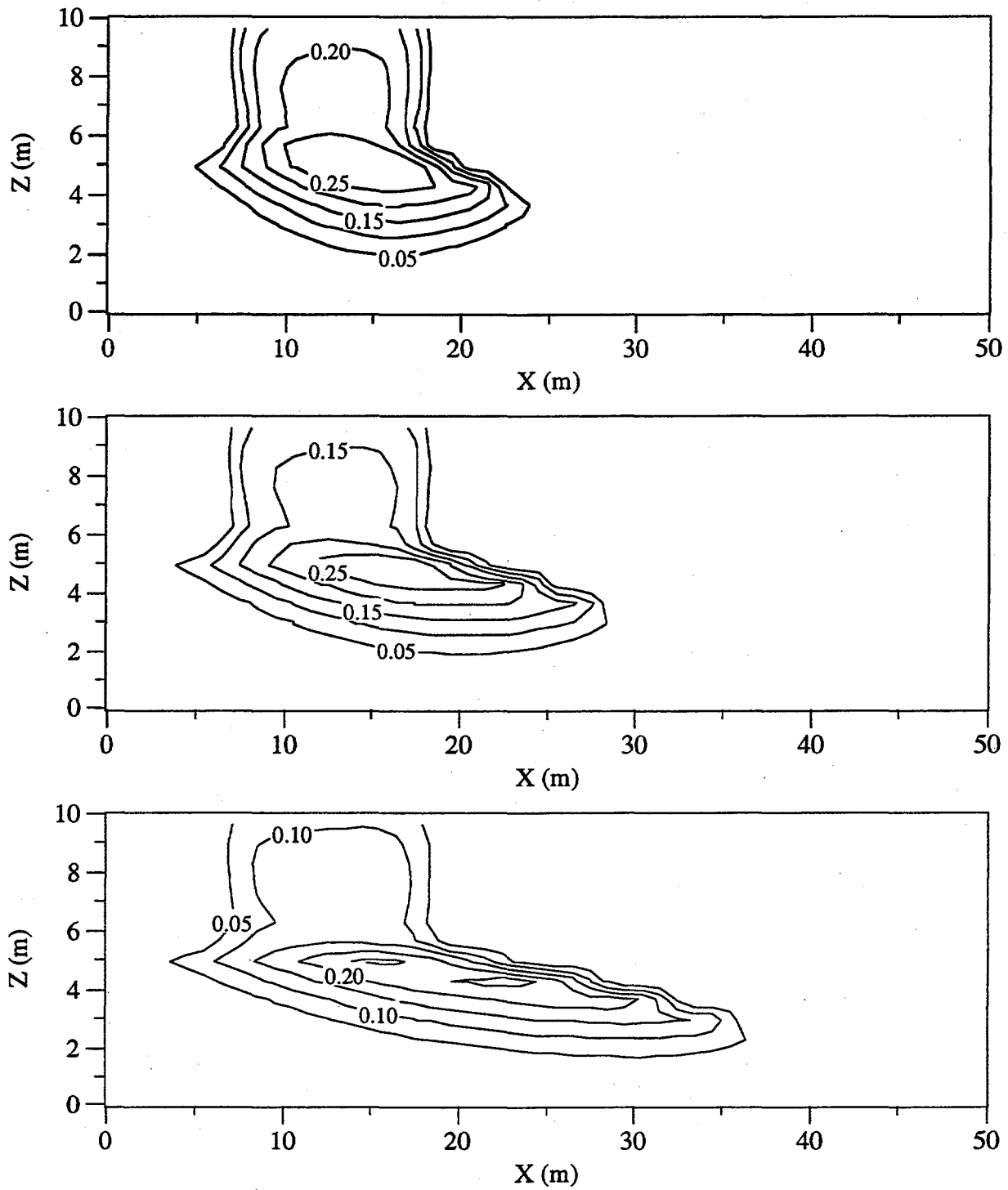


Figure 8.1-5. NAPL saturations for $\rho_n = 800 \text{ kg/m}^3$, and $\mu_n = 0.002 \text{ Pa s}$ after (a) 25 days, (b) 50 days, and (c) 100 days

$$C_{ww} \frac{\partial h_w}{\partial t} + C_{wo} \frac{\partial h_o}{\partial t} = \frac{\partial}{\partial x_i} \left[K_{w_{ij}} \left(\frac{\partial h_w}{\partial x_i} + u_j \right) \right]$$

Equation 8.1-1

$$C_{ow} \frac{\partial h_w}{\partial t} + C_{oo} \frac{\partial h_o}{\partial t} = \frac{\partial}{\partial x_i} \left[K_{o_{ij}} \left(\frac{\partial h_o}{\partial x_i} + \rho_{ro} u_j \right) \right]$$

Equation 8.1-2

where C_{pq} is the pq phase fluid capacity for $p = o$ (oil) or w (water), t is time, x_i is the i -direction coordinate, $K_{p_{ij}}$ is the p phase conductivity tensor for phase p , h_p is the water height equivalent head of p phase, ρ_w is the density of water, g is the gravitational acceleration, ρ_{ro} is the specific gravity of oil, u_j is the unit gravitational vector where z is the elevation, and

$$C_{pq} = n \frac{\partial S_p}{\partial h_q}$$

Equation 8.1-3

where n is the porosity, S_p is the p phase fluid saturation, and $p, q = o, w$.

Celia et al. (1990) and Katyal and Parker (1992) demonstrated that a mixed form of the governing equations gives results that are superior to those from the split time derivative. The STOMP simulator uses the mixed form, which avoids expanding the time derivative term (White and Oostrom, (1996)). Kaluarachchi and Parker (1994) selected Case B (high density and low viscosity) to compare the mixed formulation with their previously reported results. The plume generated with the mixed formulation looks similar to the plume generated with STOMP for the same case.

8.1.4 Summary

Four NAPL spills in a hypothetical aquifer were simulated and compared with results produced with the MOFAT code (Kaluarachchi and Parker). It was observed that the plumes

computed with the STOMP code move much faster than the plumes produced with the MOFAT code. In a recent paper, Kaluarachchi and Parker indicated that the results of their 1989 paper were erroneous.

Exhibit 8.1-1. STOMP Input File for Oil Redistribution in 2D Aquifer

<u>Line</u>	<u>Input File</u>
1	-Simulation Title Card
2	1,
3	Kaluarachi and Parker (1989 and 1994),
4	STOMP Application Guide,
5	Pacific Northwest Laboratory,
6	June 1995,
7	9:30 AM PST,
8	1,
9	Van Genuchten, Mualem,
10	
11	-Solution Control Card
12	Normal,
13	Water-Oil,
14	1,
15	0,s,60,hr,0.01,hr,2.5,hr,1.04,8,1.e-06,
16	1,day,1,day,20000,
17	Variable Aqueous Diffusion,
18	0,
19	
20	-Grid Card
21	Cartesian,
22	50,1,15,
23	0,m,50@1.0,m,
24	0,m,1.0,m,
25	0,m,15@0.66666667,m,
26	
27	
28	-Rock/Soil Zonation Card
29	1,
30	Fine Sand,1,50,1,1,1,15,
31	
32	-Mechanical Properties Card
33	Fine Sand,2650,kg/m ³ ,0.43,0.43,,Millington and Quirk,
34	
35	-Hydraulic Properties Card
36	Fine Sand,2.1,hc cm/hr,,2.1,hc cm/hr,
37	
38	-Saturation Function Card
39	Fine Sand,Nonhysteretic Van Genuchten,0.007,1/cm,2.1,0.0,1.0,1.8,2.25,,
40	
41	-Aqueous Relative Permeability Card
42	Fine Sand,Mualem,,
43	
44	-NAPL Relative Permeability Card
45	Fine Sand,Mualem,,
46	
47	-Volatile Organic Compound Properties Card
48	Soltrol,
49	170.34,g/mol,-9.55,C,225.35,C,385.05,C,
50	18.2,bar,713,cm ³ /mol,0.24,0.0,0,debyes,
51	-9.328,1.149,-0.0006347,1.359e-07,
52	Equation 2,77.628,10012.5,-9.236,10030.0,
53	Constant,1200.,kg/m ³ ,
54	Constant,0.002,Pa s,
55	1.0e10,Pa,

Exhibit 8.1-1. (Contd)

<u>Line</u>	<u>Input File</u>
56	
57	-Initial Conditions Card
58	Aqueous Pressure,151114.2,Pa,-851.24,1/m,,,-9789.284,1/m,1,50,1,1,1,15,
59	NAPL Pressure,-1.e9,Pa,,,,,,,,1,50,1,1,1,15,
60	
61	-Boundary Conditions Card
62	2,
63	Top,Zero Flux,Dirichlet NAPL,11,15,1,1,15,15,2,
64	0,s,-1.e9,Pa,0.0,101425,Pa,
65	4.25,d,-1.e9,Pa,0.0,101425,Pa,
66	West,Hydraulic Gradient,Zero Flux NAPL,
67	1,1,1,1,1,15,1,
68	0,s,151114.2,Pa,0.0,-1.e9,Pa,
69	East,Hydraulic Gradient,Zero Flux NAPL,
70	50,50,1,1,1,15,1,
71	0,s,110052.2,Pa,0.0,-1.e9,Pa,
72	
73	-Output Options Card
74	5,
75	13,1,15,
76	13,1,13,
77	13,1,11,
78	13,1,9,
79	13,1,7,
80	1,1,s,cm,4,4,4,
81	2,
82	Aqueous Saturation,,
83	NAPL Saturation,,
84	4,
85	25,d,
86	50,d,
87	100,d,
88	200,d,
89	2,
90	Aqueous Saturation,,
91	NAPL Saturation,,
92	
93	-Surface Flux Card
94	1,
95	NAPL Volumetric Flux,1/min,1,Top,11,15,1,1,15,15,
96	

Exhibit 8.1-2. Parameters File for Oil Redistribution in 2D Aquifer

<u>Line</u>	<u>Parameters File</u>
1	C-----C
2	C STOMP Parameter File
3	C-----C
4	C
5	C--- Number of lines of simulation notes
6	C Number of execution periods ---
7	C
8	PARAMETER(LNOTES=10, LEPD=10)
9	C
10	C--- Number of nodes in the x or r coordinate direction
11	C Number of nodes in the y or theta coordinate direction
12	C Number of nodes in the z coordinate direction
13	C Number of active nodes
14	C Number of active dimensions
15	C Minimum of (LFX*LFY, LFX*LFZ, LFY*LFZ) ---
16	C
17	PARAMETER(LFX=50, LFY=1, LFZ=15)
18	PARAMETER(LAN=750, LAD=2, LMNP=15)
19	C
20	C--- Energy equation switch (0 = off, 1 = on)
21	C Water mass equation switch (0 = off, 1 = on)
22	C Air mass equation switch (0 = off, 1 = on)
23	C VOC mass equation switch (0 = off, 1 = on)
24	C Solute transport equation switch (0 = off, 1 = on)
25	C Freezing conditions switch (0 = off, 1 = on) ---
26	C Dissolved salt transport equation switch (0 = off, 1 = on) ---
27	C Dissolved oil transport equation switch (0 = off, 1 = on) ---
28	C
29	PARAMETER(LT=0, LL=1, LG=0, LN=1, LC=0, LFC=0, LS=0, LD=0)
30	C
31	C--- Banded matrix linear equation solver switch (0 = off, 1 = on)
32	C Conjugate gradient linear equation solver switch (0 = off, 1 = on) ---
33	C Unsymmetric-pattern multifrontal package switch (0 = off, 1 = on) ---
34	C
35	PARAMETER(LBD=1, LCG=0, LUM=0)
36	C
37	C--- Number of boundary condition surfaces
38	C Number of boundary condition times ---
39	C
40	PARAMETER(LBC=35, LBTM=4)
41	C
42	C--- Number of sources
43	C Number of source times ---
44	C
45	PARAMETER(LSR=1, LSTM=1)
46	C
47	C--- Number of rock/soil types
48	C Number of solutes
49	C
50	PARAMETER(LRC=1, LSOLU=1)
51	C
52	C--- Number of reference nodes
53	C Number of print times
54	C Number of integration surfaces ---
55	C

Exhibit 8.1-2. (Contd)

<u>Line</u>	<u>Parameters File</u>
56	PARAMETER(LREF=5, LPTM=6, LSF=5)
57	C
58	C--- Number saturation and relative permeability table entries
59	C Number of hysteretic scanning paths
60	C Number of chemical reactions
61	C
62	PARAMETER(LTBL=1, LPATH=3, LCHEM=1)
63	C
64	C--- Computed Parameters ---
65	C
66	PARAMETER(LUK=LT+LL+LG+LN+LS+LD, LPH=LL+LG+LN, LCMP=LL+LS+LD)
67	PARAMETER(LFX=LFX*LFY, LFY=LFX*LFY, LFZ=LFX*LFY, LFZX=LFZ*LFX)
68	PARAMETER(LFD=LFX*LFY*LFZ)
69	PARAMETER(LNE=(LUK*LUK*(7*LFD-2*LFX-2*LFY-2*LFZ))*LUM)
70	PARAMETER(LHBW=LUK*LMNP+LUK-1)
71	PARAMETER(LJA=LBD + LCG*LAN*LUK + LUM*LAN*LUK)
72	PARAMETER(LJB=(2*LAN*LUK)**LUM, LJC=LAN**LUM)
73	PARAMETER(LJD=LBD*(3*LHBW+1) + LCG*LAN*LUK + LUM*6*LNE)
74	PARAMETER(LJE=LBD*LAN*LUK + LCG*((2*LAD+1)*LUK+2*LAD) + LUM)
75	PARAMETER(LJF=LAN*LUK)
76	PARAMETER(LJG=LBD*(3*LHBW+1) + LCG*LAN*LUK + LUM)
77	PARAMETER(LJH=LBD*LAN*LUK + LCG*(2*LAD+1) + LUM)
78	PARAMETER(LJJ=LBD*LAN*LUK + LCG + LUM)
79	PARAMETER(LSV=LUK+2, LSFV=2*LUK+1)
80	PARAMETER(LSX=(LFX+1)*LFY*LFZ)
81	PARAMETER(LSY=LFX*(LFY+1)*LFZ)
82	PARAMETER(LSZ=LFX*LFY*(LFZ+1))
83	PARAMETER(LFDT=LFD**LT, LFDL=LFD**LL, LFDG=LFD**LG, LFDN=LFD**LN)
84	PARAMETER(LFDC=LFD**LC, LFDI=LFD**LFC, LFDS=LFD**LS, LFDD=LFD**LD)
85	PARAMETER(LSXT=LSX**LT, LSXL=LSX**LL, LSXG=LSX**LG, LSXN=LSX**LN)
86	PARAMETER(LSXC=LSX**LC, LSXS=LSX**LS, LSXD=LSX**LD)
87	PARAMETER(LSYT=LSY**LT, LSYL=LSY**LL, LSYG=LSY**LG, LSYN=LSY**LN)
88	PARAMETER(LSYC=LSY**LC, LSYS=LSY**LS, LSYD=LSY**LD)
89	PARAMETER(LSZT=LSZ**LT, LSZL=LSZ**LL, LSZG=LSZ**LG, LSZN=LSZ**LN)
90	PARAMETER(LSZC=LSZ**LC, LSZS=LSZ**LS, LSZD=LSZ**LD)
91	PARAMETER(LRCT=LRC**LT, LRCL=LRC**LL, LRCG=LRC**LG, LRCN=LRC**LN)
92	PARAMETER(LRCC=LRC**LC, LRCL=LRC**LFC, LRCS=LRC**LS, LRCD=LRC**LD)
93	PARAMETER(LBCT=LBC**LT, LBCL=LBC**LL, LBCG=LBC**LG, LBCN=LBC**LN)
94	PARAMETER(LBCC=LBC**LC, LBCI=LBC**LFC, LBCS=LBC**LS, LBCD=LBC**LD)
95	PARAMETER(LBCU=LUK+LPH+LT+2, LBCV=LBCU+LSOLU)
96	PARAMETER(LOUPV=200+11*(LSOLU))
97	PARAMETER(LJI=LBD*LAN*LUK + LCG + (3*LNE+23*LFD*LUK+9)*LUM)
98	PARAMETER(LSCHR=18)
99	

8.2 Infiltration and Redistribution of Dense and Light Nonaqueous Phase Liquids in Partially Saturated Sand Columns

In this section, STOMP generated data are compared with experimentally determined fluid saturations during the infiltration and redistribution of a LNAPL (Soltrol[®]) and a DNAPL (carbon tetrachloride) in a partly saturated one-dimensional column (Oostrom et al. (1995)). The main objective is to evaluate the performance of the Brooks and Corey and the van Genuchten pressure-saturation relations in combination with either the Burdine or Mualem pore-size distribution model (White and Oostrom 1996). The experimentally determined fluid saturations are compared with simulated results from four relative permeability-saturation-pressure ($k-S-p$) models. The four models are the Brooks and Corey-Burdine (BCB), Brooks and Corey-Mualem (BCM), van Genuchten-Burdine (VGB), and van Genuchten-Mualem (VGM) models.

Problem Features: 8.2

- Water-Oil operational mode
- LNAPL and DNAPL transport
- one dimensional (z)
- variable saturation
- uniform Cartesian grid
- van Genuchten function
- Brooks & Corey function
- Burdine and Mualem functions
- homogeneous, isotropic media
- experimental data comparison

8.2.1 Problem Description and Parameters

The experiments were conducted in a 1-m column with a 7.6 cm inside diameter. For each experiment, the column was filled with 80 cm of a uniform 40/50 sand under water saturated conditions. After the packing process, the column was slowly drained in small increments until the water table was 70 cm below the sand surface. During drainage, water pressures and saturations were obtained experimentally at several locations. The saturations and the pressures were used to determine two-phase (air-water) van Genuchten and Brooks-Corey parameters using the RETC code (van Genuchten 1980). After water drainage has ceased, a slug of either dyed CCl_4 or Soltrol[®] was applied uniformly at a constant rate (2 ml/min) to the sand surface. The downward movement of the dyed NAPL was monitored visually and by determining fluid saturations.

The one-dimensional domain was discretized into 160 0.5 cm long cells. The lower boundary was assumed to be permeable to water flow and impermeable to the movement of the NAPLs. The initial conditions were obtained by allowing the saturated column to drain from $z = 80$ cm to $z = 10$. After equilibrium had been reached, the NAPL slug was added by using a Neumann flux-specified boundary condition at the top. Input values for the permeability of the porous medium, the interfacial tensions of the fluid pairs, and the viscosity of the fluids were

obtained in independent experiments. The operational modes of STOMP used for the simulations reported in this report, the Nonvolatile Three-Phase (NVTP) mode and the Volatile Three-Phase (VTP) mode, have been designed to solve subsurface flow and transport problems involving multiphase systems with isothermal conditions. The NVTP mode is most appropriate for systems involving organic compounds with low vapor pressures, such as Soltrol[®], while the VTP mode is appropriate for VOCs with moderate to high vapor pressures, such as CCl₄, where gas-phase transport through advection or diffusion may be significant. The STOMP input files for a Soltrol and carbon tetrachloride case are shown in Exhibit 8.2-1 and Exhibit 8.2-2, respectively.

8.2.2 Simulations

In Figure 8.2-1 and Figure 8.2-2, the measured and simulated Soltrol[®] saturations are shown as a function of elevation at $t = 4$ hr and $t = 72$ hr, respectively, after allowing 100 ml of Soltrol[®] to infiltrate with a rate of 2 ml/min. A plot of measured and simulated carbon tetrachloride saturations versus time at $z = 74$ cm (6 cm below the surface). In this case, a total of 60 ml was allowed to infiltrate with a rate of 2 ml/min. In Figure 8.2-4, measured and simulated carbon tetrachloride saturations are shown as a function of elevation at $t = 4$ hr.

8.2.3 Analysis

Visual observations and gamma system measurements show that the Soltrol[®] moves down rather uniformly through the unsaturated part of the column. At later times, the Soltrol[®] collects in the upper part of the capillary fringe. Both the BCB and VGB models predict the Soltrol[®] distribution with reasonable accuracy. The VBM and BCM models allow the Soltrol[®] to move considerably faster through the unsaturated zone. After 4 hours, the latter models predict that the Soltrol[®] is already collecting in the top of the capillary fringe (Figure 8.1-1). At the end of the experiment, at $t = 72$ hours (Figure 8.2-2), movement of the Soltrol[®] has virtually ceased. The simulated results of all four models at $t = 72$ hr are fairly close. The VGB and VGM models show some tailing in the lower part of the column. At even later times, the simulations indicate that with the VGM and VGB models, the Soltrol[®] continues to move slowly to the bottom of the column. With the BCB and BCM models, the fluid distributions depicted in Figure 8.2-2 remain unaltered. The difference between the van Genuchten and Brooks-Corey models at later times can be explained by the non-wetting fluid (=Soltrol[®]) pressures required to replace the wetting fluid (=water) at a certain elevation. In the van Genuchten models, the Soltrol[®] pressure only has to be greater than the water pressure in order to replace the water. In the Brooks-Corey models, the

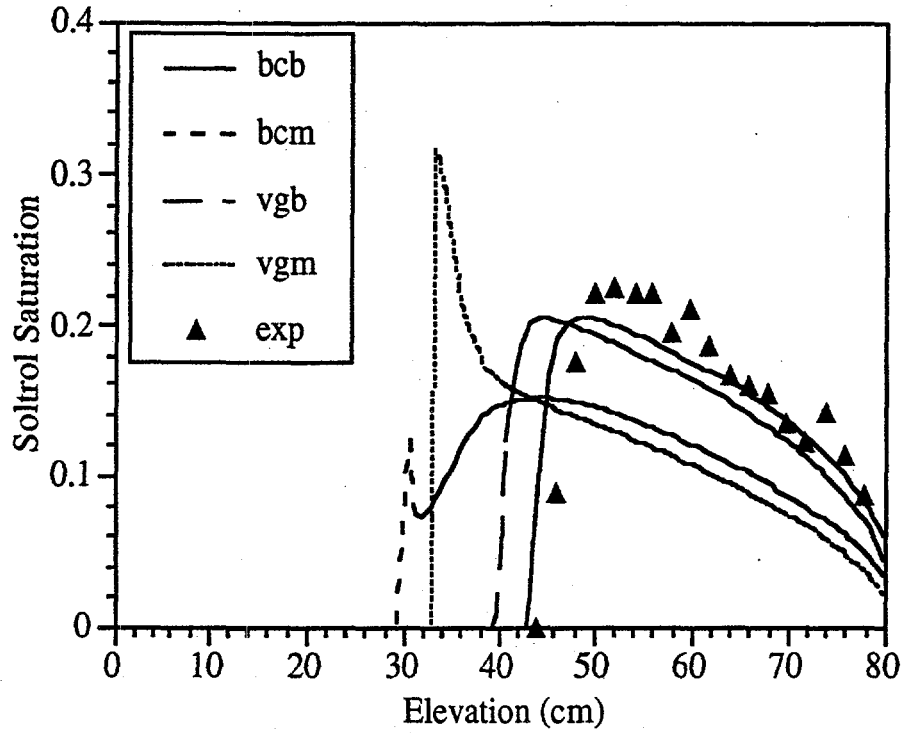


Figure 8.2-1. Soltrol® saturation versus elevation at $t = 4$ hr. A total of 100 ml Soltrol® infiltrated into the column at a rate of 2 ml/min

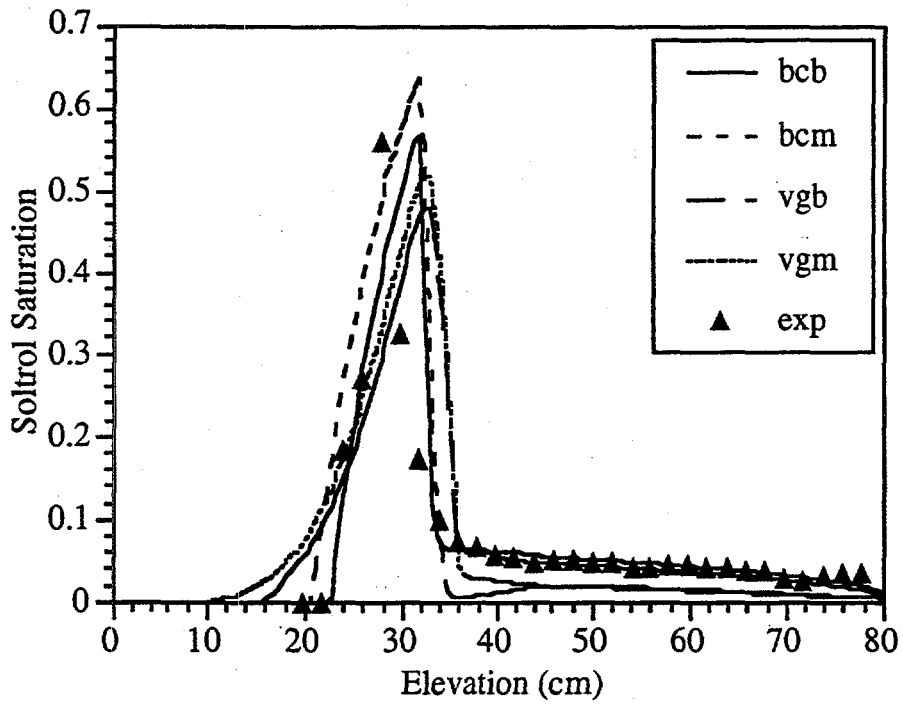


Figure 8.2-2. Soltrol® saturation versus elevation at $t = 72$ hr

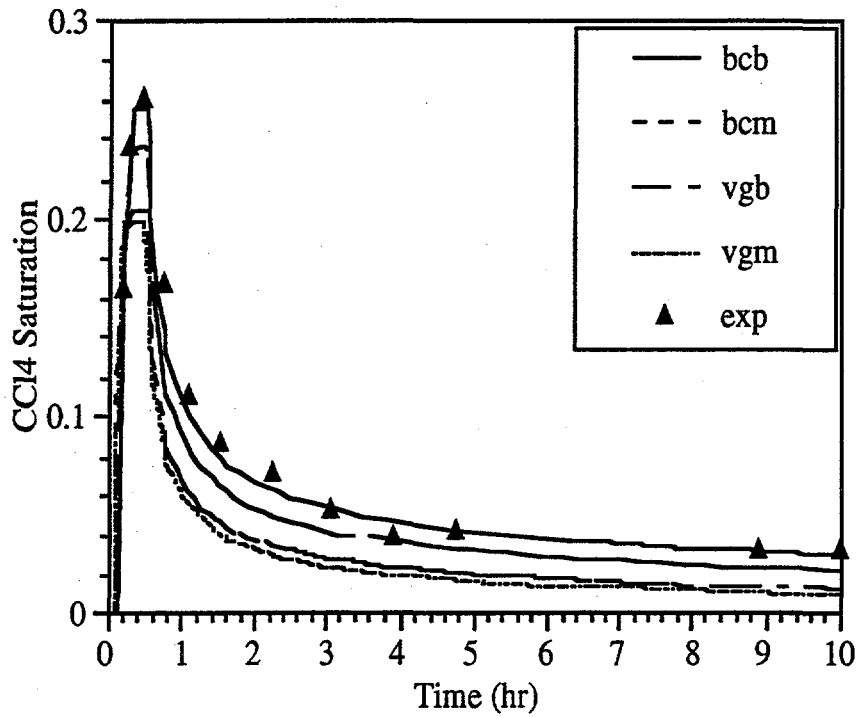


Figure 8.2-3. Carbon tetrachloride breakthrough curve at $z = 74$ cm. A total of 60 ml was allowed to infiltrate into the column at a rate of 2 ml/min

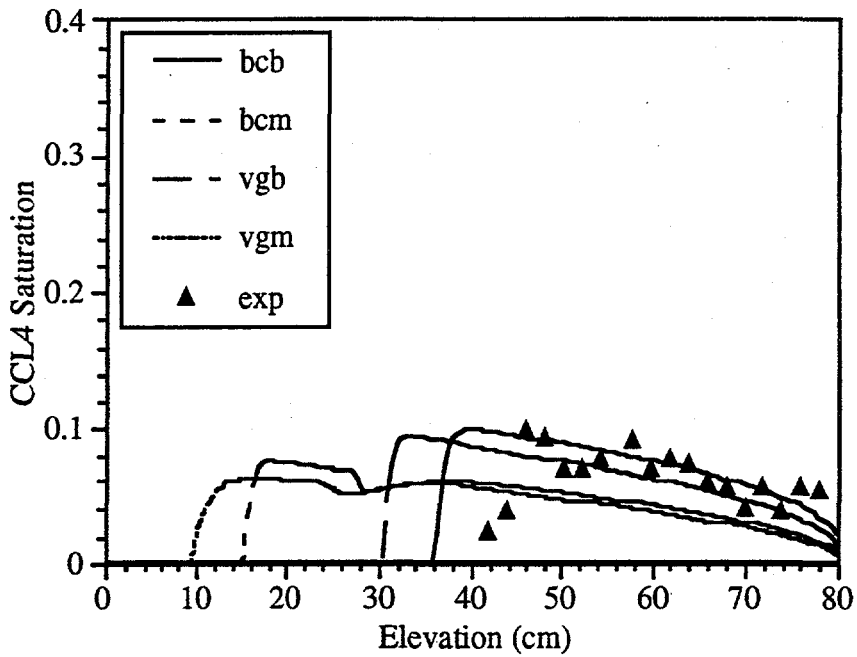


Figure 8.2-4. Carbon tetrachloride saturation versus elevation at $t = 4$ hr

Soltrol[®] pressure has to exceed the water pressure by an amount which is a reflection of the pore size distribution of a porous medium.

With a relatively small infiltration rate of 2 ml/min, the carbon tetrachloride moved uniformly through the unsaturated zone of the column. A plot of the carbon tetrachloride saturation versus time at $z = 74$ cm (6 cm below the top), for an experiment with a total slug of 60 ml, indicates that the movement through the unsaturated region is described best with the BCB model (Figure 8.2-3). This model captures both the peak saturation and the decrease in saturation at later times accurately. The BCM and VGM models predict smaller NAPL saturations during and after front passage.

In Figure 8.2-4, measured and simulated saturations are shown as a function of elevation at $t = 4$ hr. Again, the BCB model shows the best results, although the predicted depth of infiltration with this models is somewhat larger than what is experimentally observed. At $t = 4$ hr, the BCM and VGM models already predict penetration into the capillary fringe. In the experiments, carbon tetrachloride showed a tendency to 'finger' in the capillary fringe and even below the water table before relatively large amounts collected at the interface of the very fine sand and the 40/50 sand.

8.2.4 Summary

STOMP generated data were compared with experimentally determined fluid saturations during the infiltration and redistribution of a LNAPL (Soltrol[®]) and a DNAPL (carbon tetrachloride) in a partly saturated one-dimensional column. It was shown that Brooks-Corey capillary-pressure relations in combination with the Burdine pore size distribution model yield the best agreement between experimental and simulated NAPL saturations for infiltration and redistribution of Soltrol[®] and carbon tetrachloride in the unsaturated zone of a variably saturated 40/50 sand. Carbon tetrachloride has a tendency to finger in the capillary fringe and the below the water table. This phenomenon can not be predicted accurately with the code.

Exhibit 8.2-1. STOMP Input File for LNAPL and DNAPL Problem (Soltrol)

<u>Line</u>	<u>Input File</u>
1	-Simulation Title Card
2	1,
3	Soltrol infiltration 1-D experiment,
4	M.Oostrom,
5	Pacific Northwest Laboratory,
6	September 1994,
7	13:00 PM PDT,
8	1,
9	Simulation of experiment conducted in 331 building,
10	-Solution Control Card
11	Normal,
12	Water-Oil,,
13	4,
14	0,hr,50,min,1,s,60,s,1.25,8,1.e-06,
15	50,min,72,hr,1,s,60,s,1.25,8,1.e-06,
16	1,day,1,day,10000,
17	Variable Aqueous Phase Diffusion,
18	0,
19	-Grid Card
20	Uniform Cartesian,
21	1,1,160,
22	0,cm,6.9125,cm,
23	0,cm,6.9125,cm,
24	0.5,cm,
25	-Rock/Soil Zonation Card
26	1,
27	Sand 40/50,1,1,1,1,1,160,
28	-Mechanical Properties Card
29	Sand 40/50,2650,kg/m^3,0.35,0.35,0,1/m,Millington and Quirk,
30	-Hydraulic Properties Card
31	Sand 40/50,0,m^2,0,m^2,120.,hc m/day,
32	-Aqueous Relative Permeability Card
33	Sand 40/50,Burdine,,
34	-NAPL Relative Permeability Card
35	Sand 40/50,Burdine,,
36	-Volatile Organic Compound Properties Card
37	Soltrol 220,
38	170.34,g/mol,-9.55,C,225.35,C,385.05,C,
39	18.2,bar,713,cm^3/mol,0.24,0.0,0,debyes,
40	-9.328,1.149,-0.0006347,1.359e-07,
41	Equation 2,77.628,10012.5,-9.236,10030.0,
42	Constant,807.4,kg/m^3,
43	Constant,0.0047,Pa s,
44	1.0e10,Pa,
45	-Saturation Function Card
46	Sand 40/50,Nonhysteretic Brooks and Corey,19.366,cm,6.175,0.0,1.0,1.8,2.25,
47	-Initial Conditions Card
48	2,
49	Aqueous Pressure,108667,Pa,,,,,-9789.284,1/m,1,1,1,1,1,160,
50	NAPL Pressure,-1.0e+09,Pa,,,,,,1,1,1,1,1,160,
51	-Boundary Conditions Card
52	3,
53	Top,Zero Flux,Neumann,
54	1,1,1,1,160,160,2,
55	0.,hr,-1.e9,Pa,,-0.0418553,cm/min,

Exhibit 8.2-1. (Contd)

<u>Line</u>	<u>Input File</u>
56	50,min,-1.e9,Pa,, -0.0418553,cm/min,
57	Top,Zero Flux,Zero Flux,
58	1,1,1,1,160,160,2,
59	50,min,-1.e9,Pa,,,,
60	72,hr,-1.e9,Pa,,,,
61	Bottom,Dirichlet,Zero Flux,
62	1,1,1,1,1,1,2,
63	0,hr,102206.04,Pa,,,,,,
64	72,hr,102206.04,Pa,,,,,,
65	-Output Options Card
66	8,
67	1,1,158,
68	1,1,142,
69	1,1,122,
70	1,1,102,
71	1,1,82,
72	1,1,62,
73	1,1,42,
74	1,1,22,
75	1,1,sec,cm,6,6,6,
76	4,
77	total saturation,,
78	aqueous saturation,,
79	NAPL saturation,,
80	NAPL gauge pressure,cm wh,
81	4,
82	4,hr,
83	12,hr,
84	24,hr,
85	72,hr,
86	4,
87	aqueous gauge pressure,cm wh,
88	aqueous saturation,,
89	NAPL gauge pressure,cm wh,
90	NAPL saturation,,
91	-Surface Flux Card
92	1,
93	NAPL Volumetric Flux,ml/hr,ml,Top,1,1,1,1,160,160,
94	

Exhibit 8.2-2. STOMP Input File for LNAPL and DNAPL Problem (Carbon Tetrachloride)

<u>Line</u>	<u>Input File</u>
1	-Simulation Title Card
2	1,
3	Carbon tetrachloride 1-D experiment,
4	M.Oostrom,
5	Pacific Northwest Laboratory,
6	September 1994,
7	13:00 PM PDT,
8	1,
9	Simulation of experiment conducted in 331 building,
10	-Solution Control Card
11	Restart,
12	Water-Oil-Air,,
13	2,
14	0,hr,0.5,hr,1,s,30,s,1.25,16,1.e-06,
15	0.5,hr,40,hr,1,s,3600,s,1.25,16,1.e-06,
16	1,day,1,day,10000,
17	Variable Aqueous Phase Diffusion,
18	Variable Gas Phase Diffusion,
19	0,
20	-Grid Card
21	Uniform Cartesian,
22	1,1,160,
23	6.9125,cm,
24	6.9125,cm,
25	0.5,cm,
26	-Rock/Soil Zonation Card
27	1,
28	Sand 40/50,1,1,1,1,1,160,
29	-Mechanical Properties Card
30	Sand 40/50,2650,kg/m ³ ,0.35,0.35,0,1/m,Millington and Quirk,
31	-Hydraulic Properties Card
32	Sand 40/50,0,m ² ,0,m ² ,120,hc cm/hr,
33	-Aqueous Relative Permeability Card
34	Sand 40/50,Burdine,,
35	-NAPL Relative Permeability Card
36	Sand 40/50,Burdine,,
37	-Gas Relative Permeability Card
38	Sand 40/50,Burdine,,
39	-Volatile Organic Compound Properties Card
40	Carbon tetrachloride,
41	153.823,g/mol,250,K,349.9,K,556.4,K,
42	45.6,bar,275.9,cm ³ /mole,0.272,0.193,0,Debyes,
43	40.072,0.2049,-0.000227,8.843e-08,
44	Equation 1,-7.07139,1.71497,-2.8993,-2.49466,
45	Constant,1594,kg/m ³ ,
46	Constant,0.00097,Pa s,
47	3.2e+07,Pa,
48	-Saturation Function Card
49	Sand 40/50,Nonhysteretic Brooks and Corey,22.2,cm,6.52,0.06,1.0,1.6,2.6666666,
50	-Initial Conditions Card
51	5,
52	Aqueous Pressure,109156.43,Pa,,,,,-9789.284,1/m,1,1,1,1,1,160,
53	NAPL Pressure,-1.0e+09,Pa,,,,,1,1,1,1,1,160,
54	Gas Pressure,101325,Pa,,,,,1,1,1,1,1,160,
55	Temperature,22.0,C,,,,,1,1,1,1,1,160,

Exhibit 8.2-2. (Contd)

<u>Line</u>	<u>Input File</u>
56	Air Partial Pressure,96800,Pa,,,,,,,,1,1,1,1,1,160,
57	-Boundary Conditions Card
58	3,
59	Top,Zero Flux,Dirichlet,Neumann,
60	1,1,1,1,160,160,2,
61	0.,hr,-1.e9,Pa,101325,Pa,-0.0418553,cm/min,1.0,1.0,
62	0.5,hr,-1.e9,Pa,101325,Pa,-0.0418553,cm/min,1.0,1.0,
63	Top,Zero Flux,Dirichlet,Zero Flux,
64	1,1,1,1,160,160,2,
65	0.5,hr,-1.e9,Pa,101325,Pa,-1.e9,Pa,1.0,1.0,
66	40,hr,-1.e9,Pa,101325,Pa,-1.e9,Pa,1.0,1.0,
67	Bottom,Dirichlet,Zero Flux,Zero Flux,
68	1,1,1,1,1,1,2,
69	0,hr,102206.04,Pa,-1.e9,Pa,-1.e9,Pa,1.0,0.0,
70	40,hr,102206.04,Pa,-1.e9,Pa,-1.e9,Pa,1.0,0.0,
71	-Output Options Card
72	7,
73	1,1,158,
74	1,1,142,
75	1,1,122,
76	1,1,102,
77	1,1,82,
78	1,1,62,
79	1,1,2,
80	10,10,hr,cm,6,6,6,
81	4,
82	aqueous saturation,,
83	aqueous gauge pressure,cm wh,
84	NAPL saturation,,
85	NAPL gauge pressure,cm wh,
86	5,
87	4,hr,
88	8,hr,
89	12,hr,
90	24,hr,
91	40,hr,
92	4,
93	aqueous gauge pressure,cm wh,
94	aqueous saturation,,
95	NAPL gauge pressure,cm wh,
96	NAPL saturation,,
97	-Surface Flux Card
98	1,
99	NAPL Volumetric Flux,ml/hr,ml,Top,1,1,1,1,160,160,
100	

8.3 Density-Dependent Gas Advection of Trichlorethylene (TCE)

In this section, results obtained with STOMP are compared to experimentally determined TCE gaseous concentrations. The experimental investigation was conducted to evaluate whether vapor-density effects are important in moving contaminant vapors through the subsurface. TCE was studied because it represents a volatile organic compound (VOC) that has a high vapor pressure and molecular weight and it is a ubiquitous contaminant in the subsurface. VOCs such as solvents and hydrocarbon fuels, are commonly found in the subsurface at many sites. Typically, industrial VOCs have entered the subsurface as nonaqueous-phase liquids (NAPLs) via chemical spills, leaks in storage or transmission structures, and direct disposal to waste sites. VOCs have characteristically a high vapor pressure at normal temperatures and pressures near the earth's surface; therefore, a substantial mass of VOCs will likely be present in the gaseous phase of the subsurface.

Problem Features: 8.3

- Water-Oil-Air operational mode
- VOC transport
- two dimensional (x, z)
- variable saturation
- uniform Cartesian grid
- van Genuchten function
- Mualem function
- homogeneous, isotropic media
- experimental data comparison

Once in the subsurface, VOCs can exist as a separate phase (i.e., a NAPL), as a component of the gaseous phase, and as a component of the aqueous phase. VOCs may also be adsorbed on solid material, either organic or inorganic. The movement of VOCs in the subsurface can occur by advective, diffusive, and dispersive fluxes of the separate fluid phases. Therefore, to model VOC transport in the gaseous phase, advection, diffusion, and dispersion processes need to be considered.

Gas-phase advection is controlled by the network of pores that contain gas, the viscosity of the gaseous phase, and a spatial difference in the gas-phase total potential, which is commonly defined as the sum of the gas-pressure potential and the gravitational potential. Very small gradients in the gas-phase total potential can yield significant advective fluxes because the resistance to gas flow is small (i.e., negligible gas-phase viscosities), and the gaseous phase is contained in the largest pores of liquid-unsaturated porous media.

8.3.1 Problem Description and Parameters

The experiment was conducted in an intermediate-scale experimental cell. The cell has a porous-media chamber that was 2-m-long by 1-m-high by 7.5-cm-thick (Figure 8.3-1). Stainless-

steel screens separate the porous medium from the fluid reservoir chambers, which are located on each side of the porous-media chamber. The fluid levels in the reservoir chambers could be adjusted via outlets at the base of the reservoirs so that a flowing groundwater regime could be simulated. The cell can also be rotated vertically to allow coring (i.e., sampling) of the porous media following an experiment. The top of the cell can be sealed to prevent vapors from escaping into the work place. There is an outlet in the top cover that can be connected to tubing to maintain atmospheric gas conditions in the flow cell. The cell walls were metal-bar-reinforced plexiglas that had 55 sampling ports for extracting gas or water (Figure 8.3-1). The sand was packed in the flow cell by pouring through a 6-8 cm layer of water. The water layer was assumed not to cause any size segregation of the sand grains. The sand was mixed periodically to dislodge any entrapped air and to provide some degree of homogenization to the packing. Therefore, an initially water-saturated condition was assumed with a constant bulk density. Measurements of bulk densities following the experiment yielded an average value of 1.40 g cm^{-3} with a coefficient of variability of 3.2 per cent. The final thickness of the sand in the flow cell was 1 m.

During packing the flow cell, a chamber was placed in the flow cell that was used to direct TCE vapors into the sand. The chamber was 27-cm long by 10-cm high by 7.5-cm wide and was constructed with metal. There was a 8.5-cm-long by 7.5-cm-wide opening at the base of the chamber. This opening was the source area for TCE vapors entering the packed sand. The chamber and sand were placed in the flow cell at the same time to ensure that the sand was packed adjacent to the chamber walls. A 12-cm-long by 7.5-cm-wide metal section that was attached to each side of the opening in the chamber base to direct the vapors downward (Figure 8.3-1).

Approximately 24 hours after the packing was completed, the water table was lowered from slightly above the upper sand surface (i.e., an elevation of 102 cm) to an elevation of 15.5 cm at the water-supply fluid reservoir chamber and at an elevation of 15 cm at the outlet fluid reservoir chamber. A 0.5 cm height difference in fluid levels was maintained over the 2-m cell length to cause water to flow at rates comparable to field velocities. As the water drained, sand was evacuated from the chamber and a glass container, filled with dry sand, was placed on posts and centered in the source chamber. Sand was placed in the glass container to increase the surface area of the liquid TCE-air interfaces. The surface of the sand directly below the chamber was at an elevation of 90 cm, and the surface of the sand elsewhere was at an elevation of 100 cm (Figure 8.3-1). Three sampling ports were located within the domain of the source chamber. One port was used to supply liquid TCE to the glass container, one port was used to characterize TCE vapor concentrations in the supply chamber, and the other port was used to investigate if there would be any increase in total gas pressure, via a manometer, because of TCE volatilization and source

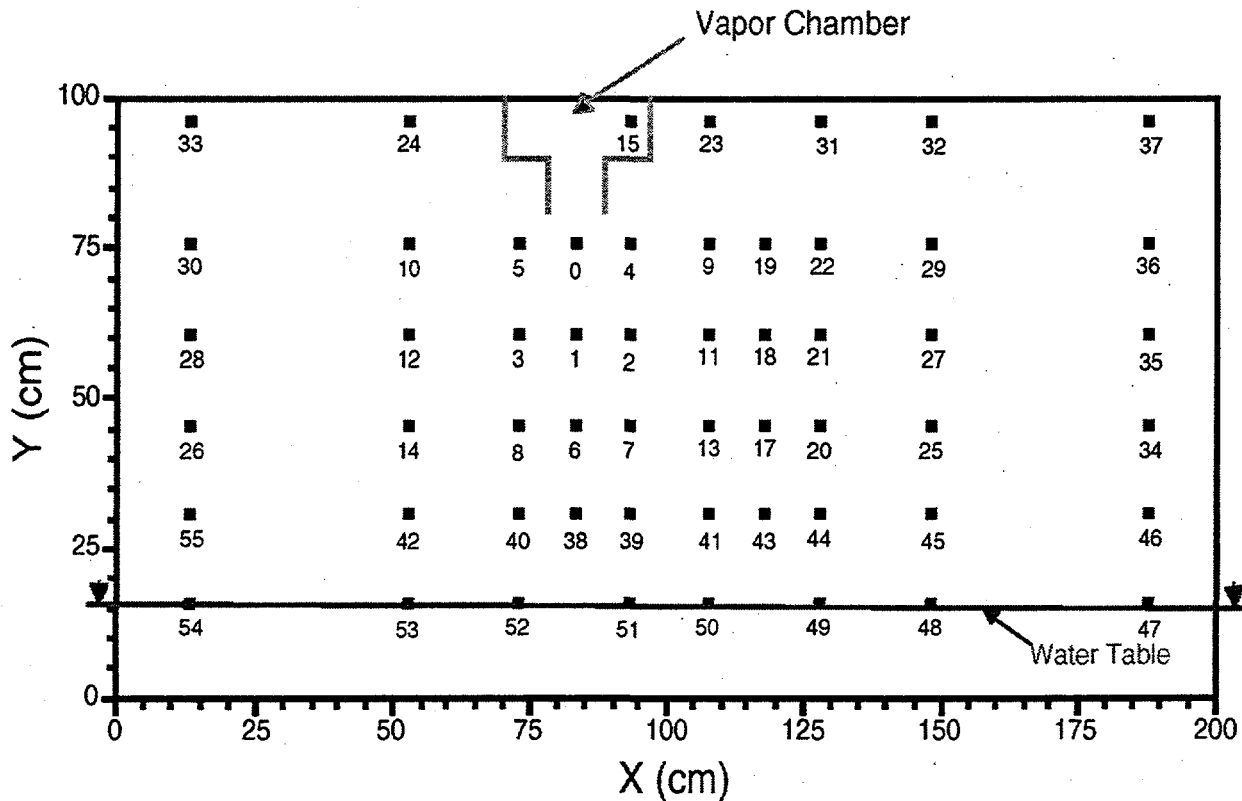


Figure 8.3-1. Illustration of the Configuration of the Flow Cell Including the Measurement Ports with Associated Numbers, the Vapor Chamber, and the Water Table

chamber design. The TCE-vapor concentrations in the void spaces of the sand were characterized by extracting 25- μ l gas samples from the measurement ports using a gas-tight syringe.

In the simulations with STOMP, the lower gas-phase boundary condition was no-flow, as were the side boundary conditions. The upper gas-phase boundary condition was atmospheric pressure with time-dependent TCE concentrations equal to those measured above the sand during the experiment (measurement port not shown in Figure 8.3-1). Boundary conditions corresponding to the vapor-source chamber were no-flow along the chamber boundaries and the vertical 12-cm-long metal sections that were used to direct the vapors downward, except for the 8.5-cm opening at the base of the chamber. At this interface, the boundary conditions were atmospheric pressure and time-dependent TCE concentrations measured via port 15 (Figure 8.3-1). These conditions more accurately matched the experimental conditions, i.e., the TCE concentrations in the vapor chamber did not instantaneously achieve their saturated values and TCE concentrations above the sand were not zero (there was some out-gassing). The upper and side aqueous-phase boundary conditions were no-flow. The lower aqueous-phase boundary condition

was constant pressures that caused water to flow at a rate equal to a reduction in head of 0.5 cm over a 2-m length. The two-dimensional domain was discretized into 880 (40 x 22) cells. The simulations consisted of two parts. In the first part the initial steady state conditions were created. The second part, the actual TCE distribution was simulated. The STOMP input file for the second part is shown in Exhibit 8.3-1. The parameters file of this problem is shown Exhibit 8.3-1. The experiment and numerical simulations are described in detail by Lenhard et al. (1995).

8.3.2 Simulations

In Figure 8.3-2 through Figure 8.3-4, the measured and simulated TCE concentrations are shown for three locations (port 6, port 9, and port 45, respectively), as a function of time. The measured concentrations are compared with numerical simulations considering diffusion only and with simulations considering both diffusion and gaseous advection as a result of density differences. To ignore vapor density effects in the simulations, it was assumed that the molecular weight of TCE was such that its vapor densities were not significantly higher than that from subsurface ambient conditions.

8.3.3 Analysis

For port 6 (refer to Figure 8.3-1 for location of ports), which is directly below the source chamber, the agreement between the experimental data and the simulation results when vapor-density effects are considered are very good. The agreement between the experimental data and the simulation results when vapor-density effects are ignored are very poor. This suggests that for at least directly below the source chamber density-driven vapor advection is important and should be considered when modeling vapor transport. For port 9, which is to the right of the source-chamber base, the results are similar to that of port 6. This implies that good agreement was obtained between the experimental data and TCE-concentration predictions when vapor-density effects were considered. Conversely, poor agreement was obtained between the experimental data and TCE-concentration predictions when vapor-density effects were ignored. For port 45, which is located slightly above the water-saturated capillary fringe to the right of the source chamber, the results are similar to ports 6 and 9.

Port 6

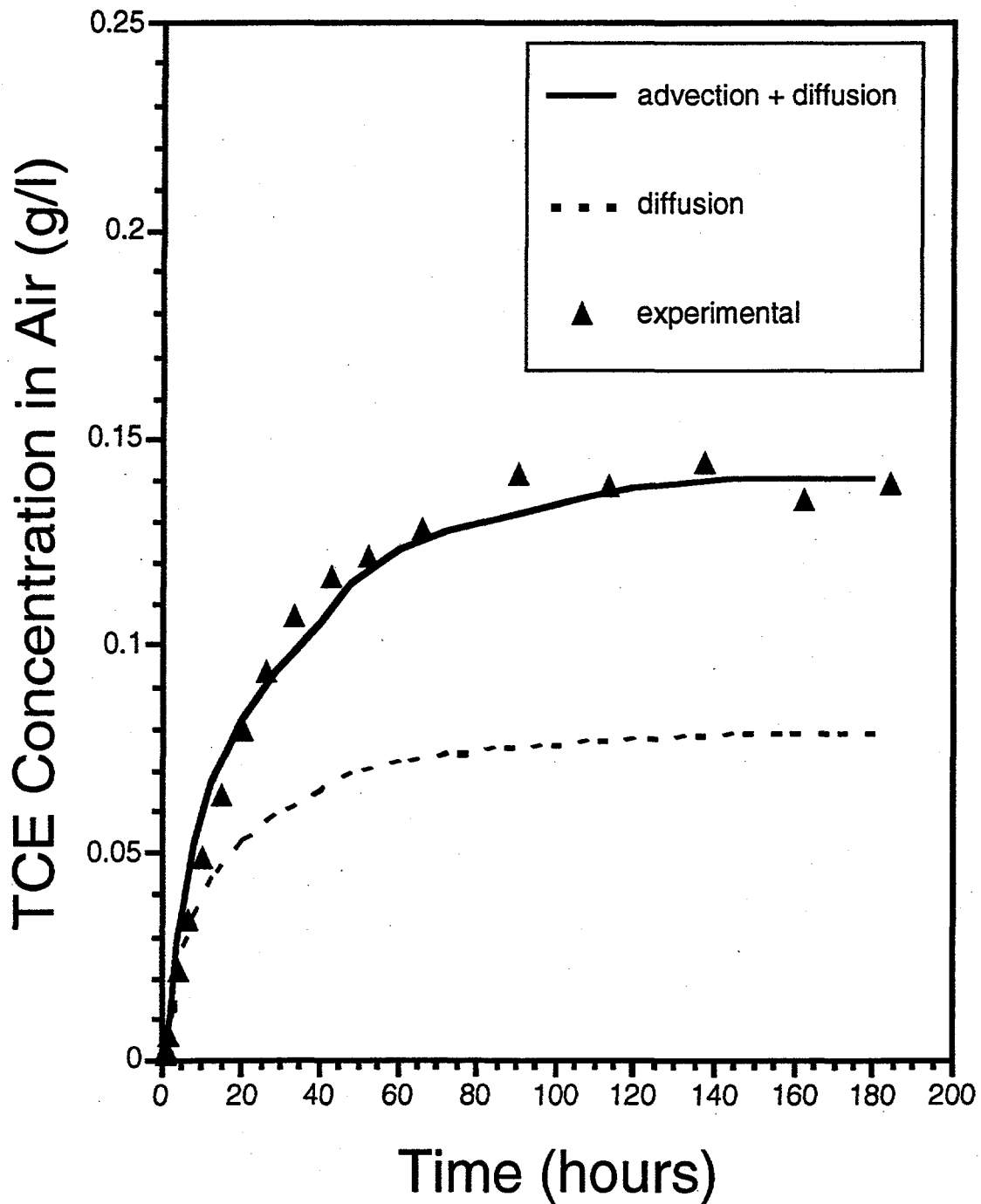


Figure 8.3-2. Comparison Between Experimental TCE Concentrations and Predictions Made by STOMP when Vapor Density is Considered (solid lines) and Ignored (broken lines) for Port 6.

Port 9

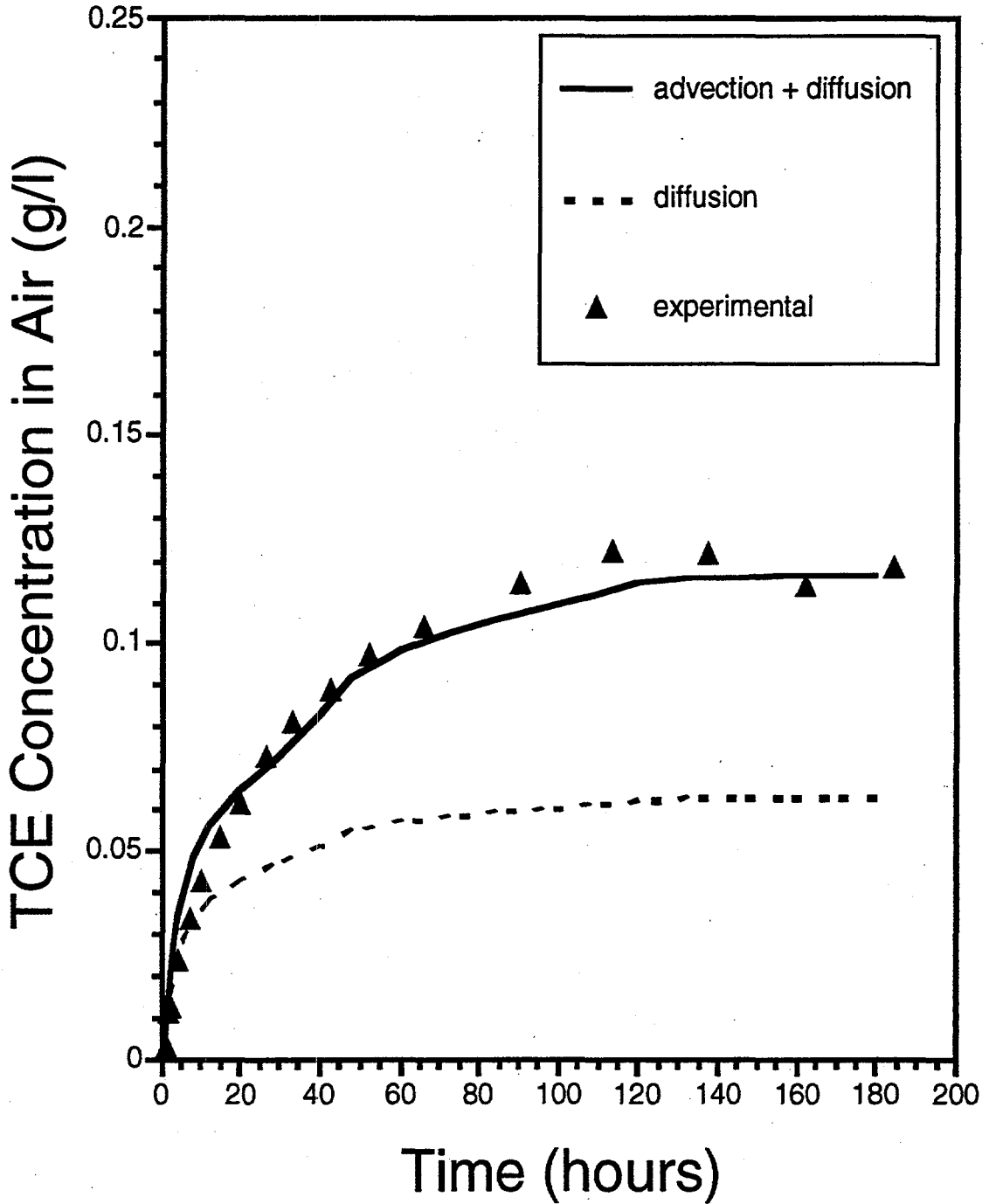


Figure 8.3-3. Comparison Between Experimental TCE Concentrations and Predictions Made by STOMP when Vapor Density is Considered (solid lines) and Ignored (broken lines) for Port 9

Port 45

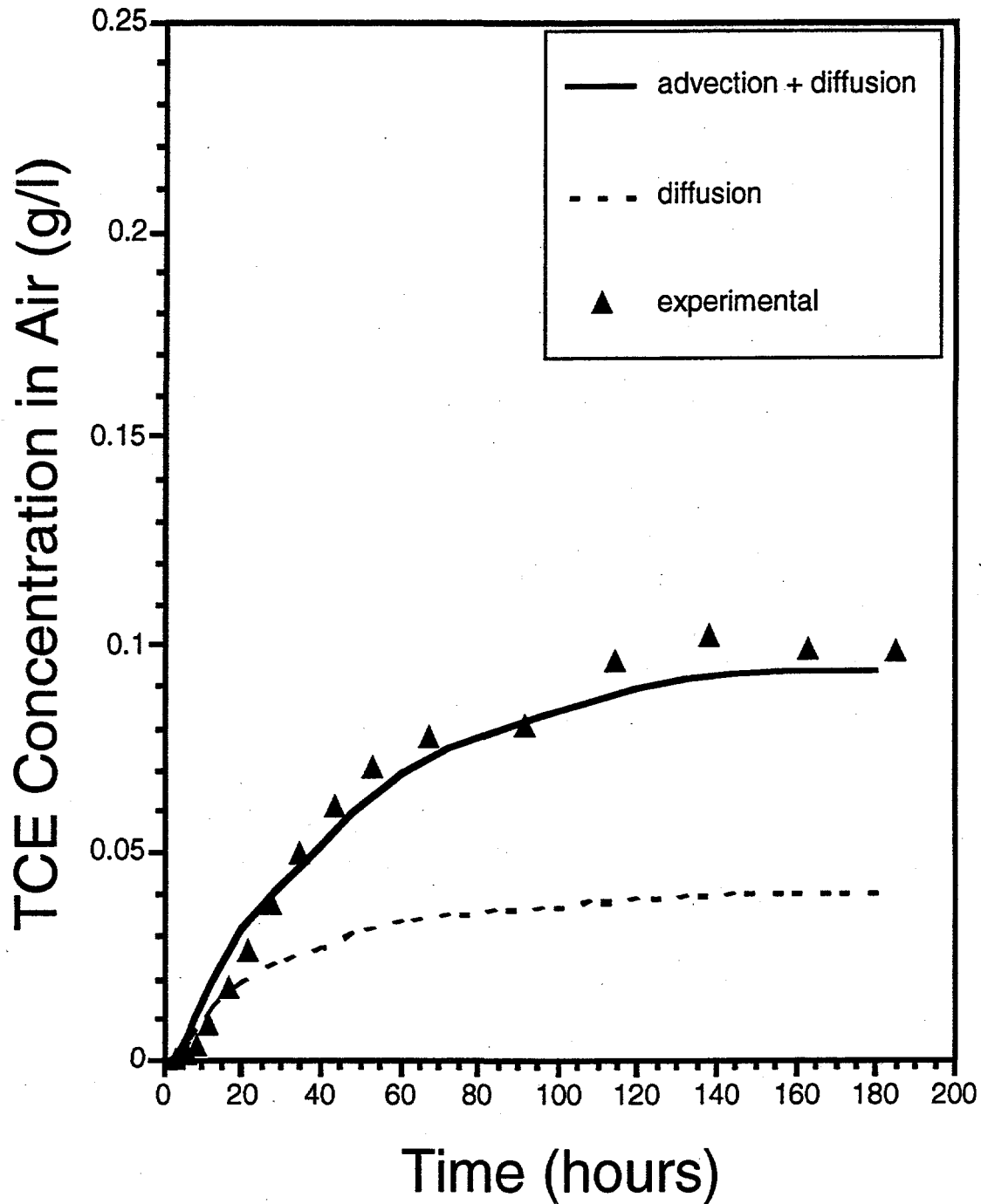


Figure 8.3-4. Comparison Between Experimental TCE Concentrations and Predictions Made by STOMP when Vapor Density is Considered (solid lines) and Ignored (broken lines) for Port 45

The reason why better agreement was obtained with simulations that include vapor-density effects for ports below the source chamber and for ports to the sides of the chamber is that whole domain of the flow cell is being affected by vapor-density effects. Because of spatial differences in vapor densities, there will be gradients in the total gas potential (i.e., sum of the gas pressure and gravitational potentials), which will induce advective gas flow and the TCE concentrations of all of the ports will be affected. The gas-flow regime, as obtained from the simulation results when vapor-density effects are considered, are shown in Figure 8.3-5 for $t = 1$ hour and $t = 180$ hours. The size of the arrows in Figure 8.3-5 reflect the magnitude of the Darcian gas velocities; the larger is the arrow, the greater is the gas velocity. It can be seen in Figure 8.3-5 that gas-flow convection cells develop. For port 6, the gas velocities are moderate and are always directed downward. At port 9, for early times, there are moderate gas velocities, but at later times, there are only minor to negligible gas velocities. For port 37, which is in the upper right corner of the flow cell, there are minor gas velocities at early times, and moderate gas velocities at later times, which are always directed upward. The development of convection cells because of vapor-density effects is not unique for the experimental design we employed. Hence, spatial TCE concentrations are likely to be also affected in the field as they were in our experiment. Therefore, for VOCs with mass densities significantly larger than ambient conditions, vapor-density effects need to be considered when evaluating VOC vapor transport through the subsurface, at least for porous media similar to that used in the experiment.

8.3.4 Summary

The experimental and modeling results suggest that vapor-density effects may be very important for moving gaseous compounds through the subsurface and should therefore be included in simulations of vapor movement for compounds and conditions in which vapor densities may deviate from ambient vapor densities. To accurately predict VOC vapor distributions in sandy subsurface media, density-driven advection must be considered.

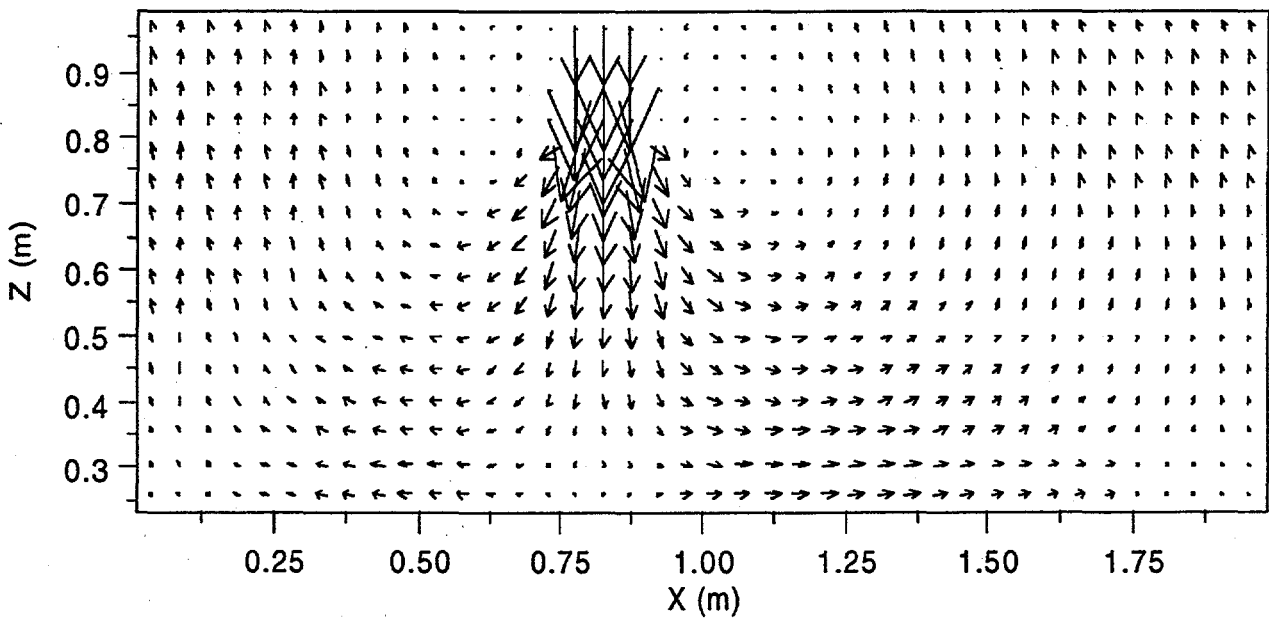
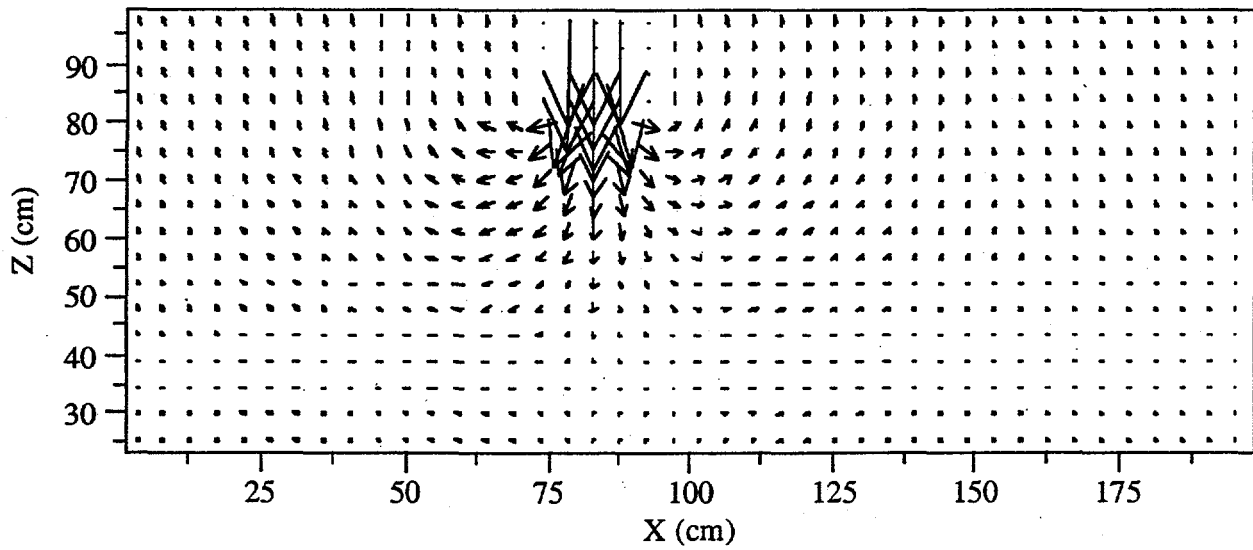


Figure 8.3-5. Darcian Velocities (m/s) of the Gas Phase in the Experimental Cell Predicted Using STOMP when Vapor Density Effects are Considered for (a) $t = 1$ h, and (b) $t = 180$ h

Exhibit 8.3-1. STOMP Input File for Two-Dimensional Vapor Flow Problem

<u>Line</u>	<u>Input File</u>
1	# -----
2	-Simulation Title Card
3	# -----
4	1,
5	Vapor flow experiment simulations,
6	M.Oostrom,
7	Pacific Northwest Laboratory,
8	January 1994,
9	10:00 AM PDT,
10	1,
11	TCE vapor experiment in 2D flow container
12	# -----
13	-Solution Control Card
14	# -----
15	Restart,
16	Water-Oil-Air,,
17	0,s,180,hr,1,s,4,hr,1.25,8,1.0e-06,
18	1,day,1,day,5000,
19	Variable,
20	Constant,0.9e-06,m ² /s,
21	0,
22	# -----
23	-Grid Card
24	# -----
25	Cartesian,
26	40,1,22,
27	0,cm,5,cm,10,cm,15,cm,20,cm,25,cm,30,cm,35,cm,40,cm,45,cm,
28	50,cm,55,cm,60,cm,65,cm,70,cm,77.5,cm,80,cm,85,cm,87.5,cm,95,cm,
29	100,cm,105,cm,110,cm,115,cm,120,cm,125,cm,130,cm,135,cm,140,cm,145,cm,
30	150,cm,155,cm,160,cm,165,cm,170,cm,175,cm,180,cm,185,cm,190,cm,195,cm,
31	200,cm,
32	0,cm,7.5,cm,
33	0,cm,2.5,cm,7.5,cm,12.5,cm,22.5,cm,25,cm,27.5,cm,32.5,cm,37.5,cm,42.5,cm,
34	47.5,cm,52.5,cm,57.5,cm,62.5,cm,67.5,cm,72.5,cm,77.5,cm,82.5,cm,87.5,cm,90,cm,
35	92.5,cm,97.5,cm,100,cm,
36	# -----
37	-Inactive Domain Card
38	# -----
39	3,
40	16,16,1,1,19,19,
41	18,18,1,1,19,19,
42	15,19,1,1,20,22,
43	# -----
44	-Rock/Soil Zonation Card
45	# -----
46	1,
47	Coarse Sand,1,40,1,1,1,22,
48	# -----
49	-Mechanical Properties Card
50	# -----
51	Coarse Sand,2650,kg/m ³ ,0.47,0.47,0,1/m,Millington and Quirk,
52	# -----
53	-Hydraulic Properties Card
54	# -----
55	Coarse Sand,175.0,hc m/day,0,m ² ,175.0,hc m/day,

Exhibit 8.3-1. (Contd)

<u>Line</u>	<u>Input File</u>
56	# -----
57	-Aqueous Relative Permeability Card
58	# -----
59	Coarse Sand,Mualem,,
60	# -----
61	-Gas Relative Permeability Card
62	# -----
63	Coarse Sand,Mualem,,
64	# -----
65	-NAPL Relative Permeability Card
66	# -----
67	Coarse Sand,Mualem,,
68	# -----
69	-Volatile Organic Compound Properties Card
70	# -----
71	Trichloroethylene,
72	131.4,g/mol,186.8,K,360.4,K,572.0,K,
73	50.5,bar,256.0,0.265,0.213,0.9,Debyes,
74	30.17,0.2287,-0.0002229,8.244e-08,
75	Equation 1,-7.3819,1.94817,-3.03294,-5.345365,
76	Constant,1460.0,kg/m^3,
77	Constant,0.00057,Pa s,
78	2.4167e+07,Pa,
79	# -----
80	-Saturation Function Card
81	# -----
82	Coarse Sand,Nonhysteretic,0.156,1/cm,4.28,0.0,1.0,1.89,2.4,
83	# -----
84	-Initial Conditions Card
85	# -----
86	4,
87	Aqueous Pressure,102680.9,Pa,-25,1/m,,,-9789.284,1/m,1,40,1,1,1,22,
88	NAPL Pressure,-1.0e+09,Pa,,,,,,1,40,1,1,1,22,
89	Gas Pressure,101336.47,Pa,,,,,-11.619,1/m,1,40,1,1,1,22,
90	Temperature,22.0,C,,,,,,1,40,1,1,1,22,
91	# -----
92	-Boundary Conditions Card
93	# -----
94	5,
95	Top,Zero Flux,Dirichlet,Zero Flux,
96	1,14,1,1,22,22,5,
97	0,s,-1.e9,Pa,,,101325,Pa,1.0,0.0,-1.e9,Pa,
98	24,hr,-1.e9,Pa,,,101325,Pa,1.0,0.0,-1.e9,Pa,
99	48,hr,-1.e9,Pa,,,101325,Pa,1.0,0.05,-1.e9,Pa,
100	120,hr,-1.e9,Pa,,,101325,Pa,1.0,0.11,-1.e9,Pa,
101	180,hr,-1.e9,Pa,,,101325,Pa,1.0,0.11,-1.e9,Pa,
102	Top,Zero Flux,Dirichlet,Zero Flux,
103	16,18,1,1,19,19,5,
104	0,s,-1.e9,Pa,,,101326.161873769,Pa,1.0,0.0,-1.e9,Pa,
105	0.5,hr,-1.e9,Pa,,,101326.161873769,Pa,1.0,0.75,-1.e9,Pa,
106	6.0,hr,-1.e9,Pa,,,101326.161873769,Pa,1.0,0.85,-1.e9,Pa,
107	48,hr,-1.e9,Pa,,,101326.161873769,Pa,1.0,1.0,-1.e9,Pa,
108	180,hr,-1.e9,Pa,,,101326.161873769,Pa,1.0,1.0,-1.e9,Pa,
109	Top,Zero Flux,Dirichlet,Zero Flux,
110	20,40,1,1,22,22,5,

Exhibit 8.3-1. (Contd)

<u>Line</u>	<u>Input File</u>
111	0,s,-1.e9,Pa,,,101325,Pa,1.0,0.0,-1.e9,Pa,
112	24,hr,-1.e9,Pa,,,101325,Pa,1.0,0.0,-1.e9,Pa,
113	48,hr,-1.e9,Pa,,,101325,Pa,1.0,0.05,-1.e9,Pa,
114	120,hr,-1.e9,Pa,,,101325,Pa,1.0,0.11,-1.e9,Pa,
115	180,hr,-1.e9,Pa,,,101325,Pa,1.0,0.11,-1.e9,Pa,
116	West,Hydraulic Gradient,Zero Flux,Zero Flux,
117	1,1,1,1,1,5,1,
118	0,s,102680.9,Pa,,, -1.e9,Pa,1.0,0.0,-1.e9,Pa,
119	East,Hydraulic Gradient,Zero Flux,Zero Flux,
120	40,40,1,1,1,5,1,
121	0,s,102630.958,Pa,,, -1.e9,Pa,1.0,0.0,-1.e9,Pa,
122	# -----
123	-Output Options Card
124	# -----
125	46,
126	3,1,21,
127	3,1,16,
128	3,1,13,
129	3,1,10,
130	3,1,7,
131	11,1,21,
132	11,1,16,
133	11,1,13,
134	11,1,10,
135	11,1,7,
136	15,1,16,
137	15,1,13,
138	15,1,10,
139	15,1,7,
140	17,1,16,
141	17,1,13,
142	17,1,10,
143	17,1,7,
144	19,1,16,
145	19,1,13,
146	19,1,10,
147	19,1,7,
148	22,1,21,
149	22,1,16,
150	22,1,13,
151	22,1,10,
152	22,1,7,
153	24,1,16,
154	24,1,13,
155	24,1,10,
156	24,1,7,
157	26,1,21,
158	26,1,16,
159	26,1,13,
160	26,1,10,
161	26,1,7,
162	30,1,21,
163	30,1,16,
164	30,1,13,
165	30,1,10,

Exhibit 8.3-1. (Contd)

<u>Line</u>	<u>Input File</u>
166	30,1,7,
167	39,1,21,
168	39,1,16,
169	39,1,13,
170	39,1,10,
171	39,1,7,
172	1,1,hr,m,
173	3,
174	x gas vol,m/day,
175	z gas vol,m/day,
176	gas voc conc,kg/m ³ ,
177	6,
178	4,hr,
179	8,hr,
180	12,hr,
181	24,hr,
182	48,hr,
183	180,hr,
184	1,
185	gas phase voc comp,kg/m ³ ,
186	

Exhibit 8.3-2. STOMP Parameters File for Two-Dimensional Vapor Flow Problem

<u>Line</u>	<u>Parameters File</u>
1	C-----C
2	C STOMP Parameter File
3	C-----C
4	C
5	C--- Number of lines of simulation notes
6	C Number of execution periods ---
7	C
8	PARAMETER(LNOTES=10, LEPD=10)
9	C
10	C--- Number of nodes in the x or r coordinate direction
11	C Number of nodes in the y or theta coordinate direction
12	C Number of nodes in the z coordinate direction
13	C Number of active nodes
14	C Number of active dimensions
15	C Minimum of (LFX*LFY, LFX*LFZ, LFY*LFZ) ---
16	C
17	PARAMETER(LFX=40, LFY=1, LFZ=22)
18	PARAMETER(LAN=863, LAD=2, LMNP=22)
19	C
20	C--- Energy equation switch (0 = off, 1 = on)
21	C Water mass equation switch (0 = off, 1 = on)
22	C Air mass equation switch (0 = off, 1 = on)
23	C VOC mass equation switch (0 = off, 1 = on)
24	C Solute transport equation switch (0 = off, 1 = on)
25	C Freezing conditions switch (0 = off, 1 = on) ---
26	C Dissolved salt transport equation switch (0 = off, 1 = on) ---
27	C Dissolved oil transport equation switch (0 = off, 1 = on) ---
28	C
29	PARAMETER(LT=0, LL=1, LG=1, LN=1, LC=0, LFC=0, LS=0, LD=0)
30	C
31	C--- Banded matrix linear equation solver switch (0 = off, 1 = on)
32	C Conjugate gradient linear equation solver switch (0 = off, 1 = on) ---
33	C Unsymmetric-pattern multifrontal package switch (0 = off, 1 = on) ---
34	C
35	PARAMETER(LBD=1, LCG=0, LUM=0)
36	C
37	C--- Number of boundary condition surfaces
38	C Number of boundary condition times ---
39	C
40	PARAMETER(LBC=12, LBTM=17)
41	C
42	C--- Number of sources
43	C Number of source times ---
44	C
45	PARAMETER(LSR=1, LSTM=10)
46	C
47	C--- Number of rock/soil types
48	C Number of solutes
49	C
50	PARAMETER(LRC=1, LSOLU=1)
51	C
52	C--- Number of reference nodes
53	C Number of print times
54	C Number of integration surfaces ---
55	C

Exhibit 8.3-2. (Contd)

<u>Line</u>	<u>Parameters File</u>
56	PARAMETER(LREF=46, LPTM=6, LSF=1)
57	C
58	C--- Number saturation and relative permeability table entries
59	C Number of hysteretic scanning paths
60	C Number of chemical reactions
61	C
62	PARAMETER(LTBL=1, LPATH=7, LCHEM=1)
63	C
64	C--- Computed Parameters ---
65	C
66	PARAMETER(LUK=LT+LL+LG+LN+LS+LD, LPH=LL+LG+LN, LCMP=LL+LS+LD)
67	PARAMETER(LFX=LFX*LFY, LFYZ=LFY*LFZ, LPZX=LPZ*LPX)
68	PARAMETER(LFD=LFX*LFY*LFZ)
69	PARAMETER(LNE=(LUK*LUK*(7*LFD-2*LFX-2*LFYZ-2*LPZX))*LUM)
70	PARAMETER(LHBW=LUK*LMNP+LUK-1)
71	PARAMETER(LJA=LBD + LCG*LAN*LUK + LUM*LAN*LUK)
72	PARAMETER(LJB=(2*LAN*LUK))*LUM, LJC=LAN*LUM)
73	PARAMETER(LJD=LBD*(3*LHBW+1) + LCG*LAN*LUK + LUM*6*LNE)
74	PARAMETER(LJE=LBD*LAN*LUK + LCG*((2*LAD+1)*LUK+2*LAD) + LUM)
75	PARAMETER(LJF=LAN*LUK)
76	PARAMETER(LJG=LBD*(3*LHBW+1) + LCG*LAN*LUK + LUM)
77	PARAMETER(LJH=LBD*LAN*LUK + LCG*(2*LAD+1) + LUM)
78	PARAMETER(LJJ=LBD*LAN*LUK + LCG + LUM)
79	PARAMETER(LSV=LUK+2, LSFV=2*LUK+1)
80	PARAMETER(LSX=(LFX+1)*LFY*LFZ)
81	PARAMETER(LSY=LFX*(LFY+1)*LFZ)
82	PARAMETER(LSZ=LFX*LFY*(LFZ+1))
83	PARAMETER(LFDT=LFD**LT, LFDL=LFD**LL, LFDG=LFD**LG, LFDN=LFD**LN)
84	PARAMETER(LFDC=LFD**LC, LFDI=LFD**LFC, LFDS=LFD**LS, LFDD=LFD**LD)
85	PARAMETER(LSXT=LSX**LT, LSXL=LSX**LL, LSXG=LSX**LG, LSXN=LSX**LN)
86	PARAMETER(LSXC=LSX**LC, LSXS=LSX**LS, LSXD=LSX**LD)
87	PARAMETER(LSYT=LSY**LT, LSYL=LSY**LL, LSYG=LSY**LG, LSYN=LSY**LN)
88	PARAMETER(LSYC=LSY**LC, LSYS=LSY**LS, LSYD=LSY**LD)
89	PARAMETER(LSZT=LSZ**LT, LSZL=LSZ**LL, LSZG=LSZ**LG, LSZN=LSZ**LN)
90	PARAMETER(LSZC=LSZ**LC, LSZS=LSZ**LS, LSZD=LSZ**LD)
91	PARAMETER(LRCT=LRC**LT, LRCL=LRC**LL, LRCG=LRC**LG, LRCN=LRC**LN)
92	PARAMETER(LRCC=LRC**LC, LRCL=LRC**LFC, LRCS=LRC**LS, LRCD=LRC**LD)
93	PARAMETER(LBCT=LBC**LT, LBCL=LBC**LL, LBCG=LBC**LG, LBCN=LBC**LN)
94	PARAMETER(LBCC=LBC**LC, LBCI=LBC**LFC, LBCC=LBC**LS, LBCC=LBC**LD)
95	PARAMETER(LBCU=LUK+LPH+LT+2, LBCV=LBCU+LSOLU)
96	PARAMETER(LOUPV=200+11*(LSOLU))
97	PARAMETER(LJI=LBD*LAN*LUK + LCG + (3*LNE+23*LFD*LUK+9)*LUM)
97	PARAMETER(LSCHR=18)
99	

8.4 References

- Celia MA, ET Bouloutas, and RL Zabra. 1990. "A general mass conservative numerical solution for the unsaturated flow equation." *Water Resources Research*, 26(7), 1483-1496.
- Kaluarachchi JJ, and JC Parker. 1989. "An efficient finite element method for modeling multiphase flow." *Water Resources Research*, 25(1), 43-54.
- Kaluarachchi JJ, and JC Parker. 1994. "Correction to "An efficient finite element method for modeling multiphase flow"." *Water Resources Research*, 30(8), 2485-2486.
- Katyal AK, and JC Parker. 1992. "An adaptive solution domain algorithm for solving multiphase flow equations." *Computers in Geosciences*, 18(1), 1-9.
- Lenhard RJ, M Oostrom, and MD White. 1995. "Investigation of density-dependent gas advection of trichloroethylene: experiment and a model validation exercise." *Journal of Contaminant Hydrology*, 19(1), 47-67.
- Oostrom M, RJ Lenhard, and MD White. 1995. "Infiltration and Redistribution of dense and light nonaqueous phase liquids in partly saturated sand columns," In *Proceedings of Fifteenth Annual American Geophysical Union Hydrology Days*, Fort Collins, Colorado, 215-226.
- Ségol G. 1994. *Classic Groundwater Simulations: Proving and Improving Numerical Models*, Prentice-Hall, Englewood Cliffs, New Jersey.
- van Genuchten MT. 1980. "A closed form equation for predicting the hydraulic conductivity of unsaturated soils." *Soil Science Society of America Journal*, 44, 982-998.
- White MD, and M Oostrom. 1996. *STOMP Subsurface Transport Over Multiple Phases Theory Guide*, PNNL-11217, Pacific Northwest National Laboratory, Richland, Washington.

9.0 Additional STOMP Applications

In addition to the applications illustrated in this report, several other published examples of STOMP applications exist. This section provides a brief synopsis of each, and the relevant reference so that the reader may locate further examples that interest them.

White et al. (1995) and Lenhard et al. (1995b) provide a description of model theory development and associated numerical and experimental results.

Two applications in this guide, Section 8.1 (Infiltration and Redistribution of Oil in a Hypothetical, Two-Dimensional Aquifer) and Section 8.2 (Infiltration and Redistribution of Dense and Light Nonaqueous Phase Liquids in Partially Saturated Sand Columns), dealt with modeling nonaqueous phase liquids. The numerical treatment of dense and light nonaqueous phase liquids (DNAPLs and LNAPLs) is examined in greater detail in Oostrom et al. (1995), Oostrom and Lenhard (1997), Oostrom et al. (1997a), and White and Oostrom (1997). These papers discuss the processes of infiltration and redistribution of these special classes of contaminants in the unsaturated zone of sand columns.

A simple radon generation problem was examined in this guide in Section 5.4 (Radon Vapor Transport into Dwellings) of this report. A more detailed look at the issue of radon generation in groundwater can be found in Oostrom and Lenhard (1996) and Oostrom et al. (1996b).

An especially difficult problem in radioactive waste issues has been modeling associated with waste storage tank issues at the Hanford Nuclear Reservation. STOMP has been applied recently to begin developing a model for saltcake waste tanks (Simmons et al. 1997).

Validation against field experimental data is demonstrated in Rockhold et al. (1996), where tritium transport in variably saturated soils is modeled and compared to data from the Las Cruces Trench Site in New Mexico. Rockhold et al. (1996) use the STOMP code with a new method combining similiar media scaling and geostatistical analyses to obtain relatively good matches between observed and simulated flow and transport behavior. Another example of validation is found in Oostrom et al. (1996a), in which a two-dimensional flow cell experiment is simulated with STOMP for comparison to flow cell data.

Two density-driven liquid flow problems were examined in Section 4 (Henry's Problem and Elder's Problem). In Lenhard et al.(1995a), density-dependent gas advection of TCE is examined through experiment and STOMP modeling.

Aimo and Oostrom (1997) provides a new model, PMFCT-2D, that employs a fast and efficient Flux-Corrected Transport (FCT) algorithm for accurate simulation of advective-dispersive transport in variably saturated, heterogeneous porous media, with nonuniform aquifer thickness in the third dimension under high Peclet number (Pe) conditions. The PMFCT-2D code is easily coupled to any flow simulator via generated velocity, saturation, and cell thickness fields. STOMP is coupled to PMFCT-2D for the demonstrations provided in Aimo and Oostrom (1997).

An additional example of multifluid flow modeling can be found in Oostrom et al. (1997b). STOMP has also been used for numerical verification of a simple way to convert Brooks-Corey parameters to van Genuchten parameters using a soil parameter equivalence expression (Morel-Seytoux et al. 1996).

STOMP was used by Smoot and Williams (1996) to compare the results of the mathematical model with a database describing the spatiotemporal movement of water injected into unsaturated sediments at the Hanford Site in Washington State. The objective of this work was to adapt geostatistical tools commonly used for model parameter estimation to the problem of estimating the spatial distribution of the dependent variable to be calculated by the model.

9.1 References

Aimo NJ, and M Oostrom. 1997. "PMFCT-2D: A solute-transport simulator for various grid Peclet numbers." *Ground Water*, 35(1), 30-38.

Lenhard RJ, M Oostrom, and MD White. 1995a. "Investigation of density-dependent gas advection of trichloroethylene: experiment and a model validation exercise." *Journal of Contaminant Hydrology*, 19(1), 47-67.

Lenhard RJ, M Oostrom, and MD White. 1995b. "Modeling fluid flow and transport in variably saturated porous media with the STOMP simulator. 2. Verification and validation exercises." *Advances in Water Resources*, 18(6), 365.

Morel-Seytoux HJ, PD Meyer, M Nachabe, J Touma, MT van Genuchten, and RJ Lenhard. 1996. "Parameter equivalence for the Brooks-Corey and van Genuchten soil characteristics: Preserving the effective capillary drive." *Water Resources Research*, 32(5), 1251-1258.

- Oostrom M, C Hofstee, JH Dane, and MD White. 1996a. "Simulation of a quantitative two dimensional multi-fluid flow experiment," In Proceedings of *XI International Conference on Computational Methods in Water Resources*, 449-556.
- Oostrom M, C Hofstee, and JH Danes. 1997a. "Light non-aqueous phase liquid movement in a variably saturated sand." *Soil Science Society of America Journal*(In Press).
- Oostrom M, C Hofstee, RC Walker, JH Dane, RJ Lenhard, and MD White. 1997b. "Physical modeling of multifluid behavior in porous media," In Proceedings of *Seventeenth Annual American Geophysical Union Hydrology Days*, Colorado Springs, Colorado, 241-254.
- Oostrom M, and RJ Lenhard. 1996. "Radon transport into dwellings: considering groundwater as a source." *Geophysical Research Letters*, 23(13), 1577.
- Oostrom M, and RJ Lenhard. 1997. "Comparison of relative permeability-saturation-pressure parametric models for infiltration and redistribution of a light nonaqueous phase liquid in sandy porous media." *Advances in Water Resources*(In Press).
- Oostrom M, RJ Lenhard, and MD White. 1995. "Infiltration and Redistribution of dense and light nonaqueous phase liquids in partly saturated sand columns," In Proceedings of *Fifteenth Annual American Geophysical Union Hydrology Days*, Fort Collins, Colorado, 215-226.
- Oostrom M, RJ Lenhard, and MD White. 1996b. "Numerical evaluation of groundwater as a supply for radon into dwellings," In Proceedings of *XI International Conference on Computational Methods in Water Resources*, 193-200.
- Rockhold ML, RE Rossi, and RG Hills. 1996. "Application of similar media scaling and conditional simulation for modeling water flow and tritium transport at the Las Cruces Trench Site." *Water Resources Research*, 32(3), 595-609.
- Simmons CS, NJ Aimo, MJ Fayer, and MD White. 1997. *Developing a Model for Moisture in Saltcake Waste Tanks: Progress Report*, PNNL-11595, Pacific Northwest National Laboratory, Richland, Washington.
- Smoot JL, and RE Williams. 1996. *A Geostatistical Methodology to Assess the Accuracy of Unsaturated Flow Models*, NUREG/CR-6411 (PNL-10866), U.S. Nuclear Regulatory Commission, Washington, D.C.
- White MD, and M Oostrom. 1997. "Mathematical modeling of surfactant-enhanced mobilization and kinetic dissolution of DNAPLS in soil columns," In Proceedings of *Seventeenth Annual American Geophysical Union Hydrology Days*, Colorado Springs, CO, 349-364.
- White MD, M Oostrom, and RJ Lenhard. 1995. "Modeling fluid flow and transport in variably saturated porous media with the STOMP simulator. 1. Nonvolatile three-phase model description." *Advances in Water Resources*, 18(6), 353-364.

Distribution

OFFSITE

D. Augustijn
Water Resources & Management Dept
University of Twente
P.O. Box 217
7500 AE Enschede
The Netherlands

M. Brusseau
429 Schantz Building
Soil Water and Environmental Sci. Dept
University of Arizona
Tucson, 85721 AZ

R. Cady
U. S. Nuclear Regulatory Commission
Office of Nuclear Regulatory Research
Mail Stop T9-B3
Washington, DC 20555

J. Dane
202 Funches Hall
Agronomy and Soils Department
Auburn University, AL 36849

M. Hassanizadeh
Faculty of Civil Engineering
Delft University of Technology
Stevinweg 1
2628 CN Delft
The Netherlands

W. Herkelrath
US Geological Survey
Water Resources Division
345 Middlefield Road, MS 496
Melo Park, CA 94025

C. Hofstee
Universitaet Stuttgart
Institut fuer Wasserbau
Pfaffenwaldring 61
D-70550 Stuttgart (Vaihingen)
Germany

F. Leij
US Salinity Laboratory
450 West Big Springs Road
Riverside, CA 92507-4617

A. Leijnse
Department of Water Resources
Wageningen Agricultural University
Nieuwe Kanaal 11
6709 PA Wageningen
The Netherlands

T. J. Nicholson
U. S. Nuclear Regulatory Commission
Office of Nuclear Regulatory Research
Mail Stop T9-F33
Washington, DC 20555

M. Schroth
Department of Civil Engineering
Oregon State University
202 Apperson Hall
Corvallis, OR 97331-2302

R. van Genuchten
US Salinity Laboratory
450 West Big Springs Road
Riverside, CA 92507-4617

ONSITE

Pacific Northwest National Laboratory
(42)

N. J. Aimo
A. Chilakapati
C. R. Cole
M. J. Fayer
M. D. Freshley
G. W. Gee
T. J. Gilmore
C. T. Kincaid
P. D. Meyer
W. E. Nichols (10)
M. Oostrom (5)
M. L. Rockhold
C. S. Simmons
G. P. Streile
A. L. Ward
M. D. White (5)
M. D. Williams
S. K. Wurstner
Information Release (7)